Distinct conformations, aggregation and neuronal internalisation of different tau strains

by

Thomas Kwaku Karikari

A Thesis Submitted

for the Degree of Doctor of Philosophy in Life Sciences

School of Life Sciences

University of Warwick

Coventry, United Kingdom

September 2017

Nyame ne Hene!

(God is King!)

Dedicated to my son, Jayden Ohene Karikari, who sacrificed most of his first year to enable daddy complete his PhD.

Table of Contents

List of Figures

List of Tables

Acknowledgements

I would like to express my sincere gratitude to my supervisor, Prof. Kevin G. Moffat, for his unflinching support, guidance and mentoring throughout my PhD. Kevin, thank you for the opportunity to explore this exciting new project. I will miss our humour-filled conversations!

I would also like to appreciate the members of my Advisory Panel, Prof. Bruno G. Frenguelli and Prof. David I. Roper, for their constructive feedback, which kept me on track towards building a coherent scientific argument.

The Warwick experience would not be possible without the generous studentship from the University of Warwick's Chancellor's Scholarship and the Biotechnology and Biological Sciences Research Council. You turned a dream into reality!

Special appreciation to Dr. Eric J. Hill of Aston University, Birmingham, and his lab members for bringing me up to speed with stem cell culture techniques. I would also like to thank Prof. Alison Rodger and her group at the Department of Chemistry, for expert advice on, and access to, analytical biophysics equipment. My further thanks go to Dr. Neil Wilson, Department of Physics, and Mr. Ian Hands-Portman for training and the use of atomic force microscopy and transmission electron microscopy respectively. I am thankful to Dr. Mussa Quareshy for useful tips on protein purification, and Greg Walkowiak for assisting with microplate reader use. To the several MBio and BSc students I worked with during my PhD, including Alexandra Turner, Rachel Thomas and Sophie Keeling, thank you for offering me the opportunity to share the skills gained.

My further appreciation goes to Prof. Dominic Walsh and his research team at the Brigham and Women's Hospital, Harvard Medical School, for their time and patience in teaching me new skills and techniques during my visiting fellowship. My gratitude to the funders too.

Finally, I wish to thank my wife Rita, my son Jayden, my sister Theresa, my parents Nana and Ama, and my entire family and friends who supported me throughout this journey.

Declaration

I hereby declare that the material contained in this thesis is, to the best of my knowledge, my own original work unless otherwise cited, indicated, or is commonly known. This thesis has not been previously submitted for any degree at this or any other institution.

Thomas Kwaku Karikari
September 2017

Abbreviations

AD	Alzheimer's disease
AFM	Atomic force microscope
AF-maleimide	Alexa Fluor® 488 C5-maleimide
AGD	Argyrophilic grain disease
APP	Amyloid precursor protein
BCA	Bicinchoninic acid
BSA	Bovine serum albumin
CBD	Corticobasal degeneration
cDNA	complementary deoxyribonucleic acid
CD	Circular dichroism
CREB	cAMP Response Element Binding
CSF	Cerebrospinal fluid
DYRK1A	Dual-specificity tyrosine phosphorylation-regulating kinase 1A
ddH_2O	Double distilled water
DLS	Dynamic light scattering
DMSO	Dimethyl sulphoxide
DNA	Deoxyribonucleic acid
DPBS	Dulbecco's phosphate buffered saline
DTT	Dithiothreitol
ECL	Electrochemiluminiscent
EDTA	Ethylenediaminetetraacetic acid
EGTA	ethylene glycol-bis(β-aminoethyl ether)-N,N,N',N'-tetraacetic acid
FTD	Frontotemporal dementia
FTLD-tau	Frontotemporal lobar degeneration with tau pathology
FTDP-17	Frontotemporal dementia with Parkinsonism on chromosome 17
GSK3	Glycogen synthase kinase 3
IMAC	Immobilised metal affinity chromatography
hiPSC	human induced pluripotent stem cell
IPTG	Isopropyl β-D-1 thiogalactopyranoside
LB	Luria-Bertani

LDH	Lactate dehydrogenase
LMW	Low molecular weight
MAPT	Microtubule associated protein tau gene
MEM	Minimal essential medium
NEM	N-ethyl maleimide
NFT	Neurofibrillary tangles
NMR	Nuclear magnetic resonance
PBS	Phosphate buffered saline
PCR	Polymerase chain reaction
PHF	Paired helical filament
PiD	Pick's disease
PIPES	Piperazine-N,N′-bis(2-ethanesulfonic acid)
PSEN1	Presenilin 1
PSEN2	Presenilin 2
PSP	Progressive supranuclear palsy
RT	Room temperature
SDS	Sodium dodecyl sulphate
SDS-PAGE	Sodium dodecyl sulphate-polyacrylamide gel electrophoresis
SDM	Site directed mutagenesis
SF	Straight filament
RT	Room temperature
TCEP	Tris(2-carboxyethyl)phosphine hydrochloride
TEM	Transmission electron microscopy
TEV	Tobacco Etch Virus
ThS	Thioflavine S
ThT	Thioflavin T
UK	United Kingdom
WB	Western blot(ting)
WT	Wild type

Abstract

A shared property of several neurodegenerative diseases is the neuronal accumulation of aggregated tau protein. These include Alzheimer's disease (AD) and frontotemporal dementia (FTD). Many studies have suggested that aggregated tau accumulation in AD brains involves: (i) internalisation of extracellular tau (aggregated or not) into neurons; (ii) induction of endogenous tau aggregation by the internalised tau; and (iii) secretion of part or whole of this aggregated tau complex. This complex then initiates a new cycle of internalisation, aggregation and secretion. While this AD mechanism has strong evidential support, it is unclear if it applies to FTD. It was therefore investigated if and how two FTD-associated tau mutations, V337M and N279K, affect *in vitro* wild type (WT) tau aggregation and conformation, and studied the cell biological effects of their respective extracellular oligomers.

A library of 43 plasmids for expressing full-length and truncated tau and their FTD variants were created, in conjunction with the establishment of a new high-yield tau purification method. Consequently, *in vitro* biochemical assays showed that the FTD variants distinctively altered the immunological reactivity, the stages of aggregation, and the structural phenotypes of aggregated WT tau four-repeat domain, K18. Internalisation of WT and FTD tau K18 extracellular oligomers was significantly different in human neuroblastoma cells and human stem-cell derived neurons. Internalisation seemed to occur by endocytosis, and the internalised oligomers localised to the nucleus and cytoplasm of human neuroblastoma cells and the soma and neurites of stem cell-derived neurons. Moreover, internalised oligomers co-localised with endogenous tau and the nuclear protein nucleolin, without inducing cell death.

These findings provide new perspectives to the cell-to-cell propagation theory of aggregated tau, by demonstrating that cellular internalisation of tau variants may be tightly regulated by the given protein's folding and aggregation characteristics. This may help to explain several enigmatic aspects of the molecular pathogenesis found in different tauopathies.

1| Introduction

A major function of tau protein is to support the intact neuronal cytoskeleton, enabling efficient trafficking between sub-neuronal compartments. The dysfunction of tau is, however, implicated in the pathogenesis of many neurodegenerative diseases including the focus of this thesis, frontotemporal dementia (FTD). Whilst there is strong evidence supporting the mechanisms of disease, it is currently unclear if and how single nucleotide polymorphisms in tau associated with different forms of FTD may influence disease onset and progression. This introduction covers the structural biochemistry of tau and its functions in physiological and pathophysiological conditions. Furthermore, the mechanisms by which abnormal tau protein may lead to distinct forms of disease and the probable therapeutic targets involved are discussed. The chapter concludes with the aims of this study.

1.1 Tau protein: structure, isoforms and functional fragments

In physiological conditions, tau, encoded by the microtubule associated protein tau (*MAPT*) gene, supports microtubule (MT) assembly by inducing MTs to polymerise (Brandt et al., 1995; Drechsel et al., 1992). The human *MAPT* gene consists of 16 exons and is located on chromosome 17q21.3 (Andreadis et al., 1992; Neve et al., 1986). These exons are alternatively spliced, producing isoforms that are differentially expressed in tissues and in development (Goedert et al., 1988, 1989). There are six tau isoforms in the adult human brain, produced from alternative splicing of exons 2, 3 and 10 (Fig. 1.1). The gene structure consists of two major regions: the N-terminus projection domain, and the assembly domain (consisting of the MT-stabilisation region and the C-terminus), with the number of N- and C-terminus repeats differing between isoforms (Fig. 1.1). Exons 2 and 3 each encodes 29-amino acid inserts at the N-terminus: alternative splicing of these exons produces isoforms with zero, one or two N-terminus repeats (0N, 1N or 2N respectively; Fig. 1.1). Similarly, alternative splicing of exon 10 produces isoforms with either three MT-binding repeats (R1, R3, R4 = 3R-tau) due to exclusion of exon 10 or four repeats (R1, R2, R3, R4 =

4R-tau) due to exon 10 inclusion (Goedert and Jakes, 1990). Several tauopathies are associated with this irregular splicing of exon 10, by influencing the 3R:4R ratio (section 1.3).

Tau monomers in physiological conditions have little or no propensity to aggregate owing to their random, intrinsically disordered conformation. Using X-ray scattering and solution nuclear magnetic resonance (NMR), it has been demonstrated that tau lacks significant amounts of secondary structure (Mukrasch et al., 2009). Tau is a highly dynamic protein in terms of solubility and adaptability to different solution conditions: this property may have been acquired due to the protein's flexible disordered character. Tau has an overall hydrophilic nature and is therefore highly soluble in water (Jeganathan et al., 2008; Mukrasch et al., 2009). The protein can also adapt to high temperatures and high acidity, which adds to its flexibility (Jeganathan et al., 2008). Nonetheless, the amino acid charge distribution varies between the different regions: the N terminus, the C terminus and the MT binding region are mainly acidic, neutral and basic respectively (Kolarova et al., 2012). These differences are believed to contribute to the protein's varied functions in physiology and pathophysiology. Moreover, the tau isoforms have an anomalous behaviour with sodium dodecyl sulphate (SDS) which leads to a decrease in their mobility on SDS-polyacrylamide gel electrophoresis (SDS-PAGE) (Guo et al., 2017).

Due to the importance of the MT repeat region to both the physiological and the pathophysiological functions of tau (section 1.2), tau fragments made of specific repeat region sequences are frequently used to model aspects of the protein's function *in vitro*. These include the 4R and the 3R repeat domains commonly referred to as K18 and K19 (Fig. 1.1). These fragments are sufficient for reproducing many tau functions (section 1.2) (Stöhr et al., 2017; von Bergen et al., 2005).

1.2 Physiological and pathophysiological functions of tau

Tau is widely known for its physiological function in stabilising MTs. Nonetheless, the protein has other physiological functions. Moreover, disease-causing properties of the protein can be manifested through multiple pathways.

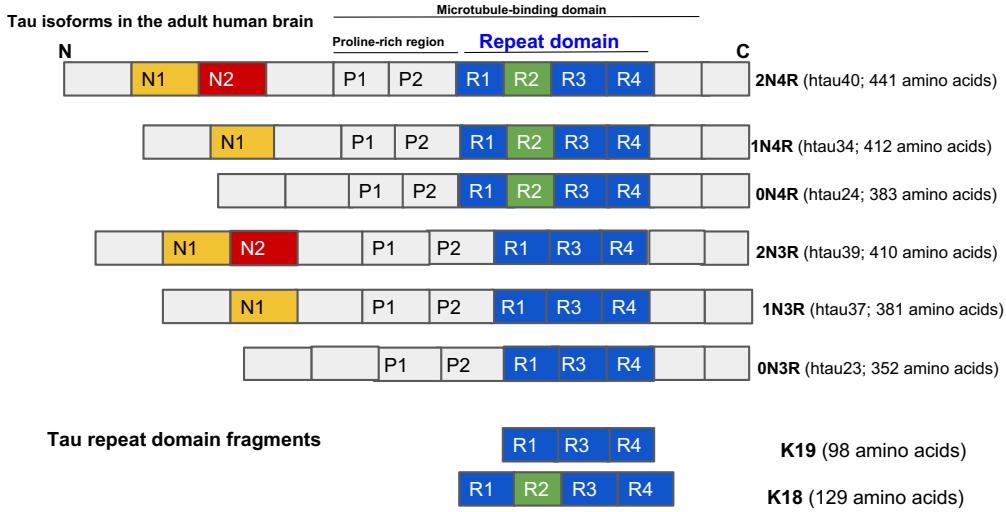

Figure 1.1. A schematic illustration of tau isoforms and functional fragments. *Alternative splicing of exons 2, 3 and 10 (colour-coded) produces six isoforms with different combinations of N terminus inserts and the C-terminus repeat domains (namely 0N3R, 1N3R, 2N3R, 0N4R, 1N4R and 2N4R). Due to the significance of the repeat domains in binding to and stabilising MTs, tau fragment constructs consisting of the two possible repeat domain combinations (repeats R1 – R4 referred to as K18 and R1-R3-R4 known as K19) are often used as functional truncation forms of tau for biochemical and cellular studies.*

1.2.1 Physiological functions of tau

Tau in the adult human brain is mostly found in axons where it binds to MTs and supports MT assembly and stability (Brandt and Lee, 1993). MTs are dynamic helical assemblies of α- and β-tubulin which serve as tracks for axonal transport (Conde and Cáceres, 2009). The binding of tau to MTs occurs at the α- and β-tubulin heterodimer interface, with specific amino acid stretches located in the repeat domain region being responsible for this function: residues 224-237 and 245-253 in R1, 275 – 284 in R2, and 300 – 317 between R2 and R3 (Kadavath et al., 2015). After the tau-MT complex is formed, a local hairpin structure involving residues ^{275}VQIINK^{280} and ^{306}VQIVYK^{311} becomes evident (Kadavath

et al., 2015). These two hexapeptide motifs are critical for tau aggregation, and therefore suggests that MT binding and self-aggregation are conflicting functions of tau (section 1.2.2.2). Due to its extra repeat region, 4R tau binds MTs more efficiently than 3R tau (Goedert and Jakes, 1990; Zhong et al., 2012). The projection domain binds to the neuronal plasma membrane and may contribute to neurite development (Brandt et al., 1995). Moreover, the length of the projection domain is a determining factor of axon diameter and MT filament spacing length (Chen et al., 1992). Deleting or reducing *MAPT* expression leads to impaired MT density and morphology, indicating that intact tau may be essential for cellular function (Bolkan and Kretzschmar, 2014).

Tau can also regulate axonal transport, by modulating the actions of the motor proteins dynein and kinesin, which function to ensure efficient protein trafficking from the axon to the soma (retrograde) and from the soma to the axon (anterograde) respectively (Dixit et al., 2008; Stamer et al., 2002). This is achieved through competition of tau with dynein and kinesin for MT binding, moderating retrograde and anterograde transport and altering the accumulation of cargo in the soma (Dixit et al., 2008; Stamer et al., 2002). As a result, tau can influence the number of kinesin molecules bound to MTs by occupying binding sites on MTs or by the interaction of its N-terminus with specific enzymes that regulate MT-kinesin binding (Kanaan et al., 2011). Furthermore, tau can modulate axonal transport by binding to the dynein interacting partner, dynactin (Magnani et al., 2007). As the functions of dynein and kinesin oppose each other (Belyy et al., 2016), tau is able to contribute to the control of both anterograde and retrograde transport.

While most neuronal tau is located in axons, small quantities of dendritic tau have recently been reported (Frandemiche et al., 2014). Dendritic tau is thought to have a crucial role in controlling synaptic plasticity: electrical stimulation of synapses causes tau in cultured mouse neurons to migrate to dendritic spines, where its interaction with actin may contribute to spine remodelling that triggers synaptic plasticity (Frandemiche et al., 2014).

Tau has also been found in eukaryotic nuclei, both in neurons and non-neuronal cells (Loomis et al., 1990; Sultan et al., 2011). Nuclear tau in human and monkey kidney cell lines co-localise with Tau-1, a pan-isoform tau antibody (Loomis et al., 1990). In these cells, Tau-1 co-localisation occurs in the nucleolar organiser region of the chromosome, suggesting that tau may have a role in regulating genomic deoxyribonucleic acid (DNA) (Loomis et al., 1990). Notably, tau homologues were not found in non-primate cells, possibly due to a conserved function of nuclear tau in primates (Loomis et al., 1990). Fig. 1.2 provides a schematic illustration of the neuronal location and physiological functions of tau.

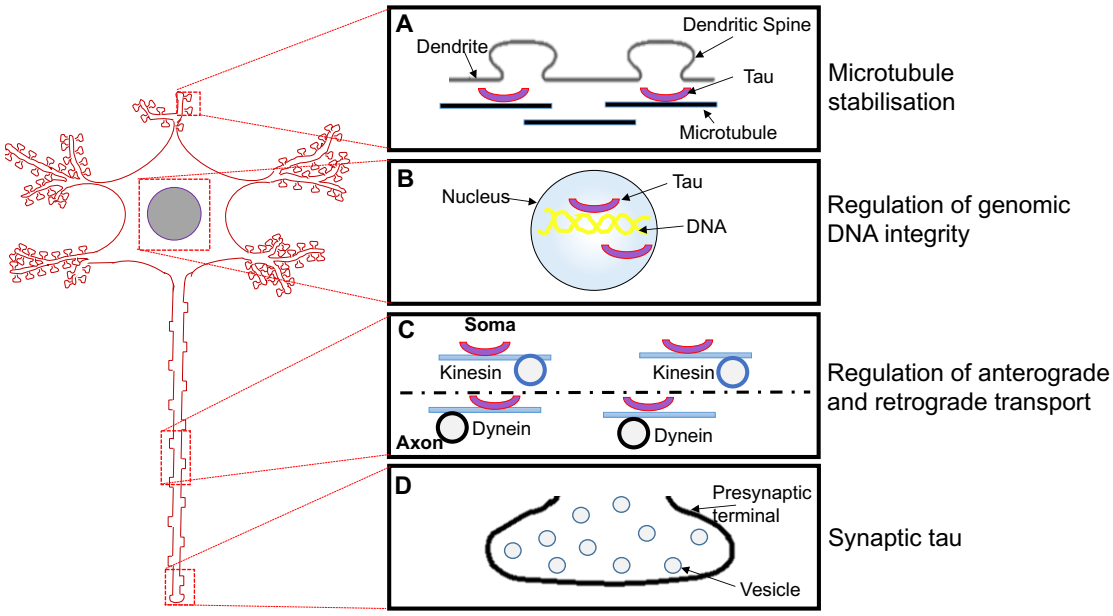

Figure 1.2. Physiological functions of tau.
(A) The most widely characterised role of tau is the stabilisation of MTs and the promotion of MT assembly. (B) In the nucleus, tau binds to specific chromosomal regions and possibly regulates the integrity and activity of genomic DNA. (C) Another function of axonal tau is the modulation of axon-soma shuttling of cellular material through the anterograde and the retrograde transport mechanisms, by regulating the interaction between MTs and the motor proteins kinesin and dynein required for these processes. (D) Synaptic tau is believed to be important for synaptic plasticity, although little is known about this property. Figure design concept taken from Wang and Mandelkow (2016).

1.2.2 Pathophysiological functions of tau

Tau dysfunction has been identified as a cause of several neurodegenerative diseases. The main pathways to tau pathophysiology can be grouped into two: either due to loss of its physiological functions or gain of new abnormal

functions. Loss of function effects of tau include: (i) decrease in tau expression levels, which reduces the amount of tau required for efficient MT stabilisation; and (ii) loss of the MT stabilisation function due to abnormal phosphorylation. Examples of the gain of function effects include: (i) self-polymerisation of soluble, free tau to form disease-associated aggregates; (ii) disease-associated mutations that change disease-causing pathways; and (iii) extracellular release and trans-synaptic propagation of misfolded tau.

1.2.2.1 Pathophysiology arising from loss of physiological functions

Elimination or reduction of tau levels

Reducing or abolishing tau expression can lead to disease-related manifestations. Although other MT-associated proteins may be able to compensate for the MT stabilisation function in the absence of tau, this seems inadequate as aged tau knock-out mice exhibit behavioural dysfunction reminiscent of those observed in neurodegeneration (Lei et al., 2014). For example, the levels of the MT-associated protein MAP1A is increased in several tau knock-out mice lines at birth, but decreases with age when motor and behavioural deficits become evident (Dawson et al., 2001; Fujio et al., 2007; Harada et al., 1994; Lei et al., 2014). It would therefore appear that the need for a critical level of physiological forms of tau increases with age, which high levels of MAP1A cannot necessarily account for. In neuronal cultures, tau reduction using antisense ribonucleic acid blocks axonal extensions (Caceres and Kosik, 1990). These data suggest that a certain level of tau expression is required to maintain MT integrity and efficient axonal transport throughout development and growth, and that reduction or elimination of protein expression has detrimental consequences. Experiments aimed at silencing tau expression using small interfering ribonucleic acid strategies have produced mixed results. Whilst it led to no evidence of neurotoxicity (Xu et al., 2014) and even neuroprotection (Vossel et al., 2015) in some cases, others reported enhanced mitochondrial dysfunction (Manczak and Reddy, 2013).

Loss of the MT stabilisation function

Adjacent to the MT-binding region are proline-rich regions (P1 and P2 in Fig. 1.1) that contain many phosphorylation sites, although many other sites are distributed across the entire tau sequence (Hanger et al., 2007). Excessive phosphorylation of tau reduces its ability to bind to MTs, hence disrupting the protein's main physiological function (Wang et al., 2013). Increasing levels of phosphorylation may lead to a complete loss of the protein's affinity to MTs, resulting in soluble tau accumulation in neurons, impairing neuronal homeostasis either by the sheer space occupied or by interfering with specific processes such as the protein degradation system (Stoothoff and Johnson, 2005). Moreover, the loss of tau's MT binding affinity can lead to MT disassembly, disrupting cargo transport. Because the extent of tau phosphorylation directly corresponds to reduction in MT binding, which may have disease-causing implications (Stoothoff and Johnson, 2005), the amount of phosphorylated tau is used as a biomarker in staging AD and other tau-positive diseases (Hampel et al., 2010). Importantly for this thesis, free forms of MT-detached tau can self-aggregate into large structures that may define disease progression (section 1.2.2.2).

1.2.2.2 Pathophysiology arising from gain of new toxic functions

Self-polymerisation of free tau to form aggregates

In its hyperphosphorylated state, the MT domain of tau cannot effectively bind MTs: this results in free floating forms of soluble tau (Fig. 1.3). These MT-unbound forms of tau can lead to disease through self-aggregation. The two hexapeptide motifs ^{275}VQIINK^{280} and ^{306}VQIVYK^{311} at the beginning of repeats R2 and R3 respectively are critical for the ability of monomeric tau molecules to aggregate. Removal of one or both motifs reduces or abolishes tau's aggregation competence (Bergen et al., 2000; Li and Lee, 2006). These motifs modulate the structural conversion of natively unfolded monomeric tau to β-sheet-rich aggregates; β-sheet content increases proportionally with cumulative aggregation (von Bergen et al., 2005). Data from solid state NMR experiments have shown that the ^{306}VQIVYK^{311} motif is an essential site for the initial monomer-monomer

contacts leading to tau aggregation (Xiang et al., 2017), suggesting that this motif regulates tau aggregation. It is therefore unsurprising that this structural peptide is capable of forming tau aggregates independently of the surrounding tau sequences (Stöhr et al., 2017), and that tau protein lacking this structural peptide is unable to aggregate (Li and Lee, 2006).

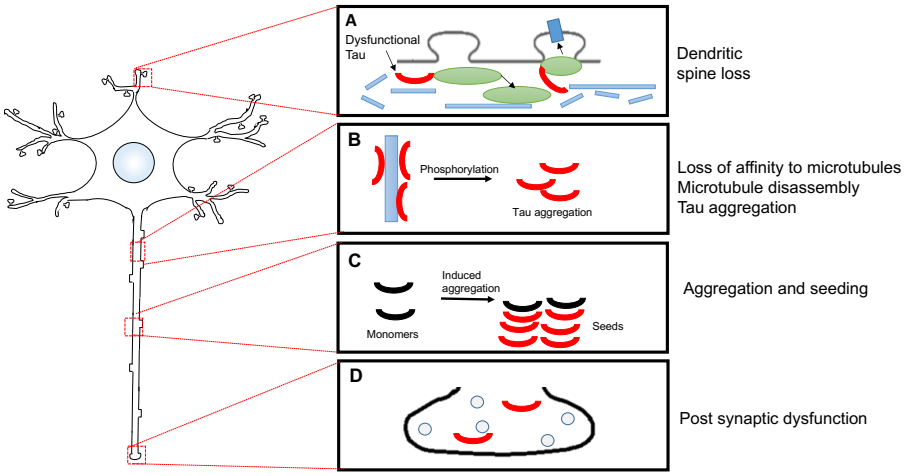

Figure 1.3. Pathophysiological functions of tau.
Dysfunctional tau, generated due to overproduction or abnormal phosphorylation, can lead to disease through different routes, such as: (A) presynaptic terminal mislocalisation, causing spine loss through a cascade of events; (B) lost affinity to MTs resulting in MT disassembly, impaired axonal transport and tau aggregation; (C) aggregated tau acting as seeds or templates to induce further aggregation; and (D) impaired neurotransmission by affecting the production and/or activity of specific post-synaptic proteins. Figure design concept taken from Wang and Mandelkow (2016).

Another mechanism by which tau aggregation can occur is intermolecular disulphide bonding. Tau monomers have one or two cysteine residues, depending on the isoform. 3R and 4R isoforms have one and two native cysteine residues respectively, at positions 291 and 322 (Bhattacharya et al., 2001; Kim et al., 2015; Schweers et al., 1995). Disulphide interactions between tau monomers promote aggregation whilst intramolecular bonding is thought to prevent aggregation (Fig. 1.4). Therefore, 4R tau aggregates faster and more efficiently than 3R tau, due to the capacity of 4R tau to form hierarchical chains of disulphide-bonded aggregates compared to 3R tau whose cysteine-dependent aggregation is limited to dimer formation (Zhong et al., 2012). However, the presence of the pro-

aggregant hexapeptide structural element ^{275}VQIINK^{280} in 4R isoforms also likely contribute to their higher aggregation rates.

In vitro tau aggregation is thought to follow a nucleation–elongation mechanism (Congdon et al., 2008; Friedhoff et al., 1998) where monomers dissociated from MTs due to hyperphosphorylation are aggregation-incompetent due to their unfolded conformation (Fig. 1.5). Monomer-monomer interactions, involving either disulphide bonding or the hexapeptide motifs, lead to a conformational change from an unfolded, disordered structure for monomers to a β-sheet-rich element that begins to adopt an aggregation-competent, structured conformation. This conformational change appears to be triggered by the formation of dimers, the minimal forms of aggregated tau (Congdon et al., 2008; Friedhoff et al., 1998). Dimer formation, thermodynamically disfavoured at physiological conditions, promotes further aggregation to form a critical nucleus of aggregated tau sufficient to overcome the rate-limiting step. Subsequent steps involve the addition of assembly-competent monomers and dimers to form larger oligomers, protomers, paired helical or straight filaments (PHFs or SFs respectively) and neurofibrillary tangles (NFTs). The neuronal accumulation of NFTs is linked to neurologic disorders involving tau, collectively referred to as tauopathies. The severity of NFT inclusion is used clinically to diagnose and stage tauopathies (Arriagada et al., 1992). Structural phenotypes of NFTs are of two major types: PHFs and SFs (Goedert and Jakes, 2005). Notably, both PHFs and SFs can be described as two strands wound round each other to form a filament, but perhaps the main distinguishing factor is that PHFs have easily recognised crossover points whereas SFs do not (Wischik et al., 1985) (Fig. 1.6). While PHFs and SFs may have identical protomer composition (made of residues 306 – 378), their structural distinction is in the molecular arrangements of protomers (Fitzpatrick et al., 2017). Being a mutation hotspot (Fig.1.7), the protomer core, and therefore PHF and SF structures, could be altered in FTD. Because tau filaments assembled *in vitro* from recombinant proteins tend to share close characteristics with AD brain-derived filaments (Fig. 1.6), recombinant tau is often used to model the mechanistic forms of tauopathies.

Tau aggregation can be accelerated *in vitro* by external agents that help to overcome the thermodynamic barrier required for nucleation. An example is inducing monomer aggregation with aggregated tau (PHFs or oligomers) used at suboptimal concentrations (Falcon et al., 2015; Guo and Lee, 2011). Such reactions record aggregation much quicker compared to unseeded controls, as the seeds readily overcome the initial rate determining steps of the reaction. Tau aggregation *in vivo* and in cultured cellular models is thought to proceed in a mechanism similar to the *in vitro* seeded aggregation: by the templated aggregation of the exogenous tau delivered into the cell by recruiting endogenous tau of same or similar conformation (Frost et al., 2009; Stancu et al., 2015). Other approaches that can accelerate tau aggregation include the use of metallic cofactors (Bader et al., 2011; Du et al., 2014; Nübling et al., 2012; Zhou et al., 2007) or chemical inducers, including heparin and arachidonic acid (King et al., 2000; Ramachandran and Udgaonkar, 2011). The mechanism by which these agents enhance tau aggregation is not fully understood but a general consensus is that they circumvent the rate limiting step, bypassing the need to form a critical mass of aggregated tau to enable aggregation. Furthermore, tau aggregation can be modulated by specific disease-associated mutations (section 1.4).

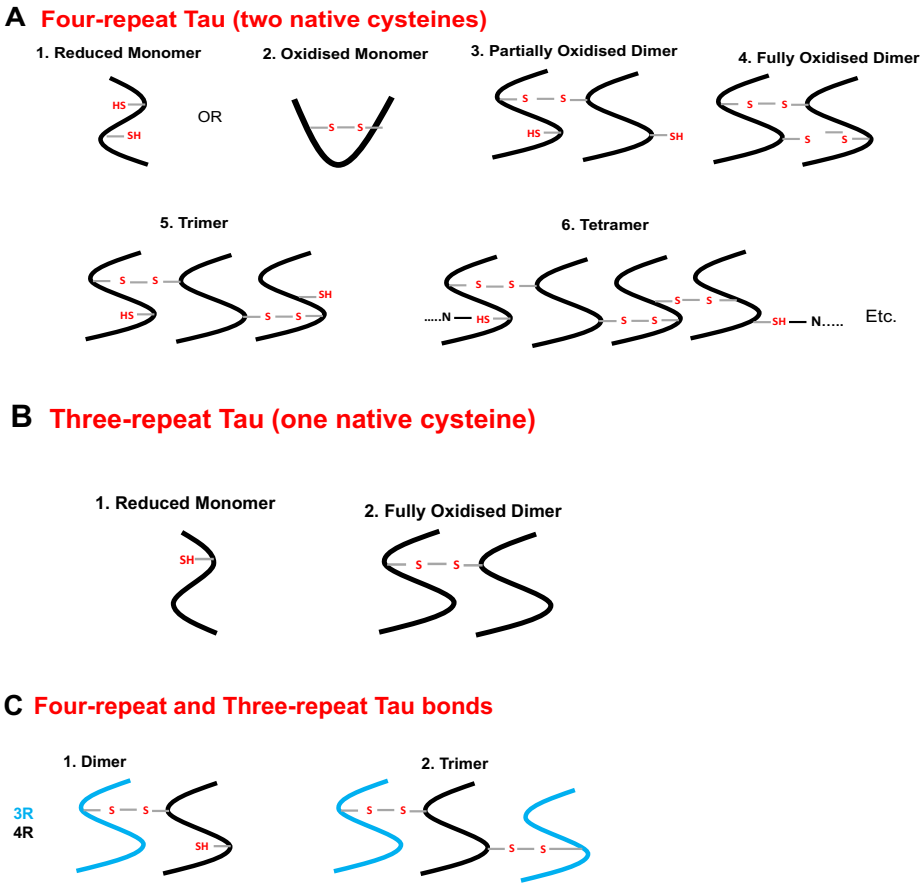

Figure 1.4. Cysteine-dependent tau aggregation is isoform-specific.
(A) 4R tau isoforms have two native cysteine residues that can engage in intermolecular disulphide bonding to form dimers, trimers and tetramers and higher aggregates, as illustrated here. (B) 3R tau isoforms have a single cysteine residue each, and can consequently aggregate only through dimer formation. (C) putative 4R-3R disulphide bonding mechanisms leading to tau aggregation.

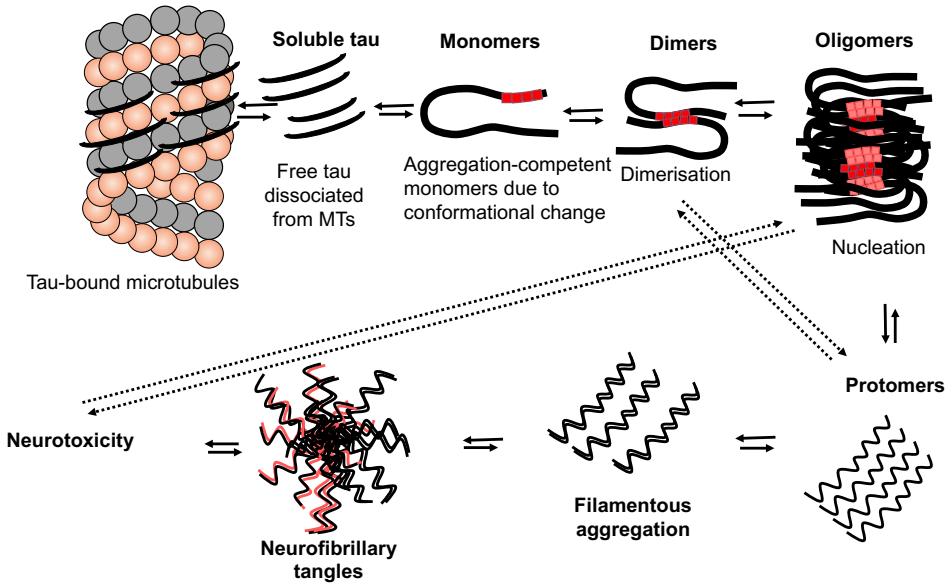

Figure 1.5. Schematic illustration of the "nucleation-elongation" mechanism of tau aggregation. *Hyperphosphorylation causes tau to detach from MTs into a pool of free, floating proteins. These aggregation-incompetent tau proteins undergo a conformational change, which enable them to make intermolecular contacts either through the hexapeptide motifs (red) or by disulphide bonding. Successive aggregation results in the formation of a critical nucleus of aggregated tau that is sufficient to overcome the thermodynamic barrier and promote further aggregation to form filamentous aggregates, and then into NFTs (different colours highlight possible structural heterogeneity in tangle composition). NFT and oligomer accumulation in affected human brains can lead to neurotoxicity through several mechanisms as described in Fig. 1.3. Specific aggregation processes leading to NFT formation may be reversible under defined conditions. High concentrations of dimers and/or other small oligomers may be able to by-pass the nucleation stage of aggregation.*

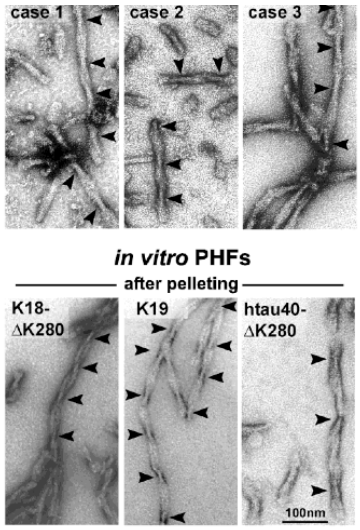

Figure 1.6. Electron micrographs of tau aggregates isolated from AD brains (upper panel; three patients – cases 1 – 3) and in vitro polymerised filaments from recombinant tau K19, and disease variant forms of K18 and htau40 (bottom panel).
The recombinant PHFs, assembled in the presence of the polyanionic cofactor heparin, share close features (such as a paired helical characteristic, 10-25 nm width and a crossover repeat of ~80 nm) with the brain-derived PHFs. Figure taken from Barghorn et al., (2004).

1.3 Tauopathies: disease classification, clinical diagnosis, progression, and differential roles of tau isoforms

Neurodegeneration in tauopathies is characterised by a gradual dysfunction and subsequent loss of affected neurons due to the activities of abnormal tau. Notwithstanding the strong similarities, the molecular mechanisms and the clinical presentations differ between various tauopathies, and these form the basis of their classification (Dickson et al., 2011; Rademakers et al., 2012). Tauopathies can be segregated based on multiple pathological factors, including histopathological findings, ultrastructure of tau inclusions and the tau isoforms mainly affected. The commonest tauopathy is AD, followed by a heterogeneous group of tau-positive diseases that have both sporadic and familial causes (Rademakers et al., 2012). These include frontotemporal lobar degeneration with tau pathology (FTLD-tau; also known as FTD). Common forms of FTD include frontotemporal dementia and parkinsonism linked to chromosome 17 (FTDP-17), corticobasal degeneration (CBD), progressive supranuclear palsy (PSP), Pick's disease (PiD) and argyrophilic grain disease (AGD).

A major clinical feature of AD is intraneuronal NFT accumulation consisting of PHFs and SFs polymerising from both 4R and 3R tau (Wischik et al., 1988). Tau filaments in AD are mostly PHFs, with crossover distances of ~80 nm and width of 10–20 nm, and SFs 15 nm wide (Wischik et al., 1988). A strong evidence supporting a causative role for tau in AD is obtained from amyloid-β processing. Amyloid-β is a proteolytic product of the transmembrane protein amyloid precursor protein (APP) whose processing occurs by two broad pathways: amyloidogenic and non-amyloidogenic, with the former leading to amyloid-β production through γ-secretase-mediated proteolysis of APP (O'Brien and Wong, 2011). As a multiprotein complex consisting of, among other proteins, presenilin 1 (PSEN1) and presenilin 2 (PSEN2), γ-secretase activity can influence APP proteolysis and hence amyloid-β generation (Bergmans and De Strooper, 2010). For example, substituting the aspartyl residues D257 and D385 in PSEN1 to Alanine reduces APP cleavage and hence amyloid-β production (De Strooper et al., 1998; Wolfe et al., 1999). Since amyloid-β is primarily an extracellular protein, its intracellular effects are triggered by activating specific channels and receptors (e.g., tyrosine kinase receptors and Ca^{2+} channels). Extensive interactions between candidate protein kinases (phosphatases, serine/threonine kinases, and tyrosine kinases) lead to increased tau phosphorylation, which then induces NFT formation and subsequent neurodegeneration and neuronal loss (Hanger et al., 2009). Based on this pathway, tau toxicity manifests downstream of abnormal amyloid-β production. Pathological mutations in *APP, PSEN1* and *PSEN2* would then induce and/or require tau dysfunction to cause disease. For example, 87% of a cohort of early-onset AD patients carrying APP or PSEN1, or PSEN2 mutations had abnormal cerebrospinal fluid (CSF) levels of total tau, phosphorylated tau and amyloid-β (Lanoiselée et al., 2017). Moreover, the V717I APP mutation causes increased amounts of amyloid-β by enhancing γ-secretase cleavage of APP in stem cell-derived neurons, which then leads to increased total and phosphorylated tau levels (Muratore et al., 2014). Importantly, total tau overproduction was rescued by amyloid-β-specific antibody treatment, suggesting a causal link between altered amyloid-β production and tau levels (Muratore et al., 2014). Furthermore, altered APP metabolism increases tau production and phosphorylation, suggesting APP regulation of tau processing beyond amyloid-β

levels (Moore, et al., 2015). This connected pathway of events, referred to as the amyloid cascade hypothesis, provides evidence demonstrating that dysfunctional tau has a central role in AD pathogenesis, dependent on altered APP metabolism and/or amyloid-β levels (Hardy and Allsop, 1991). Another piece of evidence supporting this hypothesis is that tau knock-out mice do not develop NFTs, suggesting that upstream dysfunctional APP and/or amyloid-β activity is required for tau toxicity (Chin et al., 2004, 2005). Indeed, reduction in tau levels is neuroprotective due to its obstruction of amyloid-β-induced toxicity (Vossel et al., 2015).

NFT accumulation in AD first occurs in the transentorhinal cortex, and tends to extend to other brain regions including the neocortex and the hippocampus. This gradual development of tau pathology in distinct anatomical brain regions is used in staging AD, as first described over two decades ago (Braak and Braak, 1991). NFT development in AD often occurs alongside memory and cognitive decline (Guillozet et al., 2003; Nelson et al., 2012).

NFT formation in CBD has exclusive phosphorylated 4R tau involvement (Ksiezak-Reding et al., 1996). Another feature of CBD is cortical neurodegeneration in the superior parietal lobule and the frontal gyrus (Litvan et al., 2000). Clinically, CBD may present with apraxia of speech, dystonia and asymmetrical limb rigidity (Litvan et al., 2000). CBD diagnosis is not always straightforward because patients' signs and symptoms frequently overlap with other diseases such as PSP, usually with no differentiating biomarker. For example, cases of symmetrical rigidity and apraxia with dystonia have been reported (Boeve et al., 1999; Ling et al., 2010). Due to these challenges, definitive diagnosis are usually made only at the post-mortem stage where the NFT ultrastructure can be taken into account (Dickson et al., 2011). PSP is another tauopathy whose hallmark is selective 4R tau pathology. The disease shares several clinical features with CBD and atypical forms of parkinsonism, hence a subset of PSP is referred to as PSP-Parkinson's disease (Williams et al., 2005). Brain regions affected in PSP include the substantia nigra, basal ganglia and subthalamic region (Hauw et al., 1994) with cortical neurodegeneration

sometimes present (Josephs et al., 2008). CBD and PSP both form predominantly SFs with few twisted filaments which are often 15-30 nm wide (Ksiezak-Reding et al., 1996; Takauchi et al., 1983). However, the crossover periodicity of SFs in the two diseases tends to differ, being ~100 nm and 160 nm for PSP and CBD respectively (Ksiezak-Reding et al., 1996; Takauchi et al., 1983). Tau aggregation in PiD involves mainly 3R isoforms, and leads primarily to SFs 160 nm in periodicity and 15 nm wide (Kato and Nakamura, 1990). As a rare form of frontal lobe dementia, PiD mainly affects the cortex and limbic lobe (Barker et al., 2002). PiD can be due to sporadic or familial causes, with the latter due to specific tau mutations (Hogg et al., 2003; Murrell et al., 1999).

FTDP-17 has several shared clinical features with the other FTDs – PiD, CBD, and PSP – including the affected anatomical regions (cortex, brainstem, and basal ganglia), clinical features (dementia, psychosis, and focal cortical syndrome), and tau isoforms involved (either 4R only or 4R and 3R jointly) (Dickson et al., 2011). The majority of familial FTDP-17 are caused by tau mutations (section 1.4), with the rest often occurring due to mutations in the *GRN* gene on chromosome 17q21 that codes for progranulin (Cruts et al., 2006), and *C9orf72* on chromosome 9p21 (DeJesus-Hernandez et al., 2011; Renton et al., 2011). FTD patients with progranulin mutations have TDP-43 pathology, which explains the absence of tau-positive inclusions (Cenik et al., 2012; Perry et al., 2013; Rademakers et al., 2012).

1.4 Tau mutations as modulators of familial FTD

Aside from dysfunctions of the wild type (WT) tau, many disease-associated mutations in tau have been identified (Coppola et al., 2012; Hogg et al., 2003; Murrell et al., 1999; Rosso et al., 2002; Tacik et al., 2015). The Alzforum website listed 107 of such mutations as of 8th September, 2017 (http://www.alzforum.org/mutations/search?genes%5B%5D=492&diseases=&keywords-entry=&keywords=#results). Most mutations are missense mutations involving single amino acid changes whilst a few others involve single amino acid deletions. While mutations in exons 1, 9, 11, 12 and 13 affect all isoforms, mutations in or around exon 10 affect only the 4R isoforms (Andreadis et al., 1992, 1995). The fact that the majority of the mutations are located in the MT

repeat region emphasises the importance of this region not only in tau physiology but also pathophysiology. Moreover, because many tau mutations cluster around exon 10, they can only be produced through alternative splicing which may alter the isoform balance (Fig. 1.7).

Many mutations in *MAPT* are associated with familial forms of FTD, including FTDP-17, CBD, PiD, AGD, and PSP (Goedert and Jakes, 2005) The pathological *MAPT* mutations underlying these tauopathies may confer disease in a number of ways: (i) at the mRNA level (through alternative splicing) or (ii) at the protein level (by altering MT-binding efficiency or by enhancing/reducing protein aggregation). As shown in Table 1.1, familial FTDP-17 exhibits extensive heterogeneity in disease characteristics which overlaps with features of other FTDs.

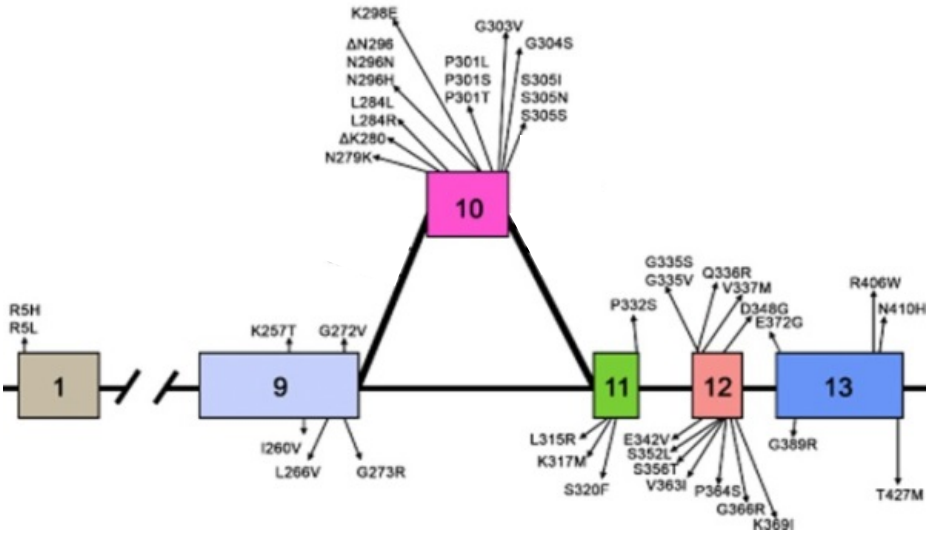

Figure 1.7. Exonic distribution of disease-associated tau mutations.
Over 100 mutations in the MAPT gene are associated with different brain disorders involving dysfunctional tau. Majority of these mutations are single point changes or deletions that change the protein's amino acid composition. These alterations can impact physiological functions such as MT stabilisation and can lead to disease through reduced MT binding, changes in aggregation kinetics, and isoform imbalance. Most mutations cluster around the MT repeat region, which spans part of exon 9 through to exon 12. Mutations in exon 10 are only evidence in 4R tau isoforms. Figure from Ghetti et al., (2015).

Many mutations found within the MT binding region exert their main effects either by reducing MT binding and stabilisation or by altering the aggregation rate. For example, P301L and R406W isolated from FTDP-17 brains reduced tau

MT binding whilst V337M and R406W decreased tau's ability to promote MT stabilisation (Hong et al., 1998). Other mutations that reduce MT binding *in vitro* include N279K, G272V and ΔK280 (Barghorn et al., 2000). The ability to alter MT binding is not limited to mutations in the MT binding region, as A152T, R5L and R5H in the N terminus also cause reduction in MT binding of tau (Coppola et al., 2012; Magnani et al., 2007). Since truncation at glutamine 124 in AD brains alters tau MT-binding abilities (Derisbourg et al., 2015), the N-terminus mutations may have direct functions in tau-MT association

Table 1.1. MT binding effects and clinical phenotypes of some *MAPT* mutations associated with FTDP-17
Table adapted from Liu and Gong, (2008)

Exon	Mutation	Effect on MT binding	Tau isoforms involved	Clinical phenotype
1	R5H	N/A	Mostly 4R	PSP
1	R5L	N/A	1N3, 4R	AD
9	K257T	Reduced	3R>4R	PiD
9	I260V	N/A	Mostly 4R	N/A
9	L266V	N/A	3R	PiD
9	G272V	N/A	3R	PiD
10	N279K	Variable*	4R	PSP
10	ΔK280	Reduced	3R>4R	FTDP-17
10	L284L	No change	4R maybe	AD
10	N296N	No change	Mostly 4R	CBD
10	N296H	N/A	Mostly 4R	FTDP-17
10	ΔN296	Reduced	N/A	PSP
10	P301L	Increased	4R	FTDP-17
10	P301S	N/A	Mostly 4R	FTDP-17 and CBD
10	G303V	N/A	Mostly 4R	PSP
10	S305N	No change	Mostly 4R	CBD
10	S305S	N/A	Mostly 4R	PSP
11	L315L	No change	N/A	N/A
11	S320F	Reduced	N/A	PiD
11	S320Y	N/A	N/A	PiD
12	Q336R	Increased	N/A	PiD
12	V337M	Reduced	3R, 4R	FTDP-17
12	E342V	N/A	Mostly 4R	FTDP-17, PiD
12	S352V	N/A	3R, 4R	PiD
13	G389R	Reduced	4R>3R	PiD
13	R406W	N/A	3R, 4R	PSP

N/A = not available
Inhibit exon 10 inclusion
Enable exon 10 inclusion
**variable MT binding effects reported from different studies*

Other *MAPT* mutations have additional suggested mechanisms. Mutations located in exon 10 have additional effects in the form of increased 4R isoform production which can influence the overall isoform distribution and lead to dysfunction through the overproduction of tau. As shown by Hong et al., (1998), insoluble human brain-derived tau aggregates from patients with N279K or P301L have exclusive involvement of 4R tau contrary to those from V337M and R406W brains that separated with both 3R and 4R tau in SDS-PAGE assays. How exon 10 mutations such as N279K increase 4R production and selectively induce 4R tau aggregation is unclear as this appears independent of MT binding effects. This could occur by promoting exon 10 splicing at the mRNA level, possibly by altering a splicing enhancer element that regulates exon 10 synthesis (Dawson et al., 2007; Hong et al., 1998). Although P301L is located in exon 10, it has opposite effects on MTs compared to N279K, indicating the two may be acting independently. Contrary to N279K, mutations such as G272V ΔK280, and L266V all inhibit exon 10 inclusion, thus reducing 4R tau production (Liu and Gong, 2008).

The aggregation of tau containing specific mutations, irrespective of the isoforms involved, can also lead to neurodegeneration via differential aggregation kinetics. P301L and ΔK280 increase thioflavine S-based tau aggregation, independent of the presence of the N terminus region (Barghorn et al., 2000). However, V337M, R406W, N279K, G272V, P301L and ΔK280 increase htau40 aggregation whilst V337M and G272V reduce K18 aggregation, suggesting that effects on aggregation kinetics are mutation-specific (Barghorn et al., 2000). A152T reduces tau aggregation, promoting oligomer but not PHF formation (Coppola et al., 2012). Using arachidonic acid as an inducer, htau40 aggregation was reduced by K369I and L315R but was increased in the presence of G272V, P301L, V337M and S320F (Combs and Gamblin, 2012). Importantly, tau mutations do not change the natively unfolded structure of monomers, and the β-sheet ordered conformation associated with aggregation (Barghorn et al., 2000). This suggests that the mutations do change the rate but perhaps not the overall mechanism of aggregation.

1.5 Theories of tau pathology: aggregation and conformational change

As discussed (section 1.2.2), a well-known route to tau dysfunction is hyperphosphorylation, which disrupts the protein's MT stabilisation function. This therefore suggests that gain-of-function effects of tau that occur downstream of MT destabilisation, such as aggregation, will be dependent on the protein's phosphorylation status. Motivated by this hypothesis, the tau research field has conducted intensive research aimed at identifying critical tau phosphorylation sites and kinases that may regulate aggregation (Šimić et al., 2016). It has however been found that tau aggregation can occur independently of phosphorylation, indicating that hyperphosphorylation may not be the sole route to disease-related aggregation (Tepper et al., 2014). Although there are disagreements as to which stage of tau aggregation (e.g., oligomers and PHFs; section 1.7) best correlates with disease, it is generally accepted that tau aggregation can lead to disease (Goedert, 2016; Goedert and Spillantini, 2017). If WT tau aggregation can cause disease, how then do FTD mutations affect this mechanism and therefore clinical outcomes? As specific mutations can alter tau's MT-stabilisation and aggregation functions (Table 1.1; section 1.2), it can be hypothesised that they do so by modifying tau's mechanism of disease. This could occur through multiple means, including: (i) by inducing conformational changes that make the mutated protein a more preferred substrate for aggregation (Jicha et al., 1999); (ii) by influencing the aggregation rate, as illustrated by significant lag time changes in kinetic aggregation assays (Combs and Gamblin, 2012); and (iii) by reducing the protein's affinity for MTs (which may also occur due to conformational change) (Table 1.1).

The effects of FTD mutations can therefore be broadly grouped into two: aggregation and conformational change, although the two are interconnected because reduced binding of mutant tau to MTs increases the amount of free, cytoplasmic tau capable of forming aggregates (Hong et al., 1998; Vogelsberg-Ragaglia et al., 2000). Aggregation changes are likely to occur in the nucleation-elongation mechanism (Fig. 1.5), where specific mutations would influence the

rate of nucleation and/or elongation, as shown previously (Barghorn et al., 2000; Combs and Gamblin, 2012) . However, these induced effects are likely to act downstream of the initial conformational change that tends to enable or enhance aggregation competence. For example, a "correct turn" conformational change in the third repeat region is essential to induce aggregation even in the presence of the ^{306}VQIVYK^{311} hexapeptide motif, as tracked by time-dependent NMR assays (Jiji et al., 2016). Such a conformational change which influences initiation of aggregation should perhaps occur before the nucleation stage (Fig. 1.5). Another form of conformational change could occur at the elongation stage of tau aggregation. In early stage AD (Braak stages I and II) brains: the monoclonal antibody MC1 recognises soluble forms of aggregated tau that appear before PHF and NFT formation in vulnerable brain areas, indicating that the MC1 epitope is an early pathological signal (Weaver et al., 2000). The conformational significance of the MC1 epitope may be the reason why the S320F FTD mutation causes reduced MT binding (Rosso et al., 2002).

1.5.1 Biochemical and biophysical tools for studying tau aggregation and conformation

Much of the insights into tau conformation and aggregation have been obtained from *in vitro* experiments on recombinant or brain-derived proteins using biochemical and biophysical tools. Those used in this thesis are introduced here.

Kinetic assays – using fluorescent dyes

Tau aggregation is rate-dependent: there are different reaction phases that can be monitored kinetically. As tau on its own does not give measurable chemical signals during aggregation (Sahara et al., 2007; Sui et al., 2015), fluorescence changes in the presence of specific chemicals that bind tau are used to estimate the protein's aggregation. Probably the most widely used is the benzothiazole salt thioflavin T (ThT) or its alternative thioflavine S (ThS), which is a mixture of several sulphonated compounds. When bound to tau monomers, ThT-tau and ThS-tau interactions lead to spectroscopic changes that alter the reported fluorescence signal. Following a brief lag phase, an exponential increase in fluorescence is recorded which is believed to indicate cumulative aggregation until filament formation when the curve reaches a plateau (Biancalana and Koide,

2010). Nonetheless, this property is dependent on the forms of tau used, buffer conditions, spectrophotometer and the tau-ThT/S ratio (Xue et al., 2017). The principle of ThT/S binding to tau filaments has been applied in clinical histopathology to diagnose tauopathies (Bussière et al., 2004; Rajamohamedsait and Sigurdsson, 2012). The mechanism of ThT/S binding to tau is not fully understood: one model suggests that ThT binds to amino acid side surface chains that are arranged in parallel to the β-sheet axis of tau filaments (Biancalana and Koide, 2010). Binding to proteinopathic aggregates can drastically increase the fluorescence intensities of both ThT and ThS, but the main difference is that a corresponding forward shift in emission spectrum is observed for ThT but not ThS for which no change in the excitation or the emission spectra is recorded (Groenning, 2010; LeVine, 1999). This results in a consistently high background fluorescence in the case of ThS, making it unsuitable for quantitative analysis (LeVine, 1999).

Secondary structure determination: circular dichroism (CD)

CD spectroscopy is routinely used to ascertain the structural transition of tau from its random coiled conformation to β-sheet formation. A CD spectrum is obtained due to a sample's differential absorption of left and right circularly polarised light. The extent to which a test molecule absorbs the two light waves which are arranged 90 ^{O} out of phase leads to the generation of an electrical field signal. The resultant differences in the electric field generated by the clockwise- and anti-clockwise-facing lights is calculated to give the CD readout at each wavelength. Signature CD spectra measured in the far UV range differ for given proteins depending on their predominant secondary structure content (Fig. 1.8). Unfolded proteins, such as monomeric tau, have negative peaks at 198 – 200 nm, β-sheet-enriched proteins like PHFs have negative peaks at ~220 nm, whilst soluble aggregated tau (e.g., oligomers) have an intermediate negative peak between 200 and 220 nm. Other proteins with majority α-helix content have two negative peaks at ~210 nm and ~220 nm (Whitmore and Wallace, 2008). CD-resolved secondary structure content can be analysed by comparing spectral signals to those in given databases (Greenfield, 2006; Kelly et al., 2005).

Ultrastructure of aggregated species: atomic force microscopy (AFM) and transmission electron microscopy (TEM)

AFM and TEM are similar techniques used to probe the ultrastructural properties of aggregated tau. AFM involves three-dimensional scanning of a sample surface with a cantilever-suspended flexible probe. Deflection of the cantilever occurs in response to probe-sample surface contacts on a piezoelectric scanner, leading to parallel images formed along the probe tracks. These images are then projected by laser signals onto photodiode detectors and processed with specific algorithms. There are three main AFM modes, depending on probe-sample interactions: contact, non-contact and tapping. Tapping mode imaging is often preferred as it eliminates the disadvantages of the other methods regarding poor resolution and frictional forces that can damage sample surfaces (Carvalho and Santos, 2012; Dufrêne, 2002).

In TEM, an electron beam passes through the sample and the micrometer-scale image formed based on electron-sample interactions is magnified to enhance resolution. As complementary techniques, TEM and AFM compensate for their shortcomings. For example, heavy metal staining in TEM can disrupt some nanoscale details. This challenge can be addressed by using AFM which does not use sample staining and therefore retains samples in their native state. Moreover, small aggregated proteins (e.g. oligomers made of <10-20 monomers) whose imaging can be problematic with TEM can be easily done with AFM. Nonetheless, AFM imaging is extremely slow and gives poor image resolutions. On the contrary, TEM images have better resolution and are achievable within shorter times (Tinker-Mill et al., 2014).

Dynamic light scattering (DLS)

DLS can be used to measure the sizes of monomeric and aggregated proteins in solution and to deduce the approximate number of monomer units that make up a given state of aggregation. The principle of DLS is based on measuring Brownian motion of proteins (or other macromolecules) when hit by solvent molecules. The detected motion is dependent on molecule size: the larger the molecule, the slower the motion and vice versa. DLS can therefore be used to efficiently deduce the sizes of a mixture of molecules (e.g. a heterogeneous mixture of aggregated

tau proteins), using the hydrodynamic radius which relates to the intensity of molecule fluctuations (Stetefeld et al., 2016).

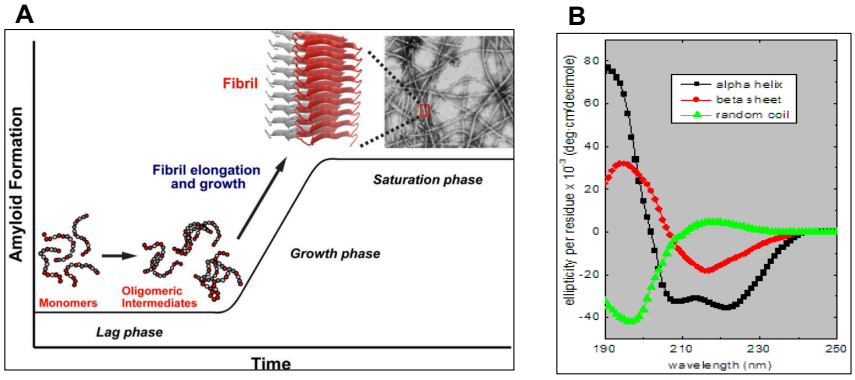

Figure 1.8. Example data from some commonly used biochemical and biophysical assays for evaluating tau aggregation and conformation.
(A) example standard curve from ThT or ThS kinetic assays (Abedini et al., 2016). (B) Standard CD spectra for proteins which have predominantly α-helices (black), β sheets (red), and unfolded/random coiled (green) conformations. Figure taken from http://www.ap-lab.com/circular_dichroism.htm, accessed on 10th September, 2017.

1.6 Proteinopathies and the prion hypothesis

Proteinopathies is a catch-all term for neurodegenerative diseases characterised by specific post translational modifications, involving the disease-related aggregation and neuronal accumulation of otherwise unstructured proteins, leading to neurodegeneration and eventual neuron loss. The term proteinopathies looks at the similarities between the molecular pathogenesis of neurodegenerative diseases such as AD, Parkinson's disease (PD) and Huntington's disease: the respective proteins underlying these diseases are tau/amyloid-β, α-synuclein, huntingtin and mutated forms of tau (in familial cases). Several other diseases have also been classified as proteinopathies (Golde et al., 2013).

A unifying characteristic of proteinopathies that continues to attract major research attention is the prion hypothesis: the mechanism by which aggregated and misfolded forms of causative proteins can be transmitted between synaptically-connected neurons. Through this strategy, abnormal forms of each

protein are gradually distributed throughout the brain, leading to synaptic dysfunction and neuron death (Frost and Diamond, 2010; Golde et al., 2013).

1.6.1 Neuronal internalisation and transmission of tau pathology: the transneuronal propagation and the selective vulnerability hypotheses

Although mounting evidence suggests that tau dysfunction causes neurodegeneration, the mechanistic basis for this association is not fully understood. Two main mechanisms have been proposed, referred to as the trans-neuronal propagation and the selective vulnerability spread hypotheses.

Transneuronal propagation

Against the backdrop that tau pathology in AD is predicted to occur in a defined, stereotypical mechanism (Braak and Braak, 1991), many scientists became interested in understanding how this may occur in experimental models. The hypothesis that misfolded tau may propagate in a transcellular manner, similar to the prion protein, was formulated and prompted a series of investigations into the cellular internalisation, secretion and propagation of dysfunctional tau. In line with this, many studies have reported that exogenously added tau protein can be internalised by both neuronal and non-neuronal cells (Clavaguera et al., 2009; de Calignon et al., 2012; Lasagna-Reeves et al., 2012a). Whilst in the cell, the internalised protein interacts with endogenous tau and propagate intracellular toxicity (Lasagna-Reeves et al., 2012; Michel et al., 2014; Usenovic et al., 2015). The mechanism of aggregation can therefore be referred to as template misfolding since the internalised protein, acting as a "seed" or "template," induces the aggregation or misfolding of endogenous tau (Stancu et al., 2015). Some of the internalised tau (perhaps in complex with some endogenous tau) is re-secreted into the extracellular environment from where propagation continues to neighbouring cells. Remarkably, all the pre-NFT (monomers, oligomers, filaments) tau species have been found to be internalised when supplied exogenously to cells and can be secreted to initiate the transmission process (Guo and Lee, 2011; Jackson et al., 2016; Lasagna-Reeves et al., 2012a; Michel et al., 2014; Usenovic et al., 2015). Moreover, these observations have been consistently made by modelling tauopathies in a range of model systems, including physiologically active whole organisms (Clavaguera et al., 2009;

Papanikolopoulou and Skoulakis, 2011), neuronal and neuron-like tissues (Michel et al., 2014; Usenovic et al., 2015; Wauters et al., 2016), *ex vivo* brain tissues (Fá et al., 2016) and post-mortem brains (Lasagna-Reeves et al., 2012a). The minimal tau peptide sequence required for this propagation behavioural is thought to be a 31-residue peptide that includes the hexapeptide motif in R3 (Stöhr et al., 2017). Neuronal accumulation and propagation of dysfunctional tau causes toxicity by impairing neurotransmission through neurite retraction and soma loss (Stancu et al., 2015; Usenovic et al., 2015), damaging electrical communication (Fá et al., 2016; Lasagna-Reeves et al., 2012a), and triggering memory and cognitive changes (Fá et al., 2016; Stancu et al., 2015).

Tau propagation is achieved through release and uptake between neighbouring neurons, for which several pathways have been reported (Fig. 1.9). In tau secretion via exocytosis for example, cytosolic tau is encapsulated in endosomal vesicles which undergo endocytic processing and later fuse with the plasma membrane to release tau in exosomes (Wang et al., 2017; Saman, et al., 2012) or ectosomes (Dujardin, et al., 2014) to the extracellular space. The secretion of tau in exosomes has been reported in cellular tauopathy models and in CSF of AD patients (Saman, et al., 2012). In the M1C human neuroblastoma cell line, exosome secreted 0N4R tau is phosphorylated at specific sites (Saman, et al., 2012). Differential release of tau isoforms (0N4R>1N4R/1N3R) has also been reported in the same cell line (Kim et al., 2010). In human AD CSF, exosome-associated tau is aggregated and phosphorylated at threonine 181, which is a diagnostic marker of AD (Saman, et al., 2012). Other mechanisms of tau secretion include tunneling nanotubular release between connected neurons (Tardivel et al., 2016; Abounit et al., 2016), and the extracellular release of tau in the membrane-free form (Chai et al., 2012). Tau in the extracellular space can be taken up by receiving neurons through several routes, with endocytosis being the commonest. Endocytosis has been reported for various forms of tau (monomers, oligomers, and fibrils), using cell lines overexpressing specific forms of tau or physiological levels of tau. (Frost et al., 2009; Guo and Lee, 2011; Michel et al., 2013; Wu et al., 2013). Furthermore, tau in exosomes can be directly transferred between neurons (Wang et al., 2017). Another mechanism is heparan sulphate-mediated macropinocytosis (Holmes et al., 2013).

Selective vulnerability model

A critique of the transneuronal propagation model argues that the physical internalisation, release and subsequent propagation proposed may be unrealistic because: (i) the model is incapable of explaining cell autonomy in degeneration and death; (ii) the Braak staging (Braak and Braak, 1991) used as a premise does not support the proposed transmission hypothesis; and (iii) the model does not address the patient heterogeneity and the brain regional vulnerability observed in proteinopathic protein accumulation. On this basis, an alternative model, referred to as the "selective vulnerability" hypothesis has been proposed. This model suggests that neuronal vulnerability to toxic insults (e.g., from misfolded tau) is selectively dependent on its viability: neurons stressed from the extracellular build-up of tau (or due to any other reason) would be easier targets compared to healthy ones. Healthy cells may become susceptible over time as the disease progresses and/or the levels of the stressor increase (Walsh and Selkoe, 2016). There are various mechanisms of transmission reported for the trans-neuronal propagation (Fig. 1.9), whilst Fig. 1.10 describes the counter selective vulnerability model.

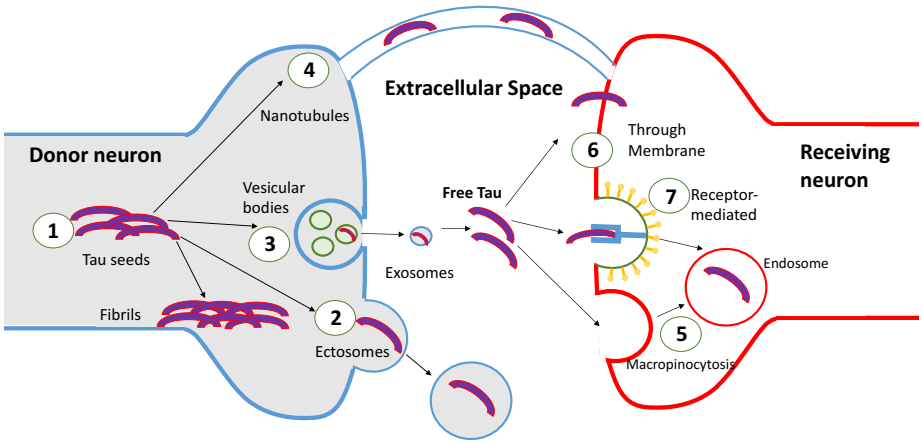

Figure 1.9. Mechanisms of misfolded tau transmission in the transneuronal propagation model for extracellular tau.
Misfolded or abnormal tau seeds (could be aggregated or not) accumulate in the neuron (1). Some of these are secreted through various routes, such as encapsulation and subsequent release by ectocytosis (2) or exocytosis (3). Nanotubular transfer between connected neuron is another possibility (4). Uptake of secreted tau can occur by naked-form passage through the plasma membrane of the receiving neuron (6), endocytosis (7), or macropinocytosis (5).

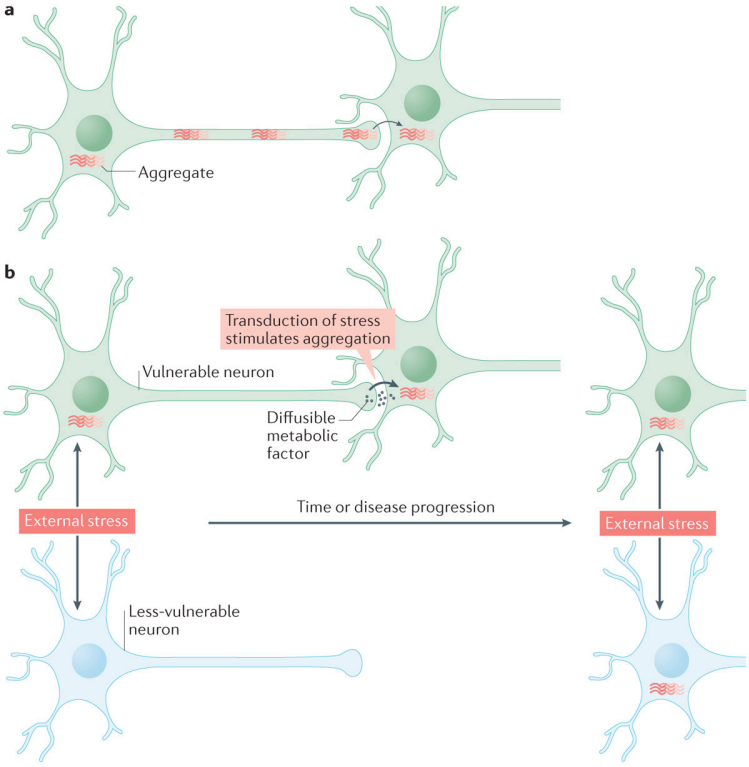

Figure 1.10. The selective vulnerability model of tau toxicity.
(A) The transneuronal spread model proposes physical transfer of misfolded tau between synaptically connected neurons, and thus brain regions, without accounting for cell autonomy. (B) The selective vulnerability model suggests that neurons of compromised viability will be first affected by possible insult from misfolded tau. Vulnerability can be transferred trans-synaptically through diffusible metabolic factors, instead of protein internalisation and release (Walsh and Selkoe, 2016).

1.7 Drug development against misfolded tau protein

The ultimate goal of research into tau-mediated neurodegeneration is to provide a knowledge base that enables effective therapy development. As tau dysfunction is triggered by phosphorylation, a primary target may be to block abnormal phosphorylation with anti-phosphorylation agents that target specific kinases or other proteins whose activities promote tau aggregation (option A; Fig. 1.11). This strategy appears promising because several candidate drugs have shown meaningful anti-phosphorylation activities. For example, the small molecule STI571 has been shown to block the activity of c-Abl tyrosine kinase, which promotes amyloid β-induced tau phosphorylation at tyrosine 15 (Cancino et al., 2008, 2011). Moreover, the candidate drug harmine inhibits the activity of dual-specificity tyrosine phosphorylation-regulating kinase 1A (DYRK1A), which

phosphorylates tau serine 202 leading to a pathology-associated conformational change (Martin et al., 2013; Seifert et al., 2008). Nonetheless, DYRK1A also phosphorylates the cAMP Response Element Binding (CREB) transcription factor, which regulates learning and memory (Yang et al., 2001). Hence, CREB inhibition is likely to lead to non-specific effects. Glycogen synthase kinase 3 (GSK3) is a tau protein kinase which has a central role in amyloid β-induced tau pathology: exposure to amyloid β increases GSK3 activity, tau phosphorylation, memory defects, apoptotic cell death and increased amyloid β expression (Hoshi et al., 1996; Takashima et al., 1996). GSK3 phosphorylates tau at multiple sites in human AD brains (Hanger et al., 2009; Martin et al., 2013), and its overexpression in NFT-forming transgenic mice causes hyperphosphorylation and neurodegeneration (Lucas et al., 2001). Lithium treatment rescues both GSK3-induced hyperphosphorylation and downstream neurodegeneration effects in transgenic mice (Klein and Melton, 1996). Other GSK3 inhibitors include specific compounds from the anilinomaleimide (Smith et al., 2001), paullone (Leost et al., 2000), indirubin (Leclerc et al., 2001), and thiadiazolidinone (Martinez et al., 2002) families. Some of these compounds are non-specific for GSK3 because they also inhibit tau kinases from the cyclin-dependent kinase family, including CDK2 and CDK5 (Bhat et al., 2004; Leclerc et al., 2001). Since CDK5 inhibition activates GSK3, such compounds may not be ideal drug candidates (Hanger et al., 2009). Whilst tau kinase inhibition may be a promising target, there is a need to be cautious in this approach because not all forms of phosphorylation may be harmful (Ittner et al., 2016).

A second approach is to prevent the conformational change that makes MT-detached tau aggregation competent, either by blocking monomer production or by immediately degrading monomers on production (option B, Fig. 1.11). Instead, preventing oligomer formation, perhaps by targeting cysteine residues and the hexapeptide motifs, as well as other forms of post translational modification that prevent oligomer formation, as shown for tau and other proteinopathic proteins (Hamano et al., 2016; Hayden et al., 2015; Soeda et al., 2015; Wen et al., 2017; Yoshitake et al., 2016, Fig. 1.11 Option C) could be an effective approach. Alternatively, agents that neutralise or clear formed oligomers, or those that prevent the accumulation of protomers may prove useful (options D and E

respectively). Formed filamentous aggregates can be otherwise targeted by degradation (option F), as explored for amyloid β (Yan et al., 2006). Should PHF degradation not prove successful, an alternative strategy will be to inhibit NFT accumulation with small molecules or immunotherapeutic agents (option H). Importantly, all the approaches proposed here should be feasible in both intra- and extra-cellular contexts.

While there are clearly several intervention points being investigated, the targeting of the cellular entry and exit of tau, which appears to be the central hub of many neurotoxic properties, may be productive in diseases involving tau and indeed other proteins (Fig. 1.10).

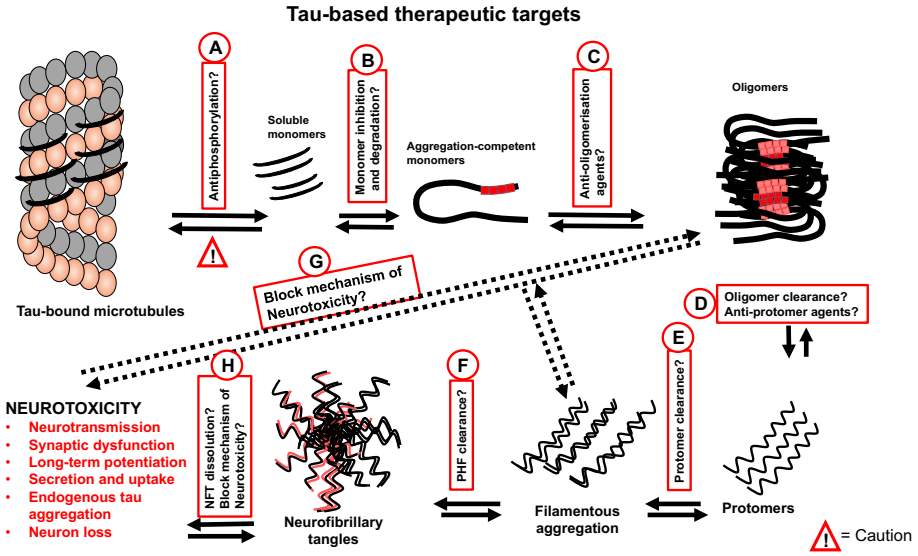

Figure 1.11. Dysfunctional tau-targeted drug development targets and approaches.
Description of each numbered approach has been provided in the text in section 1.7.

1.8 Aims of this thesis

The evidence for the transneuronal propagation of misfolded tau seems compelling. It is however unclear if the described mechanisms are translatable to mutant tau associated with FTD. While FTD mutations can cause drastic changes in tau aggregation and MT binding, these forms of tau could function through other unknown mechanisms. The aims of this thesis are therefore:

i. To develop genetic resources and a simple method of expressing and purifying tau protein and a selection of its FTD variants;

ii. To develop a new method of preparing low molecular weight (LMW) tau K18 oligomers of enhanced stability for use in biochemical and cell biology assays;

iii. To study the *in vitro* conformation and aggregation of tau K18 WT, V337M and N279K; and

iv. To investigate the cell biological effects of extracellular WT K18 tau oligomers and its FTD variants.

2| Materials and methods

2.1 Materials

BugBuster® 10X protein extraction reagent (70921-4), dimethyl sulfoxide (DMSO; K45797112 429) and DNAse I (69182) were purchased from Merck Millipore, Watford, Hertfordshire, United Kingdom (UK). Acrylamide/bisacrylamide (30 % solution; A3574-100ML), beta mercaptoethanol (M6250), bovine serum albumin (BSA; A7906-50G), bromophenol blue (B-8026), imidazole (12399-500G), retinoic acid (R2625-50MG), SH-SY5Y neuroblastoma cells (94030304), sodium chloride (S/3160/60), sodium phosphate dibasic (S9763-500G), sodium phosphate monobasic dihydrate (04269-1KG), N,N,N',N'-tetramethylethylenediamine (TEMED; T-7024), thioflavine S (T1892), thioflavin T (T3516-5G), Triton X-100 (X100-500ML) and TWEEN (P9416–100ML) were procured from Sigma Aldrich (St. Louis, Missouri, USA). X1 Amersham Protran 0.45 μm electrochemiluminescence nitrocellulose membrane (15259794), Amersham ECL Western blotting analysis system (RPN2108) and chelating sepharose fast flow (17-0575-01) were obtained from GE Healthcare, Buckinghamshire, UK. Ammonium acetate (CHE1140), ammonium persulfate (A/6160/53), glycine (G/0800/60), D-glucose (G/0500/53), ethylenediaminetetraacetic acid (EDTA; D/0700/53) and glycerol (G/0650/17) were bought from Fisher Scientific, Loughborough, UK. Ethylene glycol-bis(β-aminoethyl ether)-N,N,N',N'-tetraacetic acid (EGTA; 437012C), ethanol (20821.330) and methanol (20847.307) were purchased from VWR, Lutterworth, Leicestershire, UK. Piperazine-N,N′-bis(2-ethanesulfonic acid)(PIPES; A16090) was obtained from Alfa Aesar, Heysham, UK. Cell culture-grade DMSO (P60-36720100) was obtained from PAN-Biotech GmbH, Aidenbach, Germany. N-ethyl maleimide (23030) and CL-XPosure Film (34089) were obtained from Thermo Scientific, Rockford, Illinois, USA. CellMask® Deep Red plasma membrane stain (C10046), Hoechst 33342 (H21492) and Alexa Fluor® 488 C5-maleimide (A10254) were procured from Molecular Probes, Eugene, Oregon, USA. The Q5® site directed mutagenesis (SDM) kit (E0554S) was purchased from New England Biolabs, Ipswich, Massachusetts, USA. Lactate

dehydrogenase (LDH) cytotoxicity assay kit (88954) was obtained from Pierce Biotechnology, Rockford, Illinois, USA). The cOmplete protease inhibitor cocktail tablets (11836145001) and DNAse I (11284932001) were obtained from Roche Diagnostics GmbH (Mannheim, Germany). Isopropyl β-D-1 thiogalactopyranoside (IPTG; MB1008) was purchased from Melford Laboratories Limited (Ipswich, Suffolk, UK). Tris(2-carboxyethyl)phosphine (TCEP; A2233,0001) was procured from Applichem GmbH, Damstadt, Germany. SynaptoRed^{TM} C2 (FM4-64; 70021) was obtained from Biotium (Hayward, California, USA). The QIAprep Spin Miniprep kit (27104) was obtained from QIAGEN GmbH, Hilden, Germany. Marvel dried skimmed milk was obtained from Premier Foods Company, UK.

2.2 Cloning of tau proteins into pProEx plasmids

Three plasmids were used for recombinant expression of the WT K18 and htau40 tau proteins and four FTDP-17 variants of theirs (Fig. 2.1). For the K18 and htau40-FLAG plasmids, the protein sequences were preceded by the Tobacco Etch Virus (TEV) protease-recognition sequence ENLYFQG fused at the N-terminus to a hexa-histidine tag and a c-Myc tag. In the case of c-Myc-htau40, the c-Myc tag was placed downstream of the protein sequence. The coding sequences of the WT tau proteins were generated by polymerase chain reaction (PCR) using pCMV-FLAG-tau as template (a gift from Dr. Calum Sutherland, University of Dundee, UK) and cloned between the *Ehe*I and *Eco*RI sites of the pProEx-HTa plasmid (Invitrogen) containing ampicillin-resistance and *lacI*-encoding genes (courtesy of Dr. David Nagel, Aston University). Protein expression was controlled by a *trc* promoter, and initiated with the addition of IPTG. Plasmid sequences were confirmed by deoxyribonucleic acid (DNA) sequencing performed externally at GATC Biotech AG, Konstanz, Germany. Primers were synthesised using the standard desalting method and later diluted in 50 µl of 10 mM Tris HCl, pH 8.5 to give 500 mM stock solutions from which working solutions of 10 µM were prepared. Working solutions were diluted 1:10 with double distilled water (ddH_2O) in 10 µl sequencing reaction mixtures, in the presence of 80 ng/µl template DNA.

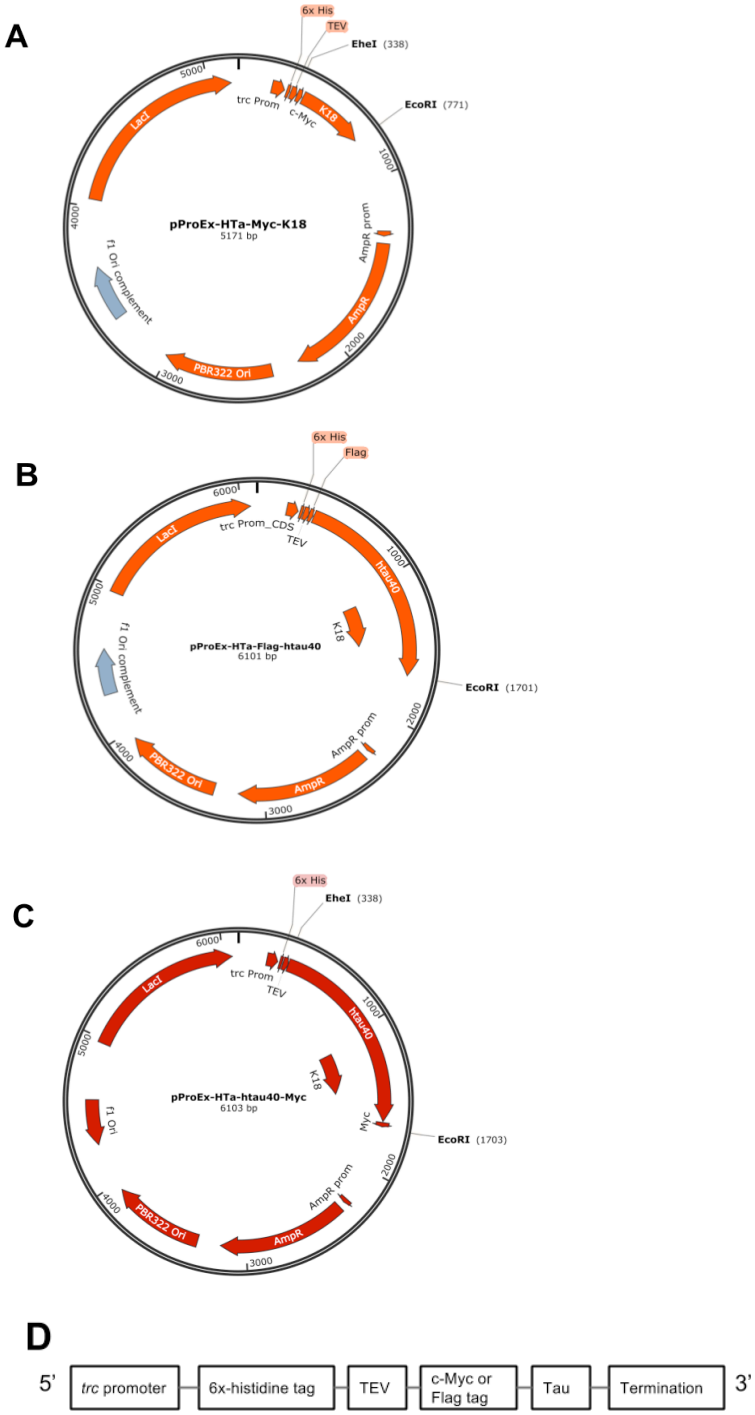

Figure 2.1. Bacterial expression plasmids used in this study.
(A-C) The pProEx-HTa-Myc-K18, pProEx-HTa-Flag-htau40 and pProEx-HTa-htau40-Myc plasmids for expressing the K18 and htau40 proteins. (D) Essential elements common to all the plasmids are shown, including a trc promoter, a hexa-histidine tag, a TEV cleavage site and a c-Myc or Flag tag followed by the tau coding sequence (note that for the plasmid in (C), the tau gene precedes the c-Myc tag).

2.3 SDM

The Q5® SDM kit was utilised to create the N279K, V337M, P301L and C291R mutations in the WT tau constructs, according to the manufacturer's instructions, using primers listed in Table 2.1 (designed using the NEBaseChanger™ programme http://nebasechanger.neb.com, version 1.2.3).

Table 2.1. Primers used in SDM to generate FTD variants of tau.
Codon changes are underlined.

Primer	Sequence (5' to 3')
N279K _Forward	GCAGATAATTAAAAAGAAGCTGGATCTT
N279K_Reverse	ACCTTCCCGCCTCCCGGC
V337M_Forward	AGGTGGCCAGATGGAAGTAAAATC
V337M_Reverse	CCTGGTTTATGATGGATGTTG
P301L_Forward	CAAACACGTCCTGGGAGGCGGCA
P301L_Reverse	ATATTATCCTTTGAGCCACACTTGGACTGG
C291R_Forward	CCAGTCCAAGCGTGGCTCAAAGG
C291R_Reverse	ACGTTGCTAAGATCCAGC

DNA samples (20 ng/µl) were exponentially amplified in the presence of 1X Q5 Hot Start 2X High Fidelity Mastermix and 0.5 µM each of the forward and reverse primers as indicated in Table 2.2. PCR was performed in an Eppendorf Mastercycler Gradient thermal cycler according to the following protocol:

i. Initial denaturation: 98 ^{o}C, 30 s
ii. Denaturation: 98 ^{o}C, 10 s
iii. Primer annealing: Ta* ^{o}C, 30 s
iv. Elongation: 72 ^{o}C, 2.5 min for K18 and 3 min for htau40
v. Final extension: 72 ^{o}C, 2 min
vi. Repeat steps ii – v for 24 times
vii. Hold at 4 ^{o}C

*Primer annealing temperatures varied for the different primer pairs: 72 ^{o}C for N279K, 62 ^{o}C for V337M, 72 ^{o}C for P301L and 63 ^{o}C for C291R.

Subsequently, 1 µl of the PCR product was treated with 1X final concentration each of the Kinase, Ligase and DpnI reaction buffer and enzyme mix and kept at room temperature (RT) for 5 min. Following the mutagenesis, 5 µl plasmid DNA was transformed into 50 µl competent NEB-5α *Escherichia coli* cells (a DH5α

derivative; genotype = *fhuA2 Δ(argF-lacZ)U169 phoA glnV44 Φ80 Δ(lacZ)M15 gyrA96 recA1 relA1 endA1 thi-1 hsdR17)*, incubated on ice for 30 min, heat shocked at 42 ^{o}C for 30 s, incubated on ice for a further 5 min, and 950 µl super optimal broth with catabolite repressor added and shaken at 37 ^{o}C for 1 h before overnight growth in Luria-Bertani (LB) broth containing 100 µg/ml ampicillin in a shaking incubator with agitation (180 rpm) at 37 ^{0}C. Plasmid DNA was isolated using the QIAprep Spin Miniprep kit according to the manufacturer's instructions.

Table 2.2. Details of PCR settings used in SDM to create FTD tau variants.

Constituent	**25 µl mix**	
	Volume (µl)	**Final concentration**
2X Q5 Hot Start 2X High Fidelity Mastermix	12.5	1X
10 µM forward primer	1.25	0.5 µM
10 µM reverse primer	1.25	0.5 µM
Template DNA 20 ng/µl	1	20 ng
Nuclease-free water	9	-

Next, the SDM process described above was utilised to modify the native cysteine residues in the tau protein constructs to alanine (C291A and C322A) and introduce a new cysteine at amino acid position 260 (I260C). Primers used in this process are provided in Table 2.3, and the annealing temperatures were: 60 ^{o}C for C291A, 61 ^{o}C for C322A and 58 ^{o}C for I260C.

The presence of the desired mutations was confirmed by DNA sequencing as described previously, using the primers listed in Table 2.4, following which plasmid DNA was transformed into BL21(DE3)*pRosetta *E. coli* cells, plated overnight on selective LB agar plates. Single colonies were then grown overnight in selective LB agar, and aliquots stored at -80 ^{o}C in 40 % glycerol until use. Primers were designed with Clone Manager Professional (Scientific and Educational Software, Denver, Colorado, USA) and synthesised by Integrated DNA Technologies (Leuven, Belgium).

Table 2.3 Primers used in SDM to introduce cysteine modifications in the WT tau constructs.
Codon changes are underlined.

Primer	Sequence (5' to 3')
C291A_Forward	CCAGTCCAAGGCTGGCTCAAAGGATAATATC
C291A_Reverse	ACGTTGCTAAGATCCAGC
C322A_Forward	GACCTCCAAGGCTGGCTCATTAGGCAAC
C322A_Reverse	ACCTTGCTCAGGTCAACTG
I260C_Forward	CAAGTCCAAGTGTGGCTCCACTGAGAACC
I260C_Reverse	ACATTCTTCAGGTCTGGC

Table 2.4. DNA sequencing primers designed and used in this study.

Tau construct	Primer	Sequence (5' to 3')
K18	Sequencing primer 1	ACAGACCATGTCGTACTACC
	Sequencing primer 2	AGGCGGCAGTGTGCAAATAG
Flag-htau40	Sequencing primer 1	GTGGCTCATTAGGCAACATC
	Sequencing primer 2	CAACGCCACCAGGATTCCAG
	Sequencing primer 3	CACGGCATCTCAGCAATGTC
htau40-myc	Sequencing primer 1	CAACGCCACCAGGATTCCAG
	Sequencing primer 2	TGGCTCATTAGGCAACATCC
	Sequencing primer 3	CACGGCATCTCAGCAATGTC

2.4 Transformation of *E. coli* BL21*(DE3) cells with tau-encoding plasmids

Five nanograms of plasmid DNA was added to 50 µl competent BL21(DE3)*pRosetta cells and incubated on ice for 30 min. Cells were heat-shocked at 42 ^{o}C for 30 s in a Clifton unstirred water bath, followed by 2 min incubation on ice. 950 µl LB broth was added and the mixture incubated at 37 ^{o}C for 1 h. Forty microlitres of the mixture was plated on LB agar supplemented with ampicillin (100 µg/ml) and chloramphenicol (35 µg/ml) and incubated overnight at 37 ^{o}C.

Genotype of BL21(DE3) = *fhuA2 [lon] ompT gal (λ DE3) [dcm] ΔhsdS*
λ DE3 = λ sBamHIo ΔEcoRI-B int::(lacI::PlacUV5::T7 gene1) i21 Δnin5

2.5 Expression of tau proteins

Single colonies of BL21(DE3)*pRosetta cells expressing specific tau proteins were inoculated into 10 ml selective LB broth and grown overnight at 37 ^{o}C. The following morning, 1 ml of the overnight culture was inoculated into 50 ml selective LB broth and grown at 37 ^{o}C with 180 rpm agitation. Cultures were

grown until reaching OD_{600} = 0.6 – 0.7, induced with 0.5 mM IPTG and grown for a further 3 h. Aliquots (1.5 ml) were centrifuged at ~ 11,000 xg for 1 min, the pellet re-suspended in 100 µl phosphate buffered saline (PBS) and sonicated for 5 s at 10 % power and re-centrifuged at ~11,000 xg for 5 min. All sonication was done in a Bandelin Sonopuls 2070 sonicator. The soluble (supernatant) fraction was pipetted into an Eppendorf tube for gel electrophoresis. The pellet was re-suspended in 500 µl PBS, sonicated (10% power, 5 s) and centrifuged (~11,000 xg for 5 min). The resultant pellet was re-suspended in 150 µl PBS, producing the insoluble fraction. Tau expression in the soluble and insoluble fractions was analysed by SDS-PAGE and Western blotting (WB) as described below.

2.6 SDS-PAGE and WB

Protein samples were separated on precast 4-20 % NuSep Tris-glycine gels or standard handcast 15 % Tris-glycine gels with (reducing gels) or without (non-reducing gels) β-mercaptoethanol and 5 min heating at 95 ^{o}C (gel and buffer preparation protocols in Table 2.5). Samples were analysed against protein ladder (#P7712 or #P7712S from New England BioLabs, size range = 11 – 245 kDa, or Precision Plus standard (#161-0374 from Biorad; size range = 10 – 250 kDa) for 35 min at 200 V in a Biorad Mini-PROTEAN Tetra system (BioRad Laboratories, California, USA) and stained with Instant Blue (Coomassie-based stain from Expedeon, Cambridge, UK) for 1 h at RT with no washing steps required and imaged using a SynGene G-Box imaging system. MagicMark^{TM} XP Western standard (#LC5602, Invitrogen) was used as a loading marker for WB. To identify tau-positive bands, WB was performed prior to antibody detection as described below.

Gels were transferred overnight at 4 ^{o}C or 2 hr at RT onto Amersham Hybond electrochemiluminescence nitrocellulose membrane and blocked for 15 min (in 5 % w/v non-fat dried milk in TBS-Tween) prior to 2 h incubation with the primary antibody. Unbound antibody was removed by 5 x 5 min washes with 10 % TBS-Tween in ddH_2O before 2 h incubation at RT with the secondary antibody and the membrane washed as previously. Antibodies used are indicated in Table 2.6. Antibody detection was performed using the Amersham

electrochemiluminescence detection reagents according to the manufacturer's instruction and bands visualised by exposure to X-ray film (Fuji Medical X-ray Film Super RX or CL-XPosure Film) and developed in an AGFA Curix 60 processor (Agfa Healthcare, Greenville, SC, USA). On a few occasions, WB detection was performed using the ImageQuant™ LAS4000 biomolecular imaging system (GE Healthcare). Densitometry analysis of protein bands was performed using ImageJ (Schneider et al., 2012), and statistically analysed with Prism 6 (GraphPad Inc., CA, USA) at the 5 % significance level.

Table 2.5. Preparation of hand-cast gels and buffers for SDS-PAGE and WB

Solution	Recipe
Loading buffer (2X Laemmli buffer)	25 mM Tris HCl pH 6.8, 25 % v/v glycerol, 2 % SDS, 0.01 % w/v bromophenol blue. Diluent = ddH_2O. For reducing gels, β-mercaptoethanol was added to 5 % final concentration in loading buffer aliquots.
Running buffer (10X)	25 mM Tris, 190 mM glycine, 0.1 % SDS.
Transfer buffer	25 mM Tris, 190 mM glycine, 20 % methanol.
15 % protein gel	Resolving gel: 50 % acrylamide/bisacrylamide, 390 mM Tris HCl pH 8.8, 0.1 % SDS, 0.1 % ammonium persulfate, 0.01 % TEMED. Stacking gel: 125 mM Tris HCl pH 6.8, 0.1 % SDS, 13.4 % acrylamide/bisacrylamide, 0.1 % ammonium persulfate, 0.1 % TEMED

2.7 Large-scale expression of tau constructs

Large cultures were produced by inoculating 500 ml selective LB broth with 10 ml overnight cultures using the expression parameters described above. Cultures were subsequently centrifuged at 4 ^{o}C for 10 min at 9800 xg. The resulting pellet was resuspended in 50 mM Na_2PO_4 pH 7.5 and frozen until use. Prior to purification, the lysate was boiled at 70 ^{o}C for 10 min to thaw, and protease inhibitor cocktail (1 tablet/~ 50 ml lysate), DNAse I and 5 ml of 1X BugBuster® protein extraction reagent added. The mixture was left to stand at RT for 1 h, sonicated at 70 % power for 1 min and centrifuged at 4 ^{o}C for 30 min at 48,000 xg. The supernatant containing the soluble fraction (crude extract) was decanted, filtered through a 0.2 μm filter and purified as below.

Table 2.6. Primary and secondary antibodies used in this study.

Antibody	Epitope	Host species	Vendor	Dilution
Polyclonal rabbit anti-human tau (#A0024)	C-terminus (amino acids 243 – 441) of the four-repeat isoforms of tau	Rabbit	Dako	1:1000 or 1:5000
Goat anti-rabbit IgG (#31460)	-	Goat	Thermo Scientific	1:1000 or 1:5000
Anti-His antibody (#27-4710-01)	6xHis tag	Mouse	GE Healthcare	1:2500
Rabbit anti-mouse IgG (#31450)	-	Rabbit	Thermofisher	1:5000
T22 oligomeric tau antibody (#ABN454)	Tau MT binding domain	Rabbit	Merck	1:1000
Anti-c-Myc (#C3956-100UG)	The Myc oncogene	Rabbit	Thermo Scientific	1:1000
HT7 anti-human tau (#MN1000)	Amino acid sequence ^{159}PPGQK^{163} of full length human tau 2N4R	Mouse	Thermo Scientific	1:100
Alexa Fluor® 594-cojugated AffiniPure goat anti-mouse	-	Goat	Jackson ImmunoResearch	1:100
Alexa Fluor® 647-conjugated anti-nucleolin (#ab198580)	Human nucleolin	Mouse	Abcam	1:500

2.8 Tau protein purification by immobilised metal affinity chromatography (IMAC)

Ni-NTA column (Econo-Pac, Biorad) was used for protein purification. Chelating sepharose resin was charged with 10 mM $NiCl_2$/CH_3COONa pH 4.0 and equilibrated with buffer A (50 mM Na_2PO_4 pH 7.0, 500 mM NaCl, 10 mM imidazole) before addition of the crude extract. The column was re-washed with buffer A, followed by buffer B (50 mM Na_2PO_4 pH 7.0, 500 mM NaCl, 25 mM imidazole) and the protein eluted with buffer C (50 mM Na_2PO_4 pH 7.0, 500 mM

NaCl, 500 mM imidazole) followed by overnight dialysis in the presence of 25 µg/ml TEV protease, against dialysis buffer (50 mM Tris HCl pH 7.5, 100 mM NaCl) to cleave the polyhistidine-TEV tag. The dialysed tau was re-purified to isolate the TEV protease-cleaved tau. Briefly, the column was equilibrated with buffer A, the cleaved protein collected as the flow-through upon elution and concentrated using Vivaspin 20 (Sartorius; 5 kDa and 10 kDa cut off for K18 and htau40 respectively) where necessary. At each step of the purification process, aliquots were taken for SDS-PAGE and WB analysis. Protein concentration and purity were estimated using the Bicinchoninic acid (BCA) assay and SDS-PAGE respectively.

2.9 Expression and purification of TEV protease

A maltose binding protein-His-TEV protease construct (kind gift of Dr. Deborah Brotherton, University of Warwick) was expressed, purified and used to cleave the polyhistidine tag on the tau proteins constructs where necessary. The MBP-His-TEV construct transformed into BL21(DE3)plus (for rare Arginine tRNA) was grown in LB broth containing 100 µg/ml carbenicllin until reaching OD_{600} = 0.6, induced with 0.4 mM IPTG and grown at 25 ^{o}C overnight. Cells were harvested by centrifugation at 9800 xg, 4 ^{o}C for 10 min and re-suspended in cell resuspension buffer (PBS, 0.3 M NaCl) at the ratio of 5 ml buffer to 1 g wet cell weight. Thereafter, the cells were lysed by 30 min boiling at 100 ^{o}C and sonication (1 min, 70 % power), and centrifuged at 150,000 xg for 30 min, 4 ^{o}C. Final concentration of 20 mM imidazole was added to the supernatant (after 0.2 µm filtering) and purified with a Ni-NTA column pre-equilibrated with purification buffer (20 mM Tris-HCl pH 7.5, 0.3 M NaCl, 3 mM dithiothreitol (DTT), 20 % glycerol) +20 mM imidazole. The washing step was done with purification buffer containing 50 mM imidazole for 20 column volumes and the purified protein eluted with purification buffer + 250 mM imidazole and dialysed overnight against 3 l of dialysis buffer (20 mM Tris-HCl pH 7.5, 0.3 M NaCl, 5 mM DTT, 30 % glycerol) at 4 ^{o}C. On the next day, the dialysed sample was further purified on a column pre-equilibrated with dialysis buffer with 20 mM imidazole and purified same as on the previous day. The eluted protein was stored at -80 ^{o}C in storage buffer (20 mM Tris-HCl pH 7.5, 0.3 M NaCl, 5 mM DTT, 50 % glycerol) with 60 % glycerol.

2.10 Protein quantification using the BCA assay

The concentrations of purified proteins were estimated using the BCA colorimetric assay (G-Biosciences, Missouri, USA). First, a linear plot was generated by monitoring the 562 nm absorbance of serial dilutions of manufacturer-provided bovine serum albumin (BSA) as the standard protein. Nine 1:2 serial dilutions of a stock 2 mg/ml BSA were prepared, thoroughly mixed and 50 µl aliquots added to 1 ml working solution (10 ml BCA reagent + 200 µl copper solution). The absorbance of each mixture was measured with an Ultrospec 2100 spectrophotometer after 30 min incubation at 37 ^{o}C. To identify the absolute protein concentration per dilution, the absorbance value for the working solution alone (the last tube in the dilution series with no protein present) was deducted from all collected absorbance values. The normalised absorbance readings were subsequently plotted against protein concentration to generate a standard curve (Fig. 2.2), which was used to estimate the concentration of purified proteins used in this work.

Concentrations in mg/ml were converted to molarity using each protein's molar mass calculated from Expasy (http://web.expasy.org/compute_pi/). For example, 1 mg/ml of purified His-tagged K18 equals 55 µM whilst 1 mg/ml of the untagged K18 is 66 µM. Indicated concentrations of tau proteins throughout this thesis refer to monomer equivalents.

2.11 Preparation of Alzheimer-like PHFs

Experiments shown in Chapter 4 (characterisation of purified tau): a method adapted from (Barghorn et al., 2005) was used. Briefly, 200 µl reaction mixtures containing 12 µM monomeric tau, 10 mM Na_2PO_4 pH 7.4, 50 mM ammonium acetate, 1 mM DTT and 6 µM heparin (MW 6000) were prepared and incubated at 37 °C for 7 days to promote filament formation.

Influence of disease mutations on tau aggregation (Chapter 6): 0.7 mg/ml (38.5 µM) of freshly-purified tau K18 or its pathologic variants were mixed with 0.75

mg/ml (125 µM) heparin and incubated for 4 days or 45 days at 37 °C before negative-stain transmission electron microscopy (TEM) analysis.

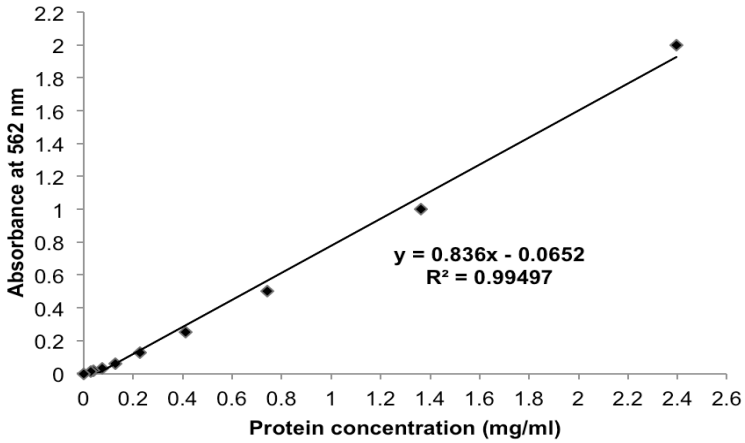

Figure 2.2. BCA assay standard plot for estimating protein concentration. *Manufacturer-supplied BSA was used to generate this standard plot for estimating the concentrations of purified tau proteins.*

2.12 CD spectroscopy

Chapter 4: following dialysis of the purified tau protein in Thermo Scientific™ Slide-A-Lyzer™ MINI Dialysis Device (10K MWCO) in excess of 10 mM Na_2PO_4 pH 7.4 buffer as per the manufacturer's instructions, 10 µM samples were diluted in the same buffer and CD spectra collected using a Jasco J-815 CD spectropolarimeter in a 1 mm path length cell. The response time was 1 s with a data pitch of 0.1 nm and the scan speed was 100 nm/min. 32 spectra accumulations were obtained for each sample at wavelengths ranging from 190 nm to 280 nm and averaged. The high-tension voltage was ≤ 550 V throughout.

PHF samples were centrifuged at 100,000 xg for 1 h at 4 °C, supernatant removed and the pellet re-suspended in 200 µl of 10 mM Na_2PO_4 pH 7.4. CD analysis on PHF samples was conducted as described above. Secondary structure elements were estimated using the DichroWeb Contin-LL (Provencher and Glockner method) reference dataset 4 (Sreerama and Woody, 2000; Whitmore and Wallace, 2008, 2004).

CD assays on tau oligomers (Chapter 6): readings were taken on 0.1 mg/ml (5.5 µM) of RT overnight-incubated samples using the above-stated conditions. For

each CD assay, three independent experiments using different batches of protein preparations were conducted.

2.13 ThT kinetic assay of tau aggregation

Freshly-prepared samples were diluted to 0.2 mg/ml (11 μM) in 10 mM Na_2PO_4 pH 7.4 and seeded at 100 μl per well (heparin-free aggregation studies) in 96-well plates (Greiner Bio-One #655077). In heparin-induced aggregation studies, 10 μl each of ThT (20 μM final concentration) and heparin (0.15 mg/ml = 25 μM final concentration) were added to 80 μl tau 0.16 mg/ml (8.85 μM; final concentration) per well of a FLUOTRAC™ 96-well plate (Greiner Bio-One #655077). Tau aggregation was monitored for up to 40 h by measuring ThT fluorescence at 440 nm excitation and 510 nm emission in a CLARIOstar microplate reader (BMG Lab Tech). Sensitivity was set to 20 % to prevent signal saturation. Fluorescence readings were taken with the top optic setting every 5 min after 200 rpm shaking for 30 s. Data analysis was done with Prism 7 (GraphPad Inc.).

2.14 TEM analysis of tau filament formation

Formvar/carbon-coated 300-mesh copper grids (Agar scientific, UK, #S162) were glow-discharged and 5 μl of sample preparations (samples in Chapter 4 were diluted 1:2) pipetted onto the grid and allowed to bind for 1 min. Excess sample was removed and 5 μl of 2% uranyl acetate added for 1 min and excess removed. The grids were imaged using a JEOL-2100F transmission electron microscope.

2.15 Dot blot assay of tau aggregation

Dot blotting without heparin (Chapter 6): freshly-purified tau proteins at 1 mg/ml (55 μM) were incubated in standard PCR tubes and heated at 37 ^{o}C to promote aggregation in quiescent conditions. Unless otherwise stated, all incubation was done in an Eppendorf Mastercycler gradient thermocycler. Aliquots taken at each time point were immediately snap-frozen and kept at -80 ^{o}C until use. Samples were diluted to 0.5 mg/ml with 10 mM Na_2PO_4 pH 7.4 before dot blotting.

Dot blotting for oligomers prepared by overnight incubation of monomers at RT (Chapter 6): Freshly-prepared tau proteins (0.1 mg/ml; 5.5 μM) were incubated at

RT overnight (~ 15 h), and used immediately for dot blot and CD or snap-frozen and kept at -80 ^{o}C until use.

Dot blotting for Alexa Fluor®-488-maleimide (AF-maleimide) and N-ethylmaleimide (NEM) labelled tau proteins (Chapter 5): The labelled and unlabelled control samples (prepared as in section 2.18 below) were each mixed with 0.75 mg/ml (125 μM) heparin, incubated at 37 ^{o}C for 48 h and aliquots taken and snap-frozen for dot blotting. Samples were diluted in half before dot blotting.

Two microlitres of the tau samples collected at the given time points were spotted onto a nitrocellulose membrane, air dried, blocked with 10 % non-fat milk in PBS overnight at 4 °C overnight or 30 min at RT, and washed five times with 10 % TBS-Tween. The nitrocellulose membrane was incubated at RT for 2 h in the primary antibody (total tau antibody #A0024 or oligomeric antibody #T22; Table 2.6), washed five times with 10 % TBS containing 0.05% Tween-20, and incubated with the secondary antibody (horse radish peroxidase-conjugated anti-rabbit IgG; Table 2.6) for a further 2 h at RT. Thereafter, the nitrocellulose paper was washed five times as previously, developed with the ECL chemiluminiscent kit, and imaged.

2.16 AFM analysis of tau aggregation

ThT end-point samples: As a complementary method to ThT analysis of tau aggregation, aliquots of tau samples after the ThT assay were taken, snap-frozen and examined by AFM.

Time-dependent aggregation of tau: to closely monitor the structural transformation of tau during aggregation, 0.7 mg/ml (38.5 μM) tau was mixed with 0.75 mg/ml (125 μM) heparin and incubated at 37 ^{o}C. Samples were taken at the indicated time points, snap-frozen and stored at -80 ^{o}C until use.

For AFM analysis, tau protein samples were adsorbed onto freshly-cleaved mica surface (Agar Scientific, #G250-3) for 15 min and unbound protein removed by washing with excess ddH_2O. Random positions on the mica surface were chosen for the collection of 1 μm^2 height images using a cantilever. The scan rate was 0.5

– 2.0 Hz, in AC Air Topography mode using an MFP3D AFM (Asylum Research, UK). Data processing was done using the "Flatten" function of the Igor Pro 6.37 software. Sample sizes were determined using Image J as previously described (Tepper et al., 2014).

2.17 Preparation of tau oligomers

Tau oligomers were prepared by diluting each given monomer sample to 0.1 mg/ml (5.5 μM) in 10 mM Na_2PO_4 pH 7.4 and incubating at RT overnight under quiescent conditions. Oligomerisation was confirmed by SDS-PAGE, WB, AFM or TEM.

2.18 AF-maleimide and NEM labelling of tau protein and the characterisation of labelled proteins

Optimisation of AF-maleimide labelling: Tau proteins were first labelled using two adapted protocols that differed in their pre-treatment with reducing agents. Following the method of Michel et al., (2014), protein samples were treated for 30 min at RT with 4X molar excess of TCEP whilst the protocol adapted from Bader et al., (2011) omitted this step. The tau proteins were treated with 4X molar excess of AF-maleimide in 10 mM Na_2PO_4 pH 7.4 or 1X BRB buffer (1 mM KCl, 80 mM PIPES, and 1 mM EGTA pH 6.8) and incubated in the dark at RT for 3 h. The reaction time was later extended to overnight to enable oligomerisation of the labelled monomers. Free fluorophore and TCEP were removed using NAP-5 chromatography column from GE Healthcare or by extensive dialysis against dialysis buffer (section 2.8) in the Thermo Scientific™ Slide-A-Lyzer™ MINI Dialysis Device (10K MWCO) perforated to increase buffer volume to about 2 l. Protein labelling and unbound fluorophore removal were confirmed with SDS PAGE. The concentration of labelled protein was routinely determined spectrophotometrically using Beer's law and molar extinction coefficient of 72000/cm/M for AF-maleimide.

Preparation of NEM-labelled tau oligomers: freshly-prepared tau (1 mg/ml) was treated with 5X molar excess of TCEP for 2 h. Subsequently, 5X molar excess of NEM was added and the reaction mix incubated at RT overnight. Oligomer formation was confirmed by dot blot and negative-stain TEM. In both cases of tau

labelling, unlabelled control samples were prepared identically except that equal volume of 10 mM Na_2PO_4 pH 7.4 was added in place of the maleimide label.

DLS: AF-maleimide labelled tau K18 oligomers at 1 mg/ml (55 µM) concentrations (100 µl) were aliquoted into a clean ZEN 040 cuvette, transferred into a Zetasizer Nano-series spectrometer (Malvern Instruments, UK) and equilibrated for 5 min at 20 ^{O}C. Eleven measurements were taken and analysed with the Zetasizer software to estimate the hydrodynamic radius of the protein.

2.19 Neuroblastoma cell culture

SH-SY5Y cells were purchased from Sigma Aldrich UK (#94030304) and maintained on 1:1 minimal essential medium (MEM)/F12 Ham medium containing 1 % L-Glutamine, 15 % foetal bovine serum, and 1 % antibiotic antimycotic acid. The cells were seeded at 200,000 cells/ml in CellView^{TM} Advanced Tissue Culture dishes (Greiner Bio-One, #627975) in the presence of 100 nM – 10 µM AF-maleimide labelled tau oligomers dissolved in the culture medium, and incubated for 24 h at 37 ^{o}C, 5 % CO_2. Thereafter, the extracellular medium was removed, the cells washed with PBS and fresh tau-free medium containing 2 µM nuclear marker Hoechst and 1:1000 dilution of the plasma membrane marker Deep Red, both added 30 min before confocal microscopy. Cells between passages two and ten were used for all experiments.

2.20 Differentiated neuroblastoma cell culture

Tissue culture plates were treated with 0.01 % poly-l-ornithine followed by 5 µg/ml laminin, and washed with PBS. Cells were seeded at same density as above in MEM-FI2 medium supplemented with 10 µg/ml retinoic acid and grown for 5 days. The media was changed to serum-free MEM-FI2 supplemented with 10 µg/ml retinoic acid and 25 ng/ml brain derived neurotrophic factor, and the differentiated cells used within 10 days.

2.21 Human induced pluripotent stem cell (hiPSC)-derived cerebral cortical neural stem cells

Neural precursors (differentiated by the supplier following a 21-day protocol) obtained from cord blood CD34+ cells of a healthy, newborn female donor were purchased from Axol Bioscience (#ax0016, Cambridge, UK). Tissue culture grade 12-well plates (Corning, USA) were each pre-coated with 250 µl/cm^2 ReadySet reagent (Axol) and incubated at 37 ^{o}C, 5 % CO_2 for 45 min and rinsed four times with ddH_2O. Thereafter, Surebond reagent (Axol) was diluted in Dulbecco's PBS (DPBS) and used at 200 µl/cm^2 and incubated at 37 ^{o}C, 5 % CO_2 to equilibrate for 1 h. Next, stem cells were seeded at 25,000 cells/cm^2 on plasma-cleaned 13 mm glass coverslips, incubated at 37 C ^{o}C, 5 % CO_2 and media changed every other day with Axol Neural Maintenance Medium kit (ax0031 a&b). Neuronal differentiation was monitored using phase contrast images obtained periodically with an EVOS XL Core Imaging System (Life Technologies). Neurons were used for experiments after 14 – 16 days *in vitro*. WT and FTD tau K18 oligomers were diluted to 5 µM in Legacy medium and added to neurons and incubated at 37 C ^{o}C, 5 % CO_2 for 24 h or 48 h, after which the spent medium was carefully removed, neurons washed with DPBS, and new tau-free medium added.

2.22 Immunohistochemistry

SH-SY5Y live cell assays: cells were treated with the appropriate antibodies (Table 2.6) or dyes and imaged without fixing. In examining the mechanism of tau internalisation, the FM4-64 endocytic marker was added to tau-free medium containing Hoechst and transferred to cells after PBS wash as described above. Confocal microscopy imaging was performed following 30 min incubation at 37 ^{o}C, 5 % CO_2. The nucleolin colocalisation test was conducted similarly using a conjugated anti human nucleolin antibody (Table 2.6) and imaged after 2 h incubation. For endogenous tau colocalisation, the HT7 antibody recognising the ^{159}PPGQK^{163} motif of full length tau but falls outside the K18 domain was added to tau-treated cultures at 22 h of incubation. The spent medium containing the HT7 antibody was removed at 24 h, washed with PBS, and new tau-free medium

with Hoechst and the Alexa Fluor® 594-cojugated AffiniPure secondary antibody. Cells were imaged after 2 h incubation. Antibody dilutions are given in Table 2.6.

hiPSC fixed tissue assays: Spent medium was removed and neurons washed with PBS after 24 h or 48 h of seeding with 5 µM tau. Neurons were then fixed with 4 % paraformaldehyde for 30 min, washed twice with DPBS and rinsed with permeabilising solution (0.2 % Triton in DPBS). Afterwards, the fixed neurons were incubated in blocking buffer (DPBS containing 0.2 % Triton and 2 % BSA) for 1 h and then primary antibody with Hoechst for another 1 h. Excess primary antibody was removed by washing thrice with blocking buffer only for 5 min each time, followed by secondary antibody incubation for 1 h and a repeat of the blocking buffer wash steps. Both antibodies were diluted in the blocking buffer. Next, the slides were rinsed with distilled water and dropped into ProLong Gold antifade mounting medium (#P36934, ThermoFisher Scientific). Neurons were observed by confocal microscopy imaging at least 24 h after curing.

2.23 Confocal microscopy

Live neuroblastoma cell imaging: 12-bit images were obtained at RT using a C-Apochromat 63x/1.20 W Korr M27 water immersion objective lens on an LSM 710 confocal microscope (Leica). hiPSC neurons were imaged using a Leica STP 6000 microscope. Images were analysed with Image J. Internalisation data were analysed as shown in the Appendix, and expressed as integrated density (area x mean fluorescent intensity).

2.24 Lactate dehydrogenase (LDH) assay of tau oligomer toxicity

The Pierce LDH Cytotoxicity assay kit was used. SH-SY5Y neuroblastoma cells were seeded at 20,000 cells/well in Falcon 96-well plates and varying concentrations of tau oligomers added. Controls included spontaneous cytotoxicity (cells + 10 µl sterile water), media only (no cells) and maximum control (membrane lysed with a manufacturer-supplied reagent). The cells were incubated for 72 h at 37 ^{o}C 5 % CO_2. After 72 h, lysis buffer was added to the maximum control wells and the plates incubated for a further 45 min. Then, 50 µl

of the sample mix in each well was transferred to a new 96-well plate and 50 µl reaction mix added to each well and incubated at RT in the dark for 30 min. Stop solution (50 µl) was added and absorbance measured at 490 nm and 680 nm with a CLARIOstar microplate reader (BMG Lab Tech). The background readings at 680 nm were subtracted from corresponding 490 nm readings and LDH release measured using the following equation:

$$\% \text{ cytotoxicity} = \frac{\text{Tau-treated LDH activity} - \text{Spontaneous LDH activity}}{\text{Maximum LDH activity} - \text{Spontaneous LDH activity}} \times 100\ \%$$

2.25 Statistical analysis

Statistical analyses were conducted with Prism 6 or 7 (GraphPad Inc., CA, USA) at the 5 % significance level. Data sets were first tested for normality using the D'Agostino and Pearson test in Prism. If appropriate, parametric analyses were performed with the Student's t-test (two variables) or one-way ANOVA (three variables). Otherwise, non-parametric analyses were performed using the Mann Whitney test (two data variables) or Kruskal Wallis test followed by Dunn's multiple comparison test. All statistics data are expressed as mean ± standard deviation.

3| A plasmid library for expressing full-length and truncated tau proteins, and their pathologic and cysteine-modified variants

3.1 Introduction

Understanding the structural, biochemical and molecular basis of tau aggregation is essential for structure-activity studies and therapy development (Cisek et al., 2014). This however requires high-yield production of tau proteins in sustainable supply. Although it is feasible to isolate reasonable amounts of tau proteins from human brain tissues, this process has many disadvantages including: (i) the need for specialised purification equipment and expertise; (ii) unsustainable supply for research purposes due to the need to process several brain tissues; (iii) potential inconsistent properties of proteins obtained from patients of diverse disease aetiologies e.g. whether genetic or sporadic. For these reasons, recombinant approaches are often used to produce homogenous tau proteins in a renewable way. Recombinant and AD brain-derived tau aggregate through the same mechanism (i.e, shift of monomers from an unfolded state towards beta sheet structures) and form filaments of the same ultrastructural properties (Barghorn et al., 2004). When recombinant tau monomers are induced with AD brain-derived tau filaments, the former aggregates into PHF of identical structural properties as the AD tau, indicating shared structural properties between the two (Morozova et al., 2013). Consistent with these findings, PHF prepared from recombinant tau closely shares structural properties of AD tau (Barghorn et al., 2004). Hence, recombinant tau will be used throughout this thesis as a validated model for studying native tau.

This thesis aims to characterise the structural, conformational and aggregation properties of different disease-linked tau proteins and to apply the insights obtained to support investigations into how extracellular tau is internalised. As a starting point in this pursuit, it was essential to obtain plasmids expressing all the tau proteins of interest. It was however realised that no such comprehensive library of

tau-expressing plasmids existed, hence one was created. In this Chapter, the rational design of a large library of plasmids for expressing a variety of full-length and truncated tau proteins is described. This collection of ~50 unique molecular clones provides a vital resource for preparing a wide variety of tau proteins for *in vitro* and *in vivo* studies.

3.2 Results

3.2.1 Creation of a library of plasmids for expressing pathologic variants of tau

Four pathologic mutations in the *MAPT* gene identified in familial cases of tauopathies (Table 3.1) were created in the htau40 and K18 tau constructs (plasmid templates in Fig. 2.1) using SDM. Protein and amino acid sequence alignments confirmed induction of the V337M, N279K, P301L and C291R mutations in the WT tau constructs are shown in Fig. 3.1 – 3.3, with a schematic illustration of this process given in Fig. 3.4. In addition to plasmids for expressing Myc-tagged pathologic tau mutants, FLAG-tagged versions of the htau40 plasmids were created to provide flexibility in plasmid selection.

Table 3.1 Details of pathological mutations created in the htau40 isoform and the K18 fragment of tau.
Note that amino acids are numbered according to the full-length brain isoform of tau (htau40).

Amino acid change	DNA codon change
N279K	AAT to AAA
V337M	GTG to ATG
P301L	CCG to CTG
C291R	TGT to CGT

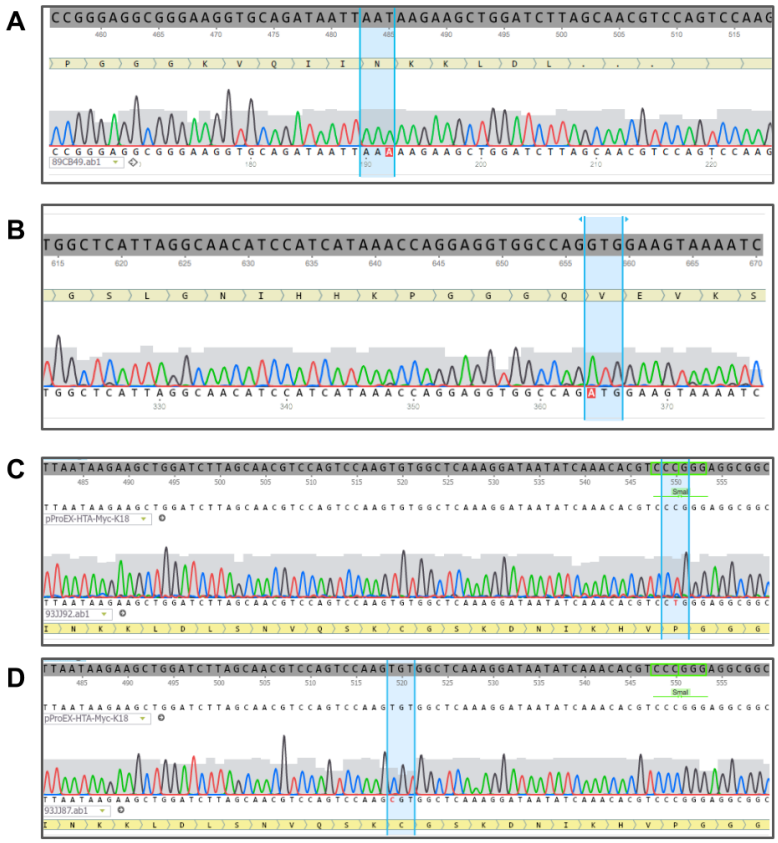

Figure 3.1. Clustal Omega sequence alignments confirming the creation of the FTD mutations N279K, V337M, P301L and C291R in the WT K18 tau construct.

(A), (B), (C), and (D) show sequence alignments demonstrating the N279K, V337M, P301L and C291R point mutations respectively. Mutation sites are highlighted in blue.

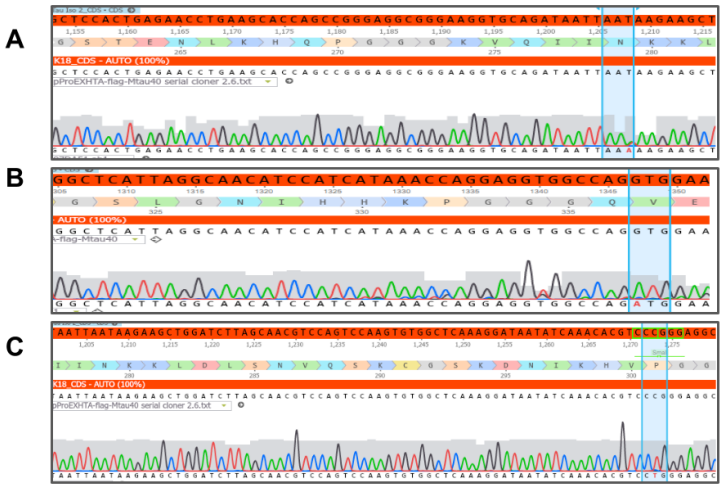

Figure 3.2. Clustal Omega sequence alignments confirming the creation of the N279K, V337M and P301L pathological mutations in the FLAG-tagged htau40 plasmid.

(A), (B) and (C) indicate the N279K, V337M and P301L mutations respectively.

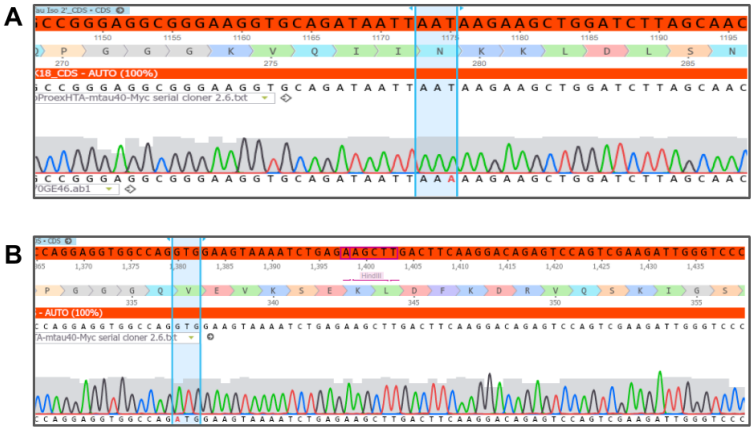

Figure 3.3. Clustal Omega sequence alignments confirming creation of the N279K and V337M mutations (A and B respectively) in the Myc-tagged htau40 plasmid.

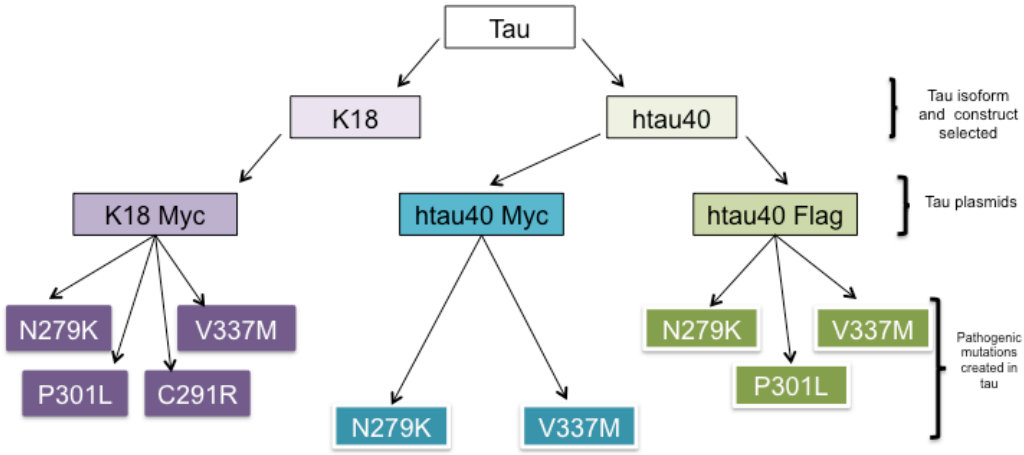

Figure 3.4. Schematic illustration of the creation of four disease-associated exonic mutations in the K18 and htau40 tau proteins.

3.2.2 Introduction of cysteine modifications into the tau proteins

A major aim of this thesis was to study the cellular internalisation of extracellular tau protein. In this regard, there was a need to use fluorescently labelled tau proteins to enable live tracking of their internalisation. A method of choice was to covalently label a single cysteine residue with a chemical fluorophore e.g., maleimide-conjugated Alexa Fluor® 488. However, the native full-length and truncated four-repeat tau proteins contain two cysteine residues, one each in the second and third repeat region. To complicate issues further, these cysteine residues are located in the protein's region believed to be required for MT binding and stabilisation (Lee

et al., 1989). To label a single cysteine residue outside of this region, the two native cysteine residues at amino acid positions 291 and C322 were modified to the nonpolar amino acid alanine and a new cysteine introduced at position 260, which is further away from the central core of the repeat region (Fig. 3.5). DNA codon changes made are shown in Table 3.2, and sequence alignments demonstrating these modifications are given in Figs. 3.6 – 3.16. For the K18-C291R construct, only two cysteine modifications (i.e., C322A and I260C) were induced due to the presence of a putative pathological mutation of unknown pathogenicity at position 291 (Marshall et al., 2015). This method of labelling tau for functional studies has previously been reported, and is believed to have no adverse effects on the protein's ability to form fibrils (Kumar et al., 2014; Michel et al., 2014; Shammas et al., 2015).

An alternative chemical labelling approach would be to directly label the two native cysteine residues without cysteine alterations, as done previously by Tepper et al., (2014). Obviously, this method would save time and avoid the potential risk of altering the protein's biochemical and structural characteristics through cysteine modification. However, the high tendency of double-cysteine tau proteins, especially the K18 truncation fragment, to form both intra- and inter-molecular disulphide bonds even in reducing conditions and at low temperatures (Barghorn and Mandelkow, 2002) presents the possible danger of "false positive labelling" i.e., not labelling cysteine residues locked up in disulphide bonding. Unfortunately, it would be difficult to remove such unlabelled proteins in post-labelling treatment steps, and may lead to irreproducible results due to the inability to quantify the contribution of unlabelled proteins to experimental outcomes.

Table 3.2. Codon changes made in the cysteine modifications induced in the tau proteins to enable chemical labelling with maleimide.
Note that these changes were made in all the tau protein constructs except the K18-C91R construct for which the C291A modification was omitted due to a pathogenic mutation at the same amino acid position.

Amino acid change	DNA codon change
C291A	TGT to GCT
C322A	TGT to GCT
I260C	ATC to TGT

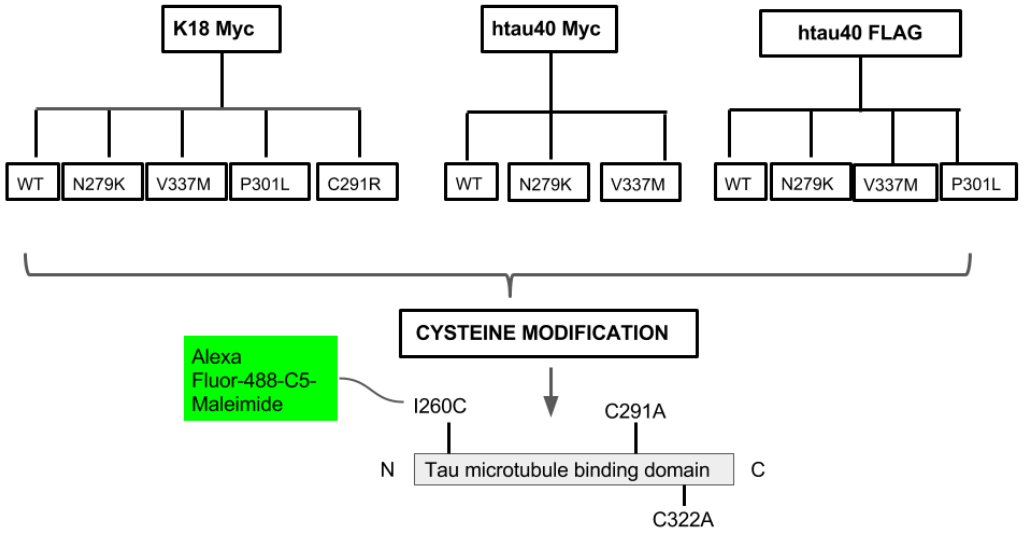

Figure 3.5. Schematic illustration of cysteine modifications induced in the tau protein-expression library hitherto created.
The DNA sequences that code for the native cysteine residues in each plasmid was modified to alanine (C291A and C322A), and a new cysteine residue introduced nearer to the N-terminus end of the MT binding domain (I260C; numbered according to the full-length tau) where it was believed not to affect tau-MT binding dynamics. The resultant plasmids will be later expressed, purified, and fluorescently labelled on the novel cysteine residue introduced at the amino acid position 260.

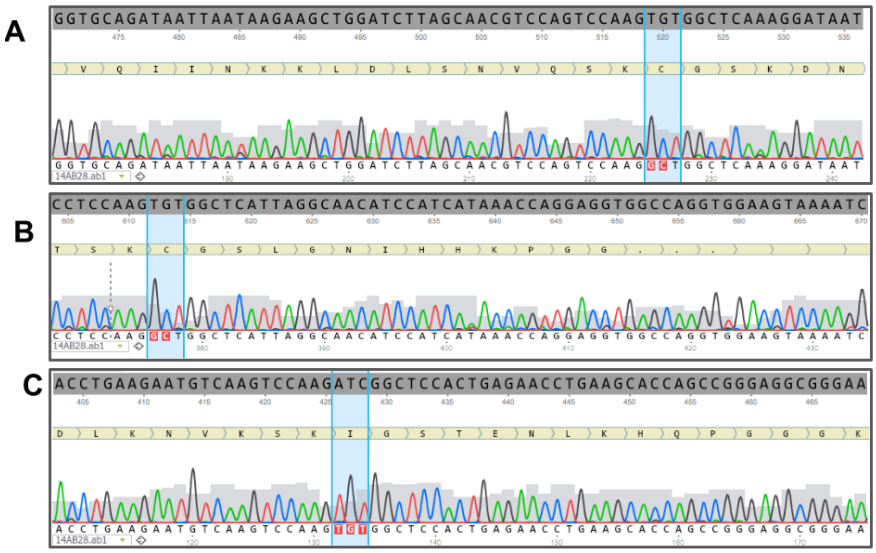

Figure 3.6. Cysteine modifications in the WT K18 sequence.
(A) and (B) refer to the modification of C291 and C322 to alanine. (C) shows the introduction of a novel cysteine residue to replace isoleucine at position 260. Nucleotide changes are highlighted in blue.

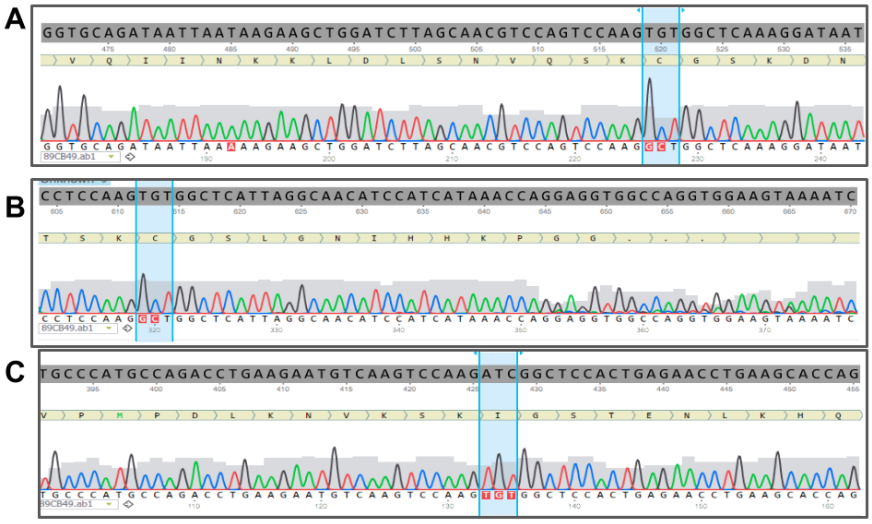

Figure 3.7. Evidence of cysteine modifications in the Myc-K18-N279K construct.

The modification of C291 and C322 to alanine is shown in (A) and (B) respectively. (C) shows the introduction of a new cysteine residue to replace isoleucine at position 260. Nucleotide changes are highlighted in blue.

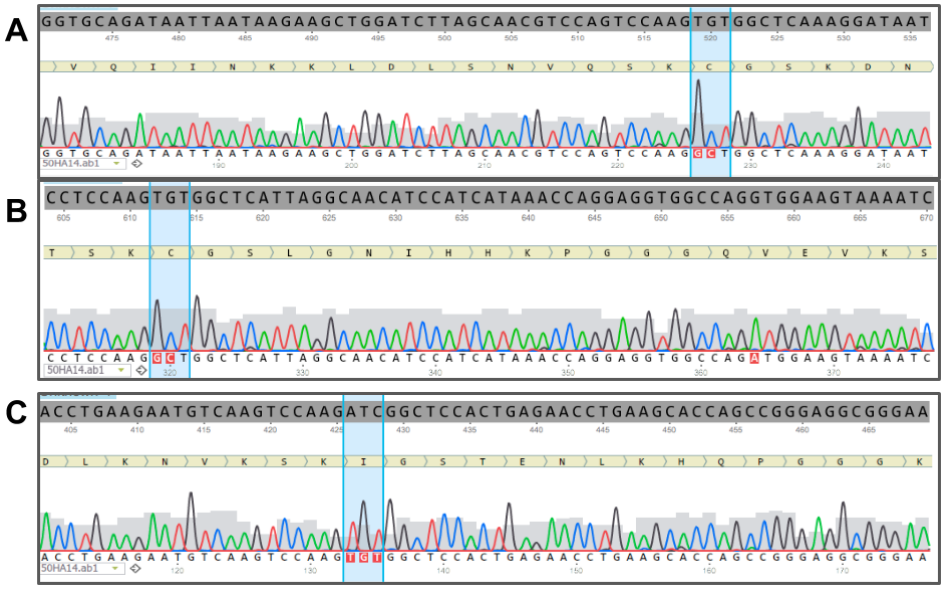

Figure 3.8. Modification of native cysteine residues in the Myc-K18-V337M construct.

(A), (B) and (C) show the generation of the C291A, C322A and I260C amino acid modifications respectively.

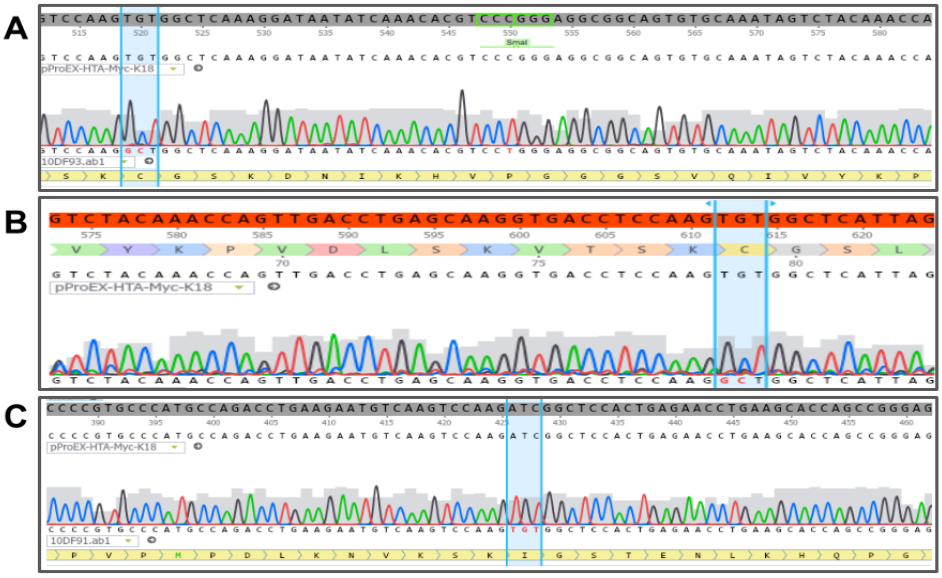

Figure 3.9. Evidence of native cysteine modification in the Myc-K18-P301L construct.

(A), (B) and (C) show the creation of the C291A, C322A and I260C amino acid modifications respectively.

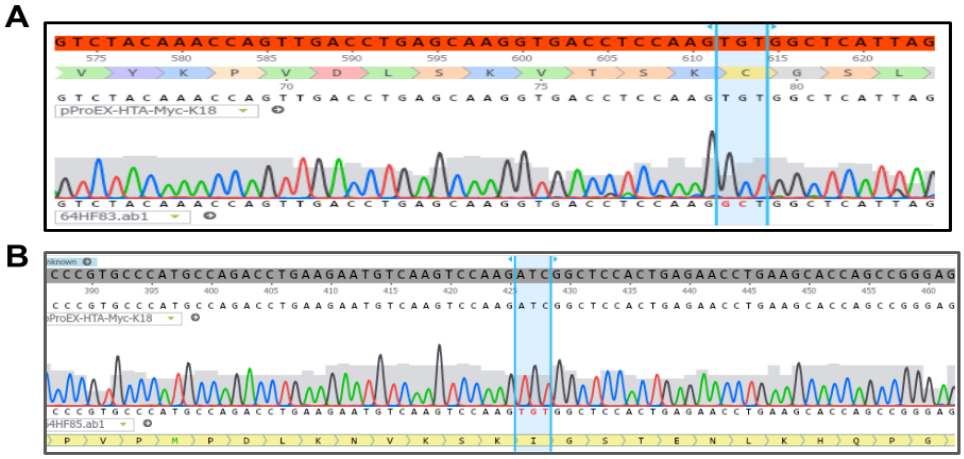

Figure 3.10. Modification of native cysteine residues in the Myc-K18-C291R construct.

(A) and (B) provide evidence of induction of the C322A and I260C amino acid modifications respectively. Note that the C291A cysteine modification was not induced for this construct due to the presence of the C291R disease-associated mutation at the same amino acid position.

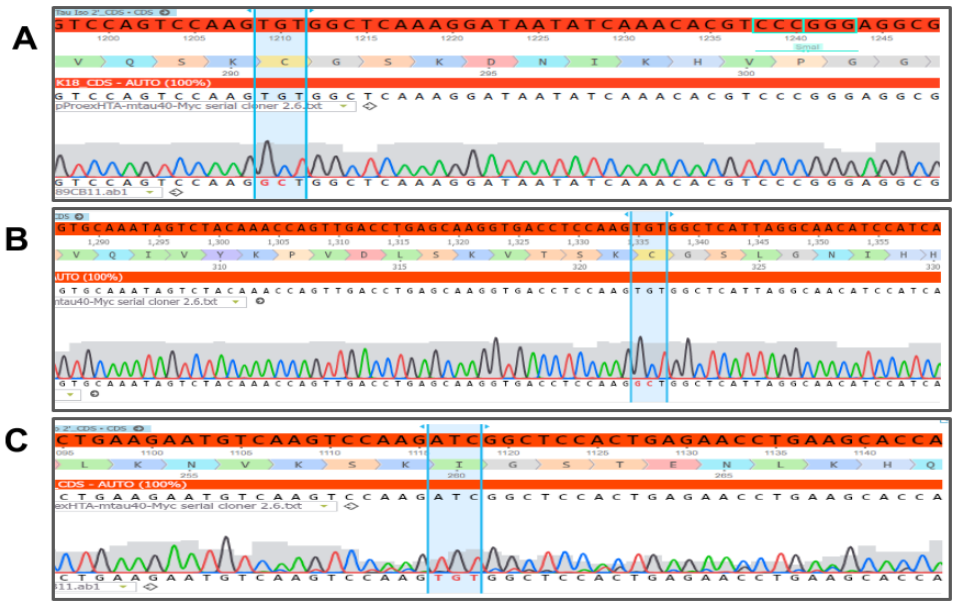

Figure 3.11. Modification of native cysteine residues in the WT Myc-htau40 construct.
The C291A, C322A and I260C amino acid changes are shown in (A), (B) and (C) respectively.

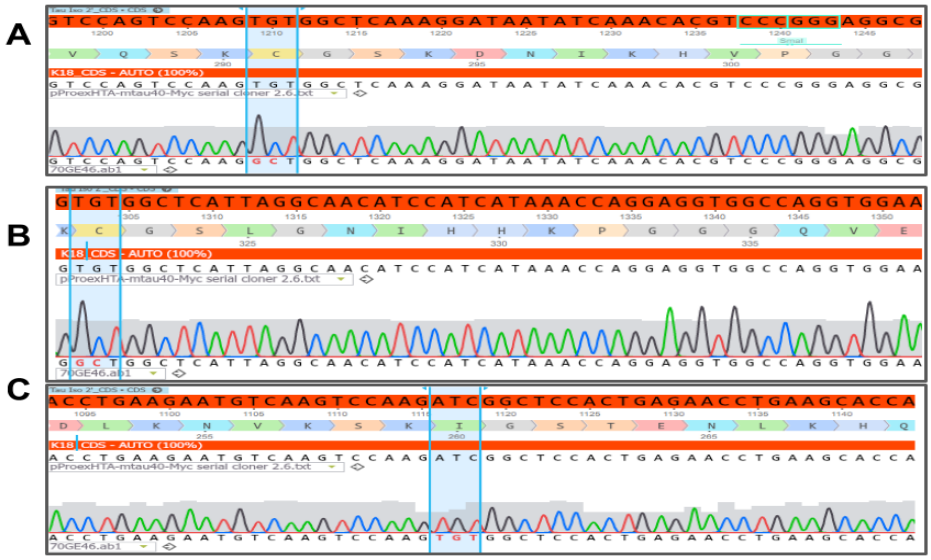

Figure 3.12. Native cysteine residue modification in the Myc-htau40-N279K construct.
The two cysteine residues in this tau construct at positions C291 and C322 were each modified to alanine, a nonpolar amino acid that does not confer an extra charge on the protein (shown in (A) and (B) respectively). (C) A new cysteine residue was introduced upstream, replacing isoleucine at position 260.

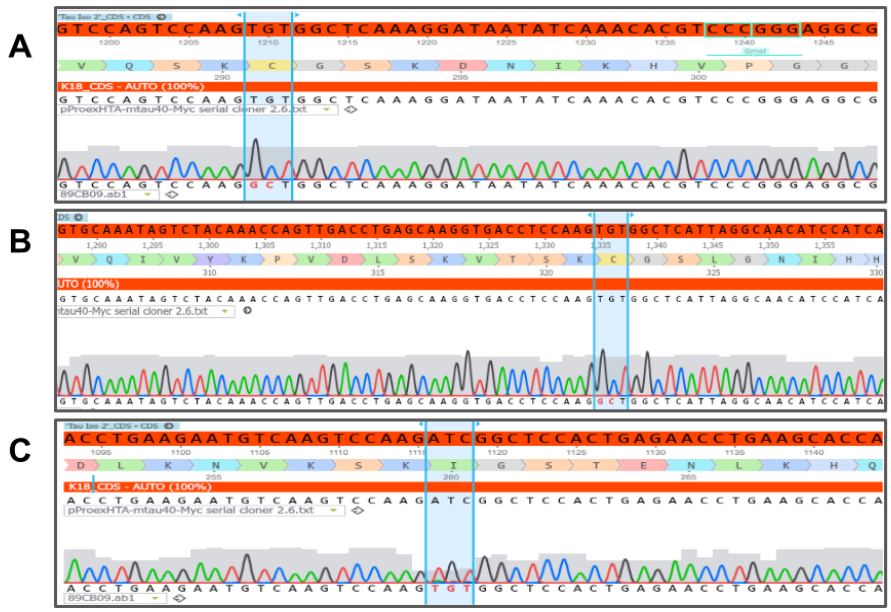

Figure 3.13. Modification of the native cysteine residues in the Myc-htau40-V337M construct.

The C291A, C322A and I260C amino acid changes created in this construct are shown in (A), (B) and (C) respectively.

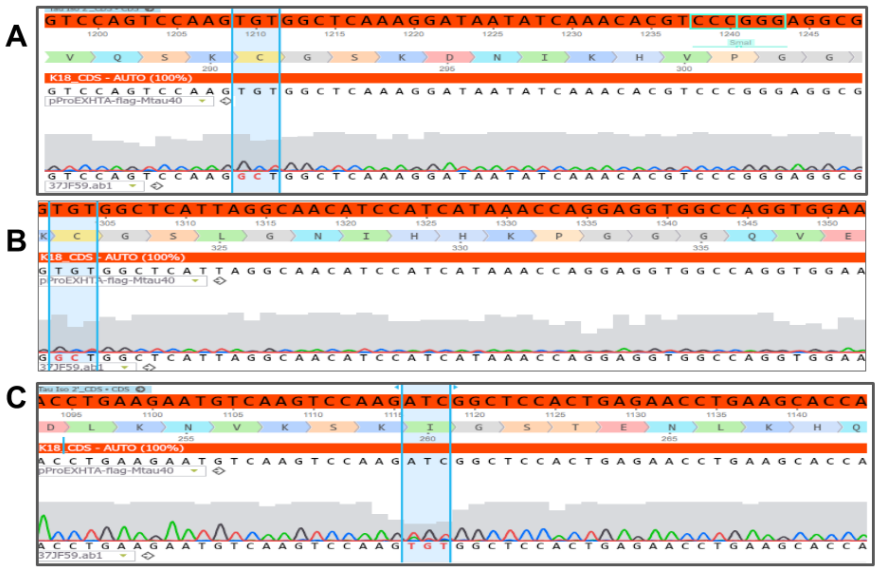

Figure 3.14. Evidence of the creation of amino acid modifications in the WT htau40-Flag construct.

(A) and (B) The native cysteine residues (C291 and C322) were each substituted with alanine. (C) A novel cysteine residue was introduced at position I260C, outside of the core of the microtubule binding region.

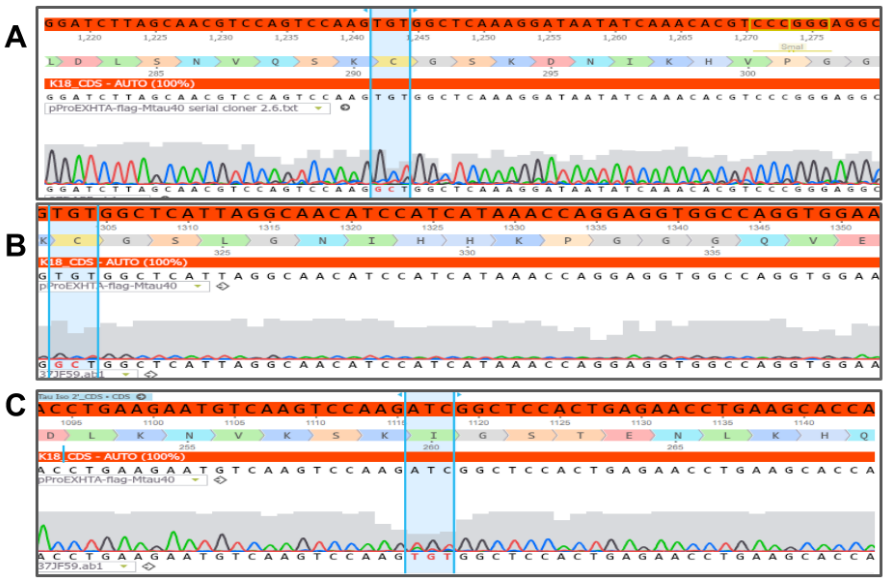

Figure 3.15. Cysteine modification in the htau40-Flag-N279K construct, showing the C291A, C322A and I260C amino acid modifications in (A), (B) and (C) respectively.

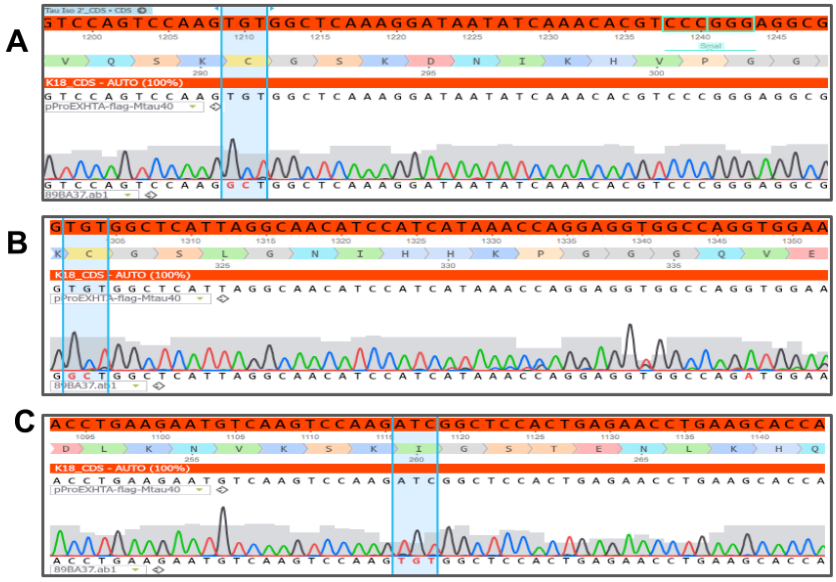

Figure 3.16. Modification of the native cysteine residues C291 and C322 to alanine (A and B respectively) and the introduction of a new cysteine residue at position 260 (C) in the htau40-FLAG-V337M construct.

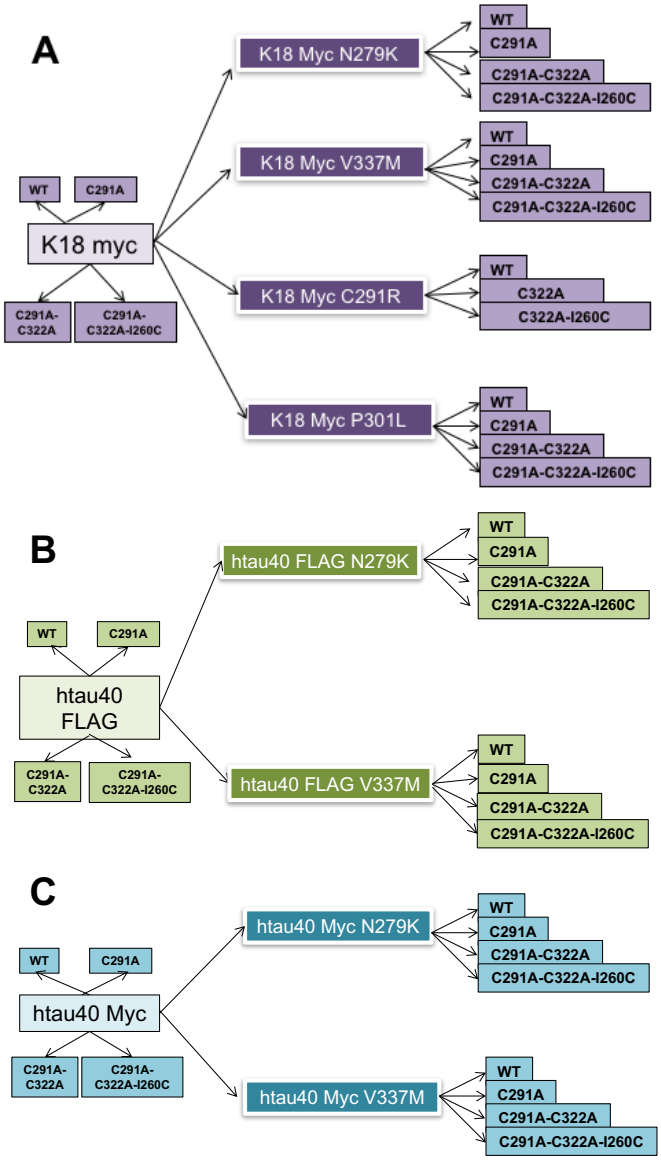

Figure 3.17. Schematic illustration of cysteine-modified tau plasmids created. *Using plasmids encoding genetic constructs for expressing WT K18 (A) and htau40 (B and C) as templates, tau constructs carrying specific disease-associated mutations and cysteine modifications were generated.*

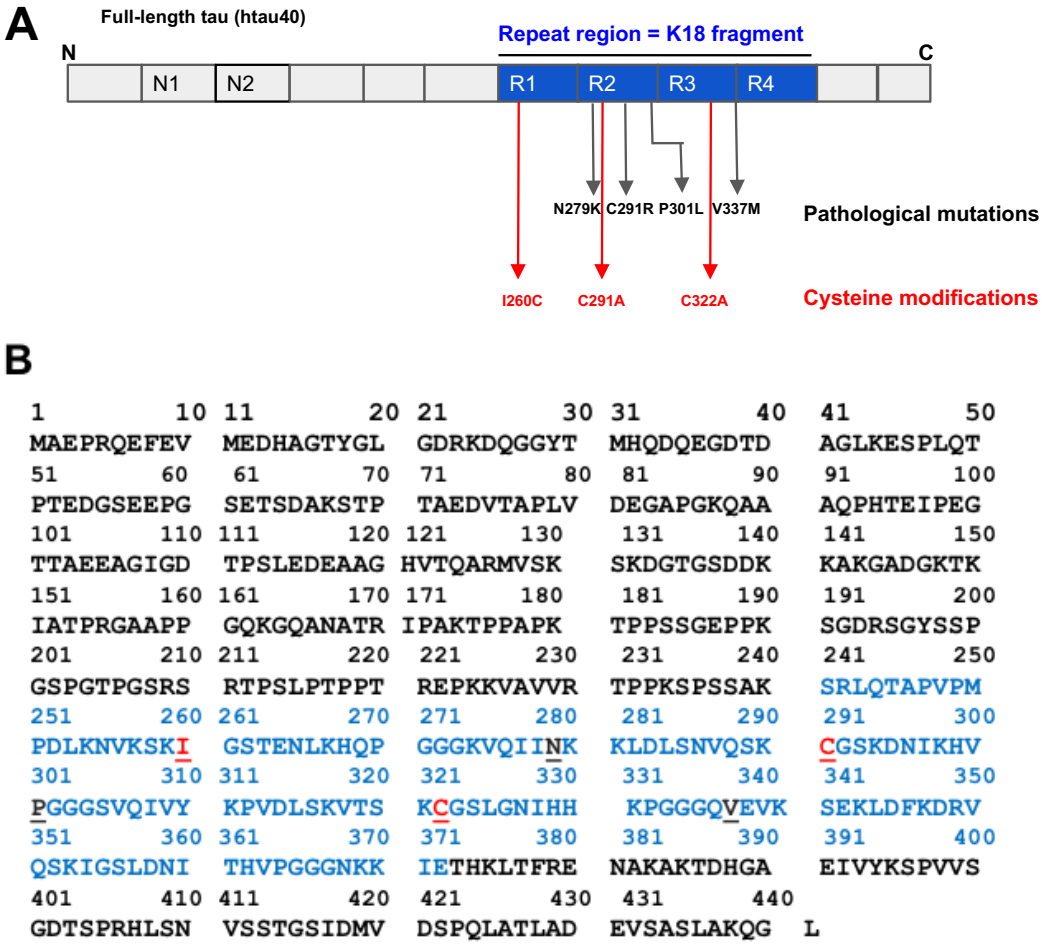

Figure 3.18. Disease-specific mutations and cysteine modifications made in the primary sequence of tau.

(A) Schematic illustration of the location of amino acid changes made in the WT tau-expressing cDNA clones (disease mutations in black and cysteine modifications in red). (B) The complete amino acid sequence of htau40, showing the K18 region (residues 241 – 372 in blue; same as regions R1 to R4 in Fig. 3.18A). Pathological mutations are shown in black and underlined. Sites for cysteine modification are given in red and are underlined. Note that residue 291 doubles as a putative pathological mutation site.

Table 3.3. A comprehensive collection of plasmids created in this study for the recombinant expression of human tau proteins, described according to the encoded genetic construct.
The tau genetic construct in each plasmid is preceded by a hexahistidine motif.

No.	Plasmid name	Tau genetic construct encoded	Description of expressed protein
	Plasmids encoding WT tau or its fragment		
1	pProEx-HTa-Myc-K18	K18	Myc-tagged fragment of the MT repeat region (amino acids 244 – 372) of the full-length human tau brain isoform
2	pProEx-HTa-FLAG-htau40	htau40	The 441-amino acid full-length human brain isoform of tau, tagged with FLAG
3	pProEx-HTa-htau40-Myc	htau40	The 441-amino acid full-length human brain isoform of tau, tagged with c-Myc
	Plasmids encoding pathological mutant versions of K18		
4	pProEx-HTa-Myc-K18-N279K	K18 incorporating the N279K mutation	Myc-tagged K18 tau fragment containing the FTD-associated N279K mutation
5	pProEx-HTa-Myc-K18-V337M	K18 carrying the V337M mutation	Myc-tagged K18 tau fragment containing the FTD-associated V337M mutation
6	pProEx-HTa-Myc-K18-C291R	K18 containing the C291R mutation	Myc-tagged K18 tau fragment consisting of the putative corticobasal degeneration-associated C291R mutation
7	pProEx-HTa-Myc-K18-P301L	K18 containing the P301L mutation	Myc-tagged K18 tau fragment containing the P301L FTD-associated mutation
	Plasmids encoding pathological mutant versions of htau40		
8	pProEx-HTa-FLAG-htau40-N279K	htau40 with the N279K mutation	FLAG-tagged full-length human tau isoform containing the N279K pathological mutation
9	pProEx-HTa-FLAG-htau40-V337M	htau40 with the V337M mutation	FLAG-tagged full-length human tau isoform containing the V337M pathological mutation
10	pProEx-HTa-FLAG-htau40-P301L	htau40 incorporating the P301L mutation	FLAG-tagged full-length human tau isoform containing the P301L pathological mutation

11	pProEx-HTa-htau40-Myc-N279K	htau40 with the N279K mutation	Myc-tagged full-length human tau incorporating the N279K mutation
12	pProEx-HTa-htau40-Myc-V337M	htau40 with the V337M mutation	Myc-tagged full-length human tau incorporating the V337M mutation
	Plasmids encoding cysteine-modified versions of WT K18		
13	pProEx-HTa-Myc-K18-C291A	K18 with C291A mutation	K18 tau fragment with one of two native cysteines (at position 291) modified to the non-polar amino acid alanine
14	pProEx-HTa-Myc-K18-C291A-C322A	K18 with C291A and C322A mutations	K18 tau fragment with both native cysteine residues modified to alanine
15	pProEx-HTa-Myc-K18-C291A-C322A-I260C	K18 with C291A, C322A and I260C mutations	K18 tau fragment with the two native cysteine residues modified to alanine, and a new cysteine introduced at position 260
	Plasmids encoding cysteine-modified versions of WT htau40		
16	pProEx-HTa-FLAG-htau40-C291A	htau40 carrying the C291A modification	FLAG-tagged full-length human tau isoform with a native cysteine replaced with alanine
17	pProEx-HTa-FLAG-htau40-C291A-C322A	htau40 carrying the C291A and C322A amino acid substitutions	FLAG-tagged full-length human tau with no cysteine residue
18	pProEx-HTa-FLAG-htau40-C291A-C322A-I260C	htau40 carrying the C291A, C322A and I260C modifications	FLAG-tagged full-length human tau with both native cysteines removed and a novel cysteine introduced at position 260
19	pProEx-HTa-htau40-Myc-C291A	htau40 carrying the C291A modification	Myc-tagged full-length human tau with a single cysteine removed
20	pProEx-HTa-htau40-Myc-C291A-C322A	htau40 carrying the C291A and C322A amino acid substitutions	Myc-tagged full-length human tau with both cysteine residues removed
21	pProEx-HTa-htau40-Myc-C291A-C322A-I260C	htau40 carrying the C291A, C322A and I260C	“Cysteineless” Myc-tagged full-length human tau with a new cysteine residue introduced at position 260C in the first repeat region

	Plasmids encoding cysteine-modified versions of pathological variants of K18		
22	pProEx-HTa-Myc-K18-N279K-C291A	K18 with N279K and C291A mutations	A single-cysteine variant of the K18 fragment with the N279K pathological mutation
23	pProEx-HTa-Myc-K18-N279K-C291A-C322A	K18 with N279K, C291A and C322A mutations	Cysteine-free variant of the K18 fragment with the N279K pathological mutation
24	pProEx-HTa-Myc-K18-N279K-C291A-C322A-I260C	K18 with N279K, C291A, C322A, and I260C mutations	The K18-N279K protein lacking native cysteine residues but has a novel cysteine at position 260
25	pProEx-HTa-Myc-K18-V337M-C291A	K18 with V337M and C291A mutations	The V337M pathological variant of tau K18 with a native cysteine residue removed
26	pProEx-HTa-Myc-K18-V337M-C291A-C322A	K18 with V337M, C291A and C322A mutations	The V337M pathological variant of tau K18 lacking both native cysteines
27	pProEx-HTa-Myc-K18-V337M-C291A-C322A-I260C	K18 with V337M, C291A, C322A and I260C mutations	The V337M pathological variant of tau K18 with both native cysteine residue removed and a new cysteine introduced in the first repeat region
28	pProEx-HTa-Myc-K18-P301L-C291A-C322A	K18 with P301L, C291A and C322A mutations	The P301L variant of tau K18 with no cysteine residue present
29	pProEx-HTa-Myc-K18-P301L-C291A-C322A-I260C	K18 with P301L, C291A, C322A and I260C mutations	The P301L variant of tau K18 with both native cysteine residues removed, and a novel cysteine introduced outside the MT binding region

30	pProEx-HTa-Myc-K18-C291R-C322A	K18 with C291R, and C322A mutations	A cysteine-free version of the C291R pathological variant of tau K18
31	pProEx-HTa-Myc-K18-C291R-C322A-I260C	K18 with C291R, C322A and I260C mutations	Tau K18-C291R with a new cysteine introduced at position 260
	Plasmids encoding cysteine-modified versions of pathological variants of htau40		
32	pProEx-HTa-FLAG-htau40-N279K-C291A	htau40 with N279K and C291A mutations	FLAG-tagged single cysteine-containing full-length tau with the N279K familial mutation
33	pProEx-HTa-FLAG-htau40-N279K-C291A-C322A	htau40 with N279K, C291A and C322A mutations	FLAG-tagged N279K variant of full-length tau, with no cysteine residue present
34	pProEx-HTa-FLAG-htau40-N279K-C291A-C322A-I260C	htau40 with N279K, C291A, C322A and I260C mutations	FLAG-tagged htau40-N279K containing a novel cysteine at position 260, but no native cysteine
35	pProEx-HTa-FLAG-htau40-V337M-C291A	htau40 with V337M and C291A mutations	FLAG-tagged single cysteine-containing full-length tau with the V337M familial mutation
36	pProEx-HTa-FLAG-htau40-V337M-C291A-C322A	htau40 with V337M, C291A and C332A mutations	The V337M variant of tau FLAG-tagged htau40 with both cysteine residues removed
37	pProEx-HTa-FLAG-htau40-V337M-C291A-C322A-I260C	htau40 with V337M, C291A and C332A mutations	FLAG-tagged htau40-V337M with native cysteine residues removed, and a novel cysteine introduced outside the MT binding core
38	pProEx-HTa-htau40-Myc-N279K-C291A	htau40 with N279K and C291A mutations	A single-cysteine variant of Myc-tagged htau40 with the N279K pathological mutation

39	pProEx-HTa-htau40-Myc-N279K-C291A-C322A	htau40 with N279K, C291A and C322A mutations	Cysteine-free variant of Myc-tagged htau40-N279K
40	pProEx-HTa-htau40-Myc-N279K-C291A-C322A-I260C	htau40 with N279K, C291A, C322A, and I260C mutations	Myc-tagged htau40-N279K with native cysteine residues removed, and a novel cysteine introduced outside the microtubule binding core
41	pProEx-HTa-htau40-Myc-V337M-C291A	htau40 with V337M and C291A mutations	A single-cysteine variant of Myc-tagged htau40 with the V337M pathological mutation
42	pProEx-HTa-htau40-Myc-V337M-C291A-C322A	htau40 with V337M, C291A and C322A mutations	Cysteine-free variant of Myc-tagged htau40-V337M
43	pProEx-HTa-htau40-Myc-V337M-C291A-C322A-I260C	htau40 with V337M, C291A, C322A and I260C mutations	Myc-tagged htau40-V337M with native cysteine residues removed, and a novel cysteine introduced outside the MT binding core

3.3 Discussion

This chapter describes the generation of a large library of plasmid clones for expressing WT tau (both full-length and truncated) and their disease-associated and cysteine-modified variants. Protein expression, purification and initial biochemical characterisation of selected constructs will be described in Chapter 4.

As the first large scale collection of molecular clones for expressing any neurodegenerative protein, this library provides a rich collection of tau proteins that will be beneficial for future studies into different aspects of the protein's physiological and toxic functions, including the influence of specific *MAPT* mutations in cellular physiology and diseases, as well as the contribution of cysteine residues/bonding to tau aggregation and its inhibition. Moreover, the library will serve as a useful resource for studying the structure-activity relationships between the different tau variants created. Furthermore, it will serve as a resourceful drug-screening platform, for instance, to investigate drug potency

against full-length tau, C-terminal truncated tau, and their respective disease variants. This library is serving members of our laboratory and collaborators, and is already being shared with colleague scientists in the neurodegenerative disease research community. Plans are advanced to share these clones in an open access repository to ensure wider, unrestricted access.

In creating these plasmids, the small molecular weights of the tau proteins (approximately 15.1 kDa for K18 and 70 kDa for htau40) ruled out the use of popular fluorescent tags such as the green and red fluorescent proteins (both ~ 27 kDa) for the intended biochemical assays of tau aggregation, and tracking of cellular internalisation of extracellular tau. These fluorescent tags, which are about twice the size of K18 and half that of htau40, have also been shown to influence protein internalisation and secretion (Baens et al., 2006), and may therefore have adverse effects on the uptake and release of tau. Another set of tags that were considered is the c-Myc and FLAG tags on the tau plasmids used (Fig. 2.1). Since these tags would require immunocytochemistry that takes several hours to days to complete, they were deemed un-ideal for quick, real-time assessment of protein spread in living cells but as secondary, confirmatory assays in cell imaging and immunoblotting. Both challenges were avoided through proposed chemical labelling with an Alexa®-Fluor 488-tagged maleimide (97.07 g/mol), which binds covalently to cysteine residues in tau.

In conclusion, a large library of molecular clones has been constructed for the recombinant expression of full-length and truncated tau proteins. Additionally, variations of these plasmids bearing specific FTD-relevant mutations as well as those with cysteine modifications have been generated. These clones are being prepared for sharing through the open access plasmid repository, Addgene, to facilitate storage, maintenance and unrestricted distribution of these ready-to-use resources for the tau research community.

Further studies in subsequent chapters will focus on the WT K18 and its N279K and V337M variants. These mutations have been selected for the following reasons: (i) The N279K is a component of the PHF6* hexapeptide motif (^{275}VQIINK^{280}) whilst the V337M is located within PHF6** (^{337}VEVKSE^{342}), and also close to the

PHF6 motif (^{306}VQIVYK^{311}). These motifs are critical for tau aggregation and seeding hence mutation in the constituent or nearby amino acids may change these pathways (Bergen et al., 2000, 2001; Falcon et al., 2015; Li and Lee, 2006). (ii) The N279K and V337M mutations fall within the second and fourth repeat regions respectively. Hence, their characterisation should offer insights into the consequences of amino acid changes in alternatively- and constitutively-spliced regions of tau. (iii) The two mutations lead to divergent pathological consequences in affected human brains (Hong et al., 1998), suggestive of differing effects on protein structure and aggregation.

4| Expression and purification of tau and its FTD variants using a cleavable histidine tag

This chapter has been published as:
Karikari TK, Turner A, Stass R, Lee LCY, Wilson B, Nagel DA, Hill EJ, Moffat KG (2017) Expression and purification of tau protein and its frontotemporal dementia variants using a cleavable histidine tag. *Protein Expression and Purification 130:44–54*. doi: 10.1016/j.pep.2016.09.009

4.1 Introduction

Tauopathies are a major neurodegenerative health concern worldwide. These include AD, FTDP-17, PiD, PSP and CBD (Spillantini and Goedert, 1998). A common feature shared by these diseases is the abundance of tau-positive NFTs that define neuropathology (Mandelkow and Mandelkow, 2012; Spillantini and Goedert, 1998). While tau is involved in MT assembly and stabilisation in physiological conditions, dysfunctional tau has been implicated in tauopathy-associated NFTs resulting from the accumulation of insoluble toxic aggregates (Arriagada et al., 1992).

Recombinant tau closely mimics important properties of the naturally-occurring human protein. To this end, recombinant tau has been used extensively to study the molecular, biochemical and cellular aspects of the protein's functions, including (i) binding to MTs in physiological and pathological conditions (ii) tau-tau interactions leading to their aggregation into toxic PHFs that are similar to those isolated from the brains of AD patients, and (iii) the transcellular spread of this toxicity in affected organisms (Barghorn et al., 2000, 2004; Hasegawa et al., 1998; Hong et al., 1998; Michel et al., 2014; Usenovic et al., 2015; Yao et al., 2003). The binding of tau to MTs is disrupted in disease and also by the presence of specific FTDP-17 mutations some of which can enhance the protein's aggregation into PHFs (Barghorn et al., 2000; Combs and Gamblin, 2012; Hasegawa et al., 1998; Hong et al., 1998). Furthermore, truncated tau constructs such as the repeat domains are *aggregation-prone* and demonstrate enhanced aggregation kinetics compared

to the full-length isoforms (Barghorn et al., 2005; Friedhoff et al., 1998). The K18 construct, for example, is sufficient for the protein's polymerisation into PHFs (Barghorn et al., 2000). When exogenously supplied, this tau fragment can be internalised by cells, engaging endogenous proteins to form toxic aggregates which spread in prion-like cell-to-cell transmission (Frost et al., 2009; Guo and Lee, 2011; Michel et al., 2014; Usenovic et al., 2015).

High-yield expression of pure tau is critical for *in vitro* tauopathy studies. However, the protein's expression and purification are complicated by its high aggregation and truncation tendencies, and time-consuming and expensive methodologies (Csokova et al., 2004). Here, we sought to identify parameters that would ensure optimal expression of tau K18 and its FTDP-17 variants V337M and N279K. The following expression conditions were investigated: the choice of *E. coli* host strain, induction temperature, duration of induction, and the presence of glucose in the culture medium. Subsequently, the newly established conditions were utilised for the large-scale protein expression and purification. The purified proteins were characterised through circular dichroism analysis of secondary structures and the assembly of Alzheimer-like PHFs.

4.2 Results

4.2.1 Preparation of tau pathogenic mutants

The K18 WT construct (Fig. 4.1A) was used as a platform for the creation of tau constructs carrying the N279K and the V337M FTDP-17 mutations. Both mutations were single point: N279K = AAT (Asn) → AAA (Lys) and V337M = GTG (Val) → ATG (Met), and were confirmed by DNA sequencing and subsequent multiple sequence alignments to the original K18 WT construct (Fig. 4.1).

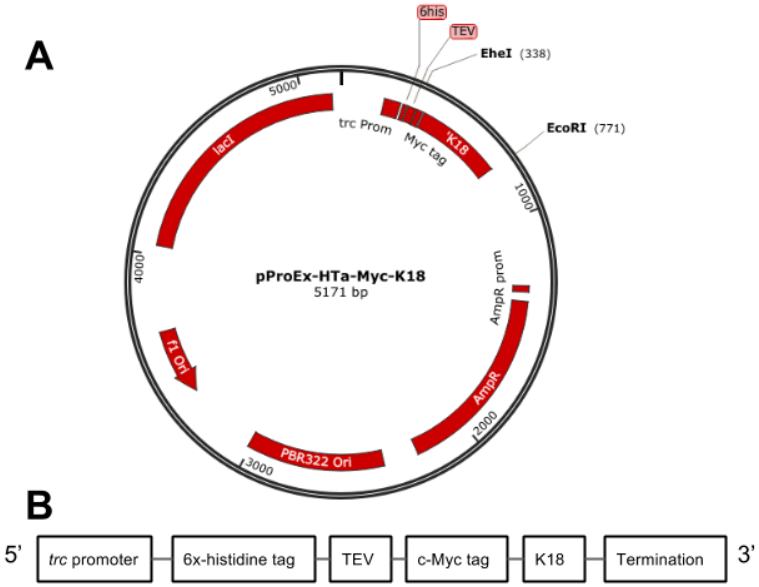

Figure 4.1. The WT K18 expression plasmid used in this study.
(A) A schematic representation of the pProEx-HTa plasmid into which the K18 tau construct was cloned. The EheI *and* EcoRI *restriction sites between which K18 was cloned are shown, as well as the genes encoding the LacI repressor (*lacI*), ampicillin resistance (AmpR), and origins of replication (f1Ori and pBR322 Ori). (B) Essential elements of the pProEx-HTa-Myc-K18 plasmid are indicated. These include a* trc *promoter, a hexa-histidine tag, a TEV site, and a c-Myc tag followed by K18.*

4.2.2 Comparison of tau expression in two different *E. coli* strains

Tau expression in two *E. coli* strains – BL21(DE3)*pRosetta and NEB-5α – was compared (Fig. 4.2). The intention was to compare expression in the former strain, which is adapted for the expression of eukaryotic proteins with the latter strain lacking this property. After IPTG induction, expressed tau proteins were positively identified with the anti-tau antibody used (Fig. 4.2A). SDS-resistant K18 WT monomers and dimers were approximately 22 kDa and 44 kDa in size respectively, with shorter fragments most likely indicating truncation products. The resistance of tau to denaturation by SDS has been previously reported (Goedert and Jakes, 1990; Schafer et al., 2013). Note that the presence of the c-Myc, poly-histidine and TEV tags, and the anomalous SDS-binding property of tau influenced the observed size of expressed tau. Higher amounts of soluble monomeric tau were recorded in the BL21(DE3)*pRosetta strain compared to NEB-5α, although this difference was not significant (two-tailed Mann Whitney test, p = 0.60; Fig. 4.2B). While

comparable levels of monomeric tau were observed in the soluble and insoluble (pellet) fractions of BL21(DE3)*pRosetta (41±18 and 42±19 respectively), expression in NEB-5α resulted in higher levels of monomeric tau in the insoluble fraction compared to the soluble fraction (42±22 and 31±4 respectively; Fig. 4.2A and B), suggesting a higher proportion of inclusion body formation in this host. For this reason, all subsequent experiments were conducted using tau transformed into BL21(DE3)*pRosetta. Note that the densitometry analysis was focused on monomers as the most abundant and primary tau protein species but due to the high tendency of the protein to form aggregation and truncation products, this may not represent overall tau production in some cases.

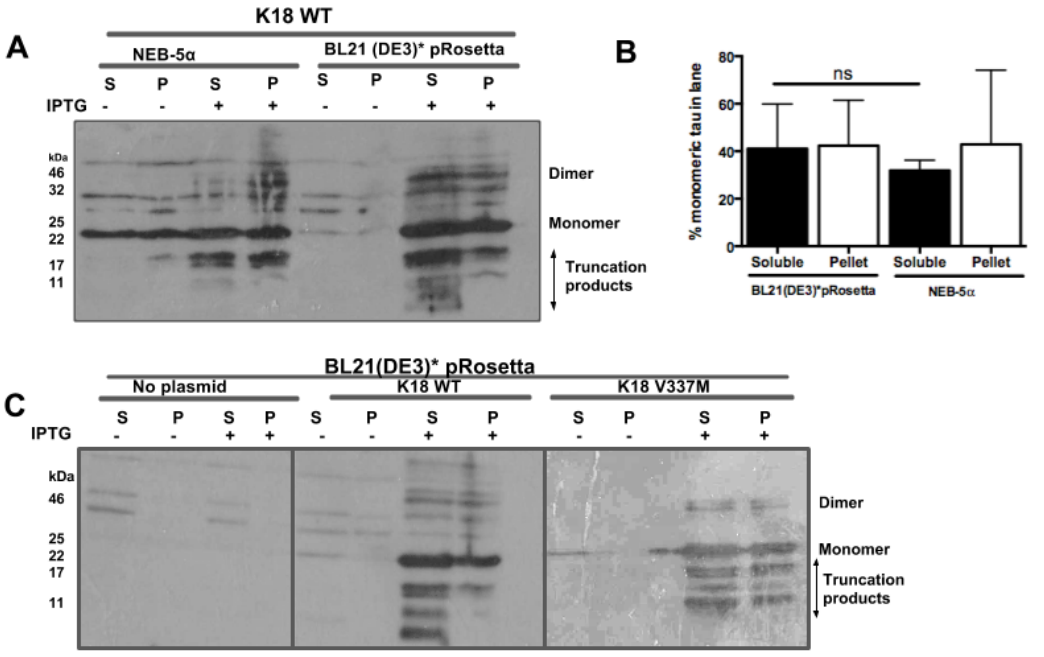

Figure 4.2. Representative WB analysis of K18 tau expression in the NEB-5α and BL21(DE3)*pRosetta E. coli strains.

*(A) Dimerisation and truncation of expressed tau protein were noticeable in both strains. (B) Densitometry analysis of soluble monomeric tau levels in the BL21(DE3)*pRosetta strain and NEB-5α. Two-tailed Mann Whitney test, p = 0.6. Data shown as mean ± SD of three independent experiments. (C) Evaluation of K18 WT and K18 V337M expression in the BL21(DE3)*pRosetta strain. S, soluble fraction; P, pellet (insoluble) fraction; IPTG, isopropyl β-D-1 thiogalactopyranoside.*

The effect of the V337M disease mutation on protein expression was also measured, since this point mutation is sufficient to reduce the MT-binding ability of tau *in vitro* (Hasegawa et al., 1998). In this experiment, similar levels of

monomeric tau expression were observed for both K18 WT and the V337M variant, suggesting that the pathogenic mutation did not affect expression levels (Fig. 4.2C). Furthermore, both proteins shared tendencies to form aggregates and truncation products, indicating that the spontaneous aggregation and truncation properties of tau were independent of this mutation (Fig. 4.2C).

4.2.3 Temperature optimisation for tau expression

Subsequently, conditions for protein expression in the BL21(DE3)*pRosetta strain were investigated. The following parameters were studied: post-induction expression temperature, length of induction, and media supplementation with glucose.

To identify an ideal expression temperature for K18 production, an initial culture of K18 WT-expressing cells was divided into three equal aliquots immediately after induction and grown for a further 3 h at 25 ^{o}C, 30 ^{o}C and 37 ^{o}C. WB analysis showed that all three temperatures were suitable for tau expression. 37 ^{o}C was found to be the best for soluble tau production, as the expression of full-length monomeric K18 WT was highest at this temperature (Fig. 4.3). However, increasing temperature appeared to favour protein aggregation and truncation.

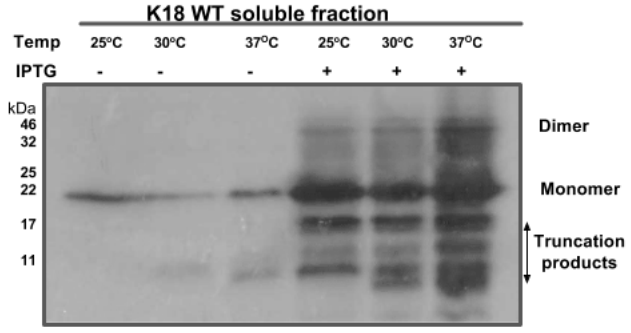

Figure 4.3. Representative WB analysis showing the influence of induction temperature on expression levels of K18 WT tau.
*Cultures of tau-encoding BL21(DE3)*pRosetta cells were grown at 37 ^{o}C until reaching OD_{600} = 0.6. After IPTG induction, the cultures were immediately split into three aliquots and grown at 25 ^{o}C, 30 ^{o}C or 37 ^{o}C for 3 h.*

4.2.4 Induction length for optimum tau expression

Optimal incubation time can vary depending on the target protein and the choice of expression system. To establish an optimum induction length for K18 WT expression, aliquots of induced cultures were taken at regular intervals post-induction and analysed by WB. Although no marked difference in monomeric tau levels was recorded at the different time points, truncation products and aggregates were least evident at 1 h (Fig. 4.4A).

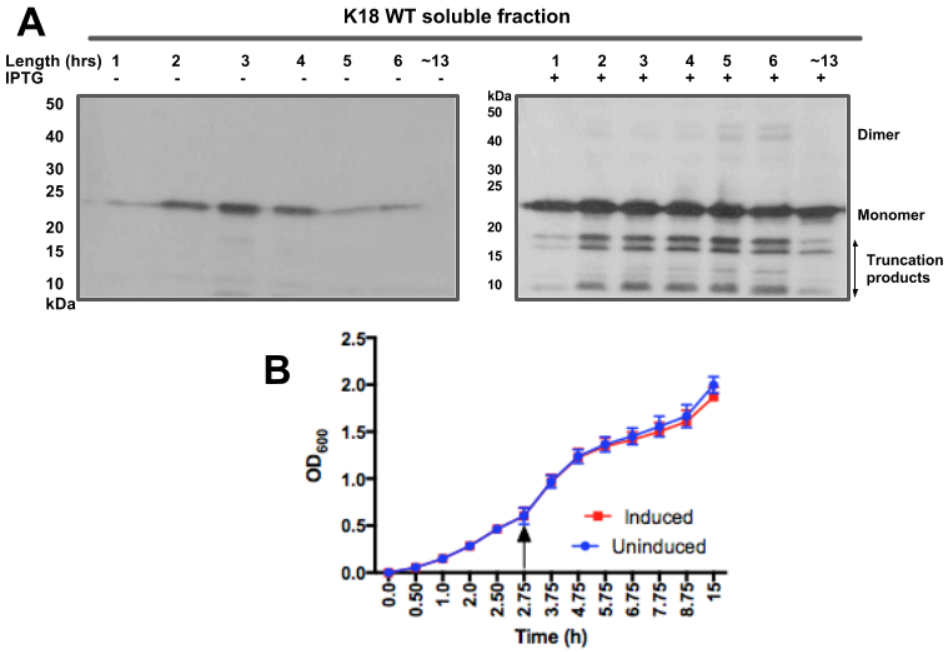

Figure 4.4. Time-course evaluation of K18 WT expression in E. coli using optical density measurement and WB.
Cultures of tau K18 WT-expressing cells were grown at 37 °C until reaching OD_{600} = 0.6. The cultures were divided into two halves, and one portion induced with 0.5 mM IPTG. Both cultures were subsequently incubated at 37 °C, and OD_{600} readings and aliquots for WB taken periodically. (A) Soluble cell fractions showing the expression of K18 WT over time. Truncation products were least evident at 1 h post-induction but increased after this time point. (B) Growth curves of IPTG-induced and un-induced cultures of tau, showing the same pattern of growth for both cultures. Arrow indicates point of induction.

Next, the growth curves of un-induced and induced cultures were monitored to ascertain whether prolonged expression resulted in accumulating toxicity. Although the un-induced culture grew at a slightly faster rate post-induction, this difference appeared minimal, suggesting that tau expression did not pose significant cellular toxicity to the bacterial system (Fig. 4.4B).

4.2.5 Media supplementation with 0.2 %w/v glucose

Glucose regulates the *lac* operon and may reduce promoter "leakiness" (detectable expression without induction) (Rosano and Ceccarelli, 2014). Glucose may therefore be provided as an extra carbon source to enhance growth of *E. coli* expressing a protein of interest. Addition of up to 1% glucose has been shown to enhance protein yield (Sivashanmugam et al., 2009). For this reason, the effect of media supplementation with 0.2 % glucose prior to IPTG induction of tau expression was investigated. The level of monomeric K18 WT was not significantly enhanced by glucose supplementation ($p = 0.6667$; Fig. 4.5A and 4.5C). Similar findings were also recorded for K18 with the two FTDP-17 variants (Fig. 4.5B).

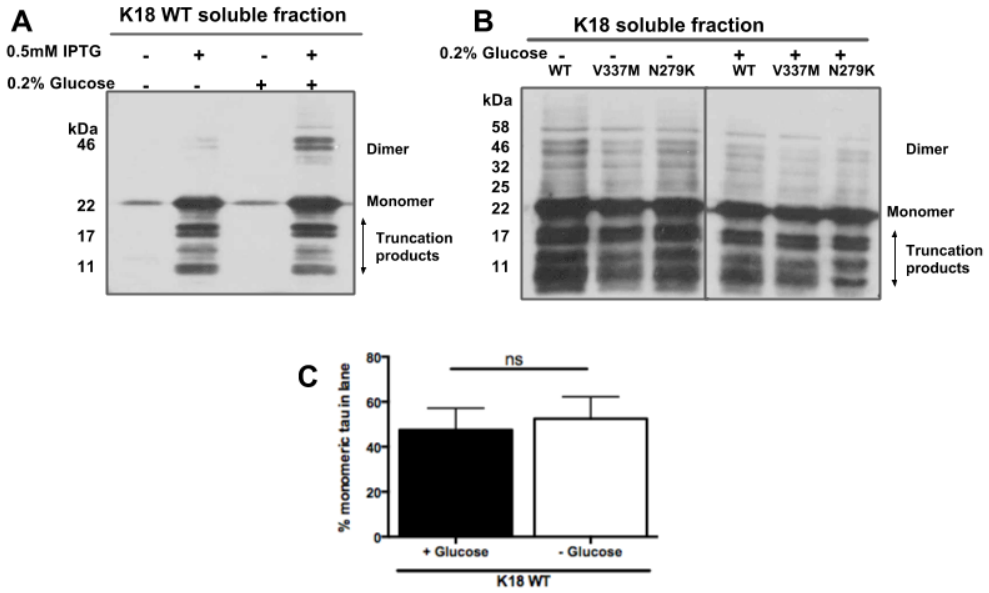

Figure 4.5. Media supplementation with 0.2% glucose did not significantly enhance tau expression.
*BL21(DE3)*pRosetta cells expressing tau were grown in selective LB media in the presence or absence of glucose. (A) Representative WB analysis of soluble cell fractions showing the expression of K18 WT in the absence and presence of 0.2% glucose. (B) WB analysis of induced protein expression in K18 WT and its FTDP-17 variants (V337M and N279K). (C) Densitometry analysis of monomeric K18 WT expression in LB media with or without glucose (two-tailed Mann Whitney test, $p = 0.6667$, $n = 3$).*

4.2.6 Purification of tau constructs

After identifying optimum conditions for expressing K18, these conditions were used in growing larger cultures of tau that were subsequently purified using IMAC. All three protein constructs (K18 WT, K18 V337M and K18 N279K) were successfully purified using this system, followed by overnight dialysis and TEV site cleavage. Tau expression and purification were confirmed by SDS-PAGE and WB (Fig. 4.6). As expected, the crude extracts contained tau in addition to contaminating cellular proteins (lanes labelled CE in Fig. 4.6). After initial separation of the crude extracts, the tau component was bound to the Ni^{2+} resin, leaving unbound proteins to filter through (UPFT lanes in Fig. 4.6). Washing the column with buffer B removed residual contaminants and loosely-bound protein (lanes B1-B3 in Fig. 4.6). Proteins were eluted with buffer C containing 500 mM imidazole (C1-C3 lanes in Fig. 4.6). and subsequently dialysed overnight with TEV protease and the purification process repeated to isolate tau proteins with the TEV site cleaved. Complete cleavage of the His tag was confirmed in WB using an anti-His antibody (Fig. 4.7). While the total tau antibody recognised K18 WT with or without the His tag (Fig. 4.7A, lanes 2 and 1 respectively), the anti-His antibody had no recognition for K18 WT and K18 N279K with the His tags cleaved (Fig. 4.7B, lanes 3 and 4 respectively) but for K18 WT with the His tag intact (Fig. 4.7B, lanes 5). Protein yield was up to ~5.5 mg/ml per 500 ml culture (Table 1). WB showed that the tau constructs were purified both in the monomeric and dimeric forms (and sometimes in higher oligomeric forms; Fig. 4.6), emphasising the characteristic tendency of the protein to readily form aggregates. Contrary to the expression experiments, truncation products were rarely observed in purified proteins. Gel electrophoresis confirmation of TEV protease purification is shown in the Appendix.

4.2.7 CD assessment of secondary structure properties of the purified tau

Following successful purification of the tau proteins, K18 WT and K18 V337M were characterised to compare their biochemical properties to those previously reported (von Bergen et al., 2005; Yao et al., 2003). Firstly, CD spectroscopy was used to investigate secondary structure conformation of the purified tau. To assess

the secondary structures of the tau proteins in solution, their CD spectra were measured in the far-ultraviolet spectral region (wavelength 190 – 280 nm) using proteins dissolved in 10 mM phosphate buffer (pH 7.4) at RT. Previous studies have reported that tau, in the mostly-monomeric state, is inherently unfolded, with predominantly random-coil conformation (Barghorn et al., 2004, 2000a; Mizushima et al., 2006; von Bergen et al., 2005; Yao et al., 2003). The analysis confirmed this observation for the purified proteins; CD spectra for both K18 WT and K18 V337M showed minimum peaks around 200 nm (Fig. 4.8A and 4.8B), characteristic of predominantly random coil structures (von Bergen et al., 2005; Yao et al., 2003). Moreover, the depth of the negative peaks were similar for both the WT and mutant constructs, suggesting that the disease-associated mutation did not cause obvious changes in secondary structure of tau as previously reported (Barghorn et al., 2000). To estimate the relative contribution of different secondary structure elements, the CD spectra were analysed with the CONTIN algorithm in DichroWeb, which showed that the secondary structures were dominated by random coils, with traces of α-helices and β-sheets (Fig. 4.8C and 4.8D).

4.2.8 Preparation of Alzheimer-like PHF and subsequent imaging using negative-stain TEM

In order to validate their authenticity, Alzheimer-like filaments were prepared from the recombinant proteins and visualised by TEM. PHFs were prepared in the presence of the reducing agent DTT and the polyanion inducer heparin. The reaction was carried out in 10 mM Na_2PO_4 pH 7.4 buffer. The use of a non-chlorine-containing buffer enabled subsequent CD investigations on the prepared PHF without having to change buffers as was previously done (Yao et al., 2003). TEM-based structural examination suggested that the filaments consisted of distinct features including two strands wound round each other, with crossover points every few nanometers (Fig. 4.9) in line with previous observations (Barghorn et al., 2004; Wischik et al., 1985).

Subsequently, the filamented tau samples were analysed by CD to assess whether PHF assembly induced a shift in secondary structure composition as suggested (von Bergen et al., 2005). The CD spectra for filamented tau showed a shift in peak to approximately 220 nm, which is indicative of β-sheet formation (Fig. 4.8). While

the soluble fractions in the PHF preparation samples consisted of monomers and low molecular weight oligomers, the insoluble PHF was predominantly made up of higher molecular weight species that were not noticeable by WB (Fig. 4.9F), consistent with previous observations (Huvent et al., 2014).

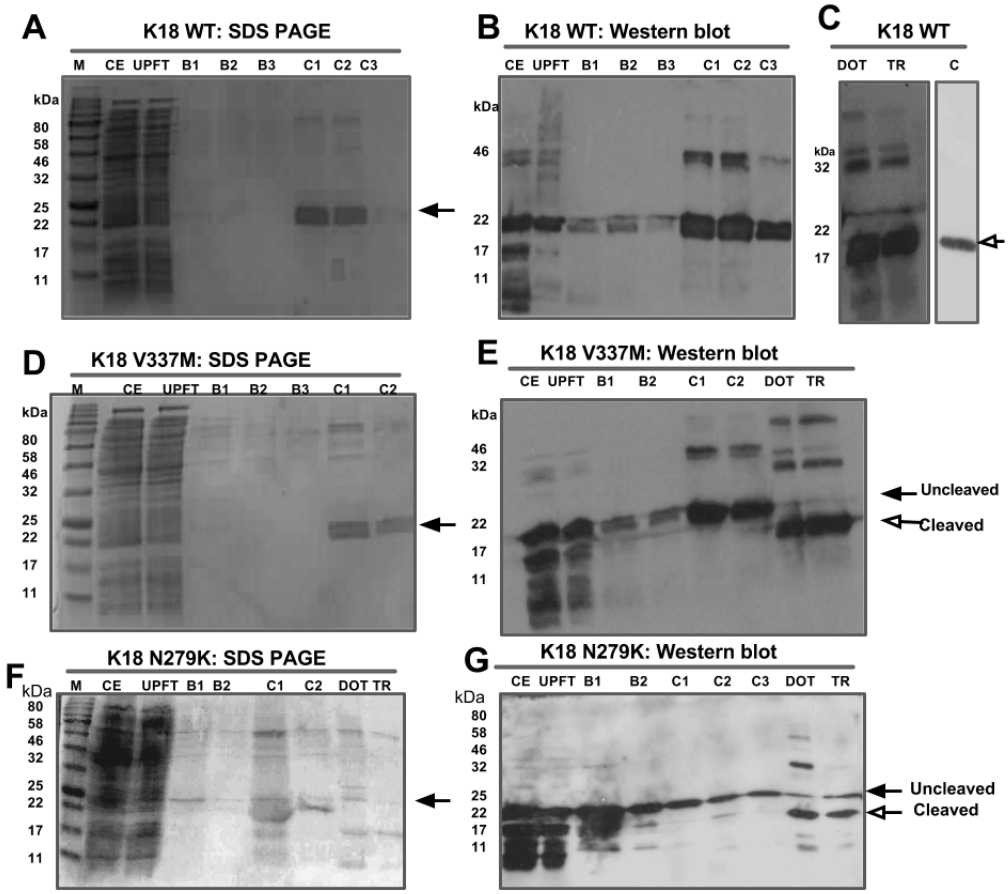

Figure 4.6. Analysis of IMAC-based tau purification using SDS-PAGE followed by WB.

Cultures were grown until reaching OD_{600} = 0.6, IPTG-induced and grown for a further 1 h after which the expressed tau protein was recovered and purified. Aliquots taken at each step of the purification process were analysed on 15% Tris-glycine SDS-PAGE gels. (A), (D) and (F) show SDS-PAGE analysis of the purification of K18 WT, K18 V337M and K18 N279K respectively. (B) and (C) are WB of K18 WT purification. ***(E)*** *and* ***(G)*** *WB analysis of the purification of K18 V337M and K18 N279K respectively. Arrows indicate monomeric tau; black arrows point to uncleaved His-tagged tau while open arrows refer to tag-free tau. M = marker protein; CE = crude extract; UPFT = unbound protein flow-through; B1, B2 and B3 = wash fractions; C1, C2 and C3 = eluted fractions; DOT = pooled eluted fractions dialysed overnight in the presence of TEV protease, against dialysis buffer; TR = eluent after TEV cleavage. C = K18 WT control protein from a previous preparation after the removal of breakdown products and aggregates, leaving homogenous monomeric tau.*

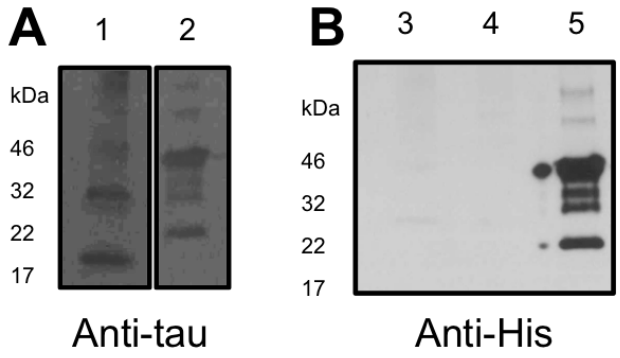

Figure 4.7. Confirmation of cleavage of the polyhistidine tag.
(A) WB using the total tau antibody (#A0024 from Dako) confirmed the presence of tau in purified K18 WT with and without the His tag cleaved (lanes 1 and 2 respectively). (B) WB using the anti-His antibody however recognised the His tagged K18 WT (lane 5) but not equal concentrations of K18 WT and K18 N279K with the His tags cleaved (lanes 3 and 4 respectively).

Table 4.1. Summary of studies on expression and purification of recombinant tau.

Study	Tau isoform or construct studied	Purification method used	Yield	Purity
This work	Wild type K18 and its N279K and V337M FTD variants	Ni^{2+} affinity chromatography	Up to ~5.5 mg/ml, 4.0 mg/ml and 3.5 mg/ml protein per 500 ml culture for K18 WT, K18 V337M and K18 N279K respectively	Up to 99 % purity for monomer only and 95 % for monomer-oligomer mix
Tepper et al. (2014)	2N4R (longest tau isoform in the adult human brain)	Tau expressed in Sf9 cells was purified by size exclusion and anion exchange chromatography	5 – 10 µM (subsequently concentrated to ~50 µM)	Not indicated
Geodert and Jakes (1990)	The six human tau isoforms	Ammonium sulphate precipitation and ion exchange chromatography	30 – 60 µg/ml culture	Up to 95 % purity
Barghorn et al (2005)	Tau isoforms and constructs	Gel permeation and cation exchange chromatography	10 – 100 mg protein/10 L culture (specific concentration for	95 % for monomer-oligomer mixtures and 99 %

	including K18		K18 not indicated)	for monomer only
Csokova et al (2004)	221-441 fragment of tau	Cation exchange, anion exchange and size exclusion chromatography	4 – 8 mg protein/500 ml culture	Up to 98 % purity

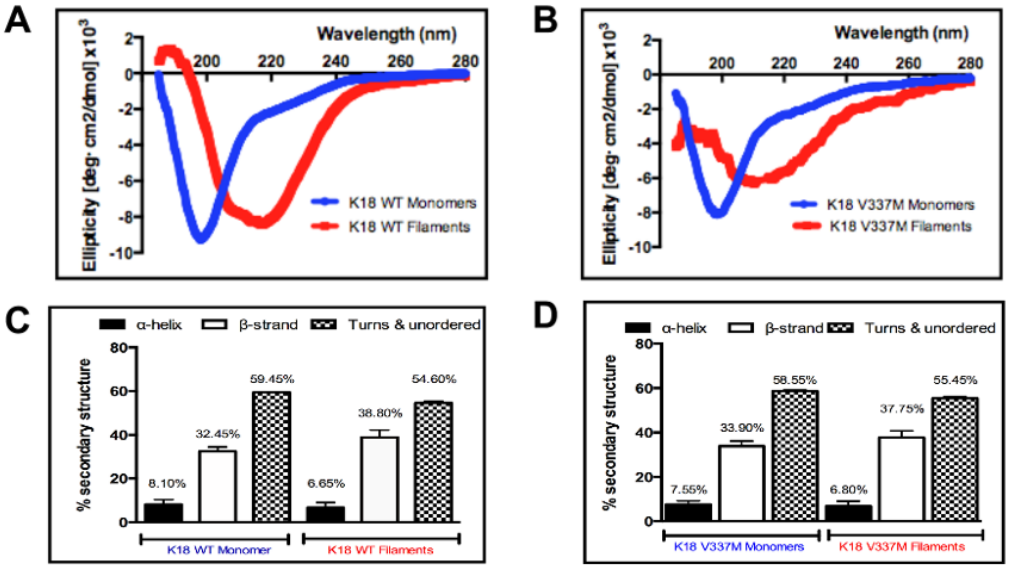

Figure 4.8. Characterisation of purified tau proteins using CD spectroscopy and the preparation of Alzheimer-like PHFs.
(A) and (B) CD spectra within the far-UV region for K18 WT and K18 V337M monomers (blue curves) and insoluble filaments (red curves). (C) and (D) Computational analysis of secondary structure content from the CD data using the CONTIN algorithm in the DichroWeb database.

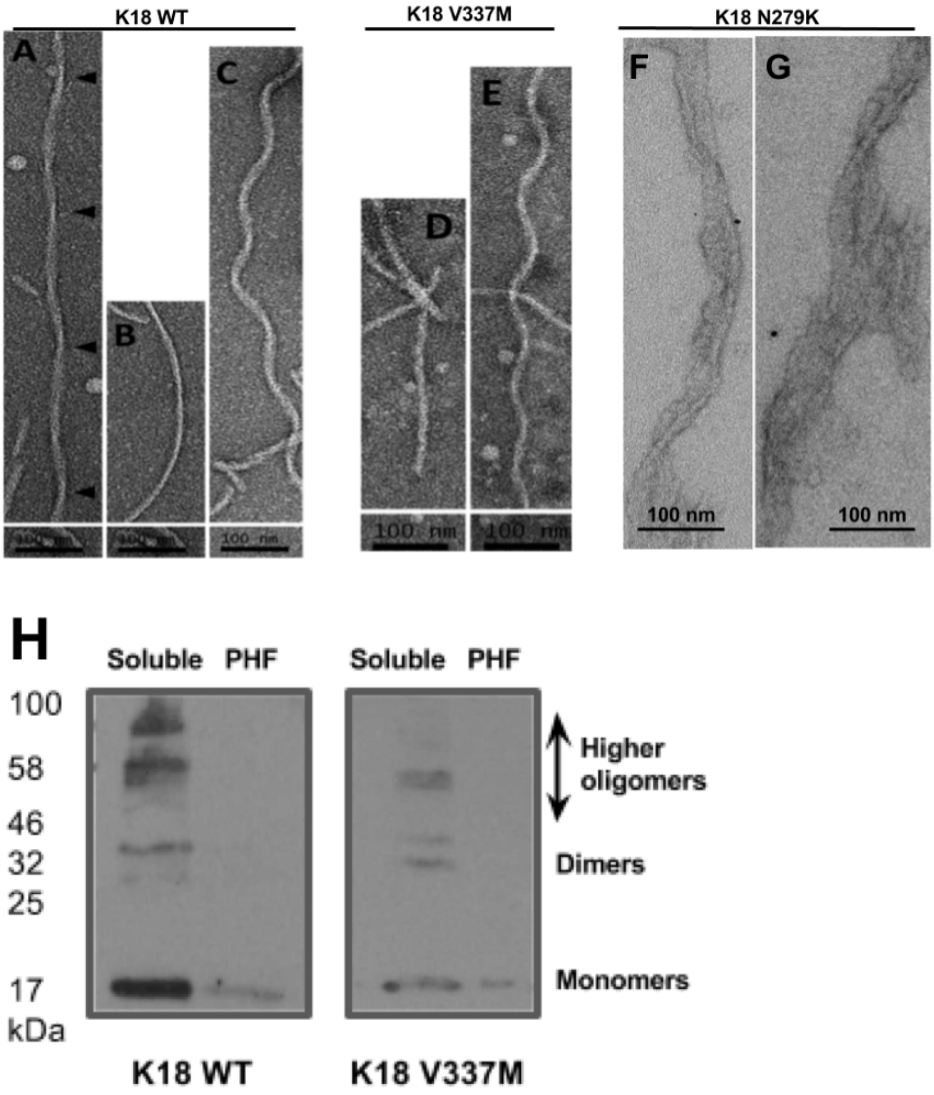

Figure 4.9. Representative electron micrographs showing negative-stained Alzheimer-like filaments of distinct morphologies prepared from the purified tau proteins.

Panels (A), (B) and (C) are from K18 WT, (D) and (E) are from K18 V337M, whilst (F) and (G) are from K18 N279K. Panel A shows PHFs of varying width. Panels B and D contain SFs with no obvious periodicity. Panels C and E display spiral-like PHFs. Panels F and G are PHFs of distinct morphological phenotypes in terms of width, crossover pattern and periodicity. Arrowheads indicate possible peak-to-peak crossover points. (H) Following heparin-induced tau aggregation, filament samples were ultra-centrifuged to isolate soluble species from insoluble PHFs. WB analysis suggested that the soluble fraction consisted of a heterogeneous mix of monomers and oligomers while the insoluble aggregates consisted mostly of higher molecular weight filaments that were not separated by gel electrophoresis.

4.3 Discussion

Tau protein has been the subject of intensive research because of its physiological importance in stabilising MTs, supporting axonal transport, neurite outgrowth and other processes involved in neuronal cell biology (Lee et al., 2012; Mandelkow and Mandelkow, 2012; Rodríguez-Martín et al., 2016). In addition, toxic aggregation of WT tau and its FTDP-17 variants is the primary hallmark of Alzheimer's disease and other tauopathies (Mandelkow and Mandelkow, 2012). Efficient production of recombinant tau is a pre-requisite for the *in vitro* and some *in vivo* modelling of these diseases. Insufficient yield of this target protein can result in several experimental pitfalls. In this study, we investigated parameters that can affect the expression and purification of WT and FTDP-17 pathogenic tau, in an attempt to identify ways to increase the yield of pure tau for downstream applications. It was shown that the presence of the V337M and N279K pathogenic mutations appeared not to affect monomeric tau expression, which was greatest at 37 ^{o}C induction temperature compared to 25 ^{o}C and 30 ^{o}C. Build-up of truncation products and aggregates was least evident at 1 h post-induction, compared to up to 13 h post-induction. Supplementing the growth medium with 0.2 % glucose did not significantly affect the percentage of monomeric tau present. The expressed protein was purified using IMAC and characterised by CD and PHF analysis. Our findings show that the described method led to the production of authentic tau proteins, which followed the known biochemical and biophysical properties. This report provides a reliable method for efficient expression and purification of tau that would be useful for further studies.

The BL21(DE3)*pRosetta strain used in this study was deficient in RNAseE, and genetically modified to be Lon and OmpT protease-deficient, making it suitable for high-yield expression of foreign genes in bacteria. WB showed that using this strain did not significantly enhance the amount of monomeric tau compared to NEB-5α (Fig. 4.2). This was possibly due to the high propensity of tau to aggregate and form truncated peptides, thus preventing efficient evaluation of monomeric tau yield. Whilst 37 ^{o}C appeared optimal for expression of monomeric tau, aggregation seemed to increase with temperature (Fig. 4.3). This corroborates previous reports

that tau polymerisation is most efficient at high temperatures (Friedhoff et al., 1998). A relatively short induction time of 1 h was optimal for the amount of monomeric protein yields achieved and a concentration of 0.1 mM – 1mM IPTG was sufficient to induce expression (data not shown). Media supplementation with glucose did not significantly enhance expression yield, suggesting that the strain can be used for tau production without glucose (Fig. 4.5). A common observation throughout the expression-optimisation experiments was the high tendency of the tau constructs to form truncation products, in both strains studied (Fig. 4.2 – 4.5). This possibly could have been reduced by the addition of protease inhibitors to the growth medium or lysis buffer, notwithstanding the reported protease resistance of the tau repeat domain (Novak et al., 1993). However, this step was omitted to allow the proteins to be observed in a native-like state. It was also observed that a considerable portion of the protein existed in the pellet fraction, which could not be recovered by additional sonication (Fig. 4.2). This was likely as a result of the formation of inclusion bodies or insoluble aggregates and not due to insufficient cell lysis, as reported for another protein (An et al., 2015).

The purified tau proteins were characterised using CD spectroscopy, PHF preparation and TEM visualisation of PHFs (Fig. 4.7). The CD data revealed that the purified tau proteins were inherently unfolded, showing negative peaks at approximately 200 nm. For direct evidence of filament formation, samples were negative-stained and imaged by TEM, which indicated that the purified tau proteins were capable of forming filaments. Filament formation was induced with the addition of heparin; the role of heparin as an inducer of PHF formation has been characterised (Ramachandran and Udgaonkar, 2011). Filament formation is promoted by hexapeptide motifs at the beginning of the second and third tau repeats (Bergen et al., 2000), both of which were intact in the 4R tau constructs used (Mizushima et al., 2006). Figs 4.8 and 4.9 indicate that the tau proteins produced were able to form filaments as expected, and that the filaments consisted of high molecular weight oligomers compared to pre-filament species. The observed structural shift in CD spectra following tau aggregation can also be achieved by incubating tau at physiological temperatures with or without heparin, although incubation times are lengthened in the absence of heparin (Kumar et al., 2014; Mizushima et al., 2006).

An advantage of the method reported here is that it enables the production of tau oligomers and monomers (the toxicity of both of which is currently under intense investigation) through one- or two-step purification protocols. The first purification step produces polyhistidine-tagged tau; the tag can be removed following TEV protease treatment during dialysis. We have confirmed that both His-tagged and tag-free tau proteins prepared using the described protocol are fully functional in terms of their aggregation tendency, ability to form Alzheimer-like filaments, and secondary structure features. These findings are in agreement with earlier studies that reported the use of untagged and His-tagged tau for *in vitro* and cell culture investigations (Kim et al., 2015; Kumar et al., 2014; Puri et al., 2009; Tepper et al., 2014), further confirming the authenticity of the proteins produced using our simplified protocol.

Whether or not the purified tau should undergo further processing before utilisation for functional studies would depend on the intended use. The preparation of monomer-oligomer mixtures, described in this report, could be used for many studies. However, if exclusively monomeric tau is required (as in Fig. 4.6C lane C), then it is possible to remove truncation products and aggregates by size exclusion chromatography. It is important to be certain about the nature of purified tau being used for downstream applications (whether consisting exclusively of monomers, oligomers or a heterogenous mixture of the two) since seemingly conflicting results have been reported for the toxicity-seeding potential of monomeric and oligomeric tau (Lasagna-Reeves et al., 2012; Michel et al., 2014; Usenovic et al., 2015).

Historically, there has been a debate as to which tau protein species is the most toxic to cells – whether monomers, oligomers, PHF or NFT (Huang et al., 2015; Krüger and Mandelkow, 2016). Recent attempts to address this question have also sought to understand if tau toxicity and pathology spread in a prion-like manner. In such studies, recombinant forms of the various protein species are injected into the brains of living experimental animals or extracellularly added to neuronal or neuron-like cells, and their ability to be internalised, secreted and co-aggregate with

endogenous proteins monitored in real time (Mohamed et al., 2013). Converging evidence has mostly suggested that oligomeric tau are the early-stage species required to initiate the trans-cellular spread, toxicity and associated learning and memory impairments (Lasagna-Reeves et al., 2012a, 2011; Usenovic et al., 2015), although others have reported that tau monomers are the fundamental toxic species (Michel et al., 2014). Although the transcellular spread of tau pathology has become a well-known, experimentally-confirmed phenomenon, the mechanisms through which this process occurs have however remained elusive. It was recently reported that the internalisation of tau K18 fibrils occurs via binding with heparan sulphate proteoglycans (Holmes et al., 2013) whilst the extracellular release of 4R0N tau occurs by exocytosis mediated by interaction with the DnaJC/Hsc70 molecular chaperone complex (Fontaine et al., 2016). It however remains unknown as to whether all tau isoforms and fragments and their FTD variants are internalised and secreted through these same processes. As the scope of research in this area grows, the importance of recombinant tau will undoubtedly increase. Certainly, recombinant tau proteins of the highest purity and yield will be essential to produce reliable and reproducible data in future studies investigating the cellular mechanisms involved in the spread of tau toxicity as well as the *in vitro* structural, biochemical and biophysical aspects of the protein's ability to cause disease. The present study has demonstrated a simple protocol for the preparation of tau K18 proteins for such investigations. This is the first report that focuses specifically on the expression and purification characteristics of K18 tau. Although Barghorn et al., (2005) earlier described a method that combines gel permeation and size exclusion chromatography for the purification of tau isoforms and constructs, a general protein yield range was provided (10-100 mg/10 L culture), with no specific value given for K18 tau. Protein yields for the tau constructs and isoforms vary (Barghorn et al., 2005), possibly due to the different structural and functional characteristics exhibited by these proteins. For this reason, studies dedicated to documenting expression and purification approaches for each tau protein is necessary to inform future research. Such reports are available for the adult human brain tau isoforms and some truncation constructs (Table 4.1), although the procedures described mostly depend on methodologies that are unavailable in many labs. In contrast, the protocol described in the present study makes use of a simple, inexpensive approach to purify both WT and mutant K18 tau proteins in high yield,

without compromising on the purity. This protocol can be adapted for the preparation of the other tau proteins. In fact, we have successfully used this protocol in our laboratory to express and purify several other tau proteins, including K18 and the full-length isoform carrying FTDP-17 mutations not described here, with similar protein quality and yield (data not shown).

4.5 Conclusion

We have investigated specific parameters affecting the production of the recombinant tau protein, reporting on conditions that may ensure optimal expression. Using these parameters, the tau MT repeat domain (K18) and two FTD variants were expressed and purified, leading to pure proteins of high concentrations. The purified proteins were natively unfolded and followed the classical fibrillisation pathway to form mature PHFs. The formation of filaments initiated a shift in secondary structure re-organisation from mostly random coils towards β-sheet formation. As such, this report demonstrates efficient methods for the production of tau protein that can be used in *in vitro* and *in vivo* studies.

5| Preparation of stable tau oligomers for cellular and biochemical studies

5.1 Introduction

The gradual intracellular accumulation of tau aggregates into NFTs is a clinical hallmark for diagnosing and staging AD (Braak and Braak, 1991). Nonetheless, tau pathology likely develops several years prior to symptom onset (Bateman et al., 2012). Indeed, cell death and synaptic lesions have been observed independent of NFT formation (Andorfer et al., 2005; Polydoro et al., 2009), prompting a need for tau biomarkers that better correlate with disease onset and progression (Beason-Held et al., 2013). Increasing evidence suggests that the activities of LMW oligomers, formed during the early nucleation stages of tau aggregation, likely associate with neurotoxicity that leads to AD pathology (Lasagna-Reeves et al., 2012a, 2012b, 2011). For example, tau oligomers induce mitochondrial, synaptic and memory defects (Lasagna-Reeves et al., 2011). Conversely, insoluble filaments have been postulated to provide neuroprotective functions since they sequester toxic oligomers into inert filaments (Gendron and Petrucelli, 2009). Many studies of tau oligomer neurotoxicity use recombinant proteins, due to the close properties they share with Alzheimer brain-derived tau (Fá et al., 2016; Frost et al., 2009; Usenovic et al., 2015). However, the transient formation and further aggregation of LMW tau oligomers presents a daunting challenge for their preparation and characterisation. Several tau oligomer preparation protocols that seek to address these difficulties have therefore been described (Bader et al., 2011; Lasagna-Reeves et al., 2010; Nübling et al., 2012b; Ren and Sahara, 2013). Nonetheless, a critical persisting challenge is the stability of the resulting oligomers. For example, htau40 oligomers prepared by seeding monomer aggregation with preformed α-synuclein or amyloid β oligomers lose their stability and aggregate completely into filaments within 48 h of incubation incubation (Lasagna-Reeves et al., 2010). This suggests that oligomers prepared *in vitro* are unstable and are prone to further aggregation, which may affect experimental outcomes and reproducibility due to the distinct conformations that tau adopts during aggregation (Combs et al., 2016;

Kumar et al., 2014). This instability has previously been demonstrated for amyloid β, another AD-linked protein, which is capable of undergoing detectable aggregation even when stored at an ultralow temperature (-80 ^{o}C) for long periods (O'Nuallain et al., 2011).

Tau aggregation occurs by two known mechanisms: (i) cysteine-dependent, whereby polymerisation occurs by intermolecular disulphide bonding (Bhattacharya et al., 2001; Schweers et al., 1995), and (ii) cysteine-independent, which occurs through the hexapeptide motifs (^{275}VQIINK^{280} and ^{306}VQIXXK^{311}) and non-covalent bonding between monomer molecules (Bergen et al., 2000; Goux et al., 2004; Li and Lee, 2006). Although either mechanism is sufficient, aggregation efficiency is increased in the presence of both (Sahara et al., 2007). It was therefore predicted that labelling cysteine residues in tau monomers would extend the stability of oligomers formed by blocking cysteine-dependent aggregation. Since maleimide binds strongly to cysteine residues, it was hypothesised that this conjugation would generate stable tau oligomers. In this chapter, a simple approach of preparing stable, LMW tau K18 oligomers by labelling cysteine residues with commercially available derivatives of maleimide, namely AF-maleimide and NEM is described. For efficient fluorescent labelling, and consistency between labelled and unlabelled proteins, cysteine modified K18 (C291A/C322A/I260C) will be used in this and the subsequent results chapter.

5.2 Results

5.2.1 Preparation of tau oligomers from monomers

Existing methods for tau oligomer preparation differ substantially in reaction constituents, as discussed above in section 5.1. Particularly, the addition of polyanion inducers to accelerate aggregation may therefore adversely affect the structure and stability of oligomer species (Ramachandran and Udgaonkar, 2011; Ren and Sahara, 2013). To circumvent these challenges, tau oligomers were prepared by overnight incubation of freshly-prepared monomers in quiescent conditions at RT, by diluting samples in 10 mM Na_2PO_4 buffer pH 7.4. The choice of Na_2PO_4 buffer was informed by its crucial role in maintaining phosphate

homeostasis in physiological conditions (Penido and Alon, 2012) and non-interference in biophysical assays including CD (Kelly et al., 2005). Overnight incubation of low starting protein concentrations of 100 μg/ml (5.5 μM) was sufficient to induce small oligomer formation, as characterised by dot blot assays confirming the presence of both total and oligomeric tau (Fig. 6.1). The total tau blot intensity was almost identical for WT and the two FTD-causing mutations, indicating equal starting concentrations (Fig. 5.1A and B). Oligomer formation was observed by immunoreactivity to the T22 antibody which is believed to react exclusively with tau oligomers (Lasagna-Reeves et al., 2012a, 2012b). By visual inspection, WT tau and N279K tau gave noticeable T22 dot blot intensities whilst V337M tau had a peculiarly poor output (Fig. 5.1). The observed V337M-T22 poor reactivity may have occurred due to one of two possibilities: (i) the T22 epitope on tau falls within the region of V^{337}, the mutation of which to methionine may have reduced the protein-antibody interaction (the exact T22 epitope is unknown); or (ii) the V337M mutation reduces initial steps of K18 oligomerisation, hence an inadequate population of oligomers was produced. This issue will be resolved by direct monitoring of oligomer formation with AFM (section 5.2.2).

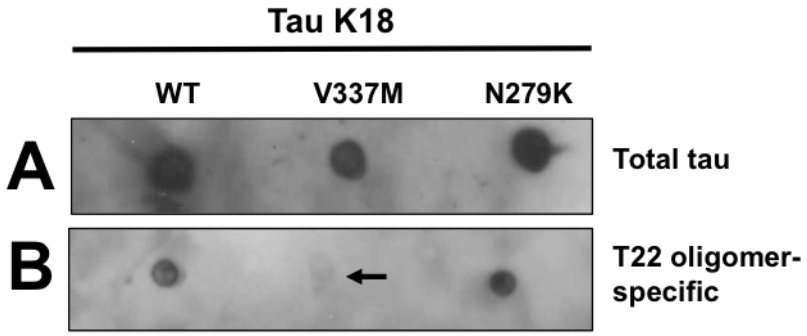

Figure 5.1. Characterisation of oligomer formation by WT and pathologic tau K18 using an oligomer-specific antibody.
(A) Dot blotting analysis of immuno-reactivity of WT K18 and its V337M and N279K pathologic variants to the A0024 total tau antibody. (B) K18 WT and K18 N279K samples, but not K18 V337M, were strongly reactive to the T22 conformation-specific antibody. Arrow points to K18 V337M dot blot.

5.2.2 Structural characterisation of tau oligomers

Having identified a viable method of oligomer preparation, the next step was to directly visualise and structurally characterise the oligomers formed. For this, AFM was used as it allows direct observation of small oligomers and preserves their

nano-structural features (shapes and sizes) akin to their native state (Tinker-Mill et al., 2014). AFM imaging revealed that overnight incubation at RT induced monomers of tau K18 WT, V337M and N279K to aggregate into a heterogeneous assembly of LMW granular oligomers (Fig. 5.2A-C). This indicates that the variable immunoreactivity of the oligomers to the T22 antibody in Fig. 5.1 was likely due to altered conformations that changed their immunoreactivity.

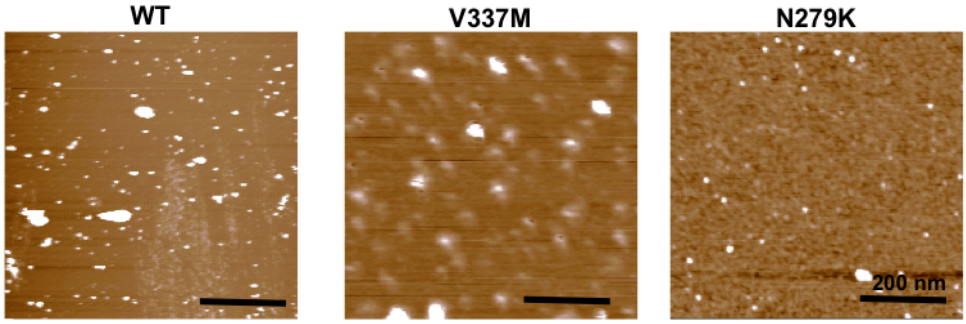

Figure 5.2. Structural characterisation of tau K18 oligomers using AFM. *Oligomers were prepared as described in section 2.17, and their structural features analysed using AFM. Granular structures were observed for each K18 variant. Scale bars = 200 nm.*

5.2.3 Oligomer preparation with regards to the aggregation pathway

One way to demonstrate authenticity of the recombinant tau monomers from which the oligomers were prepared was to investigate their capacity to undergo the Alzheimer-like aggregation process. To do this, the K18 WT protein which is known to self-polymerise from monomers into insoluble filaments was used. Freshly-purified samples were induced with heparin and their ability to undergo the tau aggregation process characterised with negative-stain TEM incubation at 37 ^{o}C. Sample aliquots were imaged without ultracentrifugation in order to identify the co-existence of different tau aggregates. As anticipated, monomers aggregated first into oligomers and subsequently into protomers and then to mature filaments (Fig. 6.3). This confirms the authenticity of the recombinant proteins used in this study.

5.2.4 The K18 tau repeat domain construct forms filaments of diverse structural morphology

WT tau K18 forms two major forms of filaments: paired helical and straight filaments (PHF and SF respectively) (Barghorn and Mandelkow, 2002). A means to characterise the authenticity of recombinant preparations of this construct is therefore to carefully observe the structural details of mature filaments and make

comparisons with the literature. Most filamentous structures (~90 %) were paired helical in appearance, with the rest being SFs (Fig. 5.4). In addition to the general PHF previously reported, it was found that these structures can further interact to form more complex aggregates through crosslinking, intertwining or by forming a "meshwork" of aggregates. Taken together, this data further confirms the authenticity of the tau proteins used in this study.

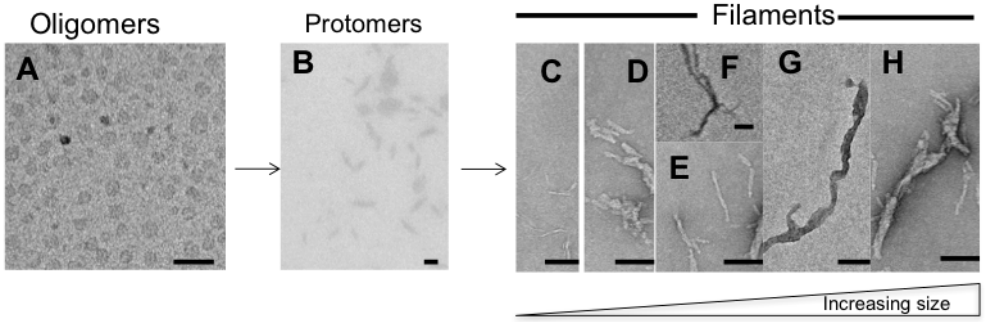

Figure 5.3. The tau monomer preparations from which the oligomers were produced were capable of recapitulating the tau aggregation pathway in vitro.
(A) Tau K18 WT monomers grow into granular oligomers. (B) The oligomers aggregate into protomers. (C) to (H) are filamentous aggregates of increasing maturity (both in terms of length and diameter) are formed. Scale bars = 100 nm.

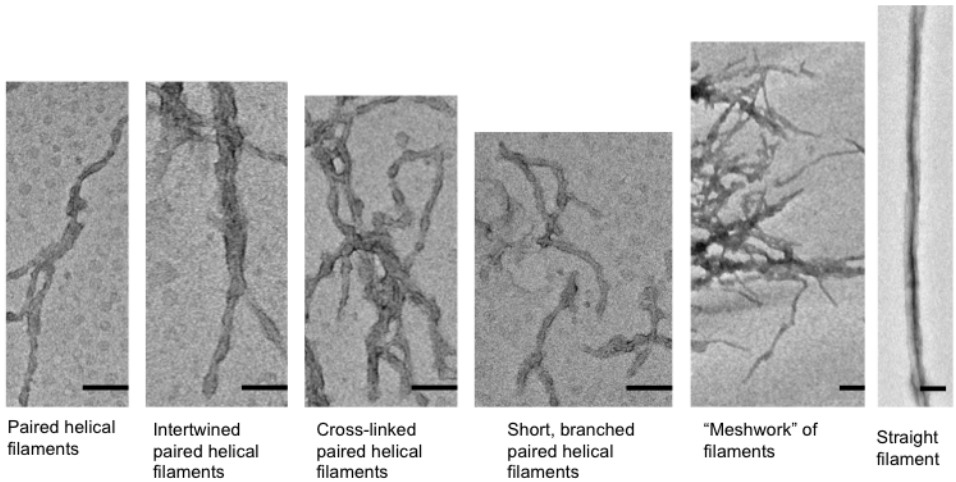

Figure 5.4. WT tau K18 forms mature filaments of diverse morphology.
The majority of filaments were PHFs, with a few others presenting as SFs and rarely a "meshwork" of filaments. Scale bars = 100 nm.

5.2.5 Preparation of fluorescently-labelled tau oligomers

The pro-aggregant MT repeat domain of tau (the K18 fragment) was used in all experiments because demonstrating oligomer stability for this aggregation-prone functional tau domain would in principle make the method applicable to the full-length isoforms which are less aggregation-prone.

Two methods of fluorescent labelling of tau with AF-maleimide were compared in an attempt to identify a more suitable option: Bader et al., (2011) and Michel et al., (2014). The main difference between these protocols is the provision of a reducing environment to hydrolyse apparent cysteine-dependent oligomers to monomers to ensure accessibility of sulfhydryl groups to fluorophores. Whilst the former method labels tau proteins irrespective of their aggregation state, the latter ensures that the proteins are initially treated with the reducing agent TCEP. Using the Bader et al., (2011) method, labelled proteins existed as a multimer of a distinct size (Fig. 5.5A). On the other hand, the Michel et al., (2014) method reduced the samples to monomers before maleimide treatment. This protocol was modified to enable oligomer preparation by overnight incubation of labelled monomers at RT without heparin. This approach was found sufficient for the preparation of small oligomers of multiple variants of tau, including: (i) WT and N279K tau K18; and (ii) His-tagged and tag-free WT K18 (Fig. 5.5 A).

The modified Michel et al., (2014) method was adopted for further use because it: (i) uses a simple "one-pot" approach for fluorescent labelling and oligomer preparation; (ii) had better labelling efficiency than the alternative method; (iii) the labelled oligomers were a heterogeneous mixture of monomers, dimers and trimers, which likely resembles the human AD brain state (Lasagna-Reeves et al., 2012a).

5.2.6 Fluorescently-labelled tau oligomers exist principally as trimers

The established method of preparing fluorescent tau oligomers was extended to prepare WT and two FTD tau K18 oligomers for application in cell culture studies. Oligomers were prepared by initially treating freshly-purified proteins with the reducing agent TCEP for 1 h to completely monomerise apparent oligomers to ensure exposure of cysteine residues. Thereafter, the exposed sulfhydryl groups

were labelled with 4x molar excess of AF-maleimide and the reaction allowed to proceed at 4 ^{o}C overnight (~ 15 h) following by extensive dialysis to remove excess dye and TCEP. Oligomerisation at low temperatures tended to increase labelling efficiency thereby reducing the likelihood of unlabelled contaminants.

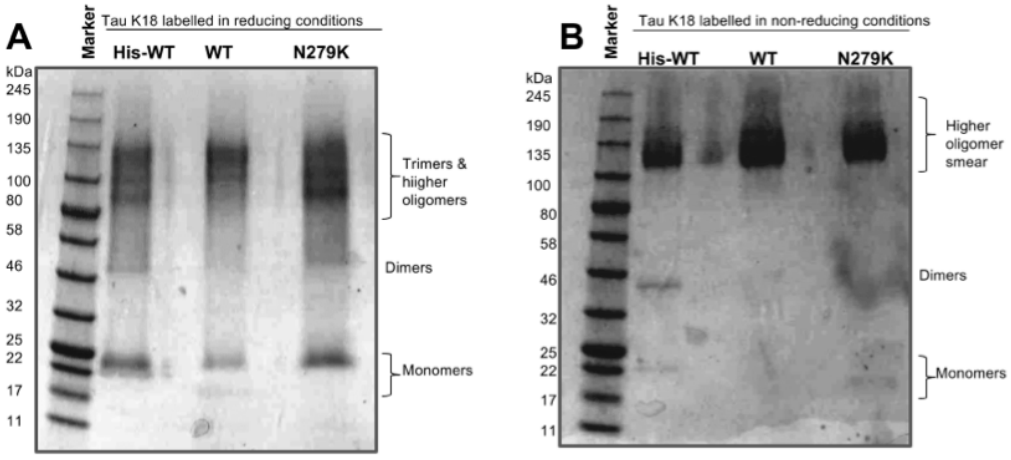

Figure 5.5. Comparison of two methods of fluorophore labelling of tau oligomers. *(A) Non-denaturing SDS-PAGE analysis of tau K18 labelling according to the protocol of Michel et al., (2013) J Biol Chem 289: 956–967. (B) Non-denaturing SDS-PAGE analysis of the AF-maleimide labelling of tau K18 proteins following the method of Bader et al., (2011) Biochem Biophys Res Commun 411:190-196.*

The labelled proteins aggregated into granular, LMW oligomers akin to those reported from other recombinant expression protocols (Lasagna-Reeves et al., 2010) (Fig. 5.6A and B). Unlabelled control proteins were prepared same way as the labelled proteins but supplied with identical volumes of buffer (10 mM Na_2PO_4 pH 7.4) instead of AF-maleimide. No detectable difference in oligomerisation patterns was observed between the labelled and unlabelled proteins (Figs. 5.6A) because unlike dimer-forming crosslinking techniques which restrict oligomerisation mainly to even ordered species, AF-maleimide does not appear to limit the polymerisation flexibility of target proteins.

5.2.7 Cysteine-specific labelling with maleimide derivatives stabilises tau oligomers

To test the hypothesis that cysteine labelling interferes with tau aggregation, the AF-maleimide labelled oligomers and unlabelled controls were challenged with the aggregation inducer heparin and heated at 37 ^{o}C under quiescent conditions for 48

h. Afterwards, aliquots were taken from each reaction solution after quick mixing and analysed by TEM. The labelled proteins existed mostly as granular oligomers (Fig. 5.7A), and were of similar structure as those imaged prior to heparin and heat treatment (Fig. 5.6Bii). On the contrary, the unlabelled protein underwent the complete aggregation process to form mature insoluble filaments, via intermediate protomers and early-stage filaments (Fig. 5.7B). These results indicate that AF-maleimide labelling stabilises tau oligomers and prevents their aggregation and conformational change into PHFs.

As a further test of tau oligomer stabilisation, conformations of the labelled and unlabelled proteins were studied by probing their immunoreactivity with a total tau antibody (A0024, Dako) and an oligomer-specific antibody (T22, Merck Millipore). Based on the above TEM findings for heparin-treated tau, it was hypothesised that the labelled proteins will be less immuno-reactive to the oligomer-specific antibody (because it formed a heterogeneous mix of monomers and LMW oligomers compared to the unlabelled protein which was additionally abundant in large oligomers and protomers which may be T22 reactive) whilst both proteins will be similarly reactive to the total tau antibody (since equimolar concentrations of monomeric tau were used). In the dot blotting experiments, the labelled and the unlabelled proteins gave near-identical reactivity to the total tau antibody (Fig. 5.7C and D). No significant difference was recorded in semi-quantitative analysis of immuno-reactivity to the A0024 antibody (based on normalised intensities to the unlabelled; Mann Whitney test, $p = 0.3429$). The situation was rather different when the proteins were probed with the T22 antibody, with immunoreactivity being significantly less for the labelled protein (Mann Whitney test, $p < 0.0286$; Fig. 5.7C and D). This corroborates earlier TEM findings that AF-maleimide labelling prevents filament formation (Fig. 5.7A). It can therefore be concluded that AF-maleimide labelling stabilises LMW tau K18 oligomers.

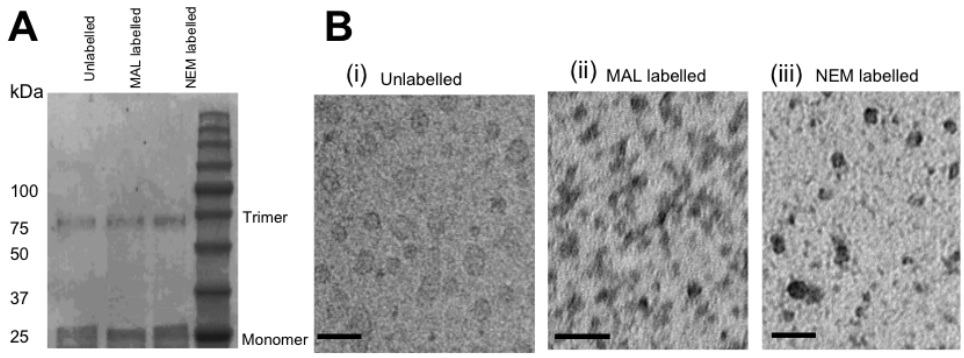

Figure 5.6. Preparation of tau K18 oligomers stabilised by crosslinking with maleimide derivatives.
(A) Non-denaturing SDS-PAGE analysis of oligomers prepared without crosslinking (Unlabelled; lane 1) or by labelling tau K18 with AF-maleimide (MAL labelled; lane 2) or NEM (NEM labelled; lane 3). (B) Negative stain TEM micrographs of oligomers prepared with or without crosslinking. Scale bars = 50 nm.

Next, the question was asked if the observed oligomer-stabilising property of AF-maleimide was shared by other maleimide derivatives. For this, the alkylating agent NEM which reacts in a similar mechanism as AF-maleimide with sulfhydryls to form stable thioesters was tested. NEM labelling of tau K18 was performed as described above, and the labelled oligomers were mainly dimeric and trimeric in distribution, same as for AF-maleimide labelled (Fig. 5.6A). To test their stability, the formed oligomers were treated with heat and heparin for 48 h and characterised by TEM and dot blotting. It was observed that, like AF-maleimide, NEM labelling stabilised tau oligomers and blocked further aggregation into filaments (Fig. 5.8A and B). Moreover, the immuno-reactivity pattern between the labelled and the unlabelled proteins was similar to what was observed earlier for AF-maleimide, with the labelled oligomers being significantly less reactive to the T22 antibody (Mann Whitney test, $p < 0.0286$) but similarly reactive to the A0024 antibody ($p = 0.6857$; Fig. 5.8C and D). Altogether, cysteine-specific labelling of the tau repeat domain with AF-maleimide and NEM appears to enhance the stability of oligomers.

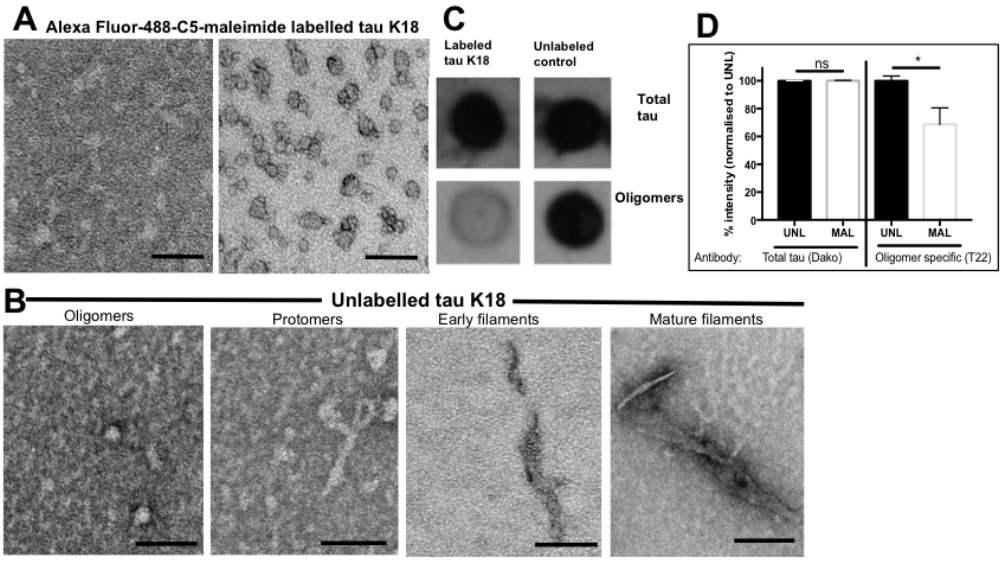

Figure 5.7. Crosslinking with AF-maleimide stabilises tau K18 WT oligomers and prevents their aggregation into Alzheimer-like filaments.
*(A) Representative TEM micrographs of tau K18 oligomers labelled with AF-maleimide. (B) Representative TEM micrographs of unlabelled control aggregates. Scale bars = 100 nm. (C) Representative dot blot data for the reactivity of labelled and unlabelled tau K18 to two tau antibodies (A0024, top panel) and T22 (bottom). (D) Semi-quantitative analysis of dot blot intensity using Image J. Mann Whitney test, * = $p<0.05$, ns = not significant.*

A model by which AD pathology propagates in the human brain is through the transmission of toxic tau proteins between neurons in some specific brain areas (Guo and Lee, 2014). A critical step in this interneuronal transmission model is the uptake of extracellular tau into neighbouring neurons, followed by their interaction with endogenous proteins and subsequence release of tau aggregates to template new internalisation cycles (Guo and Lee, 2014). For better understanding of the molecular cascade of events occurring in this process, real-time microscopic visualisation of live cells will be necessary. As oligomers are thought to be the most crucial species regulating the interneuronal transmission of tau pathology (Gerson and Kayed, 2013), the molecular fluorescence of AF-maleimide was used to study the real-time internalisation of stabilised extracellular tau K18 oligomers into the neuron-like cell line SH-SY5Y human neuroblastoma cells. Labelled tau was diluted in extracellular medium bringing the final concentration to 5 μM and supplied exogenously to cultured cells and incubated for 24 h. Thereafter, the spent medium was removed, the cells washed with warm PBS to remove non-internalised tau and the internalised fluorescent proteins visualised by confocal microscopy

after new tau-free medium containing nuclear and cell membrane markers had been added. The internalised proteins exhibited diverse morphological phenotypes, with some appearing as diffused whilst others were speckled (Fig. 5.9A). These phenotypes were similar to those reported for labelled K18 tau internalised in the same neuroblastoma cell line (Michel et al., 2014), as well as other mammalian cell lines (Sanders et al., 2014). To extend the applicability of fluorescent stabilised oligomers in cellular assays to neurons, hiPSC cortical neurons were prepared and seeded with extracellular tau prepared identically as the above. Maximum projection of z-stack confocal images revealed that tau oligomer internalisation occurred by endocytosis (since they were encapsulated by the vesicular marker FM4-64®) and that the inclusions accumulated both in the soma and neurites, hence providing insights into the subcellular localisation of tau oligomer inclusions and their morphological phenotypes (Fig. 5.9B). Altogether, these findings demonstrate that maleimide stabilisation offers a unique strategy for the characterisation of cellular internalisation of tau oligomers.

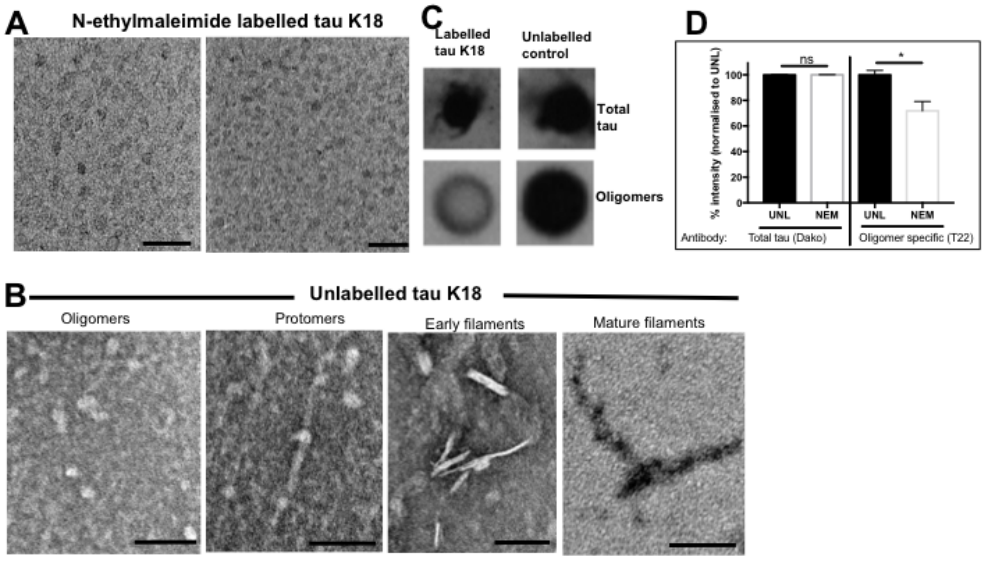

Figure 5.8. NEM labelling stabilises tau K18 oligomers in their granular conformation.

*(A) Representative TEM micrographs of NEM-labelled tau K18 oligomers. (B) Representative TEM micrographs of unlabelled control aggregates. (C) Representative dot blot data for the reactivity of labelled and unlabelled tau K18 to two tau antibodies (A0024, top panel) and T22 (bottom panel). (D) Semi-quantitative analysis of dot blot intensity using Image J. Mann Whitney test, * = $p<0.05$, ns = not significant. Scale bars = 100 nm.*

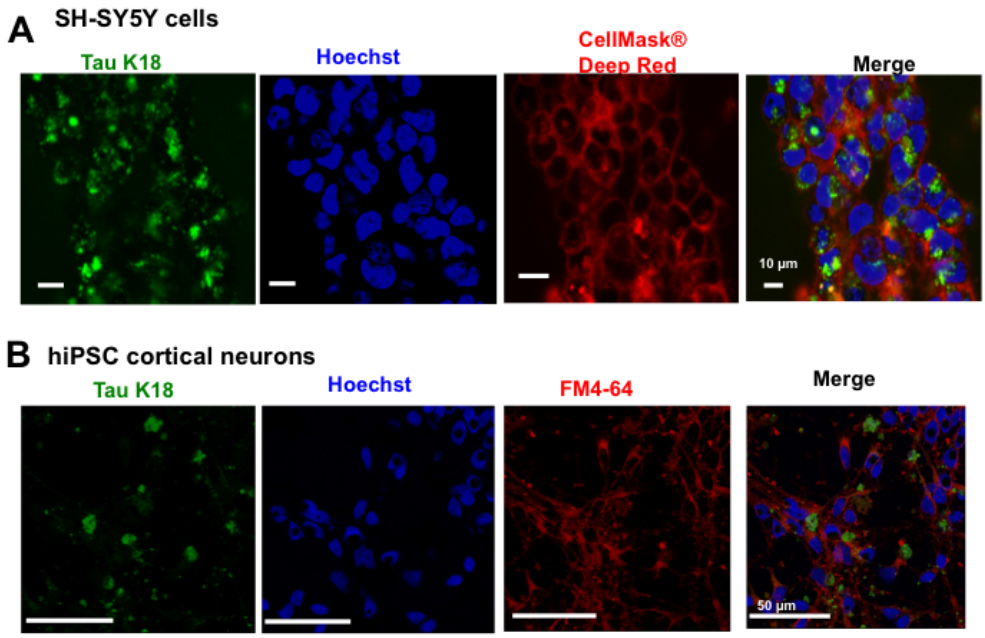

Figure 5.9. Extracellularly-applied stabilised tau K18 oligomers are internalised by human neuroblastoma cells and cortical neurons.
(A) Uptake of AF-maleimide-labelled K18 WT oligomers by SH-SY5Y cells, observed by confocal microscopy. Internalised proteins appeared localised both in the cytoplasm and nucleus. (B) Internalisation of extracellular oligomers was studied in hiPSC-derived neurons, revealing their localisation in neurites and soma. Scale bars = 10 µm in (A) and 50 µm in (B).

5.3 Discussion

Labelling with AF-maleimide or NEM provides the rare advantage of stabilising oligomers of the rather aggregation-prone tau K18. The proposed simple strategy herein described (Figs. 5.10 and 5.11) ensures that preformed tau oligomers remain in their desired authentic oligomeric state for extended periods of time, offering an exceptional opportunity to advance downstream investigations into the biochemical, biophysical and neurobiological aspects of the elusive association between tau aggregation and neurodegeneration. Important advantages of this strategy are that: (i) maleimide labelling of tau is irreversible, making oligomer hydrolysis difficult, (ii) it does not appear to directly influence the hierarchical order of aggregation. Moreover, the method is simple, time efficient and does not require expensive pre- and post-treatment stages. The proposed approach is potentially applicable to brain derived tau oligomers, and will support studies of mechanistic and conformational changes in tau oligomers that may alter the

protein's neurotoxicity and drug-reactivity profiles. Additionally, the method can be extended to other proteinopathic proteins such as huntingtin, and amyloid β containing cysteine residues. This approach has been applied to obtain novel insights into the subcellular internalisation and neuronal transmission of exogenous wild type tau K18 and several of its FTD variants (data not shown). The results indicate that this method provides a quick and reliable approach of monitoring cellular internalisation of exogenous proteins in real time, and therefore offers an advantage over fluorescent tags especially for small proteins like tau K18.

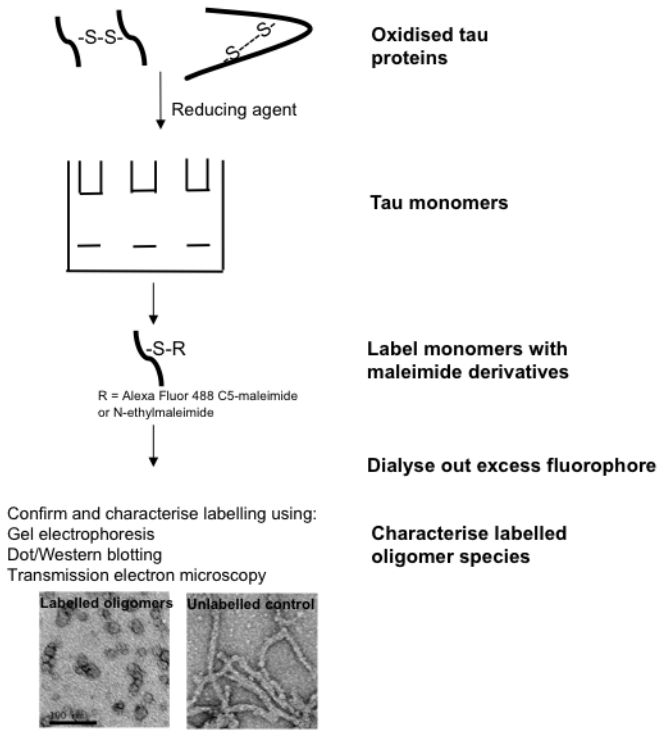

Figure 5.10. Schematic illustration of the tau oligomer stabilisation method described in this study.
Provision of a reducing environment minimises tau protein aggregation. Monomers are then labelled with AF-maleimide or NEM, and oligomer formation and stabilisation probed by heparin-induced aggregation.

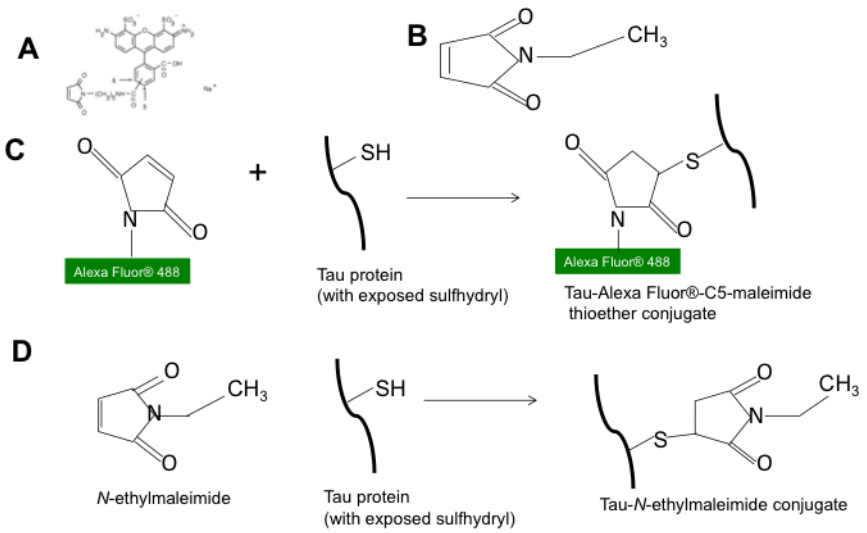

Figure 5.11. Schematic illustration of the chemical reaction involved in labelling of tau protein with maleimide derivatives.
(A) Molecular structure of AF-maleimide. (B) Reactivity of the maleimide functional group with a sulfhydryl group on tau protein to produce a stable thioether conjugate.

Furthermore, the neuronal internalisation and release of extracellular tau oligomers are regulated by protein-cell membrane interactions details about which is unclear. This oligomer stabilisation strategy offers a straightforward approach to study conformational and aggregation dynamics of protein-membrane interactions both at the single and bulk molecule levels using fluorescent spectroscopic and cell biology techniques. Additionally, stabilised oligomers are ideal immunogen candidates for antibody production against tau oligomer-targeted immunotherapy.

6| Distinct conformations, aggregation and neuronal internalisation of different tau strains

6.1 Introduction

A characteristic feature of tauopathies is the intracellular accumulation of NFTs composed of aggregated misfolded tau (Spillantini and Goedert, 2013). These misfolded proteins can be formed when tau loses its ability to bind to and support MT assembly, but rather forms insoluble aggregates that eventually develop into NFTs (Alonso et al., 1994; Barghorn et al., 2000a; Vogelsberg-Ragaglia et al., 2000). Whilst the monomeric, physiological form of tau is natively unfolded, the protein becomes increasingly enriched in β-sheets as it aggregates into soluble, granular oligomers and subsequently into protomers and then PHFs that make up the NFTs (von Bergen et al., 2005). Although mounting evidence suggests that tau dysfunction causes neurodegeneration, the mechanistic basis for this association is not fully understood, several recent studies have suggested that the characteristic stereotypical temporospatial development of tau inclusions across specific brain regions observed in AD may arise due to transmission of misfolded tau between synaptically connected neurons (section 1.6). This interneuronal propagation of misfolded tau, often referred to as "spread," is thought to initiate the functional and the structural impairments recorded in affected neurons and brain regions (Boluda et al., 2015; Usenovic et al., 2015). Therefore, the development of effective therapies for AD and other tauopathies would significantly benefit from improved understanding of the developmental pathway of this disease.

Efficiency of the interneuronal transmission of pathological tau is dependent on the conformations of the seed protein (the internalised) and the seeded (the recipient endogenous protein) (Alonso et al., 2016; Goedert et al., 2014; Scott et al., 1993). This has consequently given rise to the *tau strain hypothesis*, which suggests that misfolded tau proteins of different conformations (distinct strains) will vary in their ability to induce pathology due to variability in their interaction with endogenous proteins (Gerson et al., 2016; Narasimhan et al., 2017). By injecting human brain isolates from clinically confirmed tauopathy cases into non-tangle-forming transgenic mice brains,

Clavaguera et al., (2013) observed differential induction of tau inclusions depending on the diagnosis of the source of homogenate. Whilst tau inclusions that were formed after the intracerebral injection of isolates from human AD, PSP, AGD, tangle-only dementia, and CBD were propagated between connected brain regions, the aggregates formed in the case of PiD were limited to the inoculation site. Importantly, similar outcomes were obtained upon seeding WT mice with the same human tauopathy brain extracts, signifying that the ability of tau seeds to corrupt endogenous tau into forming aggregates was independent of the background of mice used (Clavaguera et al., 2013). Furthermore, intracerebral inoculation of human AD and CBD brain extracts into young PS19 transgenic mice led to cell type specificity in the formation and propagation of tau inclusions and induction of neuron loss (Boluda et al., 2015). Whilst tau inclusions were limited to oligodendrocytes of the fimbria and white matter around the site of injection after introducing tau from CBD patients, the tau inclusions formed after injecting AD tau were found in neuronal perikaya without evident oligodendrocyte involvement (Boluda et al., 2015). Recombinant full length and truncated tau (e.g. K18) have also been shown to propagate tauopathies by inducing endogenous tau to aggregate (Guo and Lee, 2011; Iba et al., 2013; Michel et al., 2014; Usenovic et al., 2015). This seeding capacity may be due to conformational similarity between the recombinant and endogenous tau used since the recombinant forms took on the conformation of endogenous tau from mice (Falcon et al., 2015).

It is unclear if misfolded tau conformers from FTD with tau mutations are distinct from those in AD, and also if they differ in their ability to seed endogenous tau aggregation. Whilst there is strong evidence supporting the interneuronal propagation of misfolded WT tau, little is known about same for tau-positive FTD. Answering this question will be critical to understanding the mechanisms by which AD and non-AD tauopathies develop, and to establish whether or not selectivity is required in drug development for tauopathies. In this chapter, the conformation and aggregation of tau K18 and two of its FTD tau variants, namely V337M and N279K, were studied using complementary biochemical and biophysical assays to ascertain if these mutations alter the conformation and the aggregation of the WT.

Modelling the tau interneuronal transmission process in cellular systems is challenging partly because endogenous tau is highly soluble and resists spontaneous aggregation in many cell lines, even in the presence of known pro-aggregant tau mutations such as P301L and R406W (Guo and Lee, 2011; Vogelsberg-Ragaglia et al., 2000). Additionally, genetic overexpression of tau poorly recapitulates the disease process due to its inhibition of cell division and proliferation, and compromise of MT stabilisation (Kanai et al., 1989; Vogelsberg-Ragaglia et al., 2000). To overcome these challenges, WT SH-SY5Y neuroblastoma cells and hiPSC neurons (dividing and non-dividing cells respectively) were exogenously supplied with WT and FTD tau K18 oligomers to study the biological consequences of the conformational differences (Chapter 5), as well as to investigate if these would influence their ability to be taken up by cells and to interact with endogenous tau. Since some forms of secreted tau are cleaved at the C-terminus (Plouffe et al., 2012), and the repeat region-containing forms of tau are more likely released by unhealthy neurons (Kanmert et al., 2015), focusing on the K18 fragment may provide disease-relevant understanding in the structural and neurobiological basis of tau transmission.

6.2 Results

6.2.1 FTD mutations alter tau K18 binding to ThT

The V337M and N279K mutations in the *MAPT* gene result in distinct forms of familial FTD, which reflect in differential pathology compared to tau-positive AD (Ghetti et al., 2015). The pathological consequences of the V337M and N279K tau mutations have been summarised (Table 6.1 and Fig. 6.1). To study the structural and functional biochemistry of WT and FTD K18, the ThT assay of aggregation kinetics and beta sheet formation was used. Using freshly-purified tau K18 WT, V337M and N279K samples treated with or without the polyanion inducer heparin, ThT fluorescence readings were taken every 5 min for 15 h. Analysis of pooled data from three independent experiments showed no detectable changes in fluorescence in experiments lacking heparin (data not shown). In heparin-induced aggregation, however, distinct ThT-binding behaviours were observed for each sample (Fig. 6.2). K18 WT displayed a lag time of ~5 h, following which fluorescence readings increased until 15 h (Fig. 6.2A). It is worth noting that the single-cysteine tau K18 WT (with a cysteine at positon 260) used in this study has a reduced aggregation rate but same β-sheet-enrichment mechanism of

aggregation compared to the native double-cysteine protein which was not used due to anticipated adverse effects of fluorescent labelling of cysteines located within the core of the repeat regions on MT dynamics in cell biology experiments (data not shown; Shammas et al., 2015 supplementary data). The reverse was the case for tau K18 V337M for which initial fluorescence readings at ~5000 a.u. decreased to ~3000 a.u. about halfway through the assay. No increase in fluorescence values was observed over 15 h for K18 N279K (Fig. 6.2C). These results suggest that tau K18 WT and the two variants formed aggregates of distinct conformations that were differentially recognised by ThT, consistent with findings that ThT binding to proteins of distinct β-sheet features is based on protein cavity size accommodation of ThT ions (Groenning et al., 2007). Similarly, protein aggregates of distinct morphologies have their bona fide characteristic ThT binding profiles due to differences in quantum yields that affect their inherent brightness and hence fluorescence (Lindberg et al., 2015). The increased ThT binding for WT K18 after the lag phase may be indicate of a shift from a conformation of low ThT binding to a new conformation of enhanced ThT binding during its aggregation. For K18 V337M, the conformational switch seems to have occurred from one of high ThT affinity to another of reduced ThT affinity due to the reduction in fluorescence observed in Fig. 6.2B. The conformation of N279K either did not change during the assay or the change did not reflect in altered ThT binding, hence the unchanged fluorescence measurements.

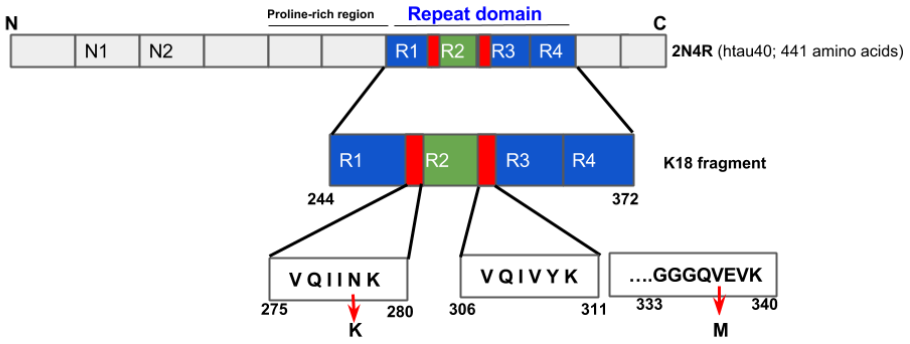

Figure 6.1. Schematic illustration of the molecular arrangement of the N279K and V337M tau mutations. *Tau K18 was constructed based on the htau40 sequence. The N279K mutation is located in the first hexapeptide motif (red) located at the start of the alternatively-spliced R2 region (green). V337M is located at the beginning of the fourth repeat region, and is a few amino acids away from the second hexapeptide motif (second red region).*

Table 6.1. Previously-reported pathological consequences of the V337M and N279K familial mutations and their impacts on aggregation and filament morphology of tau protein.

Familial mutation	Influence on tau aggregation and MT binding			Pathological consequences	References
	Aggregation kinetics and dynamics	**Dominant filament morphological phenotypes**	**MT binding**		
V337M	Aggregation rate and aggregate structures similar to the WT; increased 3R aggregation	Mostly PHFs	Reduces MT binding and stabilisation	Diffuse neuronal loss, astrogliosis, hippocampal and cortical tau deposition; delayed symptom onset; no insoluble aggregates in over-expressing cell lines; similar 4R tau levels in hiPSCs compared to WT.	(Barghorn et al., 2000; Combs and Gamblin, 2012; Domoto-Reilly et al., 2017; Ehrlich et al., 2015; Hong et al., 1998; Tanemura et al., 2002; Vogelsberg-Ragaglia et al., 2000)
N279K	Selective aggregation of 4R tau	Mostly SFs	Similar MT binding and assembly as the WT	Enhanced exon 10 splicing; tau accumulation in neurons and tufted astrocytes; higher 4R tau levels in hiPSCs compared to WT	(Barghorn et al., 2000; Dawson et al., 2007; Ehrlich et al., 2015; Hasegawa et al., 1999; Hong et al., 1998)

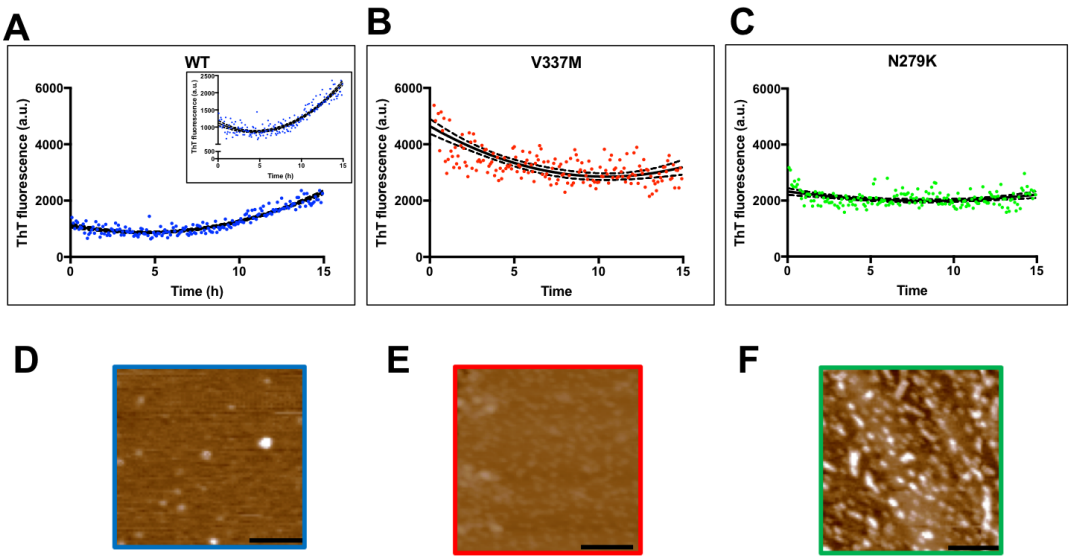

Figure 6.2. FTD mutations alter tau K18 binding to ThT. *(A), (B), and (C) Normalised ThT fluorescence readings for K18 WT, V337M, and N279K respectively (n = 3 each). (D), (E), and (F) AFM analysis of representative endpoint ThT assay samples for K18 WT, V337M, and N279K respectively (n = 3 each). Scale bars = 200 nm.*

6.2.2 AFM analysis of endpoint ThT assay samples provides insights into the aberrant binding of the tau K18 variants to ThT

Based on the unusual ThT binding characteristics of the variant tau K18 proteins, it was hypothesised that the FTD-associated proteins might be of different conformations compared to the WT. If this is true, the endpoint samples from the ThT assay should exhibit different structural features since they displayed variable ThT fluorescence at 15 h (Fig. 6.2A-C). To test this hypothesis, endpoint samples were subjected to AFM analysis to ascertain their structural properties. Distinct granular oligomers were recorded for K18 WT whilst V337M gave a mix of small and large oligomers. N279K had a combination of granular oligomers and filament-like structures. Altogether, the structural features and the stages of aggregation of endpoint WT and variant tau K18 samples appear distinct, which may explain their variable ThT binding characteristics.

6.2.3 The FTD familial mutations alter the ultrastructure of tau aggregates

Notwithstanding the importance of the ThT assay in providing insights into the stages of aggregation and folding of the tau K18 proteins, it fell short of describing the filamentous structures formed. Negative-stain TEM was therefore used to study the influence of the V337M and N279K mutations on tau K18 aggregate structures; each sample was induced with heparin and incubated at 37 °C for 4 days before being analysed. The WT protein predominantly formed PHFs and to a less extent SFs similar to those previously reported (Barghorn and Mandelkow, 2002). The PHFs structures varied in their degree of twisting, which was up to ~ 45^{o} (Fig. 6.3Ai –vii). On the other hand, SFs had no observable periodic twisting (Fig. 6.3Aviii). Tau K18 V337M formed two types of aggregates: large amorphous aggregates (Fig. 6.3Bi-iii) and short filamentous aggregates (Fig. 6.3Biv-v) whilst K18 N279K formed thick bundles of filaments of different width and length (Fig. 6.3Ci-vi).

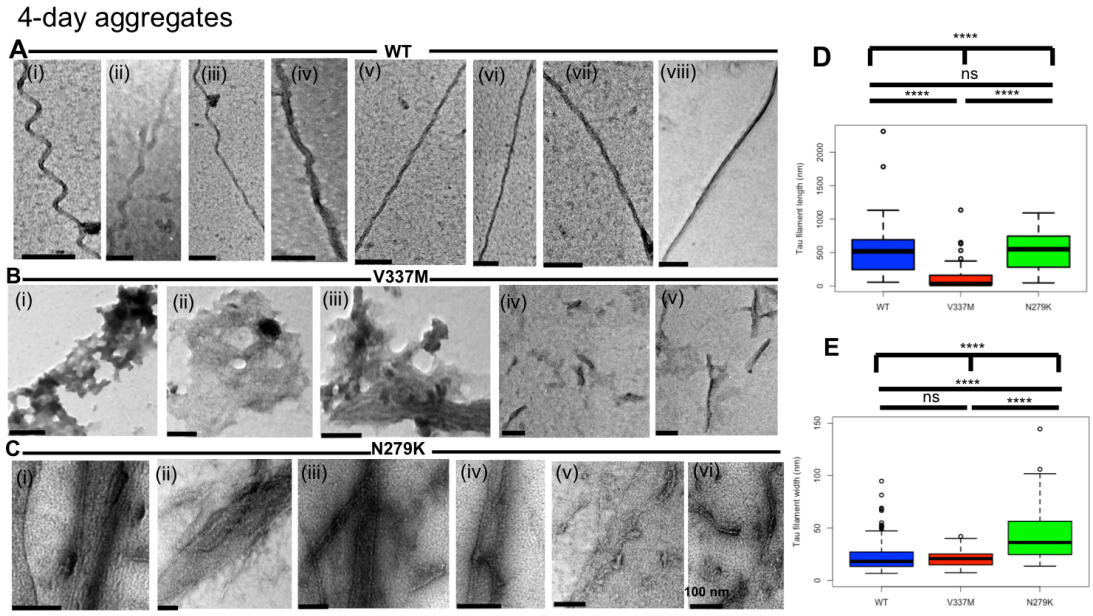

Figure 6.3. The V337M and N279K FTD mutations induce changes in the structural properties of tau K18 filaments. *(A), (B), and (C) Representative TEM micrographs for K18 WT, K18 V337M and K18 N279K aggregates respectively. Scale bars = 100 nm. (D) Boxplot of filament lengths. Kruskal Wallis test with Dunn's posthoc test, **** p<0.0001, ns = not significant. (E) Boxplot of filament widths. Kruskal Wallis test with Dunn's posthoc test, **** p<0.0001, ns = not significant.*

Quantitative information about filament structure was obtained by statistically comparing filament length and width identified from three independent experiments using Kruskal Wallis test with the Dunn's post hoc analysis. Mean filament lengths for K18 WT, V337M and N279K were 510 ± 361 nm, 106 ± 161 nm, and 534 ± 290 nm respectively. Significant difference was recorded between the mean filament lengths ($p<0.0001$). The WT formed significantly longer filaments than the V337M ($p<0.0001$) but not the N279K ($p>0.9999$). N279K filaments were also significantly longer than those of V337M ($p<0.0001$; Fig 6.3D). Moreover, filament widths for the three tau proteins were significantly different (mean filament width = 27± 64 nm for WT, 21± 7 nm for V337M and 52 ± 84 nm for N279K; $p<0.0001$), with those of the WT and V337M being comparable ($p=0.6698$; Fig. 6.3E). However, N279K filament width was significantly higher than the WT and V337M ($p<0.0001$ for both; Fig. 6.3E). Altogether, the two FTD mutations alter the morphology of tau K18 aggregates, causing a shift from PHF and SF for the WT to amorphous aggregates and significantly shorter but similarly wide filamentous aggregates for the V337M, and bundles of filaments of comparable length to the WT but increased thickness for the N279K.

6.2.4 Structural features of WT and FTD tau K18 aggregates are unchanged following prolonged incubation

Since aggregation and fracture are opposing forces in tau K18 aggregation (Meyer et al., 2016), it was investigated if the structural properties identified after 4-day incubation will be maintained on prolonged incubation. This was necessary because filament conformation is determined by the recruitment of soluble monomers and oligomers onto template conformers (Guo and Lee, 2014). It is conceivable that over extended reaction times, repeated cycles of breakdown and growth may result in the amplification of minor aggregate conformers which may not be identified in short incubation assays (Meyer et al., 2014b, 2016). Following the same experimental procedure as in Fig. 6.3, the incubation time was extended to 45 days, after which sample aliquots were analysed by TEM. The morphological phenotypes of tau aggregates formed by each protein were similar to those observed at 4 days: K18 WT formed PHF and SF whilst V337M formed both amorphous aggregates and short filaments, with N279K forming thick bundles of filament networks (Fig. 6.4). This data, combined with that in Fig. 6.3, indicate that the conformations of WT tau K18 aggregates are altered by the two FTD mutations, and that the new conformations

are stable and can withstand possible biochemical pressures when the reaction time is extended.

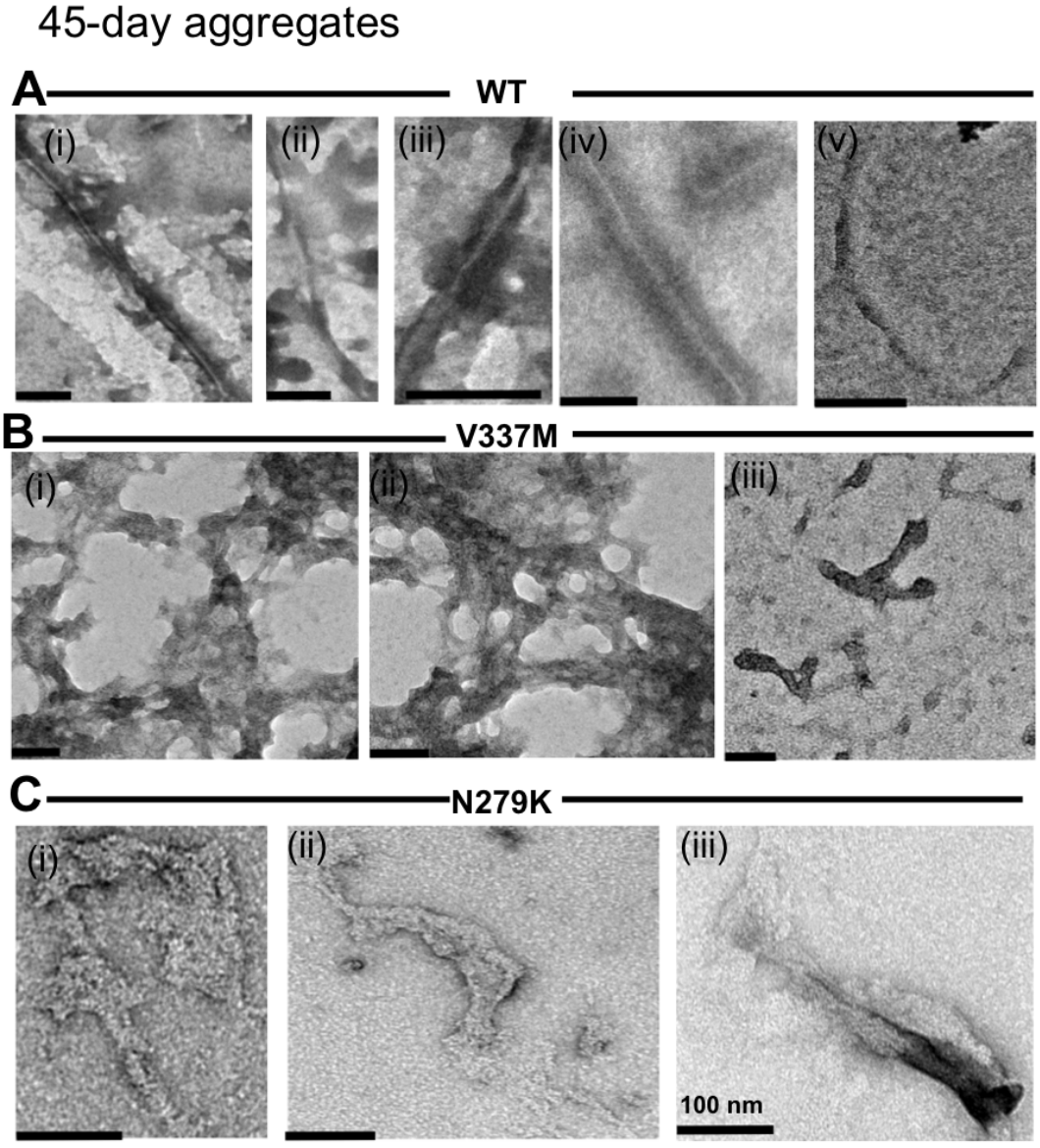

Figure 6.4. The structural distinctions between WT and FTD tau K18 aggregates are maintained following extended aggregation reactions. *(A), (B), and (C) Representative TEM micrographs for K18 WT, K18 V337M and K18 N27K aggregates respectively. Scale bars =100 nm.*

6.2.5 FTD mutations alter the dynamics of tau aggregation

Although the ThT binding data and associated AFM images (Fig 6.2) and mature filaments (Fig. 6.3 and 6.4) provided novel insights into the conformational and aggregational variability of WT and FTD tau K18, these experiments were unable to provide an understanding into the stepwise formation of aggregates. AFM was therefore used to probe

the stages of aggregation of each tau protein. To ensure consistency, the experimental setup followed that of the 4-day aggregation assay described above.

For K18 WT, samples at 0 h predominantly consisted of monomers and small oligomers of sizes 1 – 3 nm (Fig. 6.5A, green arrow) and to a limited extent small oligomers 5 – 10 nm in size (Fig. 6.5A, blue arrow). By 5.5 h, more 5 – 10 nm small oligomers had formed alongside larger oligomers 10 – 30 nm in size (red arrows) and polymers (> 30 nm). At 24 h, the polymers had shifted from the granular morphology to "stretched" structures of increased vertical length but reduced diameter. This stage likely signifies the transition to protomers. Small oligomers were still observable at this stage, indicating a gradual polymerisation process. At 72 h, short filaments of up to 100 nm could be identified (yellow arrows), which were further polymerised into complex filamentous aggregates by 96 h, similar to those observed in Fig. 6.3A.

In addition to monomers and small oligomers (1 – 3 nm), larger oligomers (5 – 30 nm) were observable for V337M at 0 h (Fig. 6.5 B). A high proportion of polymers were recognisable at 5.5 h, the diameters of which increased up to 200 nm by 24 h. Protomers and/or short filaments were also visible at 24 h (yellow arrow), with amorphous aggregates together with short filaments evident at 72 h. By 96 h, larger amorphous aggregates >1 μm (inset) were recorded in addition to short filaments. Morphologies of aggregates formed by tau K18 encoding the V337M mutation were similar to those recorded in Fig. 6.3B, providing strong evidence that the V337M mutation alters the aggregation of tau K18.

For tau K18 N279K, monomers and small oligomers were recognised at 0 h along with a few large oligomers (10–30 nm) and a few polymers (>30 nm; Fig. 6.5C). By 5.5 h, more large oligomers (red arrow) had been formed either from the amplification of small oligomers or breakdown of the polymeric aggregates observed at 0 h (orange arrow). Furthermore, globular aggregates, several of which were seen fusing together (orange arrow), were observed at 5.5 h and subsequently at 24 h (see inset). More globular aggregates were formed at 72 h through 96 h. These structures formed the "tracks" for dense networks of thick filaments (series of orange arrows at 72 h) which were more evident at lower magnification (inset at 96 h; Fig. 6.5C). Similar to the WT and V337M,

the endpoint aggregates formed by the N279K K18 tau recapitulate those recorded from earlier independent assays (Fig. 6.3C).

In summary, AFM allowed the characterisation of incipient aggregation of the three tau K18 proteins, with the results strongly corroborating initial findings from the TEM analysis of endpoint aggregation reactions. It can therefore be concluded that the V337M and N279K familial FTD mutations alter the aggregation features of tau K18, which may contribute to the phenotypic diversity observed in neurodegeneration involving WT tau and either familial mutation.

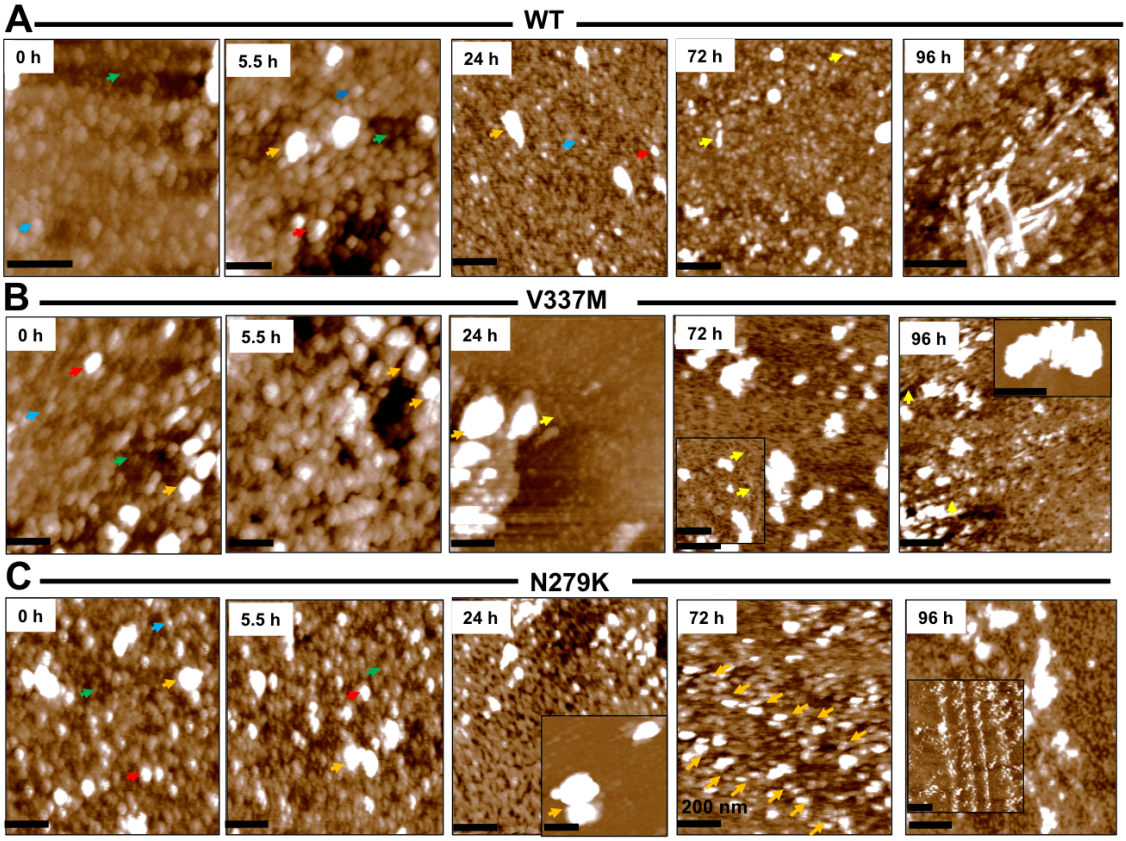

Figure 6.5. AFM imaging provides insights into the stages of tau K18 aggregation in the presence of FTD mutations. *Representative AFM images for 4-day aggregation of K18-WT, K18-V337M and K18-N279K are given in was (A), (B) and (C) respectively. Scale bars = 1 µm for the 96 h insets, and 200 nm for all other images.*

6.2.6 FTD mutations alter the immunoreactivity of aggregating tau K18

The distinctive ThT binding, structural and aggregation features of tau K18 carrying FTD alterations (Figs. 6.2 – 6.5), is consistent with the hypothesis that they alter the conformation of tau K18. Because conformational distinctions between variants of the same proteinopathic protein can lead to differential immunoreactivity profiles (Hatami et al., 2017), binding of tau K18 to specific antibodies was used to explore any further evidence of protein conformational differences. Each sample (1 mg/ml) was dissolved in 10 mM Na_2PO_4 pH 7.4 and incubated at 37 ^oC to promote polymerisation. Aliquots were taken at the specified intervals, diluted in half and then probed with the total tau antibody A0024 (Dako) or the oligomer-specific antibody T22 (Merck; (Lasagna-Reeves et al., 2012a)). Since oligomer formation is an important yet dynamic stage of tau aggregation (Fig. 6. 5), the rationale here was to probe the conformation of evolving oligomers during aggregation and as to whether aggregation induces changes in the proteins' immunoreactivity to the total tau antibody.

The WT was most reactive to the total tau antibody at 0 h when aggregation was at a minimum (Fig. 6.6 A and B, upper panels). Immuno-reactivity however quickly and consistently decreased with time, with the least intensity observed at 314 h (Fig. 6.6 A and B, upper panels). Immunoreactivity for K18 V337M was the poorest; dot blot intensity at 0 h was the highest throughout its time course, being comparable to the worst for the WT (Fig. 6.6 A and B, upper panels). Reactivity also decreased steadily from 0 h until 314 h. For K18 N279K, immuno-reactivity was similar to the WT, with high intensities in the early stages of aggregation which gradually weakened over time (Fig. 6.6 A and B, upper panels).

Next, reactivity to the oligomer-specific antibody was analysed by dot blotting and semi-quantified by densitometry. Similar to its reactivity to the total tau antibody, the WT K18 recorded higher immunoreactivity to T22 at the early stages of aggregation. This however dropped sharply from 168 h onwards, compared to the anti-total tau reactivity for the same protein (Fig. 6.6 A and B). For K18 V337M, reactivity was poor throughout the assay except at 24 h where the highest signal was recorded (Fig. 6.6 A and B; lower panels). Contrary to its reactivity to anti-total tau, K18 N279K had the least intensity to T22 which remained barely visible throughout the time course (Fig. 6.6 A and B; lower panels).

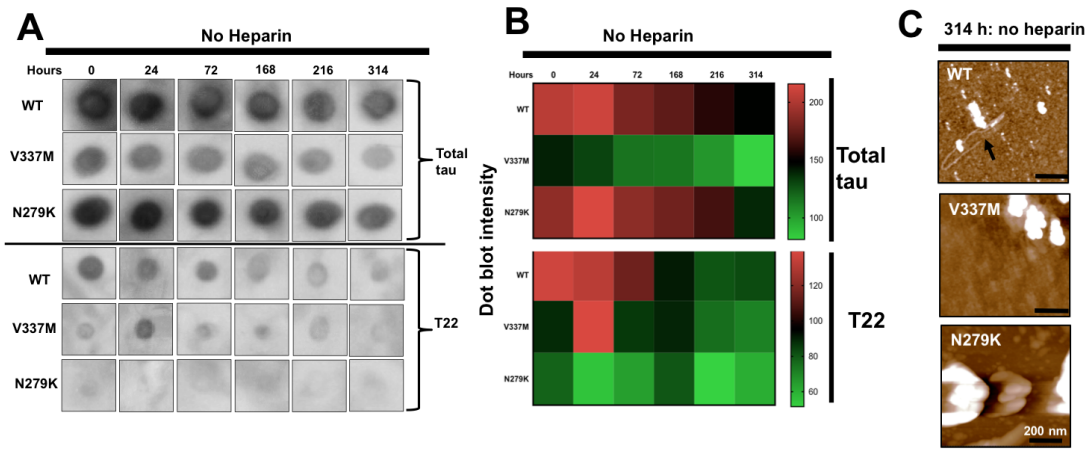

Figure 6.6. The V337M and N279K familial FTD mutations alter the immunoreactivity of tau K18. *(A) The conformations of tau K18 WT and its FTD variants aggregating without heparin were probed with the A0024 and T22 antibodies using dot blotting. (B) Semi-quantification of dot blot intensity using Image J. (C) AFM analysis of the 314 h dot blot samples. Arrow points to filaments. Scale bars =200 nm.*

6.2.7 AFM structural evidence support the variable immunological reactivity for the tau K18 proteins

As a further independent test of conformational variability, structural features of endpoint samples from the time course immunoreactivity experiments (Fig. 6.6 A and B) were analysed by AFM (Fig. 6.6C). Whilst the WT formed filamentous aggregates similar to those recorded in Figs. 6.3 – 6.5, the K18 encoding either V337M or N279K formed aggregates of distinct shapes and sizes (Fig. 6.6C). The V337M formed amorphous aggregates akin to those observed earlier whilst the N279K aggregates appeared similar to components of the dense filament networks described above (Figs. 6.3 – 6.5). Altogether, the WT and FTD K18 tau form aggregates of distinct morphologies, which in addition to the immunoreactivity data above, demonstrate that the V337M and N279K mutations modify the conformation and aggregation of tau K18.

6.2.8 WT and FTD tau K18 oligomers have distinct conformations

LMW oligomers are thought to be the seminal species responsible for tau-mediated neurodegeneration partly because they induce mitochondrial and synaptic defects independent of higher-order aggregates (Lasagna-Reeves et al., 2011). To exclude the possibility that the observed conformational diversity was limited to endpoint aggregates (Figs. 6.3 – 6.5) and aggregates in transition (Fig. 6.6), tau K18 oligomers were prepared and their conformation and structural properties characterised. After exploring several

protocols, overnight incubation of monomers at RT in the absence of inducers proved to be a viable strategy (Chapter 5). The oligomers had granular appearances, but the structural features appeared somewhat different between the WT and FTD variants (Fig. 6.7 A-C). Oligomer conformations, as measured by reactivity to the A0024 and T22 antibodies, were different (Fig. 6.7D). K18 WT and N279K had comparable reactivity to the total tau antibody whilst K18 V337M had reduced reactivity (Fig. 6.7D). K18 V337M reactivity to T22 was much lower compared to the WT, whilst K18 N279K had comparable intensity to the WT (Fig. 6.7D). Collectively, this approach for preparing LMW tau K18 oligomers allowed for the characterisation of disease mutation-specific effects on the protein's structure and conformation. Consistent with earlier findings for mature aggregates, oligomers of the V337M and N279K K18 variants adopted immunologically distinct conformations.

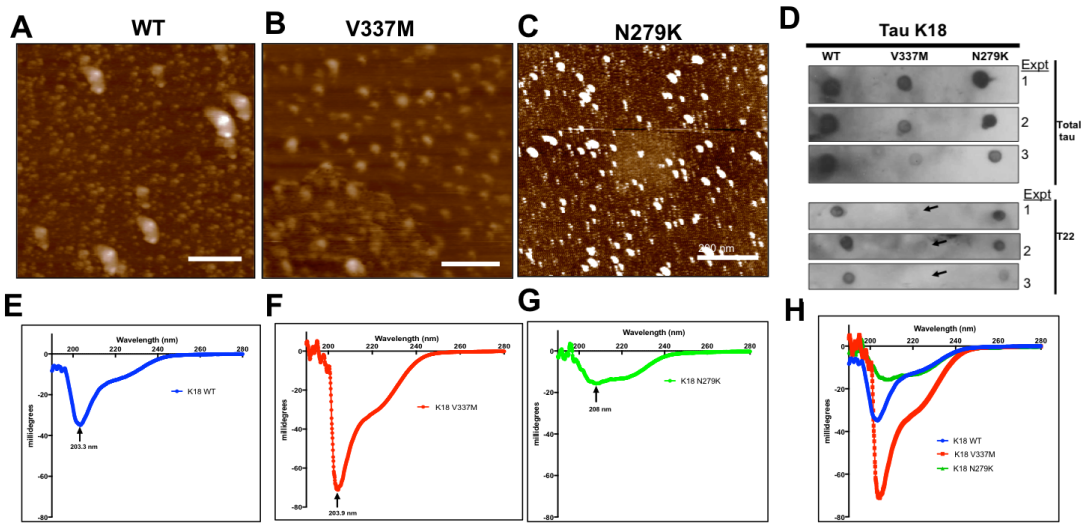

Figure 6.7. Characterisation of the conformation, shapes and size distribution of WT and FTD tau K18 oligomers. *(A), (B) and (C) are representative AFM images of tau K18 WT, V337M and N279K oligomers respectively prepared by overnight incubation of monomers RT. (D) Dot blot reactivity as a probe of oligomer conformation using two tau antibodies. Three independent experiments are shown (Expts 1, 2, and 3). Arrow points to sites of V337M blot. (E) – (H) Representative CD plots of oligomer secondary structure for K18 WT, V337M and N279K respectively, and their comparative assessment on a single graph. Scale bars =200 nm.*

6.2.9 Secondary structural features of WT and FTD tau K18

A hallmark of tau aggregation and its associated toxicity is the conversion of natively unfolded monomers to β-sheet-rich oligomers (Lasagna-Reeves et al., 2010). This rule however does not hold for all FTD variants because oligomer formation for K18 ΔK280 is

not characterised by β-sheet enrichment (Kaniyappan et al., 2017). Having previously shown that the WT K18 and its V337M variant are natively unfolded and that filamentous aggregation enhances β-sheet content (Karikari et al., 2017), oligomer secondary structure contents were investigated using CD spectroscopy. Contrary to monomers with negative peaks at 200 nm (Barghorn et al., 2000; Karikari et al., 2017), the oligomer had more appreciable β-sheet content signified by shifts in CD peaks to 203 nm for WT, 204 nm for V337M, and 208 nm for N279K (Fig. 6.7E-H). These CD peak profiles are intermediate between those of monomers and filaments (Barghorn et al., 2000; Karikari et al., 2017) and therefore indicate that the oligomers have less beta sheet content than the filaments. This means that the V337M and N279K mutations do not have detrimental effects on the ability of tau K18 oligomers to form β-sheet structures.

6.2.10 Dominant conformers of WT and FTD tau K18 are unaltered in the presence of competing species

Since specific mutations in tau K18 influence aggregate seed selection in the presence of multiple seeds of different conformations (Meyer et al., 2014a), it was investigated if the conformation of the tau proteins will be affected by the presence of competing conformers. In other words, some mutations can determine which tau seeds are preferentially polymerised over others. Although it has been established from the above that the WT and FTD tau proteins are of diverse conformations (Fig. 6.2 – 6.7), it is unclear if the observed conformations would persist as the dominant species should they be challenged with different conformers. As an initial experiment, 30-day aggregates of K18 WT (from Fig. 6.4) were used to seed monomers of all three proteins and the dominant conformers imaged by AFM after 11 days. Remarkably, the structures observed (Fig. 6.8) shared striking similarities with unseeded experiments in the presence (Fig. 6.5) or absence (Fig. 6.6C) of the inducer heparin, suggesting that the dominant conformers are unchanged when challenged with different tau strains. K18 WT, V337M and N279K formed long filaments, amorphous aggregates, and ordered "track-like" aggregates respectively (Fig. 6.8 A-C) and that these were better visualised in low and high magnifications (Fig. 6.8 D-F).

In large scale experiments designed to be consistent with the TEM and AFM characterisation of aggregation (Figs 6.3 and 6.5), 4-day preformed filaments from each protein were used to seed all three proteins and their aggregate characteristics after 4 days

of incubation was investigated through negative-stain TEM imaging. In control unseeded reactions (Fig. 6.9A), the structures observed were similar to those recorded earlier in Figs. 6.3 – 6.5: the WT recorded PHF and SF, the V337M amorphous aggregates with a few straight filaments, and the N279K thick bundled filaments. Surprisingly, the seeded reactions recorded these same features regardless of the identity of the seed (Fig. 6.9 B – D). This is consistent with the previous observations that the dominant conformations of WT and the two FTD tau K18 are distinct.

A summary of findings from the biochemical and biophysical experiments described so far has been provided in Table 6.2.

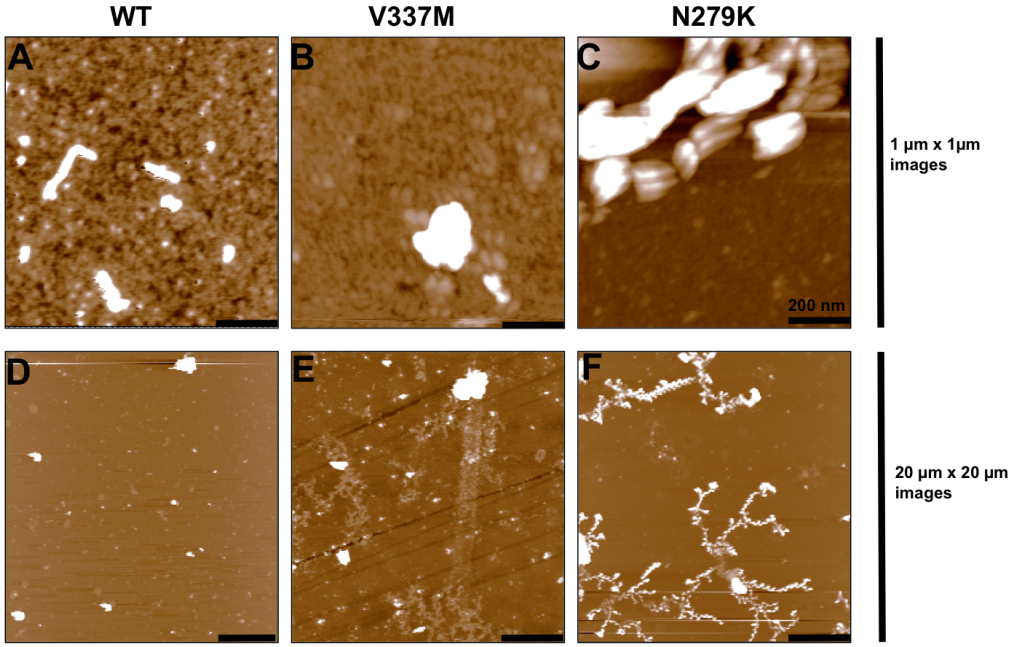

Figure 6.8. Cross-seeding of tau K18 variants with filamentous WT aggregates does not alter the morphological characteristics of aggregates formed. *Thirty-day aggregate samples of K18 WT were used to seed the aggregation of monomeric K18 WT, V337M and N279K for 11 days, and the structures formed characterised by low (1 µm x 1 µm) and high magnification (20 µm x 20 µm) AFM height images respectively for K18 WT (A and D), K18 V337M (B and E), and K18 N279K (C and F). Scale bar =200 nm for (A) – (C) and 4 µm for (D) – (F).*

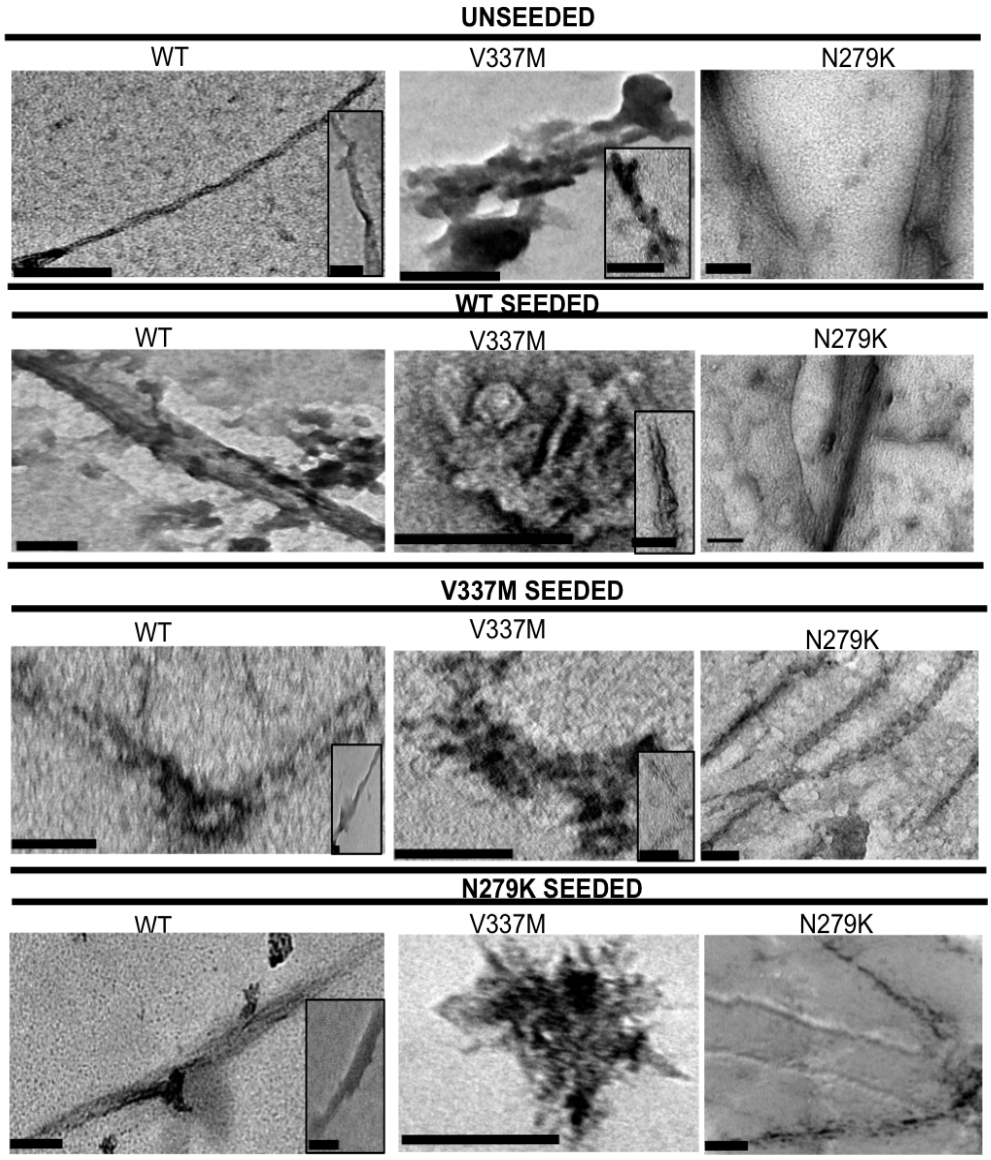

Figure 6.9. Dominant conformers of tau K18 WT, V337M and N279K are unaltered in the presence of competing conformers. *Aliquots of 4-day aggregates of K18 WT, V337M and N279K were in turn used to seed the aggregation of each protein (A, no seed; B, WT seeded; C, V337M seeded; and D, N279K seeded) and the structural features of aggregates formed analysed with TEM. Scale bars = 100 nm for all images.*

Table 6.2. Summary of biochemical and biophysical characterisation of the influence of the V337M and N279K familial FTD mutations on the conformation and aggregation of tau K18

ThT ligand-binding aggregation, followed by AFM investigation of endpoint samples		**Ultrastructural morphology following short- and long-term filament formation**		**Stages of aggregation analysed by AFM**		**Dot blotting and AFM immunological assessment of aggregation-induced conformational shift**		**CD, dot blot and AFM analysis of oligomer conformation and size distribution**		**Aggregation-seeding analysis of conformational compatibility**	
Observation	**Inference**	**Observation**	**Inference**	**Observation**	**Inference**	**Observation**	**Inference**	**Observation**	**Inference**	**Observation**	**Inference**
Differential ThT binding profiles. Endpoint samples had different structures.	WT and FTD tau K18 have different ThT binding properties.	WT formed PHFs and SFs. V337M formed amorpohous aggregates and short SFs. N279K formed dense bundles of filaments.	The V337M and N279K mutations lead to changes in the structural features of aggregated tau K18.	WT K18 monomers were converted sequentially to small and then large oligomers, and eventually PHFs or SFs. K18 V337M formed large oligomers quicker than the WT, N279K formed bundles of filaments.	The stages of tau K18 aggregation is altered in the presence of the V337M or N279K FTD mutations.	K18 V337M had reduced total tau immuno-reactivity whilst both K18 V337M and N279K had reduced oligomer reactivity. Endpoint aggregates had variable structures.	The V337M and N279K FTD mutations alter the conformation and ultrastructure of aggregating tau K18.	All proteins had similar oligomer sizes but variable immuno-reactivity. Negative CD spectra with peaks at ≥ 203 nm.	Oligomeric FTD variants of tau K18 have distinct immuno-reactivity. Oligomers were enriched in β-sheets.	Aggregate characteristics of each protein were unchanged when seeded with preformed aggregates from other proteins.	WT and FTD variants of tau K18 have distinct conformations and seed selection properties.

6.2.11 Preparation and characterisation of stabilised tau K18 oligomers for exogenous application to neurons

Differential structural properties of tau "strains" are believed to underlie variability in their functional cellular properties (Falcon et al., 2015). The observed aggregation and conformational diversity between the WT and FTD tau K18 therefore provided an important opportunity to explore relationships between their *in vitro* structural properties and their cellular functions. To achieve this, the AF-maleimide stabilisation approach from Chapter 5 was first used to prepare small oligomers of all three proteins. The oligomers produced were SDS-stable, fluorescent and existed mainly as trimers based on SDS PAGE profiles (Fig. 6.10 A, B). In agreement, TEM showed the presence of granular oligomers (Fig. 6.10 C – E) similar to those reported by others (Lasagna-Reeves et al., 2010).

Subsequently, a non-invasive biophysical method, DLS, was used to probe the oligomer size distribution for K18 WT. Because the oligomerisation protocol involved labelling with AF-maleimide in the presence of the BRB buffer, DLS studies were run on both the labelled tau reaction mix and BRB +AF-maleimide only. Two peaks were recorded for the labelled tau: a highly intense signal starting at ~ 458 nm and a less intense signal at ~ 4 nm (Fig. 6.11A). On the other hand, the signal shifted to a major peak at ~ 255 nm for BRB +AF-maleimide (likely due to the absence of TCEP) and a small peak at ~ 1 nm (most likely a buffer constituent; Fig. 6.11B). However, when the data was analysed based on size distribution by number (the Number PSD function), single peaks were obtained for both samples: one at ~ 4 nm for the labelled tau consistent with the arrowed peak in Fig. 6.11A, compared to a signal at ~ 255 nm minus tau. These outcomes are consistent with principles of DLS: in a mixture of small and large molecules (tau K18 and AF-maleimide respectively in this instance), the large molecules will scatter light the more and hence have a higher intensity score. However, the number/size distribution preferentially highlights the species with the highest number of particles (which was K18 in this case). Mean oligomer size was 4±1 nm (Fig. 6.11C; obtained from arrowed peak in Fig. 6.11A), which can be inferred to correspond with the prominent trimer band in Fig. 6.10A and B. Oligomer

distribution was 1 – 8 nm, indicating presence of n<3 and n >3 species (hydrodynamic radii = 1 – 2 nm and 5 – 8 nm respectively. The correlation plot provides information on the time-dependent scattering of light by molecules in the oligomer preparation, with fluctuations in the baseline indicating the presence of aggregated proteins (Fig. 6.11D). The DLS data is consistent with a previous report that estimated hydrodynamic radii of 3±0.2 nm for monomers and 5±1 nm for predominantly-tetrameric oligomers (Kaniyappan et al., 2017), and confirm that the oligomer preparations used in the present study consisted LMW oligomers. Since the V337M and N279K variants had the same gel electrophoresis profiles as the WT (Fig. 6.10A, B), they were hypothesised to share similar particle sizes with the WT.

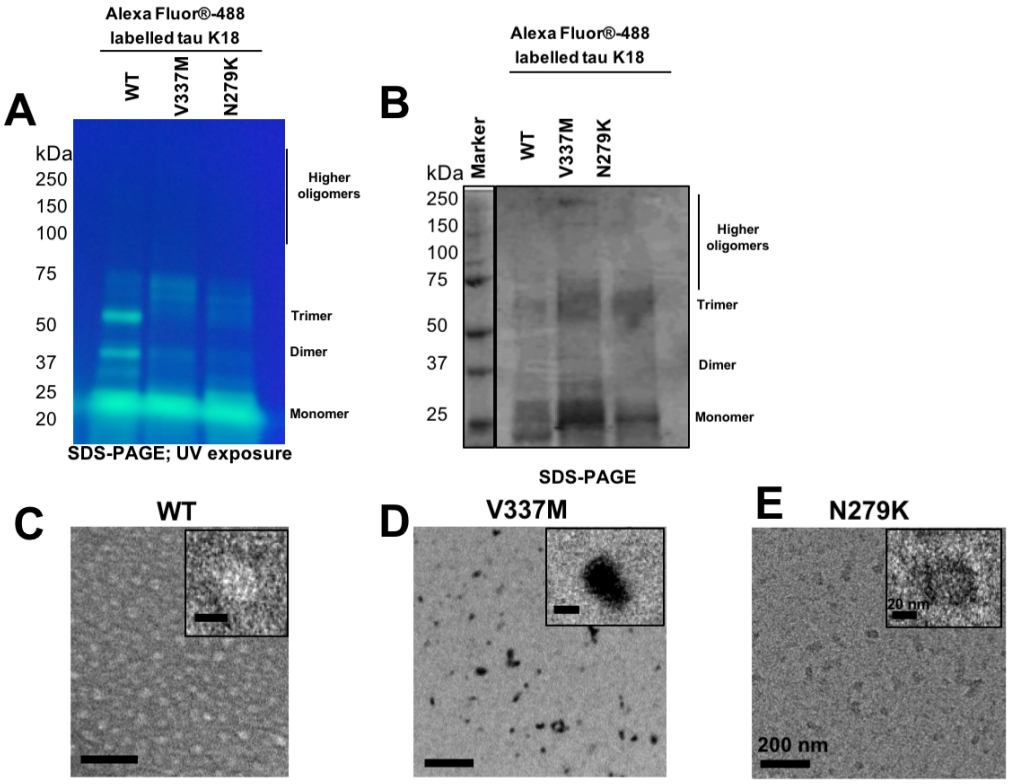

Figure 6.10. Characterisation of the size distribution of fluorescently labelled tau K18 and its V337M and N279K pathologic variants using non-denaturing SDS-PAGE and TEM*. (A) Representative non-denaturing SDS-PAGE and ultraviolet exposure showed that the labelled tau proteins consisted of a mix of monomers and LMW oligomers (i.e., dimers and trimers). (B) Non-denaturing SDS-PAGE showing that trimers were the most abundant oligomer species. (C), (D) and (E) TEM characterisation of labelled, granular oligomers of WT, V337M and N279K respectively. High magnification images are shown as insets. Scale bar = 200 nm for main images and 20 nm for insets.*

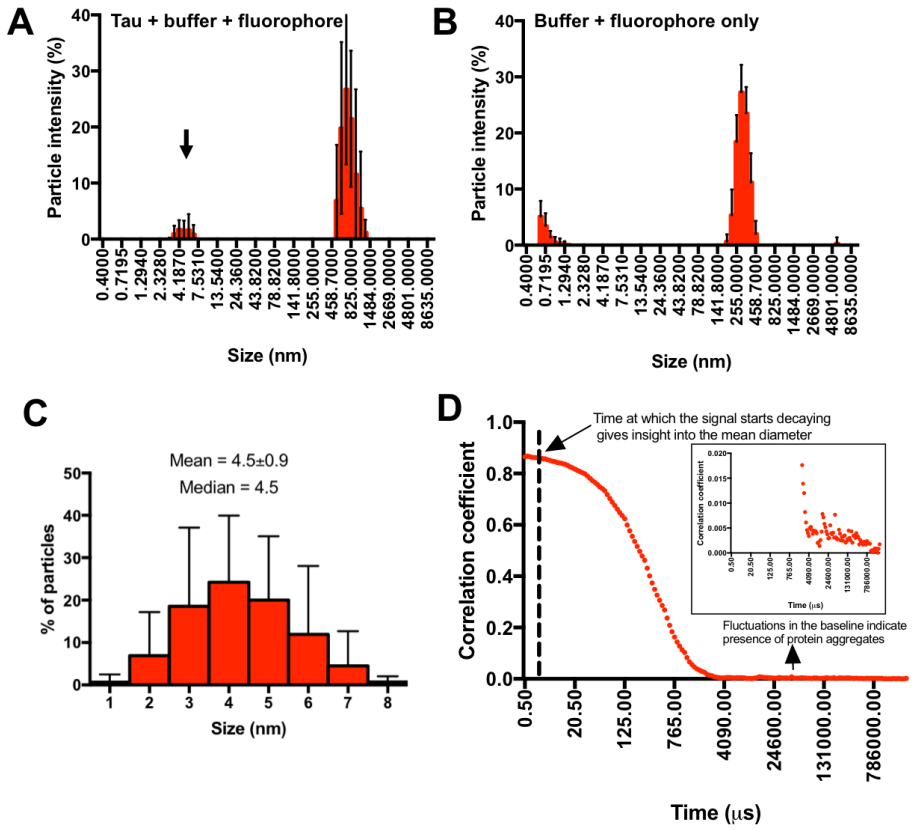

Figure 6.11. DLS assessment of the sizes of AF-maleimide–labelled tau K18 WT oligomers. *(A) The DLS intensity function gave two peaks for the labelled oligomers in the presence of the fluorophore and buffer constituents. (B) In the absence of tau, a large peak with a much-reduced size (~255 nm compared to ~825 nm in (A) was obtained. The new small peak <1 nm was likely from a buffer constituent which would bind to the tau oligomers. (C) Size distribution of tau K18 oligomers. (D) The correlation plot gives insights into the mean oligomer size, with baseline fluctuations indicating the presence of aggregated samples.*

6.2.12 Optimisation of human neuroblastoma and neuronal cell culture growth conditions

A major focus of this thesis was to study the *in vitro* structural features of tau aggregation and how this may influence cellular internalisation, which is an important step in the protein's cell–to-cell transmission. To do this, optimal cell culture conditions needed to be established. SH-SY5Y neuroblastoma cells were grown to confluence in 3-4 days in MEM/F12 medium. On splitting, different concentrations of cells were seeded in CellView^{TM} Advanced Tissue Culture dishes and their adherence and viability after 24 h of incubation analysed. It was observed that 200,000 cells/ml was a good concentration to use since the cells exhibited good adherence, growth and spacing. Moreover, the live cells stained well for the nuclear

and plasma membrane markers Hoechst and CellMask Deep Red respectively (Fig. 6.12A) as well as endogenous tau proteins, making them suitable for live cell assays of tau internalisation.

Subsequently, growth conditions for a hiPSC-derived cortical neuron line were optimised. After ~20 days in culture, the cells exhibited common neuronal properties including dense neurite networks. However, the cells appeared over-confluent with multiple layers which easily detached in a sheath-like manner. Culture duration was therefore shortened to 14 – 16 days, which proved sufficient for neurite network development (Fig. 6.12B). Additionally, the cells were characterised by their immuno-reactivity for several markers of differentiation. Differentiated neurons were immuno-negative for octamer binding transcription factor 4 (oct4), a marker of undifferentiated cells. They were also immuno-positive for the progenitor markers nestin (neuroectodermal stem cell marker), ki67 (cell proliferation marker) and GFAP (glial fibrillary acidic protein; astrocyte marker) at day 2 but expression decreased with differentiation during which Tuj1 (neuron-specific class III beta tubulin) expression increased (data not shown).

6.2.13 Familial FTD mutations increase tau oligomer internalisation in SH-SY5Y cells but not in hiPSC-derived cortical neurons

Increasing evidence suggests that oligomers may be the toxic tau species that regulate the interneuronal transmission of pathology (Lasagna-Reeves et al., 2012a). It however remains unknown if FTD characterised by familial tau mutations are transmitted through the same mechanism. To answer this question, recombinant tau K18 WT, V337M and N279K low-n oligomers were fluorescently labelled (section 5.2) and applied exogenously to cells and their internalisation dynamics investigated.

SH-SY5Y cells (Kovalevich and Langford, 2013), were first challenged with 10 μM oligomeric tau K18 for 24 h, after which un-internalised proteins were removed by washing with PBS. It was earlier observed that a single PBS wash was enough to remove all loosely-bound tau from cells. Tau internalisation was observed for all three proteins (Fig. 6.10). A careful look at the Alexa Fluor 488 channel (Fig. 6.13)

however suggested that internalisation was less intense for the WT compared to the variants. The extent of internalisation was therefore quantified. To account for both diffused and punctate phenotypes of internalisation (Fig. 6.13), integrated density (mean intensity x area occupied) was used. Internalisation was significantly different among the three proteins ($p<0.0001$). Internalisation was significantly higher for both V337M and N279K against the WT ($p<0.0001$ for each, Fig. 6.14), and also significantly higher for V337M compared to N279K ($p=0.0241$; Fig. 6.14).

Internalisation in hiPSC neurons was the opposite of what was found in SH-SY5Y cells: internalisation was highest in the WT compared to the FTD variants ($p<0.0001$). Mean values are given in Fig. 6.15B. Internalisation was better in the WT against both the V337M and the N279K ($p<0.0001$ and $p=0.0374$ respectively; Fig. 6.15). Internalisation was also better for V337M than N279K (Fig. 6.15). This suggests that the distinctive internalisation of the tau K18 oligomers may be cell line-specific.

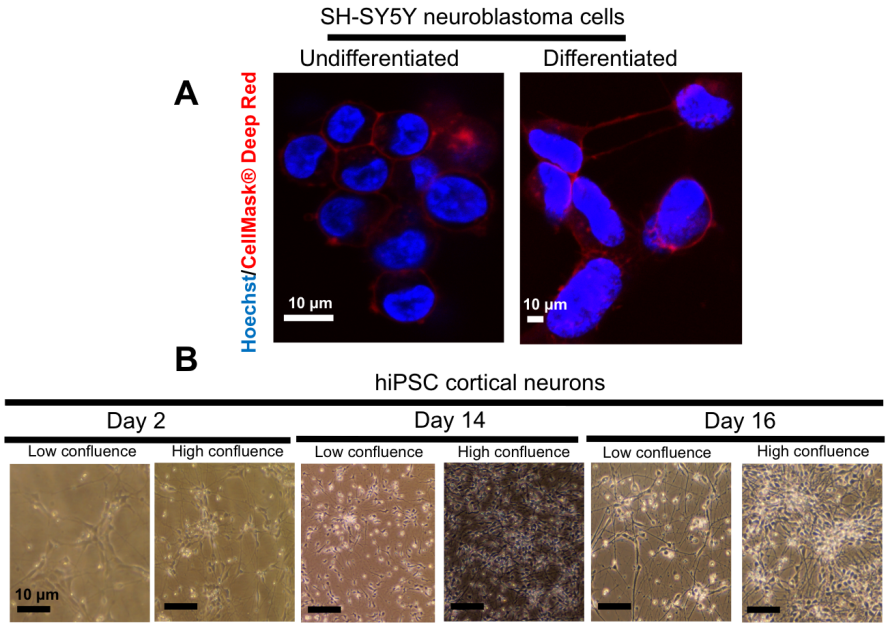

Figure 6.12. Optimisation of parameters for cell culture studies. *(A) Undifferentiated and differentiated SH-SY5Y neuroblastoma cells were seeded in CellView™ Advanced Tissue Culture dishes for 24 hrs and their adherence and staining for nuclear and plasma membrane markers studied. (B) hiPSC neurons developed neuronal morphological properties with optimal adherence within 14 – 16 days in culture. The cells also expressed markers of neural differentiation within the time frame (data not shown). Scale bars = 10 µm.*

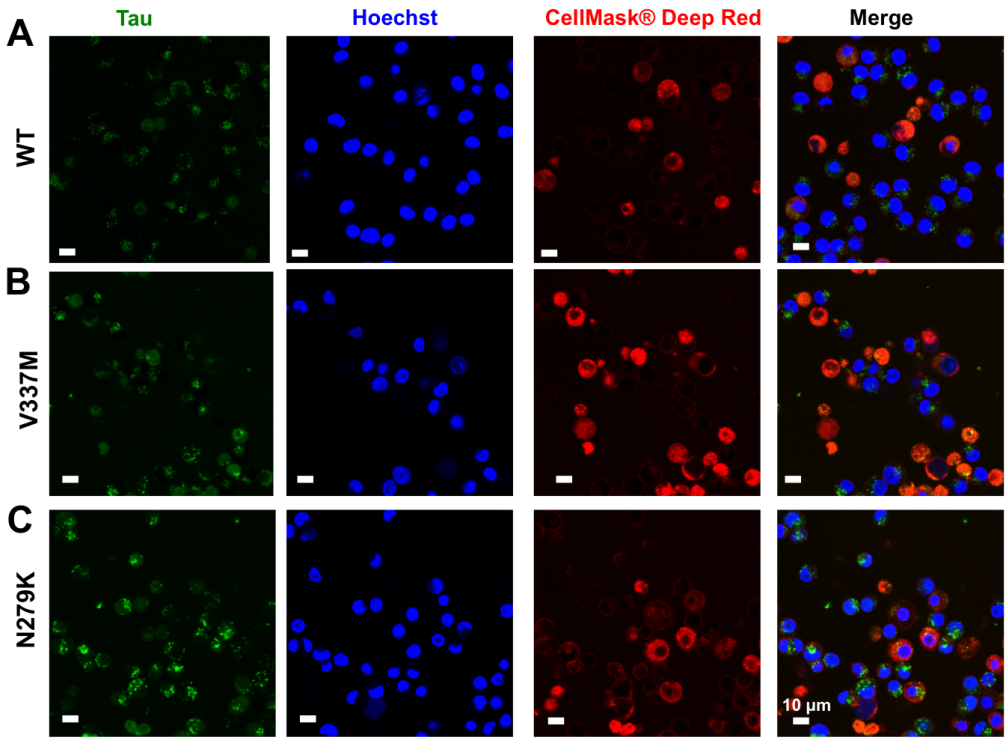

Figure 6.13. Uptake of exogenous tau K18 oligomers by SH-SY5Y cells. *Representative confocal microscopy images showing uptake of K18 WT, V337M, and N279K oligomers (A) – (C) respectively. Scale bars = 10 µm.*

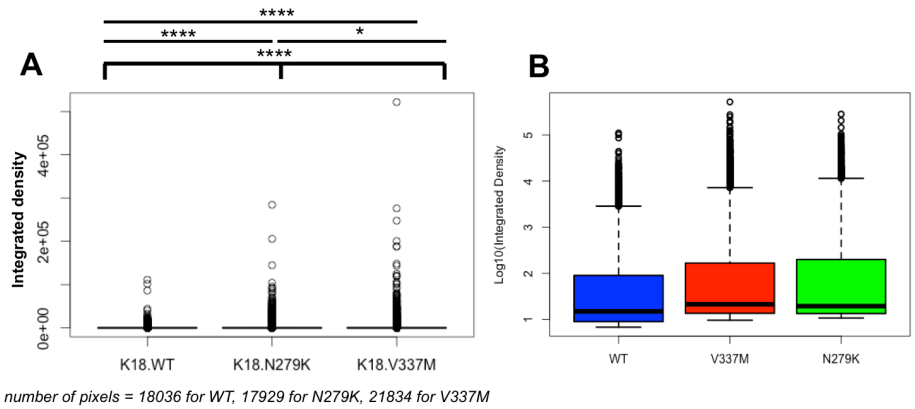

Figure 6.14. The V337M and N279K mutations significantly enhance the cellular uptake of tau K18 oligomers. *Internalised tau K18 oligomers were quantified using integrated density (mean intensity x area occupied) to account for their diverse phenotypes observed. (A) Boxplot of internalised tau K18 oligomers. Oligomer uptake significantly differed between the three proteins (Kruskal Wallis test, $p<0.0001$), being highest for V337M, followed by N279K and then WT (see text for details). (B) Log_{10} version of the internalisation boxplot given in (A).*

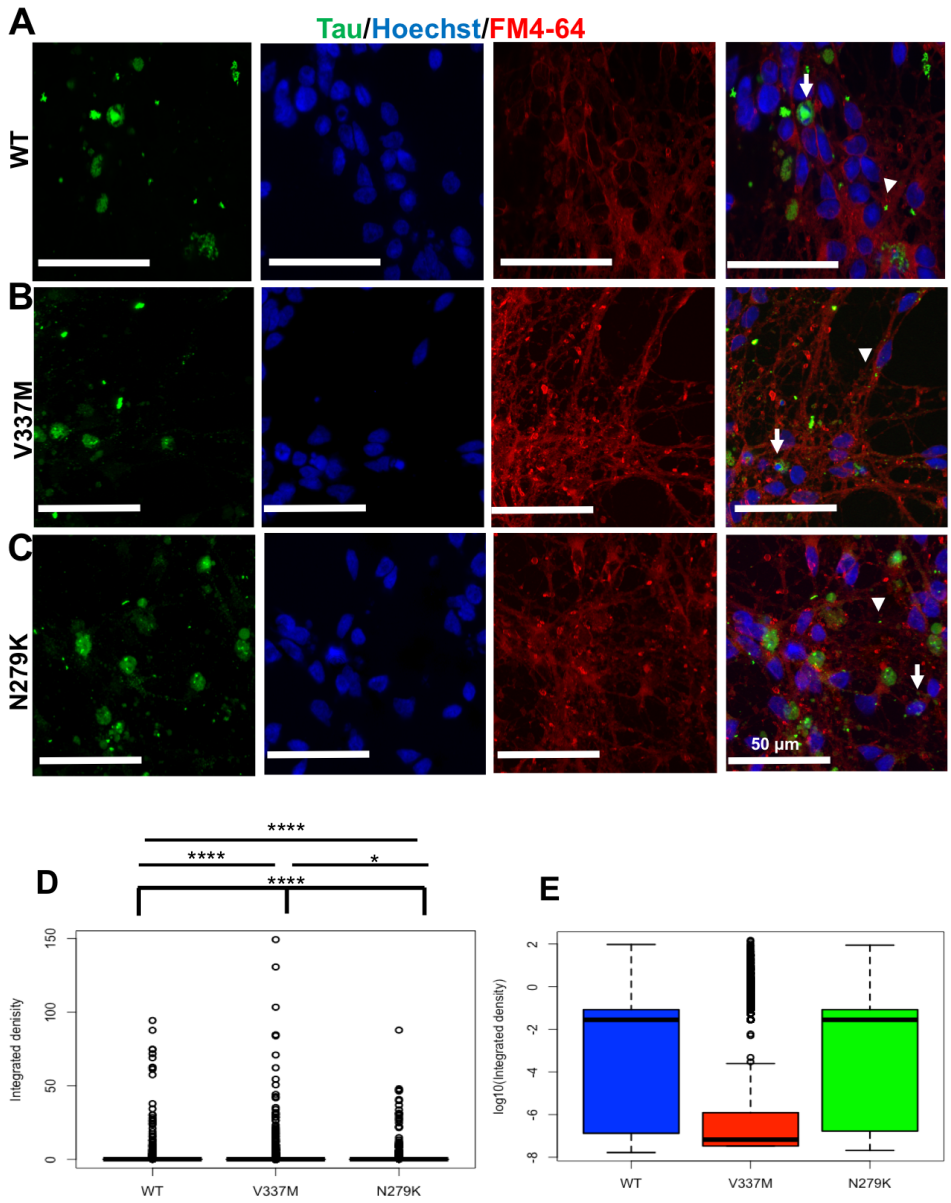

Figure 6.15. Internalisation of extracellular tau K18 oligomers in hiPSC neurons occurs by endocytosis, and the internalised oligomers localise to the cell soma and the neurites. *(A) – (C) Extracellularly applied and subsequently internalised oligomers of tau K18 WT, V337M and N279K (A – C respectively) co-localised with the FM4-64 marker of endocytosis. Some of the internalised oligomers were found in the neurites (arrowheads), whilst others were in the cell soma (arrows). Scale bars = 50 µm. (D) Internalisation boxplot for the tau K18 variants. (E) Log$_{10}$ version of the internalisation plot shown in (D).*

6.2.14 Exogenous tau K18 oligomers are internalised by endocytosis

To investigate the mechanisms by which the extracellular tau oligomers were internalised by cells, the vesicular marker FM4-64® (SynaptoRed) was used. Similar to previous reports (Guo and Lee, 2011; Michel et al., 2014), K18 WT internalisation occurred by endocytosis in SH-SY5Y cells, because internalised tau

were encapsulated in vesicles (Fig 6.16A) similar to the V337M and N279K variants (Fig 6.16 B and C respectively). Interestingly, some internalised tau and the vesicular marker both co-localised with the nucleus, suggesting that some internalised tau entered the nucleus. As a control, FM4-64® and tau oligomer treated cells were incubated at 4 ^{o}C which blocks endocytosis (Punnonen et al., 1998). Internalisation was not observed in this condition (Fig. 6.16 D-F).

Next, it was investigated if the observed vesicular transport was cell-type specific, by monitoring FM4-64 co-localisation in hiPSC neurons. Internalisation was recorded in this cell type for all tau proteins (Fig. 6.15), indicating that endocytosis is likely a common route of cell entry for exogenous tau in both cell lines.

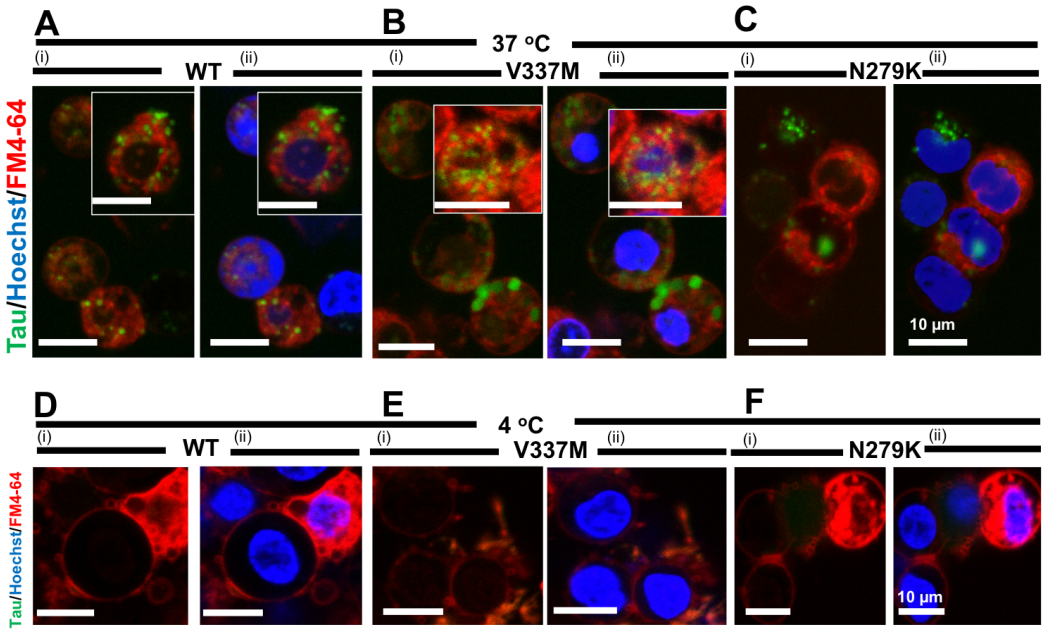

Figure 6.16. Extracellular tau K18 oligomers are taken up by SH-SY5Y cells through endocytosis. *Internalised tau K18 WT (A), K18 V337M (B), and K18 N279K (C) oligomers co-localised with the endocytic marker FM4-64. Control experiments in which tau-seeded cells were incubated at 4 ^{o}C did not show cellular uptake (D)–(F) for WT, V337M and N279K respectively. Scale bars = 10 µm.*

6.2.15 Internalised tau K18 oligomers accumulate in the cytoplasm and nucleus of SH-SY5Y cells, and the soma and axons of hiPSC-derived neurons

Whilst several studies have reported on tau internalisation, little is known about the protein's subcellular destination. The co-localisation of the endocytic marker and internalised tau with the nuclei in Figs. 6.15 and 6.16 prompted the likelihood that internalised tau may enter the nucleus. Although nuclear localisation and/or

function of internalised tau has not been previously reported, nuclear envelope associated proteins can shuttle materials between the cell surface and the nucleus, suggestive of nuclear signalling functions for endocytosed proteins (Benmerah, 2004; Chaumet et al., 2015). In SH-SY5Y cells, internalised tau was identified both in the cytoplasm and the nucleus (Fig. 6.17A-C). Similarly, internalised tau was found in the axon and soma of hiPSC neurons (Fig. 6.15A-C), indicating that nuclear targeting of exogenous tau may be a novel, previously overlooked signalling process.

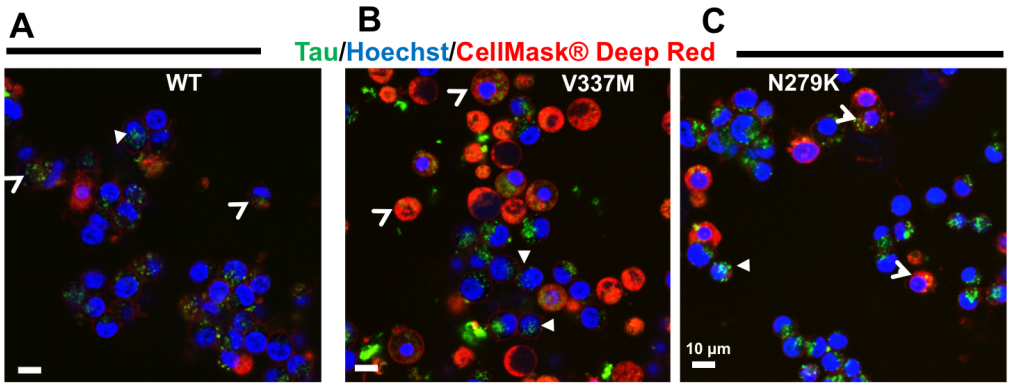

Figure 6.17. Internalised tau K18 oligomers localise to the cytoplasm and the nuclei of SH-SY5Y cells. *Exogenous oligomers of tau K18 WT (A), V337M (B), and N279K (C) taken up by SH-SY5Y cells were localised in the cytoplasm (open arrow heads) or nucleus (filled arrow heads). Scale bars = 10 µm.*

6.2.16 Internalised tau K18 oligomers co-localise with the nuclear protein nucleolin

Endogenous nuclear tau is mainly present at the nucleolar periphery, where it co-localises with the nucleolar protein nucleolin (Sjöberg et al., 2006) and protects against heat shock-induced DNA damage (Sultan et al., 2011). Following the observed nucleocytoplasmic shuttling of internalised tau in both cell lines in Figs. 6.15 – 6.17, it was investigated if exogenously-applied and nucleo-internalised tau interacted with nucleolin since this association seems critical for the nuclear transport and functions of tau (Ginisty et al., 1999). Tau co-localised with nucleolin in both cell types (Figs. 6.18 and 6.19). In SH-SY5Y cells, tau-nucleolin complexes appeared localised to the nucleolar periphery in K18 WT and K18 V337M (Fig. 6.18A,B). However, co-localisation diffused throughout the nucleus was observed for K18 N279K (Fig. 6.18C). Nucleolin co-localisation was similarly observed using hiPSC neurons (Fig. 6.19).

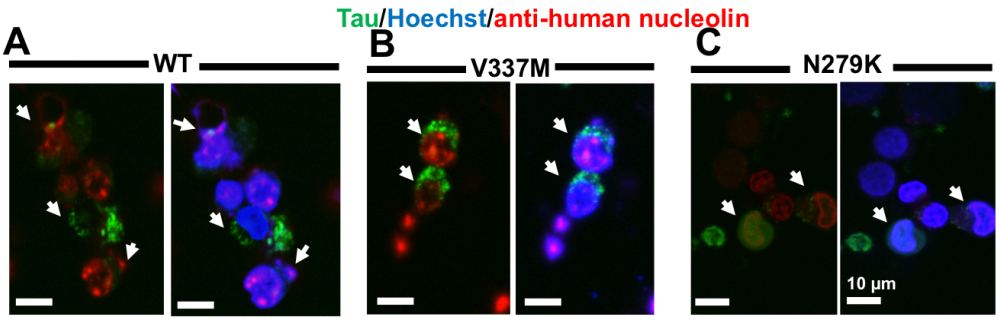

Figure 6.18. Exogenous tau K18 oligomers that are internalised in the nuclei of SH-SY5Y cells co-localise with the nucleolar protein nucleolin. *This phenomenon was observed for tau K18 WT (A), V337M (B) and N279K (C), whose co-localisation has been highlighted using images without (i) and with (ii) the nuclear marker Hoechst. Scale bars = 10 µm.*

6.2.17 Internalised tau K18 oligomers co-localise with endogenous tau

An important step in the cell-to-cell transmission of tau oligomers is the interaction of internalised tau with endogenous tau, leading to the formation of heterogeneous tau aggregates. It is however unclear if interneuronal transmission of exogenously-applied-and-internalised FTD tau variants involves interaction with endogenous tau. Using triple-stain confocal microscopy, internalised WT K18 and its FTD variants were observed to partially co-localise with endogenous tau (based on reactivity to the HT7 antibody recognising the ^{159}PPGQK^{163} epitope of full length tau). In hiPSC neurons, co-localisation was detected for all three proteins, occurring both in the neurites and soma (Fig. 6.20), suggesting that internalised tau K18 likely interacts with endogenous tau.

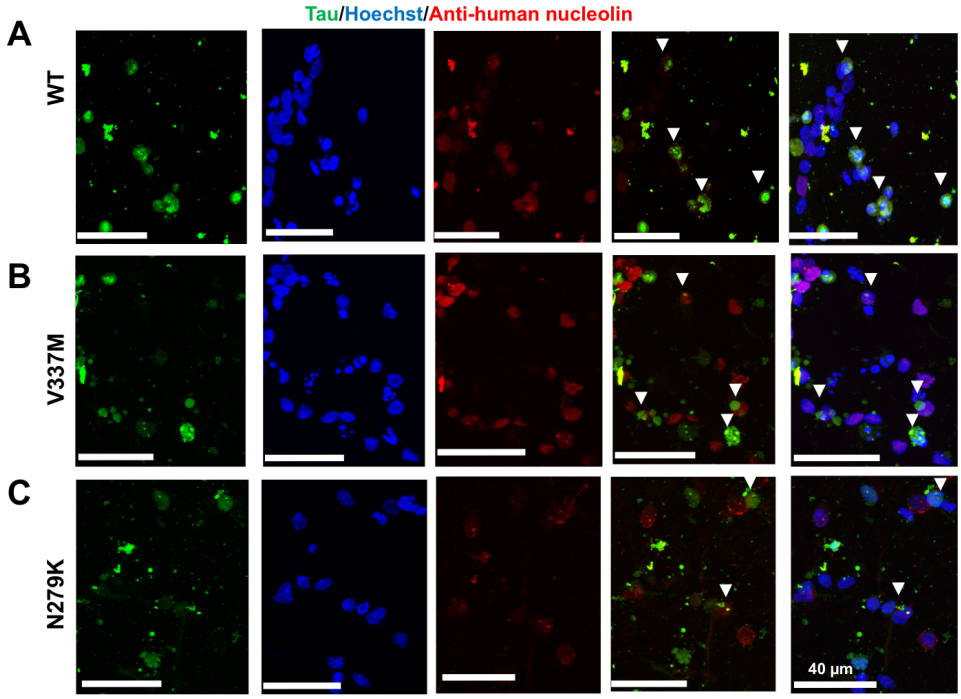

Figure 6.19. The nuclear protein nucleolin is a co-localisation partner of tau K18 oligomers internalised in hiPSC neurons. *Oligomers of K18 WT (A), V337M (B) and N279K (C) internalised in hiPSC neurons and localised to the soma were observed to interact with the nuclear protein nucleolin. Scale bars = 40 µm.*

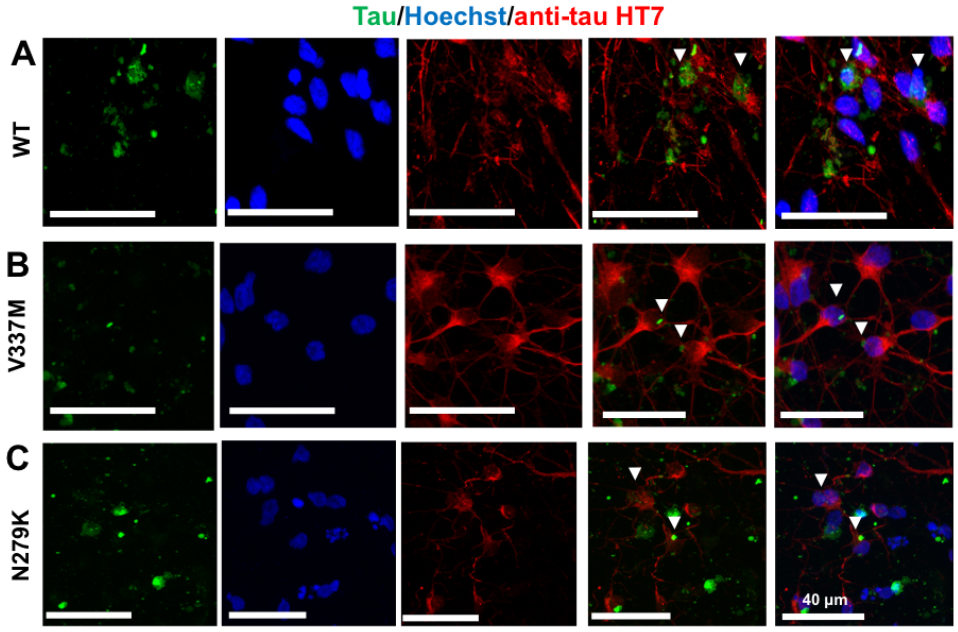

Figure 6.20. Internalised tau oligomers in hiPSC neurons co-localise with endogenous tau. *Oligomers of exogenous K18 WT (A), V337M (B) and N279K (C) internalised in hiPSC neurons co-localised with endogenous tau (white arrowheads). Scale bars = 40 µm.*

6.2.18 Morphological phenotypes of internalised tau K18

Tau proteins from diverse sources exhibit phenotypic diversity upon cellular internalisation (Boluda et al., 2015; Narasimhan et al., 2017; Sanders et al., 2014). To obtain further insights into the differential internalisation profiles for the tau K18 oligomers, morphological appearances of the internalised tau oligomers were studied. Four different phenotypes were identified and classified according to Sanders et al., (2014); (i) speckles: collection of tiny, bright puncta of different sizes, (ii) disordered: usually disc-shapes of internalised tau of non-uniform intensity, (iii) mosaic: a mix of ordered and disordered aggregates with visible puncta, and (iv) ordered: circular or spherical shapes of internalised tau of uniform or near-uniform intensity (Fig. 6.21C). These phenotypes were identified for all forms of tau internalised in both cell types (Fig. 6.21). It was uncommon to see all phenotypes per field of view in SH-SY5Y cells. However, the first three phenotypes were easily identifiable (Fig. 6.21A). In hiPSC neurons, all four phenotypes were found for all tau strains (Fig. 6.21B). Phenotypes of internalisation can therefore not be used as a distinguishing factor for K18 WT and its variants.

6.2.19 Internalised tau K18 oligomers do not induce cell death

Several studies have reported that cellular internalisation of tau K18 oligomers causes cell death and/or reduced viability (Guerrero-Muñoz et al., 2015; Lasagna-Reeves et al., 2010) whilst others have suggested that oligomer treatment is insufficient to induce cell death (Kaniyappan et al., 2017; Kumar et al., 2014). However, little is known about cytotoxic effects oligomers of the V337M and N279K forms of tau K18. SH-SY5Y cells were therefore treated with oligomer preparations from the three given proteins for 72 h and cytotoxicity analysed by measuring LDH leakage. No significant difference in viability was recorded either between cells treated with variable concentrations of the same protein oligomers or those treated with same or different concentrations of distinct proteins (Fig. 6.22). This means that the oligomer concentration-dependent variability in internalisation observed (data not shown) is not directly related to oligomer-induced cell viability. Differential outcomes from previous studies could possibly be due to assay

specificity in terms of oligomer preparation methods as well as cell lines and viability assays used.

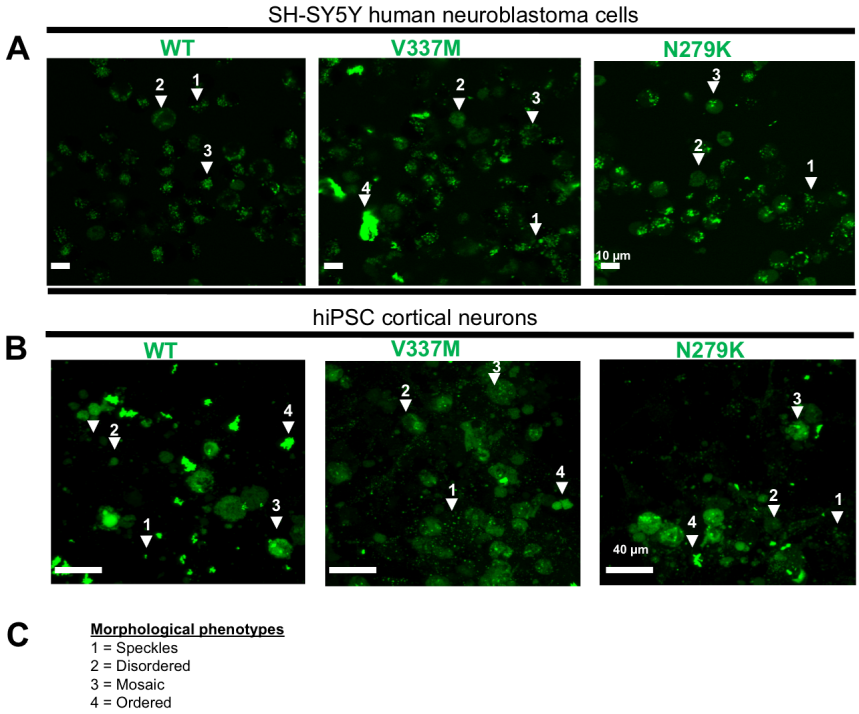

Figure 6.21. Morphological phenotypes of internalised tau K18 oligomers. *Four different phenotypes were identified and classified as speckled, disordered, mosaic and ordered. These phenotypes were recorded in both SH-SY5Y cells (A) and hiPSC neurons (B). The numbering used to annotate the different forms of internalisation is given in (C). Scale bars = 10 µm in (A) and 40 µm in (B).*

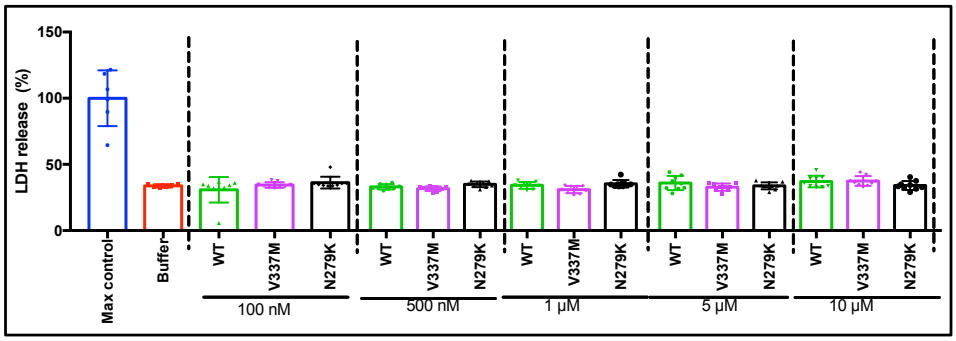

Figure 6.22. Internalisation of tau K18 oligomers does not lead to cell death. *SH-SY5Y cells were treated with variable concentrations of oligomeric tau for 72 h after which the cells were for LDH leakage. No significant difference in LDH released was recorded between the controls (maximum control or buffer only) and the three tau proteins at any of the concentrations tested (n=3 biological repeats).*

6.3 Discussion

Tau protein has intricate roles in the development of AD and FTD, among other tauopathies (Wang and Mandelkow, 2016). Whilst several theories, such as hyperphosphorylation (Alonso et al., 2001), have been explored towards understanding the mechanistic and cellular basis of AD progression to inform drug development, it has recently been identified that these diseases may occur due to a cycle of events involving: (i) the extracellular secretion of endogenous tau protein or its fragments, (ii) interaction of extracellular tau proteins leading to the accumulation of aggregated exogenous proteins, (iii) cellular entry of extracellular tau (may be aggregated or not) where it induces the aggregation of endogenous tau, and impairments in neuronal physiology and function (Guo and Lee, 2014). Whilst this interneuronal transmission hypothesis in AD is strongly supported by *in vivo*, *in vitro* and *ex vivo* data (Clavaguera et al., 2014; Guo and Lee, 2014), it is unclear if disease progression in FTD involving tau mutations occurs through the same or similar mechanisms. In this chapter, it has been shown from both biochemical and biophysical perspectives that two of the commonest FTD mutations, V337M and N279K, do alter the conformation and pathway of aggregation of tau K18. Moreover, the mutations changed the cellular internalisation of tau K18, although all proteins were internalised by endocytosis and had similar subcellular accumulation patterns. These findings may offer novel insights into both the similarities and distinctions between tauopathies involving the WT and mutated forms of tau.

Recent studies have highlighted pitfalls in using the ThT assay as a sole measure of aggregation (Coelho-Cerqueira et al., 2014; Wong et al., 2016). The ThT assay used in this chapter was therefore coupled with AFM observations of tau aggregation. This combination revealed that the extent of protein aggregation is not necessarily related to its ThT binding. Based on this outcome, it can be argued that ThT is a probe of protein conformation rather than aggregation because distinct folding dynamics may alter the exposure of ThT binding surfaces of each protein. Similar outcomes have been reached by others studying different proteinopathic proteins such as amylin (Wong et al., 2016) and amyloid β (Hatami et al., 2017),

which reinforces this observation. Indeed, the use of ThT is based on the principle of its binding to cross β-sheets which herald aggregation (Lindberg et al., 2015). However, the ability of the dye to differentiate between changing conformations of already aggregated proteins may be protein-specific and complicated.

Inferring from the ThT binding data, it was hypothesised that the FTD mutations may result in altered protein conformation and aggregation. The biochemical and biophysical evidence shown here that the V337M and N279K mutations alter the stages of aggregation, and the conformation and atomic structure of aggregated tau K18 (Figs. 6.3 – 6.9) support this hypothesis. The mutations drastically changed the immunoreactivity of tau K18 to two conformation-specific tau antibodies, which is an indication of new adopted conformations. Interestingly, the V337M recorded reduced reactivity to both antibodies whilst the N279K mutation led to nearly no reactivity to the oligomer-specific antibody notwithstanding its reactivity to the total tau antibody being comparable to the WT (Fig. 6.6). Importantly, this shows that each FTD mutation significantly shifts the protein conformation to a new, unique orientation, which in turn likely dictates its pathway to form aggregates of distinct structures. Moreover, the consistency in the observed aggregate structures of each given protein across multiple independent assays using different batches of protein preparations (heparin-induced aggregation in Figs. 6.2 – 6.5 and native-state aggregation in Fig. 6.6) strongly argues for mutation-induced specificity in protein conformations and aggregation. These data indicate that FTD mutations can lead to distinct amyloid structures of tau (referred to as tau "strains").

The tau strain hypothesis suggests that altered conformations induced by FTD mutations may underlie the differential phenotypic and disease progression profiles in FTD and AD (and other tauopathies involving WT tau). However, there is little evidence supporting this hypothesis. It was therefore investigated if the observed FTD tau proteins of different conformations may either be more toxic to cells or alter the mechanisms by which the proteins are internalised and propagated. Here, similarities and differences in exogenous oligomer propagation were observed, which highlights the shared molecular mechanisms of AD and FTD development. Whilst all proteins were taken up by cells through endocytosis, co-localised with

endogenous tau and nucleolin, and accumulated both in the cytoplasm and nucleus (neurites and soma for hiPSC-derived neurons), the extent of internalisation significantly differed between proteins and between cell lines. Speculatively, the new conformations and/or aggregation dynamics of tau in the presence of the FTD mutations may have altered its interactions with specific cell surface proteins governing endocytosis, resulting in their differential cellular trafficking. For example, the binding of aggregated tau and other proteinopathic proteins (e.g. alpha synuclein and amyloid beta) to heparan sulfate proteoglycans regulates their internalisation and transmission and that blocking heparan sulfate proteoglycan expression or activity prevents internalisation (Holmes et al., 2013; Rauch et al., 2017). Another possibility is that the internalised variant K18 had distinct degradation efficiencies or pathways, resulting in different extents of quantifiable tau. Further studies are required to elucidate the veracity of these hypotheses.

The observed interaction of all three proteins with endogenous tau is an indication that they may all propagate disease by first recruiting endogenous tau into forming larger aggregates as described (Lasagna-Reeves et al., 2012a; Michel et al., 2014). Moreover, co-localisation with nucleolin raises the possibility that: (i) internalised exogenously-applied tau can be exported into the nucleus, and (ii) nucleus-destined internalised tau may play roles in protein biosynthesis. The association of nuclear tau with nucleolin has been observed in AD brain samples for which reduction in nuclear tau levels correlate with increased NFT abundance and reduced nucleolin levels (Hernández-Ortega et al., 2016). Misfolded tau interaction with specific ribosomal proteins impairs the protein synthesis machinery (Meier et al., 2016). Importantly, this observation is not limited to the expression of WT tau but is also evident in the presence of mutated tau P301L or ΔK280 (Meier et al., 2016). The effect of tau on the protein synthesis machinery deserves to be further studied to identify how different forms of tau may affect ribosomal proteins.

6.4 Conclusion

The FTD-causing mutations V337M and N279K lead to alterations in the stages of aggregation and immunological reactivity of K18. Moreover, these mutations cause the formation of Alzheimer-like filaments that are significantly distinct from

the WT in terms of their structural properties. Oligomers prepared from WT tau K18 and its FTD variants were capable of cellular internalisation by endocytosis where they localised to the nucleus and cytoplasm of neuroblastoma cells and the axon and soma of hiPSC neurons. Furthermore, oligomers of all proteins co-localised with endogenous tau, suggestive of their ability to recruit endogenous proteins into forming potentially toxic aggregates. Moreover, oligomers of all proteins co-localised with nucleolin, a nuclear protein involved in ribosomal biosynthesis, which shows for the first time that functional defects propagated by internalised exogenous tau may be extended into the nucleus. Nonetheless, the oligomers did not induce significant cell death to SH-SY5Y cells, indicating that oligomer toxicity may be limited to functional and structural defects to neurons instead of outright lethality. The two mutations significantly enhanced the cellular internalisation of exogenous tau K18 oligomers in SH-SY5Y cells but not hiPSC neurons, and this observation may be due to the distinct conformers of tau formed by the tau variants. Taken together, these results provide evidence of the structural and functional properties of WT and FTD tau which may account for both the heterogeneity and similarities between FTD and AD (and other tauopathies involving WT tau).

7| General Discussion

The findings outlined in this thesis provide new perspectives to the cell-to-cell propagation theory of misfolded tau, by demonstrating that cellular internalisation of tau variants may be tightly regulated by the given protein's folding and aggregation characteristics. This may help to explain several enigmatic aspects of the molecular pathogenesis of different tauopathies.

7.1 Rationale

Prior to this study, many studies had shown that dysfunctional tau can be passed on from one neuron to the other, seeding the aggregation of endogenous proteins and transmitting pathology across synaptically-connected brain regions. Referred to as the cell-to-cell propagation theory, this mechanism has been demonstrated using *in vivo*, *ex vivo*, and *in vitro* models of AD, thereby building a strong evidence base in its favour (section 1.6). Some recent studies had begun to point to a new aspect of this hypothesis: different forms of misfolded tau vary in their ability to induce interneuronal spread and the robustness of the induced spread (section 6.1). For example, tau homogenates from human AD and CBD brains are propagated differently when introduced into mouse brains (Boluda et al., 2015). Based on these, I hypothesised that the capacity of tau proteins to enter neurons and seed aggregation will be dependent on their conformation, and that seeding efficiency will be determined by conformational interactions with endogenous proteins. Since specific mutations in tau lead to FTD with different pathological features from AD, I proposed that probing the role of conformational specificity in aspects of the cell-to-cell propagation may help to explain differences in disease onset, duration, and severity. I considered that *in vitro* biochemical and cellular models for this project would likely offer meaningful characterisation of tau aggregation and conformation and their cellular internalisation properties.

The aims of this thesis were four-fold:

(i) To develop genetic resources and a simple method of expressing and purifying tau K18 and a selection of its FTD variants;

(ii) To develop a new method of preparing LMW tau K18 oligomers of enhanced stability for use in biochemical and cell biology assays;
(iii) To study the *in vitro* conformation and aggregation of tau K18 WT, V337M, and N279K; and
(iv) To investigate the cell biological effects of extracellular tau K18 WT oligomers and FTD variants.

The established expression and purification methods allowed for efficient preparation of large quantities of WT and FTD tau K18 (Chapter 4), which were used for in-depth investigation of effects of the V337M and the N279K FTD mutations on time-dependent aggregation and conformation of the K18 fragment (Chapter 6). This enabled comprehensive testing of the hypothesis that these two disease-associated mutations alter the conformation and aggregation of WT tau K18. It was observed that each FTD mutation formed distinct fibril structures compared to the WT, and reacted differently to common anti-tau antibodies and the ThT stain for aggregation, leading to the conclusion that the pathological mutations induce changes in the conformation and aggregation of tau K18. Next, the extracellular-to-intracellular propagation of each tau variant was studied to ascertain if the observed distinctive biochemical properties would influence their neurobiological features. Here, the new tau oligomerisation protocol developed (Chapter 5) enabled the preparation of LMW oligomers of improved stability for use in biochemical and cell biology assays, with the added advantage of fluorescent live tracking. It was observed that both the WT and FTD tau oligomers were taken up by two human cell lines (SH-SY5Y neuroblastoma and hiPSC cortical neurons) through endocytosis and did co-localise with endogenous tau, suggesting a templated misfolding mechanism (Chapter 6). Nonetheless, the tau K18 oligomers were differentially internalised, leading to the hypothesis that the altered conformations may better associate with endocytic proteins thereby modifying their cellular entry. In addition to cytoplasmic and neuritic inclusions, some of the internalised proteins were transported into the nucleus/soma where they co-localised with nucleolin, a protein actively involved in ribosomal biosynthesis. This suggests that internalised exogenous tau may have nuclear functions.

7.2 Design and characterisation of a plasmid library for expressing full length and truncated tau proteins

The preparation of recombinant forms of tau starts with verifiable plasmids as genetic constructs for overexpressing the protein in suitable model systems, with *E. coli* being the model expression host of choice. Whilst plasmid sharing is a common practice between laboratories, it was difficult to obtain plasmids in the desired orientations at the start of this project. Since the planned experiments were aimed at direct comparison of multiple forms of tau, it was essential to use tau plasmids of similar design. It was therefore envisaged that creating an open access library of plasmids for expressing different forms tau would be beneficial both to the planned project and broadly the tauopathy research community. Four disease-associated forms of WT htau40 and K18 were created (Chapter 3). These included N279K and V337M which have been studied in detail (Chapters 4 – 6), the commonly-studied P301L which is known to accelerate tau aggregation and neurodegeneration (Lewis et al., 2000; Rodríguez-Martín et al., 2016), and the C291R novel mutation (Marshall et al., 2015). Since the availability, positioning and number of cysteine residues affect tau aggregation (Huvent et al., 2014; Sahara et al., 2007; Schweers et al., 1995; Soeda et al., 2015), plasmids for expressing both WT (K18 and htau40) and disease variants of tau containing zero, one (at different positions) or two cysteines were also created (Chapter 3). Moreover, these plasmids have cleavable hexahistidine tags to allow protein purification, as well as a c-Myc or FLAG tag for ease of immunological assessments. These tags have been observed not to have detrimental effects on tau aggregation (data not shown).

These plasmids will be shared via open access. The practice of unrestricted peer-to-peer sharing of plasmids and other experimental resources is common in areas such as synthetic biology (Constante et al., 2011) and cell biology (Chen et al., 2005; Collins et al., 1991; Hall et al., 2017), and also in some single institutions (https://plasmid.med.harvard.edu/PLASMID/Home.xhtml; accessed 17th September 2017).

7.3 Developing a new protocol for high-yield expression and purification of tau

At the start of this project the expression and purification of tau protein appeared difficult, time-consuming and resource intensive (Csokova et al., 2004). Only a few detailed protocols were available (Barghorn et al., 2005; Csokova et al., 2004). In an attempt to simplify the tau expression and purification process, a simple but high yield protocol was developed (Chapter 4). IMAC was used to purify bacterial-expressed tau followed by optional cleavage of the polyhistidine tag and a chromatographic isolation of the tag-free protein. With this protocol, the expression and purification process could be completed in 2 or 3 days for His-tagged and tag-free tau respectively, far shorter than for other published protocols (Barghorn et al., 2005; Csokova et al., 2004). At the time of writing, the method used had been further improved to produce even higher yields of tau K18 (10 mg/ml per 500 ml culture) and also adapted for the production of htau40 and its variants.

7.4 Preparation of stabilised tau oligomers

Tau oligomers have become an attractive research focus due to their abundance in tauopathy brains, ability to seed tau aggregation and propagation, and most importantly, their correlation with neurodegeneration in cellular and organismal model systems that seems to be independent of fibrils. Although patient brain-derived tau oligomers are the most disease-relevant forms of oligomers, they are often in short supply. Oligomers prepared from recombinant tau are therefore frequently used for cell biology and biochemical experiments because they closely resemble the naturally-occurring oligomers in structure and function. However, oligomer preparation methods vary considerably, in terms of buffers, inducers, and cross seeds (section 5.1). This likely affects experimental outcomes due to inconsistencies in oligomer sizes, stability and secondary structure. Moreover, some of the common methods have limited applications due to their deviation from brain-derived oligomers. For example, heparin-induced oligomers are not ideal for injection into live animal brains for *in vivo* experimentation due to the risk of haemorrhage induction (Clark et al., 1991). Furthermore, oligomers produced by

heparin induction and/or cross-seeding are unstable due to the high aggregation propensity (Lasagna-Reeves et al., 2010).

In this project, AF-maleimide labelling of tau K18 provided a simple way to stabilise oligomers, in addition to providing a fluorescent marker for their cellular internalisation. TEM analysis showed abundance of granular oligomers compared to control samples which aggregated into filaments. This finding was consistent with that of dot blotting with an aggregation stage-specific antibody (see Section 5.2). These observations suggest that AF-maleimide labelling can be used as a simple approach of preparing stable oligomers.

7.5 ThT fluorescence is not a universal indicator of proteinopathic aggregation

Outcomes of the ThT assay and the AFM single-molecule analysis of endpoint samples (Fig. 6.2) support the notion that the V337M and N279K polymorphisms lead to distinct conformations of tau K18. This exemplifies the importance of using complementary techniques in probing protein aggregation. Nonetheless, the ThT assay, mostly used in isolation, remains arguably the most widely used indicator of protein aggregation (Coelho-Cerqueira et al., 2014). The correlation between ThT fluorescence and protein aggregation is poorly defined but based on the current data and those of others (Coelho-Cerqueira et al., 2014; Hatami et al., 2017; Lindberg et al., 2017; Wong et al., 2016), two classes of this relationship can be proposed: (i) where ThT fluorescence readings have no direct relationship with the extent of aggregation because the test protein adopts conformations that do not support cumulative ThT binding, or (ii) increasing ThT fluorescence reflects enhanced aggregation kinetics due to direct correlation between protein conformation and ThT binding. The results in Fig. 6.2 provide an example of the first scenario. This is corroborated by independent observations for other proteinopathic proteins, including amyloid beta and its disease-related variants (Hatami et al., 2017) and amylin (Wong et al., 2016), arguing that adoption of dynamic conformations by neurodegenerative proteins is a common phenomenon which may not be easily elucidated by ThT binding. On the other hand, the second scenario (where increasing ThT fluorescence corresponds to aggregation kinetics) is supported by

data on monomeric and dimeric amyloid beta aggregation (O'Malley et al., 2016). The influence of experimental design and methodology on observed ThT binding features cannot be ruled out because the same protein can exhibit diverse ThT fluorescence behaviour when experimental setup (e.g., buffer composition) is varied (Wong et al., 2016). However, the fact that different proteins can assume distinct ThT binding features in identical experimental setups, as shown in Fig. 6.2 and by others (Hatami et al., 2017; Wong et al., 2016), strongly supports the proposition of ThT being an indicator of conformation and not necessary one of aggregation. The use of complementary structural characterisation techniques such as AFM or TEM is therefore recommended to avoid possible ambiguity of ThT signal's association with protein conformation and aggregation.

7.6 Internalisation of tau oligomers and the induction of neurotoxicity

The observed distinction in internalisation of the WT and the FTD forms of tau K18 could be due to a changed interaction with endocytic and/or plasma membrane proteins which facilitates their cellular entry because of their altered conformations. This hypothesis is supported by findings that internalised tau permeabilises endosomal membranes, a process closely regulated by tau-endosomal protein binding (Calafate et al., 2016). Tau internalisation can occur via multiple endocytic pathways and is therefore regulated by several proteins involved in these processes. For example, tau bound to neuronal receptors such as the muscarinic receptors M1 and M3 can be endocytosed through clathrin-dependent mechanisms (Gómez-Ramos et al., 2008). Other mechanisms of tau internalisation have been described, including those which appear to be regulated by plasma membrane proteins such as heparan sulfate proteoglycans (Holmes et al., 2013). In addition to these proteins directly involved in endocytic pathways, the binding of tau to specific AD-risk proteins, such as those encoded by the BIN1, PICALM, ApoE, and CLU genes can modulate the protein's internalisation (Ando et al., 2016; Avila et al., 2015). The most compelling evidence so far has been shown for BIN1 which negatively modulates tau endocytosis: BIN1 overexpression decreases tau internalisation and vice versa (Calafate et al., 2016). Further studies on the interaction of WT and FTD

tau with these endocysis-regulating proteins may help to understand the endocytic pathways and steps critical for the improved cellular entry of the FTD tau K18.

The previous observation that internalised tau oligomers can cause cytotoxicity was the motivation for studying effects of the tau K18 oligomers in the LDH leakage assay. The result that LDH release was not significant even at high oligomer concentrations was surprising given that some previous studies had reported the opposite (Lasagna-Reeves et al., 2010, 2012). However, the current data is consistent with others (Kaniyappan et al., 2017; Kumar et al., 2014; Tepper et al., 2014). These divergent data may be due to differences in the: (i) source of oligomers and the preparation methods, (ii) concentration of oligomers applied to cells, and (iii) other treatment conditions such as the type of cytotoxicity assay used. For example, 3 – 72 h treatment of SH-SY5Y cells or mouse primary cortical neurons with up to 10 μM WT K18 oligomers prepared from recombinant sources or extracted from Sf9 cells did not cause significant cytotoxicity in the LDH or MTT (3-(4,5-dimethylthiazol-2-yl)-2,5-diphenyltetrazolium bromide) assays (Kumar et al., 2014; Tepper et al., 2014). However, htau40 oligomers prepared by cross seeding with α-synuclein, amyloid β or AD brain-derived oligomers were significantly cytotoxic at 0.1μM – 1 μM, using the MTS (3-(4,5-dimethylthiazol-2-yl)-5-(3-carboxymethoxyphenyl)-2-(4 sulfophenyl)-2H-tetrazolium) assay (Lasagna-Reeves et al., 2010, 2012a). The ability of tau oligomers to induce cytotoxicity can therefore be said to be assay-specific.

Even if tau oligomers are cytotoxic, the immediate effect of their internalisation will most likely not be in the form of cell death because necrosis is a process rather than an event. Since one of the significant effects of tau accumulation is disturbance to synaptic processes (Yin et al., 2016), I hypothesise that the immediate effect will manifest through disruption of synaptic transmission by impairing neuronal form and function. As shown recently from Merck Laboratories, the internalisation of htau40 oligomers in hiPSC neurons can lead to impairments in neuritic processes and thereby corrupts neurotransmission and eventually leads to synaptic and neuronal loss (Usenovic et al., 2015). Moreover, internalised oligomers can cause synaptotoxicity in the form of dendritic spine loss and increments in reactive

oxygen species and intracellular calcium levels, without being cytotoxic or reducing cell viability (as measured by the LDH and the MTT tests) (Kaniyappan et al., 2017; Kumar et al., 2014; Tepper et al., 2014).

7.7 Co-localisation of internalised tau with endogenous tau

Interaction of internalised extracellular tau with endogenous tau seems to be a focal point in the cell-to-cell propagation mechanism for misfolded tau and the induction of functional toxicity (section 1.6). It was therefore investigated if the internalised tau co-localised with endogenous tau, using the HT7 antibody whose epitope is in the mid-region of full-length tau, hence outside K18. The observed co-localisation between internalised K18 and HT7-positive endogenous tau points to a likelihood that internalised tau K18 recruit endogenous tau into forming larger aggregates. This suggests a templated seeding mechanism of aggregation for K18 (Fig. 7.1). Previous reports have recorded that internalised tau K18 indeed interacts with endogenous tau to form larger aggregates some of which are subsequently secreted perhaps to seed the internalisation cycle (Michel et al., 2014). It is rather unclear if there are different forms of endogenous tau with which the WT and FTD tau K18 co-localised, because the HT7 epitope is ubiquitous to all tau isoforms. It remains to be shown if the WT and FTD tau K18 differ in their preference for endogenous tau co-localising partners, for example in terms of isoform specificity, phosphorylation, acetylation and truncation. Nevertheless, the findings here have shown that WT and FTD tau K18 may interact with endogenous mid-region-containing tau species both in the nucleus and the cytoplasm, and lays the foundation for future studies.

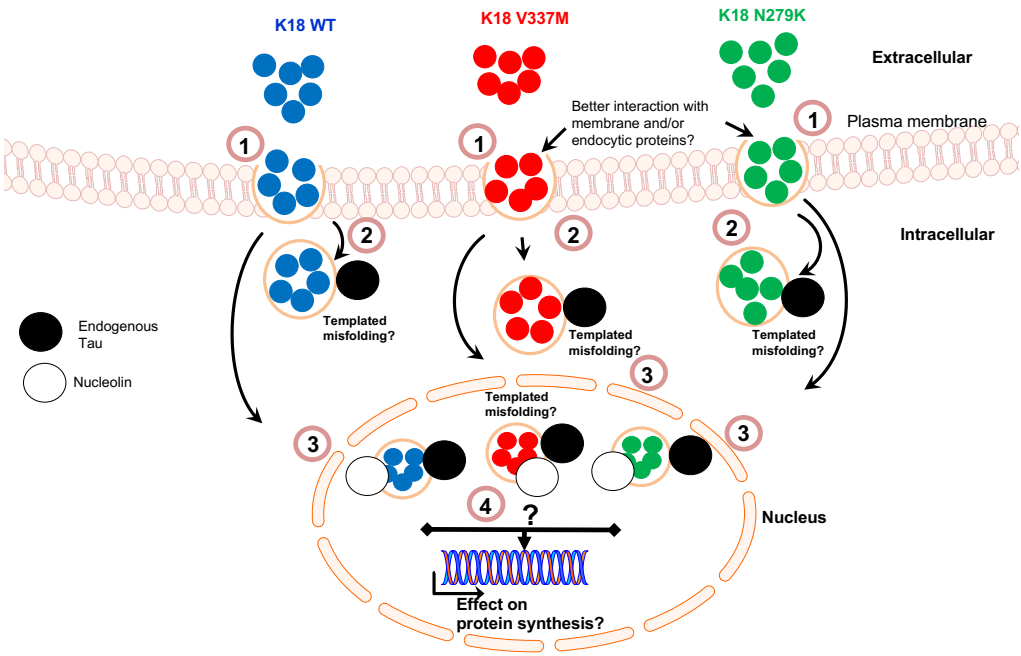

Figure 7.1 Internalised WT and FTD tau K18 likely seed the aggregation of endogenous tau and may have critical effects on ribosomal biosynthesis.
This proposed model of the cellular entry of exogenous tau K18 oligomers, and the functions and subcellular localisation of the internalised proteins suggests that: (1) some of the tau K18 proteins released into the extracellular environment, either resulting from neuronal death or secretion by physiologically active neurons, enter new neurons by initial uptake into endocytic vesicles which ensures their trafficking across the plasma membrane. The differential internalisation of the tau K18 variants may be due to their distinctive interaction with specific components of the endocytosis pathway. (2) Endocytosed tau K18 are delivered intracellularly encapsulated in endocytic vesicles. It is unclear whether the internalised tau K18 leave the intravesicular environment. However, the internalised tau (whether in vesicles or not) bind to endogenous tau and initiate a templated misfolding mechanism by possibly recruiting other endogenous proteins into forming larger aggregates. (3) Instead of neuritic deposition, some of the internalised tau K18 are transported into the nucleus (through a mechanism yet unknown) where they seed the aggregation of nuclear tau. (4) The nucleus-internalised tau K18 bind to nucleolin, and possibly other ribosomal proteins, and likely induces effects on neuronal protein synthesis. As previous reports have shown that internalised tau affects synaptic transmission, it is proposed that synaptic proteins will be among those critically affected.

Experiments aimed at demonstrating the release of internalised extracellular tau were attempted with WB using the HT7 and total tau (Dako) antibodies but perhaps the extremely low levels of released tau precluded the use of this assay to reproducibly detect tau secretion. An alternative strategy was attempted trying to confocal-image the tau-free medium that had been conditioned by cells after the initial tau K18 treatment and PBS wash. Unfortunately, the signal detection here

was small and not reproducible. To circumvent these problems in the future, the use of enzyme-linked immunosorbent assays was planned as this technique has been previously used to monitor tau release in cell lines expressing physiological levels of tau (Kanmert et al., 2015; Karch et al., 2012).

The challenges detailed above illustrate difficulties involved in the use of cells expressing physiological levels of tau to model the cell-to-cell spread mechanism, and may justify the use of cell lines overexpressing tau for WB-based detection and quantification of tau release. However, cell lines overexpressing tau were deemed unsuitable for this project.

7.8 Co-localisation of internalised tau with nucleolin

The observation that nucleolin may be an interacting partner of nucleus-destined tau (section 6.2.16) further extends the previous report that the NFT-specific antibody TG-3 binds to nucleolin, suggesting that nucleolin is a component of NFT (Dranovsky et al., 2001). Given that nucleolin plays critical roles in ribosomal biogenesis (Ginisty et al., 1999), dysfunctional tau-nucleolin interactions may be involved in the protein synthesis impairments recorded in AD patients (Ding et al., 2005; Fig. 7.1). Interestingly, nucleolin expression is decreased in the substantia nigra pars compacta of human Parkinson's disease (PD) patients, and that this appears to induce oxidative stress and proteosomal dysfunction (Caudle et al., 2009). In line with this, reduced nucleolin expression and increased nucleolin phosphorylation have been reported in AD, FTD and other tauopathies (Husseman et al., 2000). The induction of dysfunctional protein synthesis may serve to unify the tau pathology found in PD and the tauopathies.

It would be informative to study the mechanism of nuclear entry for the internalised tau, and as to whether the observed tau-nucleolin co-localisation translates to an interaction between the two proteins using co-immunoprecipitation techniques. Such experiments may also demonstrate whether this putative interaction exists exclusively between nucleolin and the internalised tau or if endogenous tau-nucleolin complexes are also present. This would help identify the exact function

that internalised extracellular tau plays in its interaction with nucleolin, compared to endogenous tau.

7.9 Conclusion

Whilst genetic determinants provide vital information about risk factors of neurodegeneration, translating these data to help understand the mechanistic basis of disease processes is challenging. The hypothesis-driven approach used in this thesis has led to some findings that are likely to influence future studies. Firstly, the differential conformation of WT and FTD tau K18 means that therapeutic agents developed primarily against WT tau may not be effective against FTD tau, and vice versa. There are strong evidences in the literature corroborating this point of view, including that of Vargas-Caballero et al., (2017) who showed that WT and FTD tau vary in their ability to rescue amyloid β-dependent impairments in long term potentiation. Moreover, the R406W FTD mutation alters membrane binding properties of WT tau (Gauthier-Kemper et al., 2011). Furthermore, the amount of secreted tau varies for cells expressing WT or FTD tau (Karch et al., 2012; Mohamed et al., 2013). Since WT tau immunotherapy and other drug discovery efforts have not been successful so far (Mably et al., 2015), future attempts are likely to expand to FTD biomarkers. The results presented here highlight the need for data in drug targeting of tau variants since these proteins may behave differently in disease processes.

Secondly, internalised extracellular tau may have functions in modulating ribosomal biosynthesis by virtue of their co-localisation with nucleolin in the human cell models used. Since neurotransmission is impaired in AD models (Usenovic et al., 2015), and the levels of nucleolin and other nucleolar and ribosomal chaperones are reduced in AD brains (Hernández-Ortega et al., 2016), further studies focusing on understanding the role of internalised extracellular tau on the synthesis of specific synaptic proteins involved in neurotransmission may help establish the destruction of synaptic protein synthesis as a form of toxicity caused by the internalised dysfunctional tau. Proteins of interest may include pre- and post-synaptic proteins whose levels are reduced in one or more tauopathies. Notably, neurogranin-1, SNAP-25, synaptotagmin and PSD-95 whose levels are

reduced in tau-dependent pathology, have been proposed as novel biomarkers for diagnosis of, and drug development for, tauopathies (Brinkmalm et al., 2014; Lista et al., 2017; Öhrfelt et al., 2016; Shao et al., 2011).

8| References

Abedini, A., Plesner, A., Cao, P., Ridgway, Z., Zhang, J., Tu, L.-H., Middleton, C.T., Chao, B., Sartori, D.J., Meng, F., Wang, H., Wong, A.G., Zanni, M.T., Verchere, C.B., Raleigh, D.P., Schmidt, A.M., 2016. Time-resolved studies define the nature of toxic IAPP intermediates, providing insight for anti-amyloidosis therapeutics. eLife 5, e12977. https://doi.org/10.7554/eLife.12977

Abounit, S., Wu, J.W., Duff, K., Victoria, G.S., Zurzolo, C., 2016. Tunneling nanotubes: A possible highway in the spreading of tau and other prion-like proteins in neurodegenerative diseases. Prion 10, 344–351. https://doi.org/10.1080/19336896.2016.1223003

Alliance Protein Laboratories, Determination of protein secondary structure by circular dichroism, Available at http://www.ap-lab.com/circular_dichroism.htm, Accessed on 10th September, 2017.

Alonso, A. del C., Zaidi, T., Novak, M., Grundke-Iqbal, I., Iqbal, K., 2001. Hyperphosphorylation induces self-assembly of τ into tangles of paired helical filaments/straight filaments. Proc. Natl. Acad. Sci. U. S. A. 98, 6923–6928. https://doi.org/10.1073/pnas.121119298

Alonso, A.C., Zaidi, T., Grundke-Iqbal, I., Iqbal, K., 1994. Role of abnormally phosphorylated tau in the breakdown of microtubules in Alzheimer disease. Proc. Natl. Acad. Sci. U. S. A. 91, 5562–5566.

Alonso, A.D., Beharry, C., Corbo, C.P., Cohen, L.S., 2016. Molecular mechanism of prion-like tau-induced neurodegeneration. Alzheimers Dement. 12, 1090–1097. https://doi.org/10.1016/j.jalz.2015.12.014

Alzforum, *MAPT* mutations, Available at: http://www.alzforum.org/mutations/search?genes%5B%5D=492&diseases=&keywords-entry=&keywords=#results, Accessed on 8th September, 2017

An, Y.D., Du, Q.Z., Tong, L.Y., Yu, Z.W., Gong, X.W., 2015. Cloning, expression and purification of penicillin-binding protein 3 from Pseudomonas aeruginosa CMCC 10104. Protein Expr. Purif. 110, 37–42. https://doi.org/10.1016/j.pep.2014.12.004

Ando, K., Tomimura, K., Sazdovitch, V., Suain, V., Yilmaz, Z., Authelet, M., Ndjim, M., Vergara, C., Belkouch, M., Potier, M.-C., Duyckaerts, C., Brion, J.-P., 2016. Level of PICALM, a key component of clathrin-mediated endocytosis, is correlated with levels of phosphotau and autophagy-related proteins and is associated with tau inclusions in AD, PSP and Pick disease. Neurobiol. Dis. https://doi.org/10.1016/j.nbd.2016.05.017

Andorfer, C., Acker, C.M., Kress, Y., Hof, P.R., Duff, K., Davies, P., 2005. Cell-Cycle Reentry and Cell Death in Transgenic Mice Expressing Nonmutant Human Tau Isoforms. J. Neurosci. 25, 5446–5454. https://doi.org/10.1523/JNEUROSCI.4637-04.2005

Andreadis, A., Broderick, J.A., Kosik, K.S., 1995. Relative exon affinities and suboptimal splice site signals lead to non-equivalence of two cassette

exons. Nucleic Acids Res. 23, 3585–3593. https://doi.org/10.1093/nar/23.17.3585
Andreadis, A., Brown, W.M., Kosik, K.S., 1992. Structure and novel exons of the human tau gene. Biochemistry 31, 10626–10633. https://doi.org/10.1021/bi00158a027
Arriagada, P.V., Growdon, J.H., Hedley-Whyte, E.T., Hyman, B.T., 1992. Neurofibrillary tangles but not senile plaques parallel duration and severity of Alzheimer's disease. Neurology 42, 631–639.
Avila, J., Gómez-Ramos, A., Marta, B., 2015. AD genetic risk factors and tau spreading. Front. Aging Neurosci. 7, 99. https://doi.org/10.3389/fnagi.2015.00099
Bader, B., Nübling, G., Mehle, A., Nobile, S., Kretzschmar, H., Giese, A., 2011. Single particle analysis of tau oligomer formation induced by metal ions and organic solvents. Biochem. Biophys. Res. Commun. 411, 190–196. https://doi.org/10.1016/j.bbrc.2011.06.135
Baens, M., Noels, H., Broeckx, V., Hagens, S., Fevery, S., Billiau, A.D., Vankelecom, H., Marynen, P., 2006. The Dark Side of EGFP: Defective Polyubiquitination. PLoS ONE 1. https://doi.org/10.1371/journal.pone.0000054
Barghorn, S., Biernat, J., Mandelkow, E., 2005. Purification of recombinant tau protein and preparation of Alzheimer-paired helical filaments in vitro. Methods Mol. Biol. Clifton NJ 299, 35–51. https://doi.org/10.1385/1-59259-874-9:035
Barghorn, S., Davies, P., Mandelkow, E., 2004. Tau Paired Helical Filaments from Alzheimer's Disease Brain and Assembled in Vitro Are Based on β-Structure in the Core Domain. Biochemistry 43, 1694–1703. https://doi.org/10.1021/bi0357006
Barghorn, S., Mandelkow, E., 2002. Toward a Unified Scheme for the Aggregation of Tau into Alzheimer Paired Helical Filaments. Biochemistry 41, 14885–14896. https://doi.org/10.1021/bi026469j
Barghorn, S., Zheng-Fischhöfer, Q., Ackmann, M., Biernat, J., von Bergen, M., Mandelkow, E.-M., Mandelkow, E., 2000. Structure, Microtubule Interactions, and Paired Helical Filament Aggregation by Tau Mutants of Frontotemporal Dementias. Biochemistry 39, 11714–11721. https://doi.org/10.1021/bi000850r
Barker, W.W., Luis, C.A., Kashuba, A., Luis, M., Harwood, D.G., Loewenstein, D., Waters, C., Jimison, P., Shepherd, E., Sevush, S., Graff-Radford, N., Newland, D., Todd, M., Miller, B., Gold, M., Heilman, K., Doty, L., Goodman, I., Robinson, B., Pearl, G., Dickson, D., Duara, R., 2002. Relative frequencies of Alzheimer disease, Lewy body, vascular and frontotemporal dementia, and hippocampal sclerosis in the State of Florida Brain Bank. Alzheimer Dis. Assoc. Disord. 16, 203–212.
Bateman, R.J., Xiong, C., Benzinger, T.L.S., Fagan, A.M., Goate, A., Fox, N.C., Marcus, D.S., Cairns, N.J., Xie, X., Blazey, T.M., Holtzman, D.M., Santacruz, A., Buckles, V., Oliver, A., Moulder, K., Aisen, P.S., Ghetti, B., Klunk, W.E., McDade, E., Martins, R.N., Masters, C.L., Mayeux, R., Ringman, J.M., Rossor, M.N., Schofield, P.R., Sperling, R.A., Salloway, S., Morris, J.C., Dominantly Inherited Alzheimer Network, 2012. Clinical and biomarker changes in dominantly inherited Alzheimer's disease. N. Engl. J. Med. 367, 795–804. https://doi.org/10.1056/NEJMoa1202753

Beason-Held, L.L., Goh, J.O., An, Y., Kraut, M.A., O'Brien, R.J., Ferrucci, L., Resnick, S.M., 2013. Changes in Brain Function Occur Years before the Onset of Cognitive Impairment. J. Neurosci. 33, 18008–18014. https://doi.org/10.1523/JNEUROSCI.1402-13.2013

Belyy, V., Schlager, M.A., Foster, H., Reimer, A.E., Carter, A.P., Yildiz, A., 2016. The mammalian dynein-dynactin complex is a strong opponent to kinesin in a tug-of-war competition. Nat. Cell Biol. 18, 1018–1024. https://doi.org/10.1038/ncb3393

Benmerah, A., 2004. Endocytosis: Signaling from Endocytic Membranes to the Nucleus. Curr. Biol. 14, R314–R316. https://doi.org/10.1016/j.cub.2004.03.053

Bergen, M. von, Barghorn, S., Li, L., Marx, A., Biernat, J., Mandelkow, E.-M., Mandelkow, E., 2001. Mutations of Tau Protein in Frontotemporal Dementia Promote Aggregation of Paired Helical Filaments by Enhancing Local β-Structure. J. Biol. Chem. 276, 48165–48174.

Bergen, M. von, Friedhoff, P., Biernat, J., Heberle, J., Mandelkow, E.-M., Mandelkow, E., 2000. Assembly of τ protein into Alzheimer paired helical filaments depends on a local sequence motif (306VQIVYK311) forming β structure. Proc. Natl. Acad. Sci. 97, 5129–5134. https://doi.org/10.1073/pnas.97.10.5129

Bergmans, B.A., De Strooper, B., 2010. gamma-secretases: from cell biology to therapeutic strategies. Lancet Neurol. 9, 215–226. https://doi.org/10.1016/S1474-4422(09)70332-1

Bhat, R.V., Budd Haeberlein, S.L., Avila, J., 2004. Glycogen synthase kinase 3: a drug target for CNS therapies. J. Neurochem. 89, 1313–1317. https://doi.org/10.1111/j.1471-4159.2004.02422.x

Bhattacharya, K., Rank, K.B., Evans, D.B., Sharma, S.K., 2001. Role of Cysteine-291 and Cysteine-322 in the Polymerization of Human Tau into Alzheimer-like Filaments. Biochem. Biophys. Res. Commun. 285, 20–26. https://doi.org/10.1006/bbrc.2001.5116

Biancalana, M., Koide, S., 2010. Molecular mechanism of Thioflavin-T binding to amyloid fibrils. Biochim. Biophys. Acta BBA - Proteins Proteomics 1804, 1405–1412. https://doi.org/10.1016/j.bbapap.2010.04.001

Boeve, B.F., Maraganore, D.M., Parisi, J.E., Ahlskog, J.E., Graff-Radford, N., Caselli, R.J., Dickson, D.W., Kokmen, E., Petersen, R.C., 1999. Pathologic heterogeneity in clinically diagnosed corticobasal degeneration. Neurology 53, 795–800.

Bolkan, B.J., Kretzschmar, D., 2014. Loss of tau results in defects in photoreceptor development and progressive neuronal degeneration in Drosophila. Dev. Neurobiol. 74, 1210–1225. https://doi.org/10.1002/dneu.22199

Boluda, S., Iba, M., Zhang, B., Raible, K.M., Lee, V.M.-Y., Trojanowski, J.Q., 2015. Differential induction and spread of tau pathology in young PS19 tau transgenic mice following intracerebral injections of pathological tau from Alzheimer's disease or corticobasal degeneration brains. Acta Neuropathol. (Berl.) 129, 221–237. https://doi.org/10.1007/s00401-014-1373-0

Braak, H., Braak, E., 1991. Neuropathological stageing of Alzheimer-related changes. Acta Neuropathol. (Berl.) 82, 239–259.

Brandt, R., Lee, G., 1993. Functional organization of microtubule-associated protein tau. Identification of regions which affect microtubule growth, nucleation, and bundle formation in vitro. J. Biol. Chem. 268, 3414–3419.
Brandt, R., Léger, J., Lee, G., 1995. Interaction of tau with the neural plasma membrane mediated by tau's amino-terminal projection domain. J. Cell Biol. 131, 1327–1340. https://doi.org/10.1083/jcb.131.5.1327
Brinkmalm, A., Brinkmalm, G., Honer, W.G., Frölich, L., Hausner, L., Minthon, L., Hansson, O., Wallin, A., Zetterberg, H., Blennow, K., Öhrfelt, A., 2014. SNAP-25 is a promising novel cerebrospinal fluid biomarker for synapse degeneration in Alzheimer's disease. Mol. Neurodegener. 9, 53. https://doi.org/10.1186/1750-1326-9-53
Bussière, T., Bard, F., Barbour, R., Grajeda, H., Guido, T., Khan, K., Schenk, D., Games, D., Seubert, P., Buttini, M., 2004. Morphological Characterization of Thioflavin-S-Positive Amyloid Plaques in Transgenic Alzheimer Mice and Effect of Passive Aβ Immunotherapy on Their Clearance. Am. J. Pathol. 165, 987–995.
Caceres, A., Kosik, K.S., 1990. Inhibition of neurite polarity by tau antisense oligonucleotides in primary cerebellar neurons. Nature 343, 461–463. https://doi.org/10.1038/343461a0
Calafate, S., Flavin, W., Verstreken, P., Moechars, D., 2016. Loss of Bin1 Promotes the Propagation of Tau Pathology. Cell Rep. 17, 931–940. https://doi.org/10.1016/j.celrep.2016.09.063
Cancino, G.I., Perez de Arce, K., Castro, P.U., Toledo, E.M., von Bernhardi, R., Alvarez, A.R., 2011. c-Abl tyrosine kinase modulates tau pathology and Cdk5 phosphorylation in AD transgenic mice. Neurobiol. Aging 32, 1249–1261. https://doi.org/10.1016/j.neurobiolaging.2009.07.007
Cancino, G.I., Toledo, E.M., Leal, N.R., Hernandez, D.E., Yévenes, L.F., Inestrosa, N.C., Alvarez, A.R., 2008. STI571 prevents apoptosis, tau phosphorylation and behavioural impairments induced by Alzheimer's β-amyloid deposits. Brain 131, 2425–2442. https://doi.org/10.1093/brain/awn125
Carvalho, F.A., Santos, N.C., 2012. Atomic force microscopy-based force spectroscopy — biological and biomedical applications. IUBMB Life 64, 465–472. https://doi.org/10.1002/iub.1037
Caudle, W.M., Kitsou, E., Li, J., Bradner, J., Zhang, J., 2009. A role for a novel protein, nucleolin, in Parkinson's disease. Neurosci. Lett. 459, 11–15. https://doi.org/10.1016/j.neulet.2009.04.060
Cenik, B., Sephton, C.F., Cenik, B.K., Herz, J., Yu, G., 2012. Progranulin: A Proteolytically Processed Protein at the Crossroads of Inflammation and Neurodegeneration. J. Biol. Chem. 287, 32298–32306. https://doi.org/10.1074/jbc.R112.399170
Chai, X., Dage, J.L., Citron, M., 2012. Constitutive secretion of tau protein by an unconventional mechanism. Neurobiol. Dis. 48, 356–366. https://doi.org/10.1016/j.nbd.2012.05.021
Chaumet, A., Wright, G.D., Seet, S.H., Tham, K.M., Gounko, N.V., Bard, F., 2015. Nuclear envelope-associated endosomes deliver surface proteins to the nucleus. Nat. Commun. 6, ncomms9218. https://doi.org/10.1038/ncomms9218

Chen, J., Kanai, Y., Cowan, N.J., Hirokawa, N., 1992. Projection domains of MAP2 and tau determine spacings between microtubules in dendrites and axons. Nature 360, 674–677. https://doi.org/10.1038/360674a0

Chen, M., Zhang, L., Zhang, H.-Y., Xiong, X., Wang, B., Du, Q., Lu, B., Wahlestedt, C., Liang, Z., 2005. A universal plasmid library encoding all permutations of small interfering RNA. Proc. Natl. Acad. Sci. U. S. A. 102, 2356–2361. https://doi.org/10.1073/pnas.0401549101

Chin, J., Palop, J.J., Puoliväli, J., Massaro, C., Bien-Ly, N., Gerstein, H., Scearce-Levie, K., Masliah, E., Mucke, L., 2005. Fyn Kinase Induces Synaptic and Cognitive Impairments in a Transgenic Mouse Model of Alzheimer's Disease. J. Neurosci. 25, 9694–9703. https://doi.org/10.1523/JNEUROSCI.2980-05.2005

Chin, J., Palop, J.J., Yu, G.-Q., Kojima, N., Masliah, E., Mucke, L., 2004. Fyn kinase modulates synaptotoxicity, but not aberrant sprouting, in human amyloid precursor protein transgenic mice. J. Neurosci. 24, 4692–4697. https://doi.org/10.1523/JNEUROSCI.0277-04.2004

Cisek, K., Cooper, G.L., Huseby, C.J., Kuret, J., 2014. Structure and mechanism of action of tau aggregation inhibitors. Curr. Alzheimer Res. 11, 918–927.

Clark, W.M., Madden, K.P., Lyden, P.D., Zivin, J.A., 1991. Cerebral hemorrhagic risk of aspirin or heparin therapy with thrombolytic treatment in rabbits. Stroke 22, 872–876. https://doi.org/10.1161/01.STR.22.7.872

Clavaguera, F., Akatsu, H., Fraser, G., Crowther, R.A., Frank, S., Hench, J., Probst, A., Winkler, D.T., Reichwald, J., Staufenbiel, M., Ghetti, B., Goedert, M., Tolnay, M., 2013. Brain homogenates from human tauopathies induce tau inclusions in mouse brain. Proc. Natl. Acad. Sci. 110, 9535–9540. https://doi.org/10.1073/pnas.1301175110

Clavaguera, F., Bolmont, T., Crowther, R.A., Abramowski, D., Frank, S., Probst, A., Fraser, G., Stalder, A.K., Beibel, M., Staufenbiel, M., Jucker, M., Goedert, M., Tolnay, M., 2009. Transmission and spreading of tauopathy in transgenic mouse brain. Nat. Cell Biol. 11, 909–913. https://doi.org/10.1038/ncb1901

Clavaguera, F., Grueninger, F., Tolnay, M., 2014. Intercellular transfer of tau aggregates and spreading of tau pathology: Implications for therapeutic strategies. Neuropharmacology 76 Pt A, 9–15. https://doi.org/10.1016/j.neuropharm.2013.08.037

Coelho-Cerqueira, E., Pinheiro, A.S., Follmer, C., 2014. Pitfalls associated with the use of Thioflavin-T to monitor anti-fibrillogenic activity. Bioorg. Med. Chem. Lett. 24, 3194–3198. https://doi.org/10.1016/j.bmcl.2014.04.072

Collins, C., Kuo, W.L., Segraves, R., Fuscoe, J., Pinkel, D., Gray, J.W., 1991. Construction and characterization of plasmid libraries enriched in sequences from single human chromosomes. Genomics 11, 997–1006.

Combs, B., Gamblin, T.C., 2012. FTDP-17 Tau Mutations Induce Distinct Effects on Aggregation and Microtubule Interactions. Biochemistry 51, 8597–8607. https://doi.org/10.1021/bi3010818

Combs, B., Hamel, C., Kanaan, N.M., 2016. Pathological conformations involving the amino terminus of tau occur early in Alzheimer's disease and are differentially detected by monoclonal antibodies. Neurobiol. Dis. 94, 18-31. https://doi.org/10.1016/j.nbd.2016.05.016

Conde, C., Cáceres, A., 2009. Microtubule assembly, organization and dynamics in axons and dendrites. Nat. Rev. Neurosci. 10, 319–332. https://doi.org/10.1038/nrn2631

Congdon, E.E., Kim, S., Bonchak, J., Songrug, T., Matzavinos, A., Kuret, J., 2008. Nucleation-dependent Tau Filament Formation. J. Biol. Chem. 283, 13806–13816. https://doi.org/10.1074/jbc.M800247200

Constante, M., Grünberg, R., Isalan, M., 2011. A Biobrick Library for Cloning Custom Eukaryotic Plasmids. PLOS ONE 6, e23685. https://doi.org/10.1371/journal.pone.0023685

Coppola, G., Chinnathambi, S., Lee, J.J., Dombroski, B.A., Baker, M.C., Soto-Ortolaza, A.I., Lee, S.E., Klein, E., Huang, A.Y., Sears, R., Lane, J.R., Karydas, A.M., Kenet, R.O., Biernat, J., Wang, L.-S., Cotman, C.W., Decarli, C.S., Levey, A.I., Ringman, J.M., Mendez, M.F., Chui, H.C., Le Ber, I., Brice, A., Lupton, M.K., Preza, E., Lovestone, S., Powell, J., Graff-Radford, N., Petersen, R.C., Boeve, B.F., Lippa, C.F., Bigio, E.H., Mackenzie, I., Finger, E., Kertesz, A., Caselli, R.J., Gearing, M., Juncos, J.L., Ghetti, B., Spina, S., Bordelon, Y.M., Tourtellotte, W.W., Frosch, M.P., Vonsattel, J.P.G., Zarow, C., Beach, T.G., Albin, R.L., Lieberman, A.P., Lee, V.M., Trojanowski, J.Q., Van Deerlin, V.M., Bird, T.D., Galasko, D.R., Masliah, E., White, C.L., Troncoso, J.C., Hannequin, D., Boxer, A.L., Geschwind, M.D., Kumar, S., Mandelkow, E.-M., Wszolek, Z.K., Uitti, R.J., Dickson, D.W., Haines, J.L., Mayeux, R., Pericak-Vance, M.A., Farrer, L.A., Alzheimer's Disease Genetics Consortium, Ross, O.A., Rademakers, R., Schellenberg, G.D., Miller, B.L., Mandelkow, E., Geschwind, D.H., 2012. Evidence for a role of the rare p.A152T variant in MAPT in increasing the risk for FTD-spectrum and Alzheimer's diseases. Hum. Mol. Genet. 21, 3500–3512. https://doi.org/10.1093/hmg/dds161

Cruts, M., Gijselinck, I., van der Zee, J., Engelborghs, S., Wils, H., Pirici, D., Rademakers, R., Vandenberghe, R., Dermaut, B., Martin, J.-J., van Duijn, C., Peeters, K., Sciot, R., Santens, P., De Pooter, T., Mattheijssens, M., Van den Broeck, M., Cuijt, I., Vennekens, K. 'l, De Deyn, P.P., Kumar-Singh, S., Van Broeckhoven, C., 2006. Null mutations in progranulin cause ubiquitin-positive frontotemporal dementia linked to chromosome 17q21. Nature 442, 920–924. https://doi.org/10.1038/nature05017

Csokova, N., Skrabana, R., Liebig, H.-D., Mederlyova, A., Kontsek, P., Novak, M., 2004. Rapid purification of truncated tau proteins: model approach to purification of functionally active fragments of disordered proteins, implication for neurodegenerative diseases. Protein Expr. Purif. 35, 366–372. https://doi.org/10.1016/j.pep.2004.01.012

Dawson, H.N., Cantillana, V., Chen, L., Vitek, M.P., 2007. The Tau N279K Exon 10 Splicing Mutation Recapitulates Frontotemporal Dementia and Parkinsonism Linked to Chromosome 17 Tauopathy in a Mouse Model. J. Neurosci. 27, 9155–9168. https://doi.org/10.1523/JNEUROSCI.5492-06.2007

Dawson, H.N., Ferreira, A., Eyster, M.V., Ghoshal, N., Binder, L.I., Vitek, M.P., 2001. Inhibition of neuronal maturation in primary hippocampal neurons from τ deficient mice. J. Cell Sci. 114, 1179–1187.

de Calignon, A., Polydoro, M., Suárez-Calvet, M., William, C., Adamowicz, D.H., Kopeikina, K.J., Pitstick, R., Sahara, N., Ashe, K.H., Carlson, G.A., Spires-Jones, T.L., Hyman, B.T., 2012. Propagation of tau pathology in a

model of early Alzheimer's disease. Neuron 73, 685–697. https://doi.org/10.1016/j.neuron.2011.11.033
De Strooper, B., Saftig, P., Craessaerts, K., Vanderstichele, H., Guhde, G., Annaert, W., Von Figura, K., Van Leuven, F., 1998. Deficiency of presenilin-1 inhibits the normal cleavage of amyloid precursor protein. Nature 391, 387–390. https://doi.org/10.1038/34910
DeJesus-Hernandez, M., Mackenzie, I.R., Boeve, B.F., Boxer, A.L., Baker, M., Rutherford, N.J., Nicholson, A.M., Finch, N.A., Flynn, H., Adamson, J., Kouri, N., Wojtas, A., Sengdy, P., Hsiung, G.-Y.R., Karydas, A., Seeley, W.W., Josephs, K.A., Coppola, G., Geschwind, D.H., Wszolek, Z.K., Feldman, H., Knopman, D.S., Petersen, R.C., Miller, B.L., Dickson, D.W., Boylan, K.B., Graff-Radford, N.R., Rademakers, R., 2011. Expanded GGGGCC hexanucleotide repeat in noncoding region of C9ORF72 causes chromosome 9p-linked FTD and ALS. Neuron 72, 245–256. https://doi.org/10.1016/j.neuron.2011.09.011
Derisbourg, M., Leghay, C., Chiappetta, G., Fernandez-Gomez, F.-J., Laurent, C., Demeyer, D., Carrier, S., Buée-Scherrer, V., Blum, D., Vinh, J., Sergeant, N., Verdier, Y., Buée, L., Hamdane, M., 2015. Role of the Tau N-terminal region in microtubule stabilization revealed by new endogenous truncated forms. Sci. Rep. 5, 9659. https://doi.org/10.1038/srep09659
Dickson, D.W., Kouri, N., Murray, M.E., Josephs, K.A., 2011. Neuropathology of Frontotemporal Lobar Degeneration–Tau (FTLD-Tau). J. Mol. Neurosci. 45, 384–389. https://doi.org/10.1007/s12031-011-9589-0
Ding, Q., Markesbery, W.R., Chen, Q., Li, F., Keller, J.N., 2005. Ribosome Dysfunction Is an Early Event in Alzheimer's Disease. J. Neurosci. 25, 9171–9175. https://doi.org/10.1523/JNEUROSCI.3040-05.2005
Dixit, R., Ross, J.L., Goldman, Y.E., Holzbaur, E.L.F., 2008. Differential Regulation of Dynein and Kinesin Motor Proteins by Tau. Science. https://doi.org/10.1126/science.1152993
Domoto-Reilly, K., Davis, M.Y., Keene, C.D., Bird, T.D., 2017. Unusually long duration and delayed penetrance in a family with FTD and mutation in MAPT (V337M). Am. J. Med. Genet. B Neuropsychiatr. Genet. 174, 70–74. https://doi.org/10.1002/ajmg.b.32443
Dranovsky, A., Vincent, I., Gregori, L., Schwarzman, A., Colflesh, D., Enghild, J., Strittmatter, W., Davies, P., Goldgaber, D., 2001. Cdc2 phosphorylation of nucleolin demarcates mitotic stages and Alzheimer's disease pathology. Neurobiol. Aging 22, 517–528. https://doi.org/10.1016/S0197-4580(00)00248-7
Drechsel, D.N., Hyman, A.A., Cobb, M.H., Kirschner, M.W., 1992. Modulation of the dynamic instability of tubulin assembly by the microtubule-associated protein tau. Mol. Biol. Cell 3, 1141–1154.
Du, X., Zheng, Y., Wang, Z., Chen, Y., Zhou, R., Song, G., Ni, J., Liu, Q., 2014. Inhibitory Act of Selenoprotein P on Cu+/Cu2+-Induced Tau Aggregation and Neurotoxicity. Inorg. Chem. 53, 11221–11230. https://doi.org/10.1021/ic501788v
Dufrêne, Y.F., 2002. Atomic Force Microscopy, a Powerful Tool in Microbiology. J. Bacteriol. 184, 5205–5213. https://doi.org/10.1128/JB.184.19.5205-5213.2002
Dujardin, S., Bégard, S., Caillierez, R., Lachaud, C., Delattre, L., Carrier, S.,

Loyens, A., Galas, M.-C., Bousset, L., Melki, R., Aurégan, G., Hantraye, P., Brouillet, E., Buée, L., Colin, M., 2014. Ectosomes: A New Mechanism for Non-Exosomal Secretion of Tau Protein. PLOS ONE 9, e100760. https://doi.org/10.1371/journal.pone.0100760

Ehrlich, M., Hallmann, A.-L., Reinhardt, P., Araúzo-Bravo, M.J., Korr, S., Röpke, A., Psathaki, O.E., Ehling, P., Meuth, S.G., Oblak, A.L., Murrell, J.R., Ghetti, B., Zaehres, H., Schöler, H.R., Sterneckert, J., Kuhlmann, T., Hargus, G., 2015. Distinct Neurodegenerative Changes in an Induced Pluripotent Stem Cell Model of Frontotemporal Dementia Linked to Mutant TAU Protein. Stem Cell Rep. 5, 83–96. https://doi.org/10.1016/j.stemcr.2015.06.001

Fá, M., Puzzo, D., Piacentini, R., Staniszewski, A., Zhang, H., Baltrons, M.A., Li Puma, D.D., Chatterjee, I., Li, J., Saeed, F., Berman, H.L., Ripoli, C., Gulisano, W., Gonzalez, J., Tian, H., Costa, J.A., Lopez, P., Davidowitz, E., Yu, W.H., Haroutunian, V., Brown, L.M., Palmeri, A., Sigurdsson, E.M., Duff, K.E., Teich, A.F., Honig, L.S., Sierks, M., Moe, J.G., D'Adamio, L., Grassi, C., Kanaan, N.M., Fraser, P.E., Arancio, O., 2016. Extracellular Tau Oligomers Produce An Immediate Impairment of LTP and Memory. Sci. Rep. 6, 19393. https://doi.org/10.1038/srep19393

Falcon, B., Cavallini, A., Angers, R., Glover, S., Murray, T.K., Barnham, L., Jackson, S., O'Neill, M.J., Isaacs, A.M., Hutton, M.L., Szekeres, P.G., Goedert, M., Bose, S., 2015. Conformation Determines the Seeding Potencies of Native and Recombinant Tau Aggregates. J. Biol. Chem. 290, 1049–1065. https://doi.org/10.1074/jbc.M114.589309

Fitzpatrick, A.W.P., Falcon, B., He, S., Murzin, A.G., Murshudov, G., Garringer, H.J., Crowther, R.A., Ghetti, B., Goedert, M., Scheres, S.H.W., 2017. Cryo-EM structures of tau filaments from Alzheimer's disease. Nature 547, 185–190. https://doi.org/10.1038/nature23002

Fontaine, S.N., Zheng, D., Sabbagh, J.J., Martin, M.D., Chaput, D., Darling, A., Trotter, J.H., Stothert, A.R., Nordhues, B.A., Lussier, A., Baker, J., Shelton, L., Kahn, M., Blair, L.J., Stevens, S.M., Dickey, C.A., 2016. DnaJ/Hsc70 chaperone complexes control the extracellular release of neurodegenerative-associated proteins. EMBO J. 35, 1537–1549. https://doi.org/10.15252/embj.201593489

Frandemiche, M.L., De Seranno, S., Rush, T., Borel, E., Elie, A., Arnal, I., Lanté, F., Buisson, A., 2014. Activity-dependent tau protein translocation to excitatory synapse is disrupted by exposure to amyloid-beta oligomers. J. Neurosci. 34, 6084–6097. https://doi.org/10.1523/JNEUROSCI.4261-13.2014

Friedhoff, P., Bergen, M. von, Mandelkow, E.-M., Davies, P., Mandelkow, E., 1998. A nucleated assembly mechanism of Alzheimer paired helical filaments. Proc. Natl. Acad. Sci. 95, 15712–15717. https://doi.org/10.1073/pnas.95.26.15712

Friedhoff, P., Schneider, A., Mandelkow, E.-M., Mandelkow, E., 1998. Rapid Assembly of Alzheimer-like Paired Helical Filaments from Microtubule-Associated Protein Tau Monitored by Fluorescence in Solution. Biochemistry 37, 10223–10230. https://doi.org/10.1021/bi980537d

Frost, B., Diamond, M.I., 2010. Prion-like mechanisms in neurodegenerative diseases. Nat. Rev. Neurosci. 11, 155–159. https://doi.org/10.1038/nrn2786

Frost, B., Jacks, R.L., Diamond, M.I., 2009. Propagation of tau misfolding from the outside to the inside of a cell. J. Biol. Chem. 284, 12845–12852. https://doi.org/10.1074/jbc.M808759200
Fujio, K., Sato, M., Uemura, T., Sato, T., Sato-Harada, R., Harada, A., 2007. 14-3-3 proteins and protein phosphatases are not reduced in tau-deficient mice. Neuroreport 18, 1049–1052. https://doi.org/10.1097/WNR.0b013e32818b2a0b
Gauthier-Kemper, A., Weissmann, C., Golovyashkina, N., Sebö-Lemke, Z., Drewes, G., Gerke, V., Heinisch, J.J., Brandt, R., 2011. The frontotemporal dementia mutation R406W blocks tau's interaction with the membrane in an annexin A2–dependent manner. J. Cell Biol. 192, 647–661. https://doi.org/10.1083/jcb.201007161
Gendron, T.F., Petrucelli, L., 2009. The role of tau in neurodegeneration. Mol. Neurodegener. 4, 13. https://doi.org/10.1186/1750-1326-4-13
Gerson, J.E., Kayed, R., 2013. Formation and propagation of tau oligomeric seeds. Neurodegeneration 4, 93. https://doi.org/10.3389/fneur.2013.00093
Gerson, J.E., Mudher, A., Kayed, R., 2016. Potential mechanisms and implications for the formation of tau oligomeric strains. Crit. Rev. Biochem. Mol. Biol. 0, 1–15. https://doi.org/10.1080/10409238.2016.1226251
Ghetti, B., Oblak, A.L., Boeve, B.F., Johnson, K.A., Dickerson, B.C., Goedert, M., 2015. Frontotemporal dementia caused by microtubule-associated protein tau gene (MAPT) mutations: a chameleon for neuropathology and neuroimaging. Neuropathol. Appl. Neurobiol. 41, 24–46. https://doi.org/10.1111/nan.12213
Ginisty, H., Sicard, H., Roger, B., Bouvet, P., 1999. Structure and functions of nucleolin. J. Cell Sci. 112 (Pt 6), 761–772.
Goedert, M., 2016. The ordered assembly of tau is the gain-of-toxic function that causes human tauopathies. Alzheimers Dement. 12, 1040–1050. https://doi.org/10.1016/j.jalz.2016.09.001
Goedert, M., Falcon, B., Clavaguera, F., Tolnay, M., 2014. Prion-like Mechanisms in the Pathogenesis of Tauopathies and Synucleinopathies. Curr. Neurol. Neurosci. Rep. 14, 495. https://doi.org/10.1007/s11910-014-0495-z
Goedert, M., Jakes, R., 2005. Mutations causing neurodegenerative tauopathies. Biochim. Biophys. Acta BBA - Mol. Basis Dis., The Biology and Pathobiology of Tau 1739, 240–250. https://doi.org/10.1016/j.bbadis.2004.08.007
Goedert, M., Jakes, R., 1990. Expression of separate isoforms of human tau protein: correlation with the tau pattern in brain and effects on tubulin polymerization. EMBO J. 9, 4225–4230.
Goedert, M., Spillantini, M.G., 2017. Propagation of Tau aggregates. Mol. Brain 10, 18. https://doi.org/10.1186/s13041-017-0298-7
Goedert, M., Spillantini, M.G., Potier, M.C., Ulrich, J., Crowther, R.A., 1989. Cloning and sequencing of the cDNA encoding an isoform of microtubule-associated protein tau containing four tandem repeats: differential expression of tau protein mRNAs in human brain. EMBO J. 8, 393–399.
Goedert, M., Wischik, C.M., Crowther, R.A., Walker, J.E., Klug, A., 1988. Cloning and sequencing of the cDNA encoding a core protein of the

paired helical filament of Alzheimer disease: identification as the microtubule-associated protein tau. Proc. Natl. Acad. Sci. 85, 4051–4055.
Golde, T.E., Borchelt, D.R., Giasson, B.I., Lewis, J., 2013. Thinking laterally about neurodegenerative proteinopathies. J. Clin. Invest. 123, 1847–1855. https://doi.org/10.1172/JCI66029
Gómez-Ramos, A., Díaz-Hernández, M., Rubio, A., Miras-Portugal, M.T., Avila, J., 2008. Extracellular tau promotes intracellular calcium increase through M1 and M3 muscarinic receptors in neuronal cells. Mol. Cell. Neurosci. 37, 673–681. https://doi.org/10.1016/j.mcn.2007.12.010
Goux, W.J., Kopplin, L., Nguyen, A.D., Leak, K., Rutkofsky, M., Shanmuganandam, V.D., Sharma, D., Inouye, H., Kirschner, D.A., 2004. The Formation of Straight and Twisted Filaments from Short Tau Peptides. J. Biol. Chem. 279, 26868–26875. https://doi.org/10.1074/jbc.M402379200
Greenfield, N.J., 2006. Using circular dichroism spectra to estimate protein secondary structure. Nat. Protoc. 1, 2876–2890. https://doi.org/10.1038/nprot.2006.202
Groenning, M., 2010. Binding mode of Thioflavin T and other molecular probes in the context of amyloid fibrils—current status. J. Chem. Biol. 3, 1–18. https://doi.org/10.1007/s12154-009-0027-5
Groenning, M., Olsen, L., van de Weert, M., Flink, J.M., Frokjaer, S., Jørgensen, F.S., 2007. Study on the binding of Thioflavin T to β-sheet-rich and non-β-sheet cavities. J. Struct. Biol. 158, 358–369. https://doi.org/10.1016/j.jsb.2006.12.010
Guerrero-Muñoz, M.J., Gerson, J., Castillo-Carranza, D.L., 2015. Tau Oligomers: The Toxic Player at Synapses in Alzheimer's Disease. Front. Cell. Neurosci. 9. https://doi.org/10.3389/fncel.2015.00464
Guillozet, A., Weintraub, S., Mash, D., Mesulam, M., 2003. Neurofibrillary tangles, amyloid, and memory in aging and mild cognitive impairment. Arch. Neurol. 60, 729–736. https://doi.org/10.1001/archneur.60.5.729
Guo, J.L., Lee, V.M.Y., 2014. Cell-to-cell transmission of pathogenic proteins in neurodegenerative diseases. Nat. Med. 20, 130–138. https://doi.org/10.1038/nm.3457
Guo, J.L., Lee, V.M.-Y., 2011. Seeding of normal Tau by pathological Tau conformers drives pathogenesis of Alzheimer-like tangles. J. Biol. Chem. 286, 15317–15331. https://doi.org/10.1074/jbc.M110.209296
Guo, T., Noble, W., Hanger, D.P., 2017. Roles of tau protein in health and disease. Acta Neuropathol. (Berl.) 133, 665–704. https://doi.org/10.1007/s00401-017-1707-9
Hall, T.E., Martel, N., Lo, H.P., Xiong, Z., Parton, R.G., 2017. A plasmid library of full-length zebrafish rab proteins for in vivo cell biology. Cell. Logist. 7, e1301151. https://doi.org/10.1080/21592799.2017.1301151
Hamano, T., Shirafuji, N., Makino, C., Yen, S.-H., Kanaan, N.M., Ueno, A., Suzuki, J., Ikawa, M., Matsunaga, A., Yamamura, O., Kuriyama, M., Nakamoto, Y., 2016. Pioglitazone prevents tau oligomerization. Biochem. Biophys. Res. Commun. https://doi.org/10.1016/j.bbrc.2016.08.016
Hampel, H., Blennow, K., Shaw, L.M., Hoessler, Y.C., Zetterberg, H., Trojanowski, J.Q., 2010. Total and Phosphorylated Tau Protein as Biological Markers of Alzheimer's Disease. Exp. Gerontol. 45, 30. https://doi.org/10.1016/j.exger.2009.10.010

Hanger, D.P., Anderton, B.H., Noble, W., 2009. Tau phosphorylation: the therapeutic challenge for neurodegenerative disease. Trends Mol. Med. 15, 112–119. https://doi.org/10.1016/j.molmed.2009.01.003

Hanger, D.P., Byers, H.L., Wray, S., Leung, K.-Y., Saxton, M.J., Seereeram, A., Reynolds, C.H., Ward, M.A., Anderton, B.H., 2007. Novel Phosphorylation Sites in Tau from Alzheimer Brain Support a Role for Casein Kinase 1 in Disease Pathogenesis. J. Biol. Chem. 282, 23645–23654. https://doi.org/10.1074/jbc.M703269200

Harada, A., Oguchi, K., Okabe, S., Kuno, J., Terada, S., Ohshima, T., Sato-Yoshitake, R., Takei, Y., Noda, T., Hirokawa, N., 1994. Altered microtubule organization in small-calibre axons of mice lacking tau protein. Nature 369, 488–491. https://doi.org/10.1038/369488a0

Hardy, J., Allsop, D., 1991. Amyloid deposition as the central event in the aetiology of Alzheimer's disease. Trends in Pharmacological Sciences 12, 383–388. https://doi.org/10.1016/0165-6147(91)90609-V

Hasegawa, M., Smith, M.J., Goedert, M., 1998. Tau proteins with FTDP-17 mutations have a reduced ability to promote microtubule assembly. FEBS Lett. 437, 207–210. https://doi.org/10.1016/S0014-5793(98)01217-4

Hasegawa, M., Smith, M.J., Iijima, M., Tabira, T., Goedert, M., 1999. FTDP-17 mutations N279K and S305N in tau produce increased splicing of exon 10. FEBS Lett. 443, 93–96. https://doi.org/10.1016/S0014-5793(98)01696-2

Hatami, A., Monjazeb, S., Milton, S., Glabe, C.G., 2017. Familial Alzheimer's Disease Mutations within the Amyloid Precursor Protein Alter the Aggregation and Conformation of the Amyloid-β Peptide. J. Biol. Chem. 292, 3172–3185. https://doi.org/10.1074/jbc.M116.755264

Hauw, J.J., Daniel, S.E., Dickson, D., Horoupian, D.S., Jellinger, K., Lantos, P.L., McKee, A., Tabaton, M., Litvan, I., 1994. Preliminary NINDS neuropathologic criteria for Steele-Richardson-Olszewski syndrome (progressive supranuclear palsy). Neurology 44, 2015–2019.

Hayden, E.Y., Kaur, P., Williams, T.L., Matsui, H., Yeh, S.-R., Rousseau, D.L., 2015. Heme Stabilization of α-Synuclein Oligomers during Amyloid Fibril Formation. Biochemistry 54, 4599–4610. https://doi.org/10.1021/acs.biochem.5b00280

Hernández-Ortega, K., Garcia-Esparcia, P., Gil, L., Lucas, J.J., Ferrer, I., 2016. Altered Machinery of Protein Synthesis in Alzheimer's: From the Nucleolus to the Ribosome. Brain Pathol. 26, 593–605. https://doi.org/10.1111/bpa.12335

Hogg, M., Grujic, Z.M., Baker, M., Demirci, S., Guillozet, A.L., Sweet, A.P., Herzog, L.L., Weintraub, S., Mesulam, M.-M., LaPointe, N.E., Gamblin, T.C., Berry, R.W., Binder, L.I., de Silva, R., Lees, A., Espinoza, M., Davies, P., Grover, A., Sahara, N., Ishizawa, T., Dickson, D., Yen, S.-H., Hutton, M., Bigio, E.H., 2003. The L266V tau mutation is associated with frontotemporal dementia and Pick-like 3R and 4R tauopathy. Acta Neuropathol. (Berl.) 106, 323–336. https://doi.org/10.1007/s00401-003-0734-x

Holmes, B.B., DeVos, S.L., Kfoury, N., Li, M., Jacks, R., Yanamandra, K., Ouidja, M.O., Brodsky, F.M., Marasa, J., Bagchi, D.P., Kotzbauer, P.T., Miller, T.M., Papy-Garcia, D., Diamond, M.I., 2013. Heparan sulfate proteoglycans mediate internalization and propagation of specific

proteopathic seeds. Proc. Natl. Acad. Sci. 110, E3138–E3147. https://doi.org/10.1073/pnas.1301440110

Hong, M., Zhukareva, V., Vogelsberg-Ragaglia, V., Wszolek, Z., Reed, L., Miller, B.I., Geschwind, D.H., Bird, T.D., McKeel, D., Goate, A., Morris, J.C., Wilhelmsen, K.C., Schellenberg, G.D., Trojanowski, J.Q., Lee, V.M.-Y., 1998. Mutation-Specific Functional Impairments in Distinct Tau Isoforms of Hereditary FTDP-17. Science 282, 1914–1917. https://doi.org/10.1126/science.282.5395.1914

Hoshi, M., Takashima, A., Noguchi, K., Murayama, M., Sato, M., Kondo, S., Saitoh, Y., Ishiguro, K., Hoshino, T., Imahori, K., 1996. Regulation of mitochondrial pyruvate dehydrogenase activity by tau protein kinase I/glycogen synthase kinase 3beta in brain. Proc. Natl. Acad. Sci. 93, 2719–2723.

Huang, Y., Wu, Z., Zhou, B., 2015. Behind the curtain of tauopathy: a show of multiple players orchestrating tau toxicity. Cell. Mol. Life Sci. 1–21. https://doi.org/10.1007/s00018-015-2042-8

Husseman, J.W., Nochlin, D., Vincent, I., 2000. Mitotic activation: a convergent mechanism for a cohort of neurodegenerative diseases. Neurobiol. Aging 21, 815–828. https://doi.org/10.1016/S0197-4580(00)00221-9

Huvent, I., Kamah, A., Cantrelle, F.-X., Barois, N., Slomianny, C., Smet-Nocca, C., Landrieu, I., Lippens, G., 2014. A functional fragment of Tau forms fibers without the need for an intermolecular cysteine bridge. Biochem. Biophys. Res. Commun. 445, 299–303. https://doi.org/10.1016/j.bbrc.2014.01.161

Iba, M., Guo, J.L., McBride, J.D., Zhang, B., Trojanowski, J.Q., Lee, V.M.-Y., 2013. Synthetic Tau Fibrils Mediate Transmission of Neurofibrillary Tangles in a Transgenic Mouse Model of Alzheimer's-Like Tauopathy. J. Neurosci. 33, 1024–1037. https://doi.org/10.1523/JNEUROSCI.2642-12.2013

Ittner, A., Chua, S.W., Bertz, J., Volkerling, A., Hoven, J. van der, Gladbach, A., Przybyla, M., Bi, M., Hummel, A. van, Stevens, C.H., Ippati, S., Suh, L.S., Macmillan, A., Sutherland, G., Kril, J.J., Silva, A.P.G., Mackay, J.P., Poljak, A., Delerue, F., Ke, Y.D., Ittner, L.M., 2016. Site-specific phosphorylation of tau inhibits amyloid-β toxicity in Alzheimer's mice. Science 354, 904–908. https://doi.org/10.1126/science.aah6205

Jackson, S.J., Kerridge, C., Cooper, J., Cavallini, A., Falcon, B., Cella, C.V., Landi, A., Szekeres, P.G., Murray, T.K., Ahmed, Z., Goedert, M., Hutton, M., O'Neill, M.J., Bose, S., 2016. Short Fibrils Constitute the Major Species of Seed-Competent Tau in the Brains of Mice Transgenic for Human P301S Tau. J. Neurosci. 36, 762–772. https://doi.org/10.1523/JNEUROSCI.3542-15.2016

Jeganathan, S., von Bergen, M., Mandelkow, E.-M., Mandelkow, E., 2008. The natively unfolded character of tau and its aggregation to Alzheimer-like paired helical filaments. Biochemistry 47, 10526–10539. https://doi.org/10.1021/bi800783d

Jicha, G.A., Rockwood, J.M., Berenfeld, B., Hutton, M., Davies, P., 1999. Altered conformation of recombinant frontotemporal dementia-17 mutant tau proteins. Neurosci. Lett. 260, 153–156. https://doi.org/10.1016/S0304-3940(98)00980-X

Jiji, A.C., Shine, A., Vijayan, V., 2016. Direct Observation of Aggregation-Induced Backbone Conformational Changes in Tau Peptides. Angew. Chem. Int. Ed. 55, 11562–11566. https://doi.org/10.1002/anie.201606544
Josephs, K.A., Whitwell, J.L., Dickson, D.W., Boeve, B.F., Knopman, D.S., Petersen, R.C., Parisi, J.E., Jack, C.R., 2008. Voxel-based morphometry in autopsy proven PSP and CBD. Neurobiol. Aging 29, 280–289. https://doi.org/10.1016/j.neurobiolaging.2006.09.019
Kadavath, H., Hofele, R.V., Biernat, J., Kumar, S., Tepper, K., Urlaub, H., Mandelkow, E., Zweckstetter, M., 2015. Tau stabilizes microtubules by binding at the interface between tubulin heterodimers. Proc. Natl. Acad. Sci. 112, 7501–7506. https://doi.org/10.1073/pnas.1504081112
Kanaan, N.M., Morfini, G.A., LaPointe, N.E., Pigino, G.F., Patterson, K.R., Song, Y., Andreadis, A., Fu, Y., Brady, S.T., Binder, L.I., 2011. Pathogenic forms of tau inhibit kinesin-dependent axonal transport through a mechanism involving activation of axonal phosphotransferases. J. Neurosci. Off. J. Soc. Neurosci. 31, 9858–9868. https://doi.org/10.1523/JNEUROSCI.0560-11.2011
Kanai, Y., Takemura, R., Oshima, T., Mori, H., Ihara, Y., Yanagisawa, M., Masaki, T., Hirokawa, N., 1989. Expression of multiple tau isoforms and microtubule bundle formation in fibroblasts transfected with a single tau cDNA. J. Cell Biol. 109, 1173–1184. https://doi.org/10.1083/jcb.109.3.1173
Kaniyappan, S., Chandupatla, R.R., Mandelkow, E.-M., Mandelkow, E., 2017. Extracellular low-n oligomers of tau cause selective synaptotoxicity without affecting cell viability. Alzheimers Dement. 13, 1270–1291. https://doi.org/10.1016/j.jalz.2017.04.002
Kanmert, D., Cantlon, A., Muratore, C.R., Jin, M., O'Malley, T.T., Lee, G., Young-Pearse, T.L., Selkoe, D.J., Walsh, D.M., 2015. C-Terminally Truncated Forms of Tau, But Not Full-Length Tau or Its C-Terminal Fragments, Are Released from Neurons Independently of Cell Death. J. Neurosci. 35, 10851–10865. https://doi.org/10.1523/JNEUROSCI.0387-15.2015
Karch, C.M., Jeng, A.T., Goate, A.M., 2012. Extracellular Tau Levels Are Influenced by Variability in Tau That Is Associated with Tauopathies. J. Biol. Chem. 287, 42751–42762. https://doi.org/10.1074/jbc.M112.380642
Karikari, T.K., Turner, A., Stass, R., Lee, L.C.Y., Wilson, B., Nagel, D.A., Hill, E.J., Moffat, K.G., 2017. Expression and purification of tau protein and its frontotemporal dementia variants using a cleavable histidine tag. Protein Expr. Purif. 130, 44–54. https://doi.org/10.1016/j.pep.2016.09.009
Kato, S., Nakamura, H., 1990. Presence of two different fibril subtypes in the Pick body: an immunoelectron microscopic study. Acta Neuropathol. (Berl.) 81, 125–129. https://doi.org/10.1007/BF00334500
Kelly, S.M., Jess, T.J., Price, N.C., 2005. How to study proteins by circular dichroism. Biochim. Biophys. Acta 1751, 119–139. https://doi.org/10.1016/j.bbapap.2005.06.005
Kim, D., Lim, S., Haque, M.M., Ryoo, N., Hong, H.S., Rhim, H., Lee, D.-E., Chang, Y.-T., Lee, J.-S., Cheong, E., Kim, D.J., Kim, Y.K., 2015. Identification of disulfide cross-linked tau dimer responsible for tau propagation. Sci. Rep. 5, 15231. https://doi.org/10.1038/srep15231
Kim, W., Lee, S., Hall, G.F., 2010. Secretion of human tau fragments resembling

CSF-tau in Alzheimer's disease is modulated by the presence of the exon 2 insert. FEBS Letters 584, 3085–3088. https://doi.org/10.1016/j.febslet.2010.05.042

King, M.E., Gamblin, T.C., Kuret, J., Binder, L.I., 2000. Differential Assembly of Human Tau Isoforms in the Presence of Arachidonic Acid. J. Neurochem. 74, 1749–1757. https://doi.org/10.1046/j.1471-4159.2000.0741749.x

Klein, P.S., Melton, D.A., 1996. A molecular mechanism for the effect of lithium on development. Proc. Natl. Acad. Sci. 93, 8455–8459.

Kolarova, M., García-Sierra, F., Bartos, A., Ricny, J., Ripova, D., 2012. Structure and Pathology of Tau Protein in Alzheimer Disease. Int. J. Alzheimer's Dis. 2012, e731526. https://doi.org/10.1155/2012/731526

Kovalevich, J., Langford, D., 2013. Considerations for the Use of SH-SY5Y Neuroblastoma Cells in Neurobiology, in: Neuronal Cell Culture, Methods in Molecular Biology. Humana Press, Totowa, NJ, pp. 9–21. https://doi.org/10.1007/978-1-62703-640-5_2

Krüger, L., Mandelkow, E.M., 2016. Tau neurotoxicity and rescue in animal models of human Tauopathies. Curr. Opin. Neurobiol. 36, 52–58. https://doi.org/10.1016/j.conb.2015.09.004

Ksiezak-Reding, H., Tracz, E., Yang, L.S., Dickson, D.W., Simon, M., Wall, J.S., 1996. Ultrastructural instability of paired helical filaments from corticobasal degeneration as examined by scanning transmission electron microscopy. Am. J. Pathol. 149, 639–651.

Kumar, S., Tepper, K., Kaniyappan, S., Biernat, J., Wegmann, S., Mandelkow, E.-M., Müller, D.J., Mandelkow, E., 2014. Stages and Conformations of the Tau Repeat Domain during Aggregation and Its Effect on Neuronal Toxicity. J. Biol. Chem. 289, 20318–20332. https://doi.org/10.1074/jbc.M114.554725

Lanoiselée, H.-M., Nicolas, G., Wallon, D., Rovelet-Lecrux, A., Lacour, M., Rousseau, S., Richard, A.-C., Pasquier, F., Rollin-Sillaire, A., Martinaud, O., Quillard-Muraine, M., Sayette, V. de la, Boutoleau-Bretonniere, C., Etcharry-Bouyx, F., Chauviré, V., Sarazin, M., Ber, I. le, Epelbaum, S., Jonveaux, T., Rouaud, O., Ceccaldi, M., Félician, O., Godefroy, O., Formaglio, M., Croisile, B., Auriacombe, S., Chamard, L., Vincent, J.-L., Sauvée, M., Marelli-Tosi, C., Gabelle, A., Ozsancak, C., Pariente, J., Paquet, C., Hannequin, D., Campion, D., Project, collaborators of the C.-M., 2017. APP, PSEN1, and PSEN2 mutations in early-onset Alzheimer disease: A genetic screening study of familial and sporadic cases. PLOS Med. 14, e1002270. https://doi.org/10.1371/journal.pmed.1002270

Lasagna-Reeves, C.A., Castillo-Carranza, D.L., Guerrero-Muñoz, M.J., Jackson, G.R., Kayed, R., 2010. Preparation and Characterization of Neurotoxic Tau Oligomers. Biochemistry 49, 10039–10041. https://doi.org/10.1021/bi1016233

Lasagna-Reeves, C.A., Castillo-Carranza, D.L., Sengupta, U., Clos, A.L., Jackson, G.R., Kayed, R., 2011. Tau oligomers impair memory and induce synaptic and mitochondrial dysfunction in wild-type mice. Mol. Neurodegener. 6, 39. https://doi.org/10.1186/1750-1326-6-39

Lasagna-Reeves, C.A., Castillo-Carranza, D.L., Sengupta, U., Guerrero-Munoz, M.J., Kiritoshi, T., Neugebauer, V., Jackson, G.R., Kayed, R., 2012a. Alzheimer brain-derived tau oligomers propagate pathology from endogenous tau. Sci. Rep. 2, 700. https://doi.org/10.1038/srep00700

Lasagna-Reeves, C.A., Castillo-Carranza, D.L., Sengupta, U., Sarmiento, J., Troncoso, J., Jackson, G.R., Kayed, R., 2012b. Identification of oligomers at early stages of tau aggregation in Alzheimer's disease. FASEB J. 26, 1946–1959. https://doi.org/10.1096/fj.11-199851

Leclerc, S., Garnier, M., Hoessel, R., Marko, D., Bibb, J.A., Snyder, G.L., Greengard, P., Biernat, J., Wu, Y.-Z., Mandelkow, E.-M., Eisenbrand, G., Meijer, L., 2001. Indirubins Inhibit Glycogen Synthase Kinase-3β and CDK5/P25, Two Protein Kinases Involved in Abnormal Tau Phosphorylation in Alzheimer's Disease A property common to most cyclin-dependent kinase inhibitors? J. Biol. Chem. 276, 251–260. https://doi.org/10.1074/jbc.M002466200

Lee, G., Neve, R.L., Kosik, K.S., 1989. The microtubule binding domain of tau protein. Neuron 2, 1615–1624.

Lee, S., Kim, W., Li, Z., Hall, G.F., 2012. Accumulation of vesicle-associated human tau in distal dendrites drives degeneration and tau secretion in an in situ cellular tauopathy model. Int. J. Alzheimers Dis. 2012, 172837. https://doi.org/10.1155/2012/172837

Lei, P., Ayton, S., Moon, S., Zhang, Q., Volitakis, I., Finkelstein, D.I., Bush, A.I., 2014. Motor and cognitive deficits in aged tau knockout mice in two background strains. Mol. Neurodegener. 9, 29. https://doi.org/10.1186/1750-1326-9-29

Leost, M., Schultz, C., Link, A., Wu, Y.Z., Biernat, J., Mandelkow, E.M., Bibb, J.A., Snyder, G.L., Greengard, P., Zaharevitz, D.W., Gussio, R., Senderowicz, A.M., Sausville, E.A., Kunick, C., Meijer, L., 2000. Paullones are potent inhibitors of glycogen synthase kinase-3beta and cyclin-dependent kinase 5/p25. Eur. J. Biochem. 267, 5983–5994.

LeVine, H., 1999. Quantification of β-sheet amyloid fibril structures with thioflavin T, in: Methods in Enzymology, Amyloid, Prions, and Other Protein Aggregates. Academic Press, pp. 274–284. https://doi.org/10.1016/S0076-6879(99)09020-5

Lewis, J., McGowan, E., Rockwood, J., Melrose, H., Nacharaju, P., Van Slegtenhorst, M., Gwinn-Hardy, K., Paul Murphy, M., Baker, M., Yu, X., Duff, K., Hardy, J., Corral, A., Lin, W.L., Yen, S.H., Dickson, D.W., Davies, P., Hutton, M., 2000. Neurofibrillary tangles, amyotrophy and progressive motor disturbance in mice expressing mutant (P301L) tau protein. Nat. Genet. 25, 402–405. https://doi.org/10.1038/78078

Li, W., Lee, V.M.-Y., 2006. Characterization of Two VQIXXK Motifs for Tau Fibrillization in Vitro. Biochemistry 45, 15692–15701. https://doi.org/10.1021/bi061422+

Lindberg, D.J., Wenger, A., Sundin, E., Wesén, E., Westerlund, F., Esbjörner, E.K., 2017. Binding of Thioflavin-T to Amyloid Fibrils Leads to Fluorescence Self-Quenching and Fibril Compaction. Biochemistry 56, 2170–2174. https://doi.org/10.1021/acs.biochem.7b00035

Lindberg, D.J., Wranne, M.S., Gilbert Gatty, M., Westerlund, F., Esbjörner, E.K., 2015. Steady-state and time-resolved Thioflavin-T fluorescence can report on morphological differences in amyloid fibrils formed by Aβ(1-40) and Aβ(1-42). Biochem. Biophys. Res. Commun. 458, 418–423. https://doi.org/10.1016/j.bbrc.2015.01.132

Ling, H., O'Sullivan, S.S., Holton, J.L., Revesz, T., Massey, L.A., Williams, D.R., Paviour, D.C., Lees, A.J., 2010. Does corticobasal degeneration

exist? A clinicopathological re-evaluation. Brain 133, 2045–2057. https://doi.org/10.1093/brain/awq123

Lista, S., Toschi, N., Baldacci, F., Zetterberg, H., Blennow, K., Kilimann, I., Teipel, S.J., Cavedo, E., Dos Santos, A.M., Epelbaum, S., Lamari, F., Dubois, B., Nisticò, R., Floris, R., Garaci, F., Hampel, H., Alzheimer Precision Medicine Initiative (APMI), 2017. Cerebrospinal Fluid Neurogranin as a Biomarker of Neurodegenerative Diseases: A Cross-Sectional Study. J. Alzheimers Dis. JAD 59, 1327–1334. https://doi.org/10.3233/JAD-170368

Litvan, I., Grimes, D.A., Lang, A.E., 2000. Phenotypes and prognosis: clinicopathologic studies of corticobasal degeneration. Adv. Neurol. 82, 183–196.

Liu, F., Gong, C.-X., 2008. Tau exon 10 alternative splicing and tauopathies. Mol. Neurodegener. 3, 8. https://doi.org/10.1186/1750-1326-3-8

Loomis, P.A., Howard, T.H., Castleberry, R.P., Binder, L.I., 1990. Identification of nuclear tau isoforms in human neuroblastoma cells. Proc. Natl. Acad. Sci. 87, 8422–8426. https://doi.org/10.1073/pnas.87.21.8422

Lucas, J.J., Hernández, F., Gómez-Ramos, P., Morán, M.A., Hen, R., Avila, J., 2001. Decreased nuclear beta-catenin, tau hyperphosphorylation and neurodegeneration in GSK-3beta conditional transgenic mice. EMBO J. 20, 27–39. https://doi.org/10.1093/emboj/20.1.27

Mably, A.J., Kanmert, D., Mc Donald, J.M., Liu, W., Caldarone, B.J., Lemere, C.A., O'Nuallain, B., Kosik, K.S., Walsh, D.M., 2015. Tau immunization: a cautionary tale? Neurobiol. Aging 36, 1316–1332. https://doi.org/10.1016/j.neurobiolaging.2014.11.022

Magnani, E., Fan, J., Gasparini, L., Golding, M., Williams, M., Schiavo, G., Goedert, M., Amos, L.A., Spillantini, M.G., 2007. Interaction of tau protein with the dynactin complex. EMBO J. 26, 4546–4554. https://doi.org/10.1038/sj.emboj.7601878

Manczak, M., Reddy, P.H., 2013. RNA silencing of genes involved in Alzheimer's disease enhances mitochondrial function and synaptic activity. Biochim. Biophys. Acta BBA - Mol. Basis Dis. 1832, 2368–2378. https://doi.org/10.1016/j.bbadis.2013.09.008

Mandelkow, E.-M., Mandelkow, E., 2012. Biochemistry and Cell Biology of Tau Protein in Neurofibrillary Degeneration. Cold Spring Harb. Perspect. Med. 2. https://doi.org/10.1101/cshperspect.a006247

Marshall, C.R., Guerreiro, R., Thust, S., Fletcher, P., Rohrer, J.D., Fox, N.C., 2015. A Novel MAPT Mutation Causing Corticobasal Syndrome Led by Progressive Apraxia of Speech. J. Alzheimers Dis. 48, 923–926. https://doi.org/10.3233/JAD-150477

Martin, L., Latypova, X., Wilson, C.M., Magnaudeix, A., Perrin, M.-L., Yardin, C., Terro, F., 2013. Tau protein kinases: Involvement in Alzheimer's disease. Ageing Res. Rev., Special Issue: Invertebrate Models of Aging 12, 289–309. https://doi.org/10.1016/j.arr.2012.06.003

Martinez, A., Alonso, M., Castro, A., Pérez, C., Moreno, F.J., 2002. First Non-ATP Competitive Glycogen Synthase Kinase 3 β (GSK-3β) Inhibitors: Thiadiazolidinones (TDZD) as Potential Drugs for the Treatment of Alzheimer's Disease. J. Med. Chem. 45, 1292–1299. https://doi.org/10.1021/jm011020u

Meier, S., Bell, M., Lyons, D.N., Rodriguez-Rivera, J., Ingram, A., Fontaine, S.N., Mechas, E., Chen, J., Wolozin, B., LeVine, H., Zhu, H., Abisambra, J.F., 2016. Pathological Tau Promotes Neuronal Damage by Impairing Ribosomal Function and Decreasing Protein Synthesis. J. Neurosci. 36, 1001–1007. https://doi.org/10.1523/JNEUROSCI.3029-15.2016

Meyer, V., Dinkel, P.D., Luo, Y., Yu, X., Wei, G., Zheng, J., Eaton, G.R., Ma, B., Nussinov, R., Eaton, S.S., Margittai, M., 2014a. Single Mutations in Tau Modulate the Populations of Fibril Conformers through Seed Selection. Angew. Chem. Int. Ed. 53, 1590–1593. https://doi.org/10.1002/anie.201308473

Meyer, V., Dinkel, P.D., Rickman Hager, E., Margittai, M., 2014b. Amplification of Tau Fibrils from Minute Quantities of Seeds. Biochemistry 53, 5804–5809. https://doi.org/10.1021/bi501050g

Meyer, V., Holden, M.R., Weismiller, H.A., Eaton, G.R., Eaton, S.S., Margittai, M., 2016. Fracture and Growth Are Competing Forces Determining the Fate of Conformers in Tau Fibril Populations. J. Biol. Chem. jbc.M116.715557. https://doi.org/10.1074/jbc.M116.715557

Michel, C.H., Kumar, S., Pinotsi, D., Tunnacliffe, A., George-Hyslop, P.S., Mandelkow, E., Mandelkow, E.-M., Kaminski, C.F., Schierle, G.S.K., 2014. Extracellular Monomeric Tau Protein Is Sufficient to Initiate the Spread of Tau Protein Pathology. J. Biol. Chem. 289, 956–967. https://doi.org/10.1074/jbc.M113.515445

Mizushima, F., Minoura, K., Tomoo, K., Sumida, M., Taniguchi, T., Ishida, T., 2006. Fluorescence-coupled CD conformational monitoring of filament formation of tau microtubule-binding repeat domain. Biochem. Biophys. Res. Commun. 343, 712–718. https://doi.org/10.1016/j.bbrc.2006.02.185

Mohamed, N.-V., Herrou, T., Plouffe, V., Piperno, N., Leclerc, N., 2013. Spreading of tau pathology in Alzheimer's disease by cell-to-cell transmission. Eur. J. Neurosci. 37, 1939–1948. https://doi.org/10.1111/ejn.12229

Moore, S., Evans, L.D.B., Andersson, T., Portelius, E., Smith, J., Dias, T.B., Saurat, N., McGlade, A., Kirwan, P., Blennow, K., Hardy, J., Zetterberg, H., Livesey, F.J., 2015. APP Metabolism Regulates Tau Proteostasis in Human Cerebral Cortex Neurons. Cell Reports 11, 689–696. https://doi.org/10.1016/j.celrep.2015.03.068

Morozova, O.A., March, Z.M., Robinson, A.S., Colby, D.W., 2013. Conformational Features of Tau Fibrils from Alzheimer's Disease Brain Are Faithfully Propagated by Unmodified Recombinant Protein. Biochemistry 52, 6960–6967. https://doi.org/10.1021/bi400866w

Mukrasch, M.D., Bibow, S., Korukottu, J., Jeganathan, S., Biernat, J., Griesinger, C., Mandelkow, E., Zweckstetter, M., 2009. Structural Polymorphism of 441-Residue Tau at Single Residue Resolution. PLoS Biol. 7. https://doi.org/10.1371/journal.pbio.1000034

Muratore, C.R., Rice, H.C., Srikanth, P., Callahan, D.G., Shin, T., Benjamin, L.N.P., Walsh, D.M., Selkoe, D.J., Young-Pearse, T.L., 2014. The familial Alzheimer's disease APPV717I mutation alters APP processing and Tau expression in iPSC-derived neurons. Hum Mol Genet 23, 3523–3536. https://doi.org/10.1093/hmg/ddu064

Murrell, J.R., Spillantini, M.G., Zolo, P., Guazzelli, M., Smith, M.J., Hasegawa, M., Redi, F., Crowther, R.A., Pietrini, P., Ghetti, B., Goedert, M., 1999. Tau gene mutation G389R causes a tauopathy with abundant pick body-like inclusions and axonal deposits. J. Neuropathol. Exp. Neurol. 58, 1207–1226.

Narasimhan, S., Guo, J.L., Changolkar, L., Stieber, A., McBride, J.D., Silva, L.V., He, Z., Zhang, B., Gathagan, R.J., Trojanowski, J.Q., Lee, V.M.Y., 2017. Pathological tau strains from human brains recapitulate the diversity of tauopathies in non-transgenic mouse brain. J. Neurosci. 1230–17. https://doi.org/10.1523/JNEUROSCI.1230-17.2017

Nelson, P.T., Alafuzoff, I., Bigio, E.H., Bouras, C., Braak, H., Cairns, N.J., Castellani, R.J., Crain, B.J., Davies, P., Del Tredici, K., Duyckaerts, C., Frosch, M.P., Haroutunian, V., Hof, P.R., Hulette, C.M., Hyman, B.T., Iwatsubo, T., Jellinger, K.A., Jicha, G.A., Kövari, E., Kukull, W.A., Leverenz, J.B., Love, S., Mackenzie, I.R., Mann, D.M., Masliah, E., McKee, A.C., Montine, T.J., Morris, J.C., Schneider, J.A., Sonnen, J.A., Thal, D.R., Trojanowski, J.Q., Troncoso, J.C., Wisniewski, T., Woltjer, R.L., Beach, T.G., 2012. Correlation of Alzheimer Disease Neuropathologic Changes with Cognitive Status: A Review of the Literature. J. Neuropathol. Exp. Neurol. 71, 362–381. https://doi.org/10.1097/NEN.0b013e31825018f7

Neve, R.L., Harris, P., Kosik, K.S., Kurnit, D.M., Donlon, T.A., 1986. Identification of cDNA clones for the human microtubule-associated protein tau and chromosomal localization of the genes for tau and microtubule-associated protein 2. Brain Res. 387, 271–280.

Novak, M., Kabat, J., Wischik, C.M., 1993. Molecular characterization of the minimal protease resistant tau unit of the Alzheimer's disease paired helical filament. EMBO J. 12, 365–370.

Nübling, G., Bader, B., Levin, J., Hildebrandt, J., Kretzschmar, H., Giese, A., 2012a. Synergistic influence of phosphorylation and metal ions on tau oligomer formation and coaggregation with α-synuclein at the single molecule level. Mol. Neurodegener. 7, 35. https://doi.org/10.1186/1750-1326-7-35

Nübling, G., Bader, B., Levin, J., Hildebrandt, J., Kretzschmar, H., Giese, A., 2012b. Synergistic influence of phosphorylation and metal ions on tau oligomer formation and coaggregation with α-synuclein at the single molecule level. Mol. Neurodegener. 7, 35. https://doi.org/10.1186/1750-1326-7-35

O'Brien, R.J., Wong, P.C., 2011. Amyloid Precursor Protein Processing and Alzheimer's Disease. Annu. Rev. Neurosci. 34, 185–204. https://doi.org/10.1146/annurev-neuro-061010-113613

Öhrfelt, A., Brinkmalm, A., Dumurgier, J., Brinkmalm, G., Hansson, O., Zetterberg, H., Bouaziz-Amar, E., Hugon, J., Paquet, C., Blennow, K., 2016. The pre-synaptic vesicle protein synaptotagmin is a novel biomarker for Alzheimer's disease. Alzheimers Res. Ther. 8, 41. https://doi.org/10.1186/s13195-016-0208-8

O'Malley, T.T., Witbold, W.M., Linse, S., Walsh, D.M., 2016. The Aggregation Paths and Products of Aβ42 Dimers Are Distinct from Those of the Aβ42 Monomer. Biochemistry 55, 6150–6161. https://doi.org/10.1021/acs.biochem.6b00453

O'Nuallain, B., Klyubin, I., Mc Donald, J.M., Foster, J.S., Welzel, A., Barry, A., Dykoski, R.K., Cleary, J.P., Gebbink, M.F.B.G., Rowan, M.J., Walsh, D.M., 2011. A monoclonal antibody against synthetic Aβ dimer assemblies neutralizes brain-derived synaptic plasticity-disrupting Aβ. J. Neurochem. 119, 189–201. https://doi.org/10.1111/j.1471-4159.2011.07389.x

Papanikolopoulou, K., Skoulakis, E.M.C., 2011. The Power and Richness of Modelling Tauopathies in Drosophila. Mol. Neurobiol. 44, 122–133. https://doi.org/10.1007/s12035-011-8193-1

Penido, M.G.M.G., Alon, U.S., 2012. Phosphate homeostasis and its role in bone health. Pediatr. Nephrol. Berl. Ger. 27, 2039–2048. https://doi.org/10.1007/s00467-012-2175-z

Perry, D.C., Lehmann, M., Yokoyama, J.S., Karydas, A., Lee, J.J., Coppola, G., Grinberg, L.T., Geschwind, D., Seeley, W.W., Miller, B.L., Rosen, H., Rabinovici, G., 2013. Progranulin mutations as risk factors for Alzheimer disease. JAMA Neurol. 70, 774–778. https://doi.org/10.1001/2013.jamaneurol.393

PlasmID repository, Harvard Medical School, Boston, USA. Available at: https://plasmid.med.harvard.edu/PLASMID/Home.xhtml; accessed 17th September 2017

Plouffe, V., Mohamed, N.-V., Rivest-McGraw, J., Bertrand, J., Lauzon, M., Leclerc, N., 2012. Hyperphosphorylation and cleavage at D421 enhance tau secretion. PloS One 7, e36873. https://doi.org/10.1371/journal.pone.0036873

Polydoro, M., Acker, C.M., Duff, K., Castillo, P.E., Davies, P., 2009. Age-Dependent Impairment of Cognitive and Synaptic Function in the htau Mouse Model of Tau Pathology. J. Neurosci. 29, 10741–10749. https://doi.org/10.1523/JNEUROSCI.1065-09.2009

Punnonen, E.L., Ryhänen, K., Marjomäki, V.S., 1998. At reduced temperature, endocytic membrane traffic is blocked in multivesicular carrier endosomes in rat cardiac myocytes. Eur. J. Cell Biol. 75, 344–352.

Puri, R., Suzuki, T., Yamakawa, K., Ganesh, S., 2009. Hyperphosphorylation and Aggregation of Tau in Laforin-deficient Mice, an Animal Model for Lafora Disease. J. Biol. Chem. 284, 22657–22663. https://doi.org/10.1074/jbc.M109.009688

Rademakers, R., Neumann, M., Mackenzie, I.R.A., 2012. Recent advances in the molecular basis of frontotemporal dementia. Nat. Rev. Neurol. 8, 423–434. https://doi.org/10.1038/nrneurol.2012.117

Rajamohamedsait, H.B., Sigurdsson, E.M., 2012. Histological Staining of Amyloid and Pre-Amyloid Peptides and Proteins in Mouse Tissue. Methods Mol. Biol. 849. https://doi.org/10.1007/978-1-61779-551-0_28

Ramachandran, G., Udgaonkar, J.B., 2011. Understanding the Kinetic Roles of the Inducer Heparin and of Rod-like Protofibrils during Amyloid Fibril Formation by Tau Protein. J. Biol. Chem. 286, 38948–38959. https://doi.org/10.1074/jbc.M111.271874

Rauch, J., Chen, J.J., Sorum, A.W., Miller, G.M., Sharf, T., See, S.K., Hsieh-Wilson, L.C., Kampmann, M., Kosik, K.S., 2017. Tau Internalization is Regulated by 6-O Sulfation on Heparan Sulfate Proteoglycans (HSPGs). bioRxiv 167874. https://doi.org/10.1101/167874

Ren, Y., Sahara, N., 2013. Characteristics of Tau Oligomers. Front. Neurol. 4. https://doi.org/10.3389/fneur.2013.00102

Renton, A.E., Majounie, E., Waite, A., Simón-Sánchez, J., Rollinson, S., Gibbs, J.R., Schymick, J.C., Laaksovirta, H., van Swieten, J.C., Myllykangas, L., Kalimo, H., Paetau, A., Abramzon, Y., Remes, A.M., Kaganovich, A., Scholz, S.W., Duckworth, J., Ding, J., Harmer, D.W., Hernandez, D.G., Johnson, J.O., Mok, K., Ryten, M., Trabzuni, D., Guerreiro, R.J., Orrell, R.W., Neal, J., Murray, A., Pearson, J., Jansen, I.E., Sondervan, D., Seelaar, H., Blake, D., Young, K., Halliwell, N., Callister, J.B., Toulson, G., Richardson, A., Gerhard, A., Snowden, J., Mann, D., Neary, D., Nalls, M.A., Peuralinna, T., Jansson, L., Isoviita, V.-M., Kaivorinne, A.-L., Hölttä-Vuori, M., Ikonen, E., Sulkava, R., Benatar, M., Wuu, J., Chiò, A., Restagno, G., Borghero, G., Sabatelli, M., ITALSGEN Consortium, Heckerman, D., Rogaeva, E., Zinman, L., Rothstein, J.D., Sendtner, M., Drepper, C., Eichler, E.E., Alkan, C., Abdullaev, Z., Pack, S.D., Dutra, A., Pak, E., Hardy, J., Singleton, A., Williams, N.M., Heutink, P., Pickering-Brown, S., Morris, H.R., Tienari, P.J., Traynor, B.J., 2011. A hexanucleotide repeat expansion in C9ORF72 is the cause of chromosome 9p21-linked ALS-FTD. Neuron 72, 257–268. https://doi.org/10.1016/j.neuron.2011.09.010

Rodríguez-Martín, T., Pooler, A.M., Lau, D.H.W., Mórotz, G.M., De Vos, K.J., Gilley, J., Coleman, M.P., Hanger, D.P., 2016. Reduced number of axonal mitochondria and tau hypophosphorylation in mouse P301L tau knockin neurons. Neurobiol. Dis. 85, 1–10. https://doi.org/10.1016/j.nbd.2015.10.007

Rosano, G.L., Ceccarelli, E.A., 2014. Recombinant protein expression in Escherichia coli: advances and challenges. Front. Microbiol. 5, 172. https://doi.org/10.3389/fmicb.2014.00172

Rosso, S.M., Van Herpen, E., Deelen, W., Kamphorst, W., Severijnen, L.-A., Willemsen, R., Ravid, R., Niermeijer, M.F., Dooijes, D., Smith, M.J., Goedert, M., Heutink, P., Van Swieten, J.C., 2002. A novel tau mutation, S320F, causes a tauopathy with inclusions similar to those in Pick's disease. Ann. Neurol. 51, 373–376. https://doi.org/10.1002/ana.10140

Sahara, N., Maeda, S., Murayama, M., Suzuki, T., Dohmae, N., Yen, S.-H., Takashima, A., 2007. Assembly of two distinct dimers and higher-order oligomers from full-length tau. Eur. J. Neurosci. 25, 3020–3029.

Saman, S., Kim, W., Raya, M., Visnick, Y., Miro, S., Saman, S., Jackson, B., McKee, A.C., Alvarez, V.E., Lee, N.C.Y., Hall, G.F., 2012. Exosome-associated tau is secreted in tauopathy models and is selectively phosphorylated in cerebrospinal fluid in early Alzheimer disease. J. Biol. Chem. 287, 3842–3849. https://doi.org/10.1074/jbc.M111.277061

Sanders, D.W., Kaufman, S.K., DeVos, S.L., Sharma, A.M., Mirbaha, H., Li, A., Barker, S.J., Foley, A.C., Thorpe, J.R., Serpell, L.C., Miller, T.M., Grinberg, L.T., Seeley, W.W., Diamond, M.I., 2014. Distinct Tau Prion Strains Propagate in Cells and Mice and Define Different Tauopathies. Neuron 82, 1271–1288. https://doi.org/10.1016/j.neuron.2014.04.047

Schafer, K.N., Cisek, K., Huseby, C.J., Chang, E., Kuret, J., 2013. Structural Determinants of Tau Aggregation Inhibitor Potency. J. Biol. Chem. 288, 32599–32611. https://doi.org/10.1074/jbc.M113.503474

Schneider, C.A., Rasband, W.S., Eliceiri, K.W., 2012. NIH Image to ImageJ: 25 years of image analysis. Nat. Methods 9, 671–675. https://doi.org/10.1038/nmeth.2089

Schweers, O., Mandelkow, E.M., Biernat, J., Mandelkow, E., 1995. Oxidation of cysteine-322 in the repeat domain of microtubule-associated protein tau controls the in vitro assembly of paired helical filaments. Proc. Natl. Acad. Sci. U. S. A. 92, 8463–8467.

Scott, M., Groth, D., Foster, D., Torchia, M., Yang, S.-L., DeArmond, S.J., Prusiner, S.B., 1993. Propagation of prions with artificial properties in transgenic mice expressing chimeric PrP genes. Cell 73, 979–988. https://doi.org/10.1016/0092-8674(93)90275-U

Seifert, A., Allan, L.A., Clarke, P.R., 2008. DYRK1A phosphorylates caspase 9 at an inhibitory site and is potently inhibited in human cells by harmine. FEBS J. 275, 6268–6280. https://doi.org/10.1111/j.1742-4658.2008.06751.x

Shammas, S.L., Garcia, G.A., Kumar, S., Kjaergaard, M., Horrocks, M.H., Shivji, N., Mandelkow, E., Knowles, T.P.J., Mandelkow, E., Klenerman, D., 2015. A mechanistic model of tau amyloid aggregation based on direct observation of oligomers. Nat. Commun. 6. https://doi.org/10.1038/ncomms8025

Shao, C.Y., Mirra, S.S., Sait, H.B.R., Sacktor, T.C., Sigurdsson, E.M., 2011. Postsynaptic degeneration as revealed by PSD-95 reduction occurs after advanced Aβ and tau pathology in transgenic mouse models of Alzheimer's disease. Acta Neuropathol. (Berl.) 122, 285–292. https://doi.org/10.1007/s00401-011-0843-x

Šimić, G., Babić Leko, M., Wray, S., Harrington, C., Delalle, I., Jovanov-Milošević, N., Bažadona, D., Buée, L., de Silva, R., Di Giovanni, G., Wischik, C., Hof, P.R., 2016. Tau Protein Hyperphosphorylation and Aggregation in Alzheimer's Disease and Other Tauopathies, and Possible Neuroprotective Strategies. Biomolecules 6, 6. https://doi.org/10.3390/biom6010006

Sivashanmugam, A., Murray, V., Cui, C., Zhang, Y., Wang, J., Li, Q., 2009. Practical protocols for production of very high yields of recombinant proteins using Escherichia coli. Protein Sci. 18, 936–948. https://doi.org/10.1002/pro.102

Sjöberg, M.K., Shestakova, E., Mansuroglu, Z., Maccioni, R.B., Bonnefoy, E., 2006. Tau protein binds to pericentromeric DNA: a putative role for nuclear tau in nucleolar organization. J. Cell Sci. 119, 2025–2034. https://doi.org/10.1242/jcs.02907

Smith, D.G., Buffet, M., Fenwick, A.E., Haigh, D., Ife, R.J., Saunders, M., Slingsby, B.P., Stacey, R., Ward, R.W., 2001. 3-Anilino-4-arylmaleimides: potent and selective inhibitors of glycogen synthase kinase-3 (GSK-3). Bioorg. Med. Chem. Lett. 11, 635–639. https://doi.org/10.1016/S0960-894X(00)00721-6

Soeda, Y., Yoshikawa, M., Almeida, O.F.X., Sumioka, A., Maeda, S., Osada, H., Kondoh, Y., Saito, A., Miyasaka, T., Kimura, T., Suzuki, M., Koyama, H., Yoshiike, Y., Sugimoto, H., Ihara, Y., Takashima, A., 2015. Toxic tau oligomer formation blocked by capping of cysteine residues with 1,2-dihydroxybenzene groups. Nat. Commun. 6, 10216. https://doi.org/10.1038/ncomms10216

Spillantini, M.G., Goedert, M., 2013. Tau pathology and neurodegeneration. Lancet Neurol. 12, 609–622. https://doi.org/10.1016/S1474-4422(13)70090-5

Spillantini, M.G., Goedert, M., 1998. Tau protein pathology in neurodegenerative diseases. Trends Neurosci. 21, 428–433. https://doi.org/10.1016/S0166-2236(98)01337-X

Sreerama, N., Woody, R.W., 2000. Estimation of protein secondary structure from circular dichroism spectra: comparison of CONTIN, SELCON, and CDSSTR methods with an expanded reference set. Anal. Biochem. 287, 252–260. https://doi.org/10.1006/abio.2000.4880

Stamer, K., Vogel, R., Thies, E., Mandelkow, E., Mandelkow, E.-M., 2002. Tau blocks traffic of organelles, neurofilaments, and APP vesicles in neurons and enhances oxidative stress. J. Cell Biol. 156, 1051–1063. https://doi.org/10.1083/jcb.200108057

Stancu, I.-C., Vasconcelos, B., Ris, L., Wang, P., Villers, A., Peeraer, E., Buist, A., Terwel, D., Baatsen, P., Oyelami, T., Pierrot, N., Casteels, C., Bormans, G., Kienlen-Campard, P., Octave, J.-N., Moechars, D., Dewachter, I., 2015. Templated misfolding of Tau by prion-like seeding along neuronal connections impairs neuronal network function and associated behavioral outcomes in Tau transgenic mice. Acta Neuropathol. (Berl.) 129, 875–894. https://doi.org/10.1007/s00401-015-1413-4

Stetefeld, J., McKenna, S.A., Patel, T.R., 2016. Dynamic light scattering: a practical guide and applications in biomedical sciences. Biophys. Rev. 8, 409–427. https://doi.org/10.1007/s12551-016-0218-6

Stöhr, J., Wu, H., Nick, M., Wu, Y., Bhate, M., Condello, C., Johnson, N., Rodgers, J., Lemmin, T., Acharya, S., Becker, J., Robinson, K., Kelly, M.J.S., Gai, F., Stubbs, G., Prusiner, S.B., DeGrado, W.F., 2017. A 31-residue peptide induces aggregation of tau's microtubule-binding region in cells. Nat. Chem. 9, 874–881. https://doi.org/10.1038/nchem.2754

Stoothoff, W.H., Johnson, G.V.W., 2005. Tau phosphorylation: physiological and pathological consequences. Biochim. Biophys. Acta BBA - Mol. Basis Dis., The Biology and Pathobiology of Tau 1739, 280–297. https://doi.org/10.1016/j.bbadis.2004.06.017

Sui, D., Liu, M., Kuo, M.-H., 2015. In Vitro Aggregation Assays Using Hyperphosphorylated Tau Protein. J. Vis. Exp. JoVE. https://doi.org/10.3791/51537

Sultan, A., Nesslany, F., Violet, M., Bégard, S., Loyens, A., Talahari, S., Mansuroglu, Z., Marzin, D., Sergeant, N., Humez, S., Colin, M., Bonnefoy, E., Buée, L., Galas, M.-C., 2011. Nuclear Tau, a Key Player in Neuronal DNA Protection. J. Biol. Chem. 286, 4566–4575. https://doi.org/10.1074/jbc.M110.199976

Tacik, P., DeTure, M., Hinkle, K.M., Lin, W.-L., Sanchez-Contreras, M., Carlomagno, Y., Pedraza, O., Rademakers, R., Ross, O.A., Wszolek, Z.K., Dickson, D.W., 2015. A Novel Tau Mutation in Exon 12, p.Q336H, Causes Hereditary Pick Disease. J. Neuropathol. Exp. Neurol. 74, 1042–1052. https://doi.org/10.1097/NEN.0000000000000248

Takashima, A., Noguchi, K., Michel, G., Mercken, M., Hoshi, M., Ishiguro, K., Imahori, K., 1996. Exposure of rat hippocampal neurons to amyloid beta peptide (25-35) induces the inactivation of phosphatidyl inositol-3 kinase

and the activation of tau protein kinase I/glycogen synthase kinase-3 beta. Neurosci. Lett. 203, 33–36.
Takauchi, S., Mizuhara, T., Miyoshi, K., 1983. Unusual paired helical filaments in progressive supranuclear palsy. Acta Neuropathol. (Berl.) 59, 225–228. https://doi.org/10.1007/BF00703207
Tanemura, K., Murayama, M., Akagi, T., Hashikawa, T., Tominaga, T., Ichikawa, M., Yamaguchi, H., Takashima, A., 2002. Neurodegeneration with tau accumulation in a transgenic mouse expressing V337M human tau. J. Neurosci. 22, 133–141.
Tardivel, M., Bégard, S., Bousset, L., Dujardin, S., Coens, A., Melki, R., Buée, L., Colin, M.,
2016. Tunneling nanotube (TNT)-mediated neuron-to neuron transfer of pathological Tau protein assemblies. Acta Neuropathologica Communications 4, 117. https://doi.org/10.1186/s40478-016-0386-4
Tepper, K., Biernat, J., Kumar, S., Wegmann, S., Timm, T., Hübschmann, S., Redecke, L., Mandelkow, E.-M., Müller, D.J., Mandelkow, E., 2014. Oligomer Formation of Tau Protein Hyperphosphorylated in Cells. J. Biol. Chem. 289, 34389–34407. https://doi.org/10.1074/jbc.M114.611368
Tinker-Mill, C., Mayes, J., Allsop, D., Kolosov, O.V., 2014. Ultrasonic force microscopy for nanomechanical characterization of early and late-stage amyloid-β peptide aggregation. Sci. Rep. 4. https://doi.org/10.1038/srep04004
Usenovic, M., Niroomand, S., Drolet, R.E., Yao, L., Gaspar, R.C., Hatcher, N.G., Schachter, J., Renger, J.J., Parmentier-Batteur, S., 2015. Internalized Tau Oligomers Cause Neurodegeneration by Inducing Accumulation of Pathogenic Tau in Human Neurons Derived from Induced Pluripotent Stem Cells. J. Neurosci. 35, 14234–14250. https://doi.org/10.1523/JNEUROSCI.1523-15.2015
Vargas-Caballero, M., Denk, F., Wobst, H.J., Arch, E., Pegasiou, C.-M., Oliver, P.L., Shipton, O.A., Paulsen, O., Wade-Martins, R., 2017. Wild-Type, but Not Mutant N296H, Human Tau Restores Aβ-Mediated Inhibition of LTP in Tau−/− mice. Front. Neurosci. 11. https://doi.org/10.3389/fnins.2017.00201
Vogelsberg-Ragaglia, V., Bruce, J., Richter-Landsberg, C., Zhang, B., Hong, M., Trojanowski, J.Q., Lee, V.M.-Y., 2000. Distinct FTDP-17 Missense Mutations in Tau Produce Tau Aggregates and Other Pathological Phenotypes in Transfected CHO Cells. Mol. Biol. Cell 11, 4093–4104. https://doi.org/10.1091/mbc.11.12.4093
von Bergen, M., Barghorn, S., Biernat, J., Mandelkow, E.-M., Mandelkow, E., 2005. Tau aggregation is driven by a transition from random coil to beta sheet structure. Biochim. Biophys. Acta BBA - Mol. Basis Dis. 1739, 158–166. https://doi.org/10.1016/j.bbadis.2004.09.010
Vossel, K.A., Xu, J.C., Fomenko, V., Miyamoto, T., Suberbielle, E., Knox, J.A., Ho, K., Kim, D.H., Yu, G.-Q., Mucke, L., 2015. Tau reduction prevents Aβ-induced axonal transport deficits by blocking activation of GSK3β. J Cell Biol 209, 419–433. https://doi.org/10.1083/jcb.201407065
Walsh, D.M., Selkoe, D.J., 2016. A critical appraisal of the pathogenic protein spread hypothesis of neurodegeneration. Nat. Rev. Neurosci. 17, 251–260. https://doi.org/10.1038/nrn.2016.13

Wang, J.-Z., Xia, Y.-Y., Grundke-Iqbal, I., Iqbal, K., 2013. Abnormal hyperphosphorylation of tau: sites, regulation, and molecular mechanism of neurofibrillary degeneration. J. Alzheimers Dis. 33 Suppl 1, S123-139. https://doi.org/10.3233/JAD-2012-129031

Wang, Y., Balaji, V., Kaniyappan, S., Krüger, L., Irsen, S., Tepper, K., Chandupatla, R., Maetzler, W., Schneider, A., Mandelkow, E., Mandelkow, E.-M., 2017. The release and trans-synaptic transmission of Tau via exosomes. Molecular Neurodegeneration 12, 5. https://doi.org/10.1186/s13024-016-0143-y

Wang, Y., Mandelkow, E., 2016. Tau in physiology and pathology. Nat. Rev. Neurosci. 17, 22–35. https://doi.org/10.1038/nrn.2015.1

Wauters, M., Wattiez, R., Ris, L., 2016. Internalization of the Extracellular Full-Length Tau Inside Neuro2A and Cortical Cells Is Enhanced by Phosphorylation. Biomolecules 6, 36. https://doi.org/10.3390/biom6030036

Weaver, C.L., Espinoza, M., Kress, Y., Davies, P., 2000. Conformational change as one of the earliest alterations of tau in Alzheimer's disease. Neurobiol. Aging 21, 719–727. https://doi.org/10.1016/S0197-4580(00)00157-3

Wen, G., Qin, W., Chen, D., Wang, Y., Yue, X., Liu, Z., Cao, Y., Du, J., Zhou, B., Bu, X., 2017. Stabilizing the monomeric amyloid-β peptide by tyrocidine A prevents and reverses amyloidogenesis without the accumulation of oligomers. Chem. Commun. 53, 3886–3889. https://doi.org/10.1039/C7CC00506G

Whitmore, L., Wallace, B.A., 2008. Protein secondary structure analyses from circular dichroism spectroscopy: Methods and reference databases. Biopolymers 89, 392–400. https://doi.org/10.1002/bip.20853

Whitmore, L., Wallace, B.A., 2004. DICHROWEB, an online server for protein secondary structure analyses from circular dichroism spectroscopic data. Nucleic Acids Res. 32, W668–W673. https://doi.org/10.1093/nar/gkh371

Williams, D.R., de Silva, R., Paviour, D.C., Pittman, A., Watt, H.C., Kilford, L., Holton, J.L., Revesz, T., Lees, A.J., 2005. Characteristics of two distinct clinical phenotypes in pathologically proven progressive supranuclear palsy: Richardson's syndrome and PSP-parkinsonism. Brain 128, 1247–1258. https://doi.org/10.1093/brain/awh488

Wischik, C.M., Crowther, R.A., Stewart, M., Roth, M., 1985. Subunit structure of paired helical filaments in Alzheimer's disease. J. Cell Biol. 100, 1905–1912. https://doi.org/10.1083/jcb.100.6.1905

Wischik, C.M., Novak, M., Thøgersen, H.C., Edwards, P.C., Runswick, M.J., Jakes, R., Walker, J.E., Milstein, C., Roth, M., Klug, A., 1988. Isolation of a fragment of tau derived from the core of the paired helical filament of Alzheimer disease. Proc. Natl. Acad. Sci. U. S. A. 85, 4506–4510.

Wolfe, M.S., Xia, W., Ostaszewski, B.L., Diehl, T.S., Kimberly, W.T., Selkoe, D.J., 1999. Two transmembrane aspartates in presenilin-1 required for presenilin endoproteolysis and gamma-secretase activity. Nature 398, 513–517. https://doi.org/10.1038/19077

Wong, A.G., Wu, C., Hannaberry, E., Watson, M.D., Shea, J.-E., Raleigh, D.P., 2016. Analysis of the Amyloidogenic Potential of Pufferfish (Takifugu rubripes) Islet Amyloid Polypeptide Highlights the Limitations of

Thioflavin-T Assays and the Difficulties in Defining Amyloidogenicity. Biochemistry 55, 510–518. https://doi.org/10.1021/acs.biochem.5b01107

Wu, J.W., Herman, M., Liu, L., Simoes, S., Acker, C.M., Figueroa, H., Steinberg, J.I., Margittai, M., Kayed, R., Zurzolo, C., Di Paolo, G., Duff, K.E., 2013. Small Misfolded Tau Species Are Internalized via Bulk Endocytosis and Anterogradely and Retrogradely Transported in Neurons. J Biol Chem 288, 1856–1870. https://doi.org/10.1074/jbc.M112.394528

Xiang, S., Kulminskaya, N., Habenstein, B., Biernat, J., Tepper, K., Paulat, M., Griesinger, C., Becker, S., Lange, A., Mandelkow, E., Linser, R., 2017. A two-component adhesive: Tau fibrils arise from a combination of a well-defined motif and conformationally flexible interactions. J. Am. Chem. Soc. https://doi.org/10.1021/jacs.6b09619

Xu, H., Rösler, T.W., Carlsson, T., de Andrade, A., Fiala, O., Hollerhage, M., Oertel, W.H., Goedert, M., Aigner, A., Höglinger, G.U., 2014. Tau silencing by siRNA in the P301S mouse model of tauopathy. Curr. Gene Ther. 14, 343–351.

Xue, C., Lin, T.Y., Chang, D., Guo, Z., 2017. Thioflavin T as an amyloid dye: fibril quantification, optimal concentration and effect on aggregation. Open Sci. 4, 160696. https://doi.org/10.1098/rsos.160696

Yan, P., Hu, X., Song, H., Yin, K., Bateman, R.J., Cirrito, J.R., Xiao, Q., Hsu, F.F., Turk, J.W., Xu, J., Hsu, C.Y., Holtzman, D.M., Lee, J.-M., 2006. Matrix Metalloproteinase-9 Degrades Amyloid-β Fibrils in Vitro and Compact Plaques in Situ. J. Biol. Chem. 281, 24566–24574. https://doi.org/10.1074/jbc.M602440200

Yang, E.J., Ahn, Y.S., Chung, K.C., 2001. Protein Kinase Dyrk1 Activates cAMP Response Element-binding Protein during Neuronal Differentiation in Hippocampal Progenitor Cells. J. Biol. Chem. 276, 39819–39824. https://doi.org/10.1074/jbc.M104091200

Yao, T.-M., Tomoo, K., Ishida, T., Hasegawa, H., Sasaki, M., Taniguchi, T., 2003. Aggregation Analysis of the Microtubule Binding Domain in Tau Protein by Spectroscopic Methods. J. Biochem. (Tokyo) 134, 91–99. https://doi.org/10.1093/jb/mvg116

Yin, Y., Gao, D., Wang, Y., Wang, Z.-H., Wang, X., Ye, J., Wu, D., Fang, L., Pi, G., Yang, Y., Wang, X.-C., Lu, C., Ye, K., Wang, J.-Z., 2016. Tau accumulation induces synaptic impairment and memory deficit by calcineurin-mediated inactivation of nuclear CaMKIV/CREB signaling. Proc. Natl. Acad. Sci. 113, E3773–E3781. https://doi.org/10.1073/pnas.1604519113

Yoshitake, J., Soeda, Y., Ida, T., Sumioka, A., Yoshikawa, M., Matsushita, K., Akaike, T., Takashima, A., 2016. Modification of Tau by 8-nitro-cGMP: Effects of Nitric Oxide-linked Chemical Modification on Tau Aggregation. J. Biol. Chem. jbc.M116.734350. https://doi.org/10.1074/jbc.M116.734350

Zhong, Q., Congdon, E.E., Nagaraja, H.N., Kuret, J., 2012. Tau Isoform Composition Influences Rate and Extent of Filament Formation. J. Biol. Chem. 287, 20711–20719. https://doi.org/10.1074/jbc.M112.364067

Zhou, L.-X., Du, J.-T., Zeng, Z.-Y., Wu, W.-H., Zhao, Y.-F., Kanazawa, K., Ishizuka, Y., Nemoto, T., Nakanishi, H., Li, Y.-M., 2007. Copper (II)

modulates in vitro aggregation of a tau peptide. Peptides 28, 2229–2234. https://doi.org/10.1016/j.peptides.2007.08.022

9| Appendix

9.1 Additional methods

9.1.1 Quantifying tau internalisation using pixel intensity and size (area) in Image J

Method adapted from Jensen (2013)

Procedure

1. Open image in Image J
2. Convert image to 8 bit
3. Edit → Invert

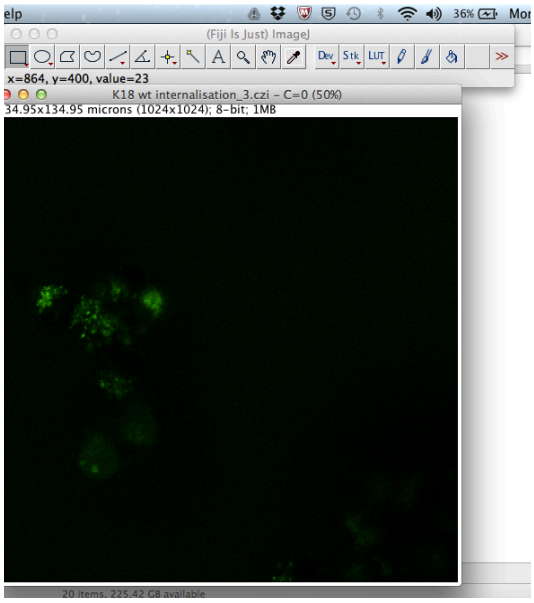

4. Image →Adjust → Threshold (adjust as appropriate, ensure tau shows red with no background noise)

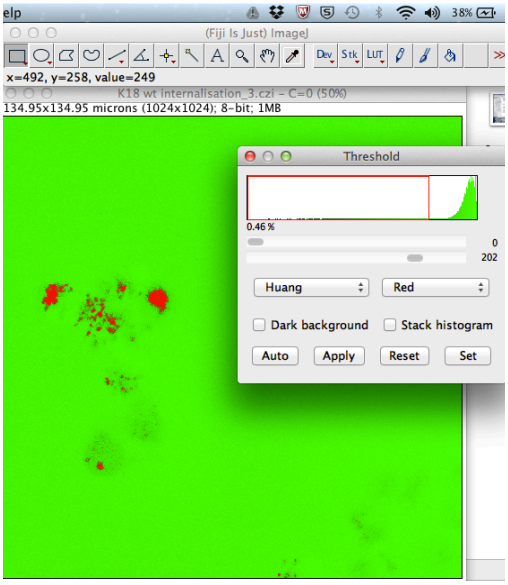

5. Change “default” on pull down menu to “Huang”. Press “Apply”. Tau positive area changes to black

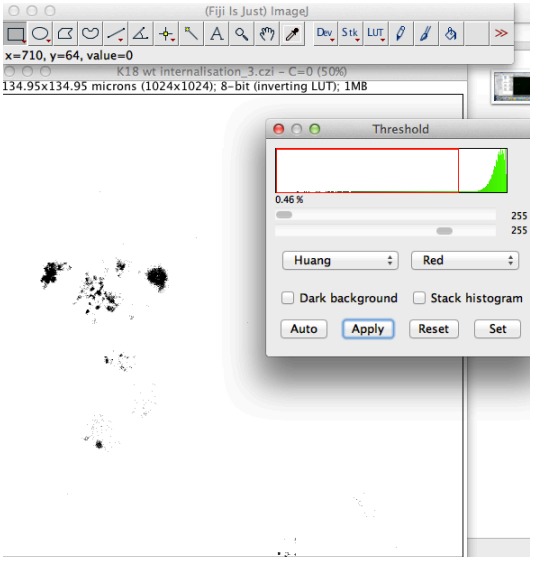

6. Exit the threshold window
7. Process → Binary → Watershed
8. Analyze → Analyze particles. Select “Add to Manager”. Click OK

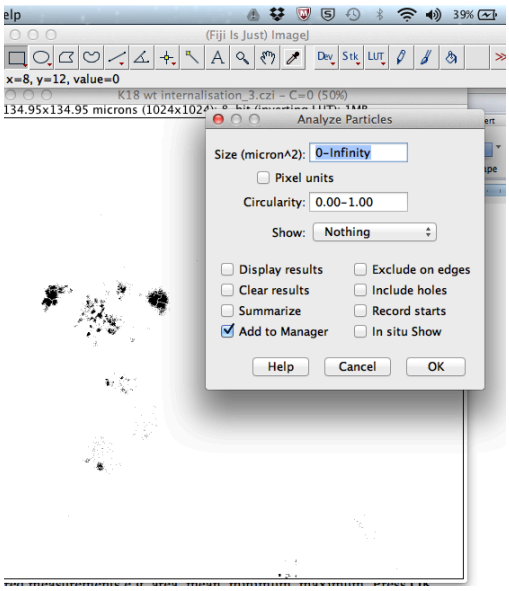

9. Close image without saving changes or closing the region of interest (ROI)

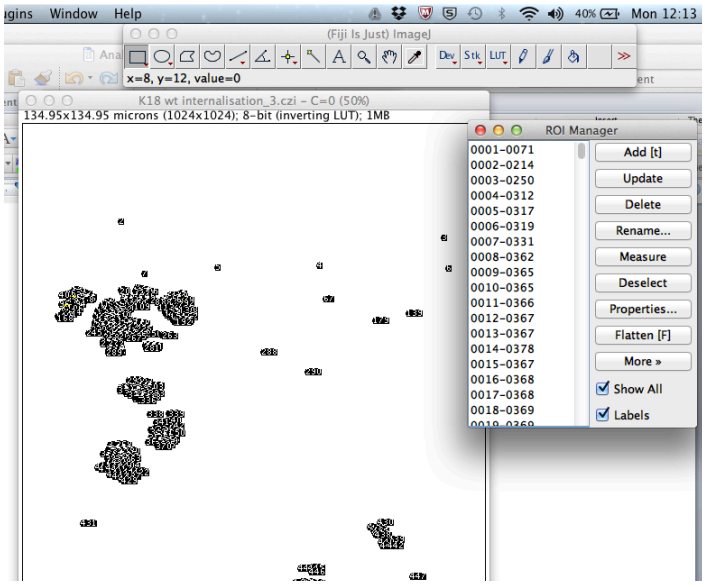

10. Reopen the original, unprocessed image. The ROI manager list of numbers will be linked to the reopened image by selecting “Show All”

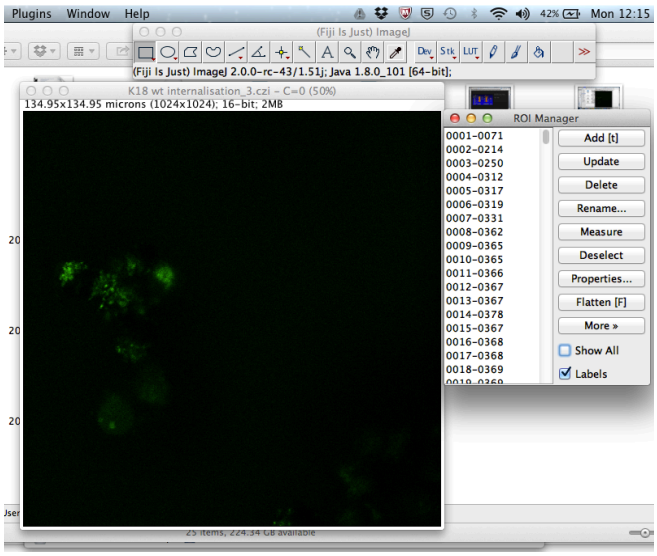

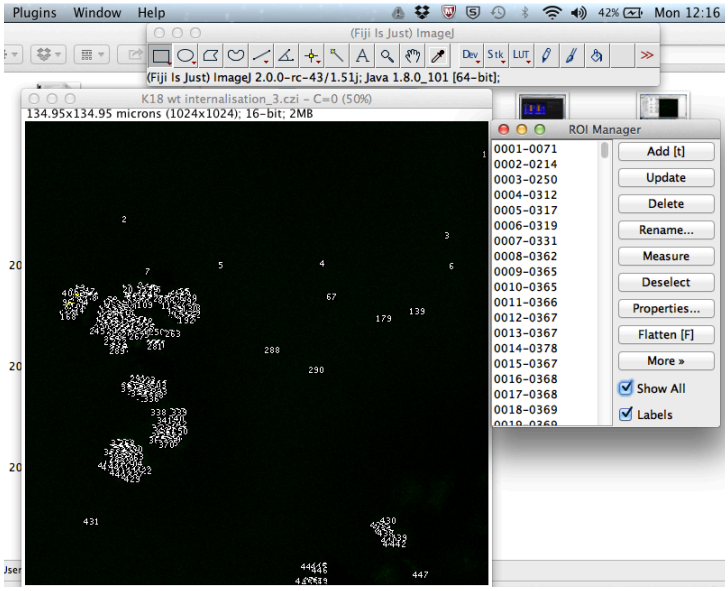

11. Analyze → set measurements
12. Select preferred measurements e.g. area, mean, minimum, maximum.
    Press OK
13. On the ROI manager, select all (Ctrl+A on Windows or Cmd+A on Mac).

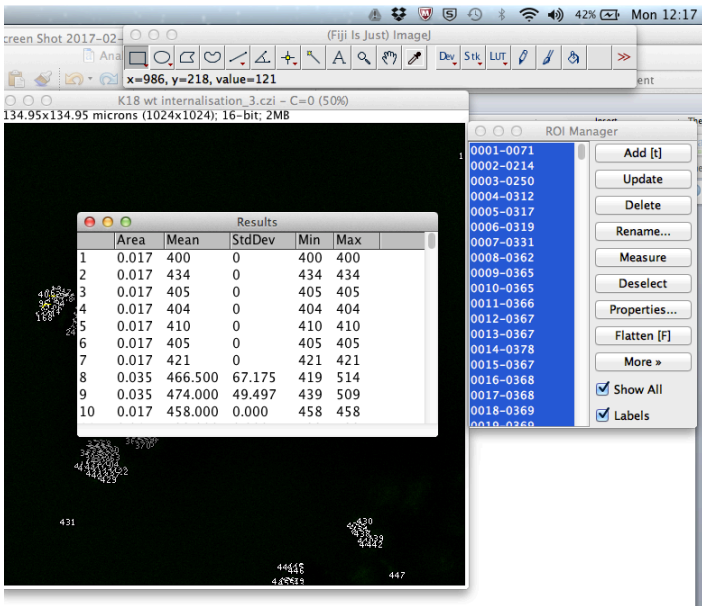

14. Press measure
15. File → Save as

Integrated density = Area x mean

Reference

Jensen, E.C., 2013. Quantitative Analysis of Histological Staining and Fluorescence Using ImageJ. Anat. Rec. 296, 378–381. https://doi.org/10.1002/ar.22641

9.2 Additional results

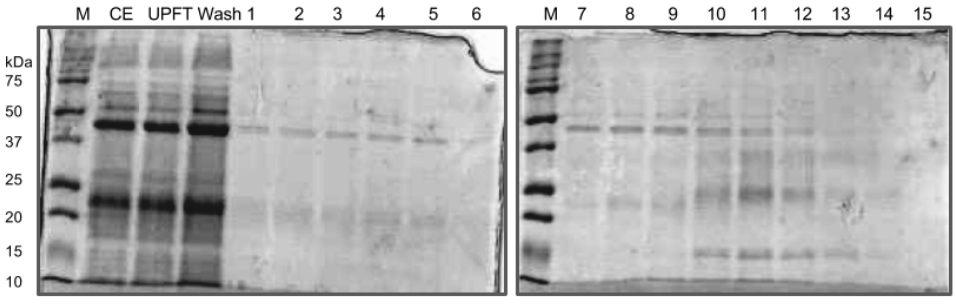

Figure 9.1. Non-reducing SDS PAGE analysis of the purity of purified TEV protease.
M = marker protein; CE = crude extract; UPFT = unbound protein flow-through; Wash = washing step aliquot; 1 - 15 = eluted fractions.